Dynamical system modeling of nonlinear complex ecological systems

Thesis
submitted for the Degree of
Doctor of Philosophy
in Science

by

Kankan Sarkar

to

Department of Mathematics
Jadavpur University
Kolkata - 700032, India
December, 2022

This thesis is dedicated to my beloved mother
Late Chhaya Sarkar

Certificate from the supervisors

This is to certify that the thesis entitled "**Dynamical system modeling of nonlinear complex ecological systems**" submitted by Sri Kankan Sarkar who got his name registered on 12th October, 2020 (Index No. 30/20/Maths./27) for the award of Ph.D. (Science) degree of Jadavpur University, is absolutely based upon his own work under the supervision of Prof. (Dr.) Prakash Chandra Mali and Dr. Subhas Khajanchi and that neither this thesis nor a part of it has been submitted for any degree/diploma or any academic award anywhere before.

19.12.2022

Dr. Prakash Chandra Mali
Professor
Department of Mathematics
Jadavpur University
Kolkata - 700032, India

**Professor
DEPARTMENT OF MATHEMATICS
Jadavpur University
Kolkata – 700 032, West Bengal**

Subhas Khajanchi 19/12/2022

Dr. Subhas Khajanchi
Assistant Professor
Department of Mathematics
Presidency University
86/1 College Street
Kolkata - 700073, India

Assistant Professor
Department of Mathematics
Presidency University
Kolkata

ACKNOWLEDGEMENT

First of all, I would like to express my deep and sincere gratitude to my supervisors, Prof. Prakash Chandra Mali, Department of Mathematics, Jadavpur University, Kolkata - 700032 and Dr. Subhas Khajanchi, Department of Mathematics, Presidency University, Kolkata - 700073 for their guidance, help and effort during my research work. Their valuable advice, inspiration, continuous support helped me a lot throughout my research work. I have been fortunate to have them as mentors during my research work. They have shared novel research idea with me and also gave me the freedom to explore on my own. It would have not been possible for me to complete this thesis without their close association, invaluable help, continuous support and co-operation. Apart from this academic supremacy, I deeply appreciate the professionalism of Dr. Subhas Khajanchi in the academic field which had smoothened my path. Dr. Subhas Khajanchi is not only my PhD supervisor but also my good friend with whom I have done my entire thesis work.

I warmly thank Prof. Abhijit Lahiri, Department of Mathematics, Jadavpur University, Kolkata for his valuable advice about my research work. I also thank Prof. Sujit Kumar Sardar for his continuous support during my research work.

I would like to express my deepest gratitude to my beloved parents, my father Sri. Nandan Sarkar, my mothers Late Chhaya Sarkar and Smt. Usha Sarkar, they always guided me to move forward with their support and inspiration. My gratefulness will never be completed without expressing my special gratitude for my beloved wife Smt. Gouri Sarkar. Her continuous inspiration, love and moral support are absolutely unforgettable. I also express my deep appreciation to my beloved daughter Aparna Sarkar.

Kankan Sarkar
19/12/2022
Kankan Sarkar

Kolkata - 700032
December, 2022

Thesis title: **Dynamical system modeling of nonlinear complex ecological systems**

Submitted by: **Kankan Sarkar**

In this thesis, we proposed and analyzed mathematical models for the predator-prey dynamics through a coupled system of differential equations. At the beginning, we studied a simple predator-prey model with different types of functional response and model exhibits rich ecological dynamics. We introduced the effect of fear on the growth of prey due to predator population. Our theoretical analysis shows strong anti-predator responses that can stabilize the predator-prey interactions by ignoring the existence of periodic behaviour. Our model system undergoes Hopf bifurcation by considering the prey birth rate as a bifurcation parameter. We extend our study on the effect of fear in an eco-epidemiological system and obtained that the increasing level of fear cannot wipe out the diseases from the system but the amplitude of the infected prey decreases as the level of fear is increased. Then, we proposed and analyzed a mathematical model for the eco-epidemiological system by incorporating disease in prey population, with particular emphasis on the influence of weak Allee effect in the growth of the predator population and the effects of incubation time delay. This study shows high-periodic oscillations due to increasing the value of time delay parameter and the disease transmission rate. We modified the fear function and proposed a more realistic fear function based on the experimental findings. We investigate how behavioural modification in prey population due to fear for predators and mutual interference among predator species can create various spatiotemporal pattern formation in population distribution. Finally, we considered a carbon-phytoplankton-zooplankton model and studied the effect of global warming and our simulation shows shifts in plankton's seasonal dynamics. The spatially explicit carbon-phytoplankton-zooplankton model shows complex spatiotemporal dynamics and patchy pattern formation. Analytical findings are validated with extensive numerical simulations. The thesis ends with a potential future direction.

19.12.2022

Prof. Prakash Chandra Mali

Subhas Khajanchi
Dr. Subhas Khajanchi 19/12/22

Kankan Sarkar
19/12/2022
Mr. Kankan Sarkar

Professor
DEPARTMENT OF MATHEMATICS
Jadavpur University
Kolkata – 700 032, West Bengal

Assistant Professor
Department of Mathematics
Presidency University
Kolkata

Contents

Chapter 1

Introduction

The study of predator-prey interactive dynamics is a very popular research topic in ecology. The dynamical interaction between a predator-prey system with different kinds of response function is a dominant theme in applied mathematics and theoretical ecology [1]. In a food chain of an ecosystem, energy is transferred from one trophic level to another by consumption of prey. The density of prey reduces due to natural death of the prey and consumption by the predators. It is very easy to observe the direct killing of prey by predators for food. But the presence of predators in an ecosystem also indirectly influences the growth of prey population. In presence of predator population, the prey population may significantly change their behavior, such an scope that it could influence the prey population more effectively than direct predation [2, 3]. Most of the investigation on predator-prey interactions, only consider the direct assassination of prey population in presence of predators, as this predation is more easy to investigate in ecological system. Some ecologists and evolutionary biologists have perceived the following fact based on the field observations: a predator-prey system should include not only the direct killing but also the cost for fear [3, 4] due to the lack of direct experimental observations, this fear effect has not been studied in the mathematical models. They noticed an attractive scenario that in presence of fear for predator population may influence the behavior and psychology for prey species more powerfully than direct assassination. The indirect effects caused by anti-predator behaviors (which incorporates foraging, habitat alterations, vigilance and various physiological alterations) for prey population may play a crucial role in governing prey demography [5]. The fear of predator population may influence the physiological situation for the prey species and it may cause a long-term loss for prey species. As for example, in the Greater Yellowstone Ecosystem, wolves (Canis lupus) influence the reproductive physiology of elks (*Cervus elaphus*) [6]. Also, the

frightened prey species naturally forages less, for which their growth rate decreases and embraces some survival mechanisms like starvation [2, 4]. Higher level of acute risk for predation can create prey species to quit habitats or foraging sites momentarily, returning only when the acute risk has passed and the prey species are relatively safe [4]. As for example, birds react to the sound of predator species with anti-predator defenses and they escape from their eyries at the first indication of danger. Such anti-predator activities may reduce the reproduction rate of the birds as long-run cost, although it is temporarily lucrative as it increases the survival probability of mature birds [4].

In the year 2011, Zanette et al. [7] studied a field experiment on song sparrows (*Melospiza melodia*) during a whole breeding season and observed that there is 40% depletion in offspring reproduction of song sparrows due to fear for predators [7]. This depletion is being happen due to the anti-predator activities which influences the growth rate, as well as the offspring survival rate because female song sparrows laid few eggs. Some of those eggs survived while most of the nestlings perished in the nest. The authors also observed that there were a variety of anti-predator responses their effect. As for illustrations, frightened parents suckled their nestlings less, their nestlings were lighter and much more likely to perish. Correlational affirmation for birds [8–11], Elk [6], Snowshoe hares [12] and dugongs [13] also give some confirmation that fear can influence the predator-prey interplays. Recently, Elliott et al. [14], conducted a field observation on *Drasophila melanogaster* as prey species and *mantid* as their predators, to quantify the affect of fear for fitness of the population in relation to species density. The authors showed that in appearance of *mantid*, the reproductive achievement of drasophila decreases, at low species density, in both their breeding as well as non-breeding seasons.

The disease in a population has been considered as one of the basic reasons for the extinction of the population. In the year 1986, Anderson and May [15] conducted a theoretical study on predator-prey system considering the infection in prey population. After this pioneer study, the predator-prey system with infected prey has grown enormously in the last three and half decades and some of these studies are [16–21]. Due to the infection in prey, the prey population become more vulnerable to the predator species [22–25]. In the year 1993, Lafferty & Morris [22] conducted an experiment to observe whether the predators hunt more on the infected prey and they observed that the infected prey (parasitized fish) are more vulnerable to predator population (bird). In different circumstances, it can also be observed that the

predator population avoid infected prey in reducing the cost of fitness [26, 27].

Due to the fear for predator species, the prey population become more vigilant and moves away from suspected predator population [28]. Thus, without killing the prey species, the food for predator species depleted by frightening of the prey. Such foraging activity of the prey reduces the chance of infection among susceptible prey by lowering the contact with the infected prey. Therefore, the fear of predators on prey population has a high impact on the dynamics in an eco-epidemiological model. The impact of fear on prey in an eco-epidemiological model have not been properly studied yet. Recently very few studies of eco-epidemiological model with disease in prey population incorporated the effect of fear [29, 30]. The theoretical study has shown that the impact fear of predator induced lower disease transmission in the prey population [29]. The fear of predator on prey can remove the chaotic oscillations from the system and the system moves towards disease free steady state [30].

Simultaneously, the most significant problems in eco-epidemiological interplays is to investigate the role of discrete time lags on stabilization of model system under consideration. Time lag is a most important scenario in eco-epidemiological modeling. A lot of significant research has been done on the population behavior, positiveness, uniform persistence, periodic solutions, oscillating behavior, bifurcation & chaotic or high periodic phenomena in population with retarded system [31–41]. Delay can destabilize the system with chaotic behavior as well as high-periodic behavior [42–46]. It is well established that a significant amount of biological processes include time lag(s) and need to be emphasized for the practical use. A two-patch predator-prey system with prey dispersal and positive density dependence growth of prey species has been studied by Sasmal & Ghosh [47].

Different kind of time lags are utilized in mathematical models to describe the phenomena more precisely. As for example, a negative feedback time lag is evaluated in the case of logistic growth rate for prey species to delineate the density related feedback procedure [48] and a positive feedback time lag is evaluated to delineate the gestation time of the predator population [49]. The infection is not an immediate interaction followed by time delay. This indicates that very soon an infected prey interacts a uninfected prey and finally become infectious. Moreover, in real scenario, there is a time lag among two events, for example, the first effective interplay among susceptible and infected prey species & the newly infected prey species become productively infectious. Shi et al. [50] investigated the effect of

3

incubation time lag in a Leslie-Gower predator-prey interaction model with prey infection. In their study, the authors observed that the non-negative co-existing steady state undergoes a Hopf bifurcation if time delay crosses a threshold value. More elaborate argument regarding the importance of time lags in useful models can be obtained in the standard book by Kuang [49].

Carbon dioxide (CO_2) is continuously exchanging among the earth's atmosphere, ocean and land surface as it is producing and absorbing by many animals, plants and microorganisms. Atmospheric CO_2 increased by nearly 40% over the past 250 years [51]. This increase is mainly caused by human fossil fuel combustion and deforestation [52]. In absence of anthropogenic activity, emissions and removal of CO_2 by these natural processes tend to balance the level of CO_2. Human activities have contributed substantially to the global warming by adding CO_2 and other green house gases to the atmosphere after the industrial revolution began around 1750 [53]. Burning of fossil fuels (oil, coal and natural gas) for energy, chemical reactions (e.g., manufacture of cement) and deforestation are the main human activity that emits CO_2 in the atmosphere. Thus, the anthropogenic activities are responsible for an intensive emission of CO_2 and other greenhouse gases to the atmosphere. In marine environment, phytoplankton are the main consumer of carbon during the photosynthesis. Hence, the study of the dynamics of carbon-phytoplankton-zooplankton system becomes very important.

Mathematical models for spatiotemporal pattern formation are now ubiquitous. Spatiotemporal pattern formation due to reaction-diffusion equation for predator-prey interplays have received substantial attention after the pioneering work by Alan Turing on chemical morphogenesis [54]. Spatiotemporal patterns are observed in different chemical, physiological and biological interactions and most of these patterns could be restored through numerical illustrations of the mathematical problems of which partial differential equations are an integral part [55–59]. The diffusion-induced instability familiar as Turing instability that leads to the generation of stationary Turing patterns like strips, spots and combination of both while the homogeneous equilibrium solution of the model undergoes unstable behavior to spatiotemporal disturbances. The patterns like spiral and target are known as non-Turing pattern that are observed occasionally in the Turing-Hopf region and occasionally in pure-Hope region in which oscillations for non-spatial Hopf bifurcation are dominant [60, 61]. Spiral patterns are normally observed around the boundary of Hopf bifurcation in which the diffusion rate is negligible [62]. Target patterns are the solutions

4

that move with same velocity in all directions and if perturbed slightly, tend to curl creating spiral waves [63].

The non-uniform motion of the population/species over the space are omnipresent. During the interplay between prey and predator species, predator species tend to diffuse due to search of prey species, and prey species migrate to circumvent predation, resulting in spatiotemporal variations [64]. This non-uniform motion resulting in a variety of interesting spatiotemporal pattern formation. The idea of Turing instability discovered by Alan Turing in the year 1952 [54] that came to light while a stable equilibrium state drops its stability due to existence of diffusion. The concept of Turing instability is used to explore the stationary and non-stationary patchy pattern formation, familiar as spatiotemporal pattern, due to interaction of prey and predator population while we include their randomness into our mathematical modeling. The reaction-diffusion system of interaction species are developed to incorporate randomness of the population into our mathematical modeling. The reaction part includes the inter and intra-species interplays while the randomness of the species within their habitat is modeled using the diffusion term. A significant number of research has been done on the basis of reaction-diffusion models for interacting species with suitable initial and boundary restrictions that are able to generate spatiotemporal pattern due to Turing instability [56, 58, 64–66]. Other than the stationary Turing pattern, the non-stationary and chaotic spatial pattern formation are equally important to explore the patchy distribution of the interacting species [58, 67–72].

1.1 Key terminology used in mathematical models

1.1.1 Functional response

Generally, the predator-prey system obey two basic principles: (i) prey species has natural birth rate and both the species has natural death rate, (ii) predator species can only grow by consuming the prey species [73]. In order to explain the predation phenomenon, Holling [74] has proposed different type of functional responses such as type-I, type-II and type-III. The response functions are the rate of prey consumption by the predator per unit time. The functional responses proposed by Holling [74] are the functions of prey density only. The response functions are independent of predator

density. The mathematical form of Holling type-I, II, and III are as follows:

$$\text{Holling type-I}: g(N) = \alpha N,$$
$$\text{Holling type-II}: g(N) = \frac{\alpha N}{1 + \beta N},$$
$$\text{Holling type-III}: g(N) = \frac{\alpha N^2}{1 + \beta N^2},$$

where α is the attack rate, β is handling time, and N is the prey density.

In the year 1975, Beddington & DeAngelis [75, 76] introduce a response function, which is alike to Holling type-II response function with an additional term, which represents the mutual interaction between the predators. Hence, Beddington-DeAngelis type response function is a function of both prey and predator density, that is, the rate of predation is a function of both prey and predator density. However, depending upon the structural complexity of the prey habitat, the response function for the predator-prey interaction may be different [77]. The mathematical form of Bedington-DeAngelis response function is as follows:

$$g(N, P) = \frac{\alpha N}{1 + \beta N + \varphi P},$$

where φ is a non-negative constant and P is the predator density. The Beddington-DeAngelis response function is a similar kind of Holling type-II response function but contains an additional term φP at the denominator. The mutual interaction between the predator population is represented by the term φP. For constant prey density, the response function $g(N, P)$ is maximum, when predator density P is minimum; again, the response function $g(N, P)$ is minimum, when predator density P is maximum. This response function is more realistic due to less mutual interaction of predators, predation will be more when predator density is less. The Bedington-DeAngelis response function is more generalized form of Holling type-I & type-II functional responses. Because, if $\varphi = 0$, then the Beddington-DeAngelis functional response is same as Holling type-II functional response. Again, if $\xi = 0$ and $\varphi = 0$, then Beddingon-DeAngelis response function is same as Holling type-I response function.

1.1.2 The Allee effect

Allee effect is one of the natural and classical phenomena in ecology. An Allee effect is the non-negative correlation among individual size/density & per-capita proliferation rate at the density of low population [78–82]. Allee

effect can be the cause of population extinction when density becomes very low and the species are unable to fertilize or unable to find mates. Allee effect primarily stratified into two distinct classes, namely strong Allee effect & weak Allee effect [82]. Sometimes, growth rate of population becomes negative and population die out below a critical level. This is known as strong Allee effect. Again, the weak Allee effect is a Allee effect without a critical population size/density. Evidence of Allee effect observed in many population of nature, including dogs [83, 84], insects [85] and plants [86]. We consider a population with logistic growth as follows:

$$\frac{dN}{dt} = r_0 N \left(1 - \frac{N}{K}\right),\qquad(1.1)$$

where N is the population density, r_0 is the intrinsic growth rate and K is the carrying capacity. Now, the model (1.1) with Allee effect becomes

$$\frac{dN}{dt} = r_0 N \left(1 - \frac{N}{K}\right)\left(1 - \frac{\alpha + \beta}{N + \beta}\right),$$

where α is the Allee threshold below which there is an extinction of population with $0 < \alpha < \beta$ (see Fig. 1.1) and β is a non-negative parameter affecting the overall shape of the population. Here, $\alpha \leq 0$ corresponds to weak Allee effect whereas $\alpha > 0$ corresponds to the strong Allee effect.
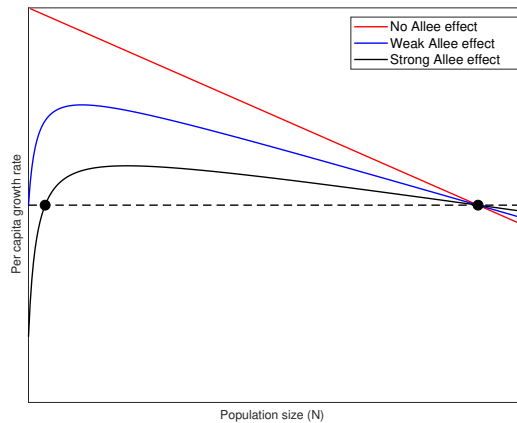
Figure 1.1: The figure shows the per-capita growth rate with respect to the population size (N). The red line shows no Allee effect, blue curve shows weak Allee effect and the strong Allee effect is shown by black curve. The black dot on the left represents the Allee threshold.

1.1.3   Fear effect

The energy is transformed from prey population to predator population by consumption of prey population. Thus, the density of prey reduces due to natural death of prey, consumption by predators and psychological effect (for example fear effect). Assassination of prey by predators is common to be observed in the ecosystem. But, in presence of predators, the prey population spend less time foraging for quality food but more time being vigilant. Due to the stress of predation, prey relocates them from the original high-risk habitat to the low-risk habitat, though the prey population may compromise with the quality food. Such anti-predator activities may instantly benefit prey by increasing their instant survival, but have a long-time negative effect on their reproduction and survival [2]. Zanette et al. [7] experimentally observed that due to the fear of predators, spring song sparrows reproduction reduced by 40%. The fear of predation affected the birth rate and the survival of song sparrow, which leads to hatching fewer eggs. It was also experimentally observed that Drosophila melanogaster shows anti-predator behaviors as exposed to scent of mantid and the growth and fitness of Drosophila melanogaster are affected due to the effect of fear [87].

Due to the lack of direct experimental observations, a very limited number of research conducted in the field of mathematical biology considered the effect of fear. In the year 2016, Wang et al. [88] has incorporated the effect of fear in a predator-prey system based on the experiment conducted by Zanette et al. [7]. The strong anti-predator behaviors of prey may exclude the existence of periodic solution and thus eliminate the phenomenon of "paradox of enrichment", also the periodic solution of the predator-prey system exclude when the anti-predator behavior of prey becomes weak [88]. As the level of fear increases, the predator-prey system enters into a steady state situation from limit cycle oscillation [89]. Some of the theoretical studies considering fear effect are [88, 90–94].

1.1.4   Reaction diffusion system

Ordinary differential equations (ODEs) is an efficient tool for modeling the ecological phenomena. But, the mathematical modeling using ODE restrict our analysis to one independent variable only (namely, time). Real world ecological system depends on both time and space. The ODE models describing the predator-prey dynamics considering the most important independent variable time and neglecting the space variation. This restriction often fails to explain the real world scenario of the predator-prey system. Hence, in such scenario, instead of using ODE model, use of

partial differential equation (PDE) becomes more appropriate as the PDE model are based on the two independent variable, namely, time as one independent variable and space as another independent variable [95]. Thus, the dynamical behavior of the predator-prey system can be explained for at least two independent variables at the same time.

For example, we consider the Lotka-Volterra model for the predator-prey system as follows:

$$
\begin{aligned}
\frac{dN}{dt} &= \alpha N - \beta NP, \\
\frac{dP}{dt} &= \gamma NP - \delta P,
\end{aligned}
\tag{1.2}
$$

where N, P represents prey and predator density, respectively, at any time t; α, β, γ and δ are non-negative constants and have their usual ecological meaning. In the system (1.2), we have considered only one independent variable time (t). To consider the movement of the prey and predator in space, we add the diffusion terms in (1.2). We consider the bounded domain Ω in $\mathbb{R}^2$ with closed boundary $\partial\Omega$. Hence, the spatiotemporal model corresponding to (1.2) is the following system of reaction-diffusion equations:

$$
\begin{aligned}
\frac{\partial N(t,x,y)}{\partial t} &= \alpha N - \beta NP + D_N \bigtriangledown^2 N, \\
\frac{\partial P(t,x,y)}{\partial t} &= \gamma NP - \delta P + D_P \bigtriangledown^2 P,
\end{aligned}
\tag{1.3}
$$

where D_N and D_P are the diffusion coefficients for prey and predator population, respectively, with $\bigtriangledown^2 \equiv \partial^2/\partial x^2 + \partial^2/\partial y^2$ is the two-dimensional Laplacian operator and (x,y) is the position in space. The equations in (1.3) are subject to the following non-negative initial conditions: $N(0,x,y) \equiv N_0(x,y) \geq 0$, $P(0,x,y) \equiv P_0(x,y) \geq 0$, for all $(x,y) \in \Omega$ with zero-flux boundary conditions: $\frac{\partial N}{\partial \hat{r}} = 0 = \frac{\partial P}{\partial \hat{r}}$, where $\hat{r}$ is the outward drawn unit normal vector on the boundary $\partial\Omega$.

1.2 Mathematical preliminaries

In this section, some definitions and theorems have been described which are used to analyze the proposed mathematical models in this thesis.

1.2.1 System of ordinary differential equations

A finite set of differential equations is known as system of ordinary differential equations, which are mainly two types (i) linear and (ii) nonlinear. A linear system of ordinary differential equations can be defined as follows:

$$\frac{d\mathbf{x}}{dt} = A\mathbf{x}, \tag{1.4}$$

with the initial condition $\mathbf{x}(\mathbf{0}) = \mathbf{x}_0$, where $\mathbf{x} \in \mathbb{R}^n$, A is an $n \times n$ matrix and

$$\frac{d\mathbf{x}}{dt} = \begin{bmatrix} \frac{dx_1}{dt} \\ \frac{dx_1}{dt} \\ \vdots \\ \frac{dx_n}{dt} \end{bmatrix}.$$

The solution of (1.4) is given by $\mathbf{x}(t) = e^{At}\mathbf{x}_0$.

Again, the nonlinear system of differential equations can be defined as follows:

$$\frac{d\mathbf{x}}{dt} = \mathbf{f}(\mathbf{x}), \tag{1.5}$$

with the initial condition $\mathbf{x}(\mathbf{0}) = \mathbf{x}_0$, where $\mathbf{f} : E \to \mathbb{R}^n$ and E is an open subset of $\mathbb{R}^n$. The nonlinear system (1.5) has unique solution through each point $\mathbf{x}_0 \in E$.

Definition 1.2.1. *A point $\boldsymbol{x}_0 \in \mathbb{R}^n$ is said to be an equilibrium point or critical point of the system of differential equations (1.5) if $\boldsymbol{f}(\boldsymbol{x}_0) = \boldsymbol{0}$.*

Definition 1.2.2. *An equilibrium point $\boldsymbol{x}_0$ of (1.5) is said to be a hyperbolic equilibrium point if none of the eigenvalues of the matrix $D\boldsymbol{f}(\boldsymbol{x}_0)$ have zero real part. Again if $A = D\boldsymbol{f}(\boldsymbol{x}_0)$, then the system (1.4) is called the linearization of the system (1.5).*

If $\mathbf{x}_0 = \mathbf{0}$ is an equilibrium point of the system (1.5), then $\mathbf{f}(\mathbf{0}) = \mathbf{0}$. Now, by Taylor's series expansion, we have

$$\mathbf{f}(\mathbf{x}) = D\mathbf{f}(\mathbf{0})\mathbf{x} + \frac{1}{2}D^2\mathbf{f}(\mathbf{0})(\mathbf{x}, \mathbf{x}) + \cdots .$$

Hence, the linear function $D\mathbf{f}(\mathbf{0})\mathbf{x}$ is a good approximation for the nonlinear function $\mathbf{f}(\mathbf{x})$ near $\mathbf{x} = \mathbf{0}$. Thus, the local behavior of the nonlinear system (1.5) near $\mathbf{x} = \mathbf{0}$ will be approximated by the behavior of its linearization at $\mathbf{x} = \mathbf{0}$.

Definition 1.2.3. *Let $\boldsymbol{x}_0$ is an equilibrium point of the nonlinear system (1.5). Now, if all the eigenvalues of $D\boldsymbol{f}(\boldsymbol{x}_0)$ have negative real part, then the equilibrium $\boldsymbol{x}_0$ is said to be a sink; again if all the eigenvalues of $D\boldsymbol{f}(\boldsymbol{x}_0)$ have positive real part, then the equilibrium $\boldsymbol{x}_0$ is said to be a source; and the equilibrium $\boldsymbol{x}_0$ is said to be a saddle if at least one eigenvalue with negative real part and at least one eigenvalue with positive real part.*

1.2.2 Positivity and boundedness

The positivity of solution of the system (1.5) indicates that the solution of the system (1.5) with non-negative initial conditions remain non-negative for all finite time t. Analytically, it can be expressed as

$$H = \left\{ \mathbf{x} \in \mathbb{R}^n : \phi(\mathbf{x}) = 0 \right\},$$

where H is positively invariant with $\mathbf{x}_0 \in H$ implies $\mathbf{x}(t, \mathbf{x}_0) \in H$ for all $t \geq 0$ and ϕ is a real-valued function.

The solution $\mathbf{x}(t, \mathbf{x}_0)$ of the system (1.5) is said to be bounded if the following condition is satisfied

$$\mid \mathbf{x}(t, \mathbf{x}_0) \mid \leq \epsilon(\mid \mathbf{x}_0 \mid, t_0), \forall \; t \geq t_0,$$

where ϵ is a non-negative constant and depends on the initial condition $\mathbf{x}(t_0) = \mathbf{x}_0$. The system (1.5) is called uniformly bounded if the solutions of (1.5) are independent of initial condition.

1.2.3 Uniform persistence

If there exists a bounded region $\Gamma \subset Int(\mathbb{R}^+)$ such that every solution $\mathbf{x}(t)$ of the system (1.5) are always positive and remains bounded in Γ, irrespective of initial conditions, then the system (1.5) is said to be uniformly persistent or permanent. Analytically, it can be written as

$$m \leq \max \left\{ \liminf_{t \to \infty} \mathbf{x}(t) \right\}, \;\; \max \left\{ \limsup_{t \to \infty} \mathbf{x}(t) \right\} \leq M,$$

where m and M are non-negative real numbers with $0 < m \leq M$.

1.2.4 Stability and Liapunov functional

In this section, we discuss the stability of the equilibrium points of the system (1.5).

Definition 1.2.4. *Let $\boldsymbol{f} \in C^1(S)$, where S is an open subset of $\mathbb{R}^n$. For $\boldsymbol{x}_0 \in S$ and $\boldsymbol{\phi}(t, \boldsymbol{x}_0)$ be the solution of the initial value problem (1.5) defined on its maximal interval of existence $I(\boldsymbol{x}_0)$. The set of mappings*

$$\boldsymbol{\phi}_t(\boldsymbol{x}_0) = \boldsymbol{\phi}(t, \boldsymbol{x}_0),$$

for $t \in I(\boldsymbol{x}_0)$, is said to be the flow of the system (1.5).

Definition 1.2.5. *The equilibrium point $\boldsymbol{x}_0$ of (1.5) is said to be stable if for any $\epsilon > 0$ there exists a $\delta > 0$ such that for all $\boldsymbol{x} \in N_\delta(\boldsymbol{x}_0)$ and $t \geq 0$, we have*

$$\boldsymbol{\phi}_t(\boldsymbol{x}) \in N_\epsilon(\boldsymbol{x}_0).$$

The equilibrium point $\boldsymbol{x}_0$ is said to be unstable if it is not stable. Again, if the equilibrium point $\boldsymbol{x}_0$ is stable and there exist a $\delta > 0$ such that for all $\boldsymbol{x} \in N_\delta(\boldsymbol{x}_0)$,

$$\lim_{t \to \infty} \boldsymbol{\phi}_t(\boldsymbol{x}) = \boldsymbol{x}_0,$$

then the equilibrium point $\boldsymbol{x}_0$ is said to be asymptotically stable.

Theorem 1.2.1. *If the equilibrium point $\boldsymbol{x}_0$ of the system (1.5) is stable, then no eigenvalue of $D\boldsymbol{f}(\boldsymbol{x}_0)$ has positive real part.*

Definition 1.2.6. *Let $\boldsymbol{\phi}_t$ be the flow of (1.5) and $\boldsymbol{f}, L \in C^1(S)$, then for $\boldsymbol{x} \in S$ the derivative of $L(\boldsymbol{x})$ along the solution $\boldsymbol{\phi}_t(\boldsymbol{x})$ is defined as follows:*

$$\dot{L}(\boldsymbol{x}) = \frac{d}{dt} L(\boldsymbol{\phi}_t(\boldsymbol{x})) \mid_{t=0} = DL(\boldsymbol{x})\boldsymbol{f}(\boldsymbol{x}),$$

where S is the open subset of $\mathbb{R}^n$.

A function $L : \mathbb{R}^n \to \mathbb{R}$ satisfying the hypotheses of the following theorem is said to be a Liapunov function.

Theorem 1.2.2. *Let $\boldsymbol{f} \in C^1(S)$ and $\boldsymbol{f}(\boldsymbol{x}_0) = \boldsymbol{0}$, where S is an open subset of $\mathbb{R}^n$ containing $\boldsymbol{x}_0$. Also, let L be a real valued function such that $L \in C^1(S)$, $L(\boldsymbol{x}_0) = 0$ and $L(\boldsymbol{x}) > 0$ if $\boldsymbol{x} \neq \boldsymbol{x}_0$. Then*

  (i) if $\dot{L}(\boldsymbol{x}) \leq 0$ for all $\boldsymbol{x} \in S$, $\boldsymbol{x}_0$ is stable;

  (ii) if $\dot{L}(\boldsymbol{x}) < 0$ for all $\boldsymbol{x} \in S \sim \{\boldsymbol{x}_0\}$, $\boldsymbol{x}_0$ is asymptotically stable;

  (iii) if $\dot{L}(\boldsymbol{x}) > 0$ for all $\boldsymbol{x} \in S \sim \{\boldsymbol{x}_0\}$, $\boldsymbol{x}_0$ is unstable.

Routh-Hurwitz criterion:

To investigate the stability of (1.5), we use Routh-Hurwitz stability criterion. The stability of (1.5) near the equilibrium point $\mathbf{x}_0$ depends upon the nature of the eigenvalues of $D\mathbf{f}(\mathbf{x}_0)$. Let the characteristic equation of $D\mathbf{f}(\mathbf{x}_0)$ be

$$\lambda^n + c_1\lambda^{n-1} + c_2\lambda^{n-2} + \cdots + c_n = 0, \tag{1.6}$$

where c_i, $i = 1, 2, \ldots, n$ are real. The system (1.5) is locally asymptotic stable if if all of the eigenvalues have negative real parts. Routh-Hurwitz criterion gives the necessary and sufficient condition for all the eigenvalues of the characteristic equation (1.6) of $D\mathbf{f}(\mathbf{x}_0)$ lies in the left half of the complex plane. If $c_i > 0$ for all $i = 1, 2, \ldots, n$, then the Routh-Hurwitz criterion is as follows [96, 97]:

$$\triangle_1 = c_1 > 0, \ \triangle_2 = \begin{vmatrix} c_1 & c_3 \\ 1 & c_2 \end{vmatrix} > 0, \ \triangle_3 = \begin{vmatrix} c_1 & c_3 & c_5 \\ 1 & c_2 & c_4 \\ 0 & c_1 & c_3 \end{vmatrix} > 0,$$

$$\triangle_i = \begin{vmatrix} c_1 & c_3 & . & . & . & . \\ 1 & c_2 & c_4 & . & . & . \\ 0 & c_1 & c_3 & . & . & . \\ 0 & 1 & c_2 & . & . & . \\ . & . & . & . & . & . \\ 0 & 0 & . & . & . & c_i \end{vmatrix} > 0, \ i = 1, 2, 3, \ldots, n.$$

If the system parameters value satisfies all the above constraints, then the system (1.5) is locally asymptotic stable at the equilibrium point $\mathbf{x}_0$.

1.2.5 Bifurcation

If a system parameter is varied, a qualitative change in behavior of the system may observed at a critical value of the parameter. Such change in behavior of the system is known as bifurcation and the corresponding critical value of the system parameter is known as bifurcation point. At the bifurcation point, small perturbation can cause qualitative change in the solution of the system. In this section, we discussed about two types of bifurcation, which are frequently observed in a system.

- **Saddle-node bifurcation:**
  Saddle-node bifurcation observed in a system, if the control parameter is varied, two equilibrium points move towards each other, collide and annihilate each other.

- **Transcritical bifurcation:**
  Transcritical bifurcation occurs in a system, if the control parameter is varied and the stability of the equilibrium points are exchanged when the control parameter passes through the critical value (that is, the bifurcation point). The equilibrium point just switches their stability and they do not disappear after the bifurcation.

Theorem 1.2.3 (Sotomayor). *Let us consider an autonomous system of n ordinary differential equations*

$$\frac{d\boldsymbol{x}}{dt} = \boldsymbol{f}(\boldsymbol{x}, \alpha), \tag{1.7}$$

where $\boldsymbol{x} \in \mathbb{R}^n$, $\alpha \in \mathbb{R}$ and the system (1.7) has a equilibrium point $\boldsymbol{x}_0$. Now, for $\alpha = \alpha^*$, $D\boldsymbol{f}(\boldsymbol{x}_0, \alpha^*)$ has an eigenvalue $\lambda = 0$, then $\left[D\boldsymbol{f}(\boldsymbol{x}_0, \alpha^*)\right]^T$ also has an eigenvalue $\lambda = 0$. Let $\boldsymbol{U}$ and $\boldsymbol{V}$ be the eigenvectors of $D\boldsymbol{f}(\boldsymbol{x}_0, \alpha^*)$ and $\left[D\boldsymbol{f}(\boldsymbol{x}_0, \alpha^*)\right]^T$, respectively, corresponding to the eigenvalue $\lambda = 0$. Also assume that $D\boldsymbol{f}(\boldsymbol{x}_0, \alpha^*)$ has p eigenvalues with negative real part and $(n-p-1)$ eigenvalues with positive real part and the following conditions are satisfied

$$\begin{aligned} \boldsymbol{V}^T \boldsymbol{f}_\alpha(\boldsymbol{x}_0, \alpha^*) &\neq 0, \\ \boldsymbol{V}^T \left[D^2 \boldsymbol{f}(\boldsymbol{x}_0, \alpha^*)(\boldsymbol{U}, \boldsymbol{U})\right] &\neq 0. \end{aligned} \tag{1.8}$$

Then there is a smooth curve of equilibrium points of (1.7) in $\mathbb{R}^n \times \mathbb{R}$ passing through $(\boldsymbol{x}_0, \alpha^*)$ and tangent to the hyperplane $\mathbb{R}^n \times \{\alpha^*\}$. The number of equilibrium point of (1.7) depends on the sign of the expressions in (1.8). The system (1.7) has no equilibrium pint near $\boldsymbol{x}_0$ when $\alpha < \alpha^*$ (or when $\alpha > \alpha^*$) and (1.7) has two equilibrium pint near $\boldsymbol{x}_0$ when $\alpha > \alpha^*$ (or when $\alpha < \alpha^*$). The two equilibrium points of (1.7) near $\boldsymbol{x}_0$ are hyperbolic and have stable manifolds of dimensions p and $p + 1$, respectively. Thus, the system (1.7) undergoes a saddle-node bifurcation at the equilibrium point $\boldsymbol{x}_0$, if the control parameter α is varied and passes through the critical value α^*. The point $\alpha = \alpha^*$ is known as the saddle-node bifurcation point.
Now, if the conditions (1.8) are changed to

$$\begin{aligned} \boldsymbol{V}^T \boldsymbol{f}_\alpha(\boldsymbol{x}_0, \alpha^*) &= 0, \\ \boldsymbol{V}^T \left[D\boldsymbol{f}_\alpha(\boldsymbol{x}_0, \alpha^*)\boldsymbol{U}\right] &\neq 0, \\ \boldsymbol{V}^T \left[D^2 \boldsymbol{f}(\boldsymbol{x}_0, \alpha^*)(\boldsymbol{U}, \boldsymbol{U})\right] &\neq 0. \end{aligned}$$

then the system (1.7) undergoes a transcritical bifurcation at the equilibrium point $\boldsymbol{x}_0$, if the control parameter α is varied and passes through the critical value α^*. The point $\alpha = \alpha^*$ is known as the transcritical bifurcation point.

- **Hopf bifurcation:**
  The system experiences Hopf bifurcation, if the control parameter is varied and the stable equilibrium point loses its stability at a critical value (that is, the bifurcation point) and limit cycle oscillation occurs.

Theorem 1.2.4. (**Hopf bifurcation**) *Let us consider an autonomous system of ordinary differential equations*

$$\frac{d\boldsymbol{x}}{dt} = \boldsymbol{f}(\boldsymbol{x}, \alpha), \tag{1.9}$$

where $\boldsymbol{x} \in \mathbb{R}^n$, $\alpha \in \mathbb{R}$ and the system (1.9) has a equilibrium point $\boldsymbol{x}_0$. Now, for $\alpha = \alpha^*$, $D\boldsymbol{f}(\boldsymbol{x}_0, \alpha^*)$ has a pair of purely imaginary eigenvalues and no other eigenvalue has zero real part. Then there is a smooth curve of equilibrium points $\boldsymbol{x}(\alpha)$ with $\boldsymbol{x}(\alpha^*) = \boldsymbol{x}_0$ and the eigenvalues, $\lambda(\alpha)$ and $\bar{\lambda}(\alpha)$ of $D\boldsymbol{f}(\boldsymbol{x}(\alpha), \alpha)$, which are purely imaginary at $\alpha = \alpha^*$, vary smoothly with α. Moreover, if

$$\frac{d}{d\alpha}\big[Re(\lambda(\alpha))\big]_{\alpha=\alpha^*} \neq 0,$$

then the system (1.9) undergoes Hopf bifurcation at the equilibrium point $\boldsymbol{x}_0$ for $\alpha = \alpha^*$.

1.2.6 Delay differential equation

If the evolution of a system at time t depends on the earlier time $t - \tau$, then the system is represented by a system of the delay differential equation (DDE). There are different type of delay differential equations. A general retarded delay differential equation (RDDE) or retarded functional differential equation (RFDE) is expressed as follows:

$$\frac{d\mathbf{x}}{dt} = \mathbf{h}(\mathbf{x}(t), \mathbf{x}(t - \tau)). \tag{1.10}$$

To evaluate the rate of change of the state variable $\mathbf{x}$ at t_0, we must have the values $\mathbf{x}(t_0)$ and $\mathbf{x}(t_0 - \tau)$. Hence, the initial value problem for a delay differential equation required the value of the state variable $\mathbf{x}$ not only at the point t_0, but also on the entire interval $[t_0 - \tau, t_0]$. Thus, for the delay differential equations (1.10), the initial value function $\mathbf{x}(t) = \mathbf{x}_0(t)$ should be defined for all $t \in [t_0 - \tau, t_0]$. The initial value function $\mathbf{x}_0(t)$ is called the initial history of the delay differential equations (1.10).

Considering the above discussions, the delay differential equation can be defined as follows: let $E \equiv E([-\tau, 0], \mathbb{R})$, $\tau > 0$ be a Banach space of all

continuous functions with the norm defined as $\parallel \rho \parallel = \sup_{-\tau \leq \alpha \leq 0} \mid \rho(\alpha) \mid$ for all $\rho \in E$. Let us assume that the non-delayed and delayed variables as $\mathbf{x}$ and $\mathbf{x}_t$, respectively, such that

$$\mathbf{x}_t(\alpha) = \mathbf{x}(t + \alpha), \ \alpha \in [-\tau, \ 0], \ t \in [t_0, \ t_0 + r],$$

where $r > 0$, $t_0 \in \mathbb{R}$, $\mathbf{x}(t) \in E\left([t_0 - \tau, \ t_0 + r], \mathbb{R}\right)$ and $\mathbf{x}_t(\alpha) \in E$. A general retarded delay differential equation or retarded functional differential equation is defined as follows:

$$\frac{d\mathbf{x}}{dt} = \mathbf{h}(t, \mathbf{x}_t), \ \mathbf{x}(t) = \mathbf{x}_0(t) = \rho(t), \ t \in [-\tau, \ 0]. \tag{1.11}$$

Now, for $t_0 \in \mathbb{R}$ and $\rho \in E$, $\mathbf{x}(t, \rho)$ is a solution of (1.11) with initial function ρ.

Again, we consider the linearized delay system as follows:

$$\frac{d\mathbf{x}}{dt} = M\mathbf{x}(t) + N\mathbf{x}(t - \tau), \tag{1.12}$$

where M and N are $n \times n$ matrices and τ is the discrete time delay. The characteristic equation of the linearized system (1.12) is

$$\det\left(\lambda I - M - Ne^{-\lambda\tau}\right) = 0,$$

which can be expressed as

$$A(\lambda) + B(\lambda)e^{-\lambda\tau} = 0, \tag{1.13}$$

where $A(\lambda)$ and $B(\lambda)$ are polynomials in λ. The local stability of the delayed system is determined by the roots of the characteristic equation, but in this case, the characteristic equation (1.13) is a transcendental equation in λ, which has infinitely many roots. Hence, the Routh-Hurwitz criteria is not applicable for the delay differential equations to find the stability of the system. Thus, the linear stability analysis of the delayed system is more difficult. To study the local stability of the delayed system, we compute the sign of the real part of characteristic roots of (1.13). The delayed system will be locally asymptotically stable if the characteristic roots of (1.13) are negative or have negative real part and the system will lost its stability if the characteristic roots are purely imaginary. The basic results regarding changing the stability is summarized in the following theorem.

Theorem 1.2.5. *The sum of orders of zeros of the characteristic equation (1.13) in the open right half plane can change only if a zero appears or passes the imaginary axis when the time delay parameter τ is varied. Furthermore, given any real number ζ, the characteristic equation (1.13) has at most a finite number of roots λ such that $Re(\lambda) \geq \zeta$.*

The study of local stability in a delayed system becomes more difficult than the non-delayed system. After introduction of delay in a system of ordinary differential equations, it is necessary to study the change in stability of the equilibrium as the delay parameter varies. If the characteristic root changes its real part from negative to positive or vise-versa, that is, the root passes the imaginary axis, as the delay parameter increases or decreases, then the equilibrium point changes its stability. This phenomenon is called Hopf bifurcation with respect to the time delay parameter τ. The system must satisfy the following two conditions to occur Hopf bifurcation:

(i) there exists a critical value $\tau = \tau^*$ for which $\lambda_{1,2}(\tau^*) = \pm i\omega$ and all other characteristic roots have negative real parts at $\tau = \tau^*$ and

(ii) **(the transversality condition)**

$$\frac{d}{d\tau}\left[Re(\lambda(\tau)) \right]_{\tau=\tau^*} \neq 0.$$

1.3 The organization of the Thesis

The aim of the present thesis is to study the dynamics of predator-prey system that include different factors/mechanisms responsible for complex behavior in multi-species mathematical models. This is an attempt to analyze models with fear factors, time delays, infections, environmental effects and spatiotemporal perturbations. An effort has been made to stabilize the complex behavior in the models. Numerical illustrations are carried out to explore the possibility of rich dynamics in the nonlinear models. The thesis is organized in the following way:

In the present chapter, we give a brief introduction to the dynamics of ecological systems. The important concepts are overviewed here. Brief discussion on tools/techniques used in this thesis is also included. A brief literature review related work in this area has also been presented.

In the **Chapter 2**, we investigate a two-dimensional mathematical model that describes the interactive dynamics of a predator-prey system with different kinds of response function such as Holling type-I, type-II and Beddington-DeAngelis type. The positivity, boundedness and uniform persistence of the system is established. We investigate the biologically feasible equilibrium points and their stability analysis. We perform a comparative study by considering different kinds of functional responses, which suggest that the dynamical behavior of the system remains unaltered but the position of the bifurcation points altered. Again, we introduce the

effect of fear in the predator-prey system with Holling type-II functional response. We investigate all the biologically feasible equilibrium points, and their stability is analyzed in terms of the model parameters. Our theoretical analysis exhibits that for strong anti-predator responses can stabilize the predator-prey interactions by ignoring the existence of periodic behaviors. The system undergoes Hopf bifurcation with respect to the prey birth rate, which indicates that a periodic solution occurs around a fixed point.

In the **Chapter 3**, we extend our study on the effect of fear in an eco-epidemiological system. We proposed and analyzed an eco-epidemiological model with disease in prey and incorporated the effect of fear on prey species due to predator population. We assume that in absence of predator species, the prey population grows logistically and the disease is limited on prey population only. Due to the fear for predators, prey population becomes more vigilant and moves away from suspected predators. Such foraging activity of prey reduces the chance of infection among susceptible prey by lowering the contact with infected prey. We assume that the fear of predator has no effect on infected prey as they are more vigilant. Positivity, boundedness and uniform persistence of the proposed model are investigated. The feasibility and stability of the equilibrium points are analyzed. We establish the conditions for Hopf bifurcation of the proposed model around the endemic steady state. As the level of fear increases, the system moves toward the steady state from limit cycle oscillation. Increasing level of fear cannot wipe out the diseases from the system but amplitude of the infected prey decreases as the level of fear is increased. The system changes its stability as the rate of infection increases and the predator extinct when the rate of infection of prey is high enough though predators are not infected by the disease.

In the **Chapter 4**, we proposed and analyzed a mathematical model for the eco-epidemiological system with disease in prey population, with particular emphasis on the effects of an incubation time delay and the influence of weak Allee effect in the growth of the predator population. The positivity, boundedness, uniform persistence of the model and the stability of the biologically feasible equilibrium points are investigated. Using the time delay as bifurcation parameter, we explored the stability of the interior equilibrium point and observe that Hopf bifurcation can occur when the incubation time delay crosses some threshold value. We have identified the stability regions associated with extinction of the population, stability of the equilibrium points and high-periodic oscillations in the level of disease transmission. Analytical findings are supported by numerical illustrations

that demonstrate the behavior of the proposed model in different dynamical regimes. Stability criteria for the biologically feasible equilibrium points were obtained and validated with numerical simulations. We found most sensitive system parameters using the PRCC sensitivity analysis. We observe that our model simulation exhibits high-periodic oscillations due to increasing the value of time delay parameter and the disease transmission rate.

In the **Chapter 5**, we developed a more realistic fear function. Based on the experimental findings, we proposed and analyzed a mathematical model that incorporates the fear-induced birth reduction in the prey population due to presence of predator. We performed qualitative behavior of the model including positivity and boundedness of solutions, existence of equilibrium points and their local stability analysis, existence of transcritical and Hopf bifurcation. We analyzed Hopf bifurcation with respect to the prey growth rate and the level of fear. The transcritical bifurcation is analyzed by varying the prey growth rate. Distribution of the population of interacting species in a large scale natural system is heterogeneous and subject to alter for different reasons. Thus, we investigate how behavioral modification in prey population due to fear for predators and mutual interference among predator species can create various spatiotemporal pattern formation in population distribution. In the spatially extended system, we provide a detailed stability analysis and obtain the conditions for Turing instability. Numerical simulations are performed to validate our analytical results for both non-spatial and spatial models. Warm spot patterns are obtained by considering three different types of initial data and discussed the biological significance of these patterns for the two-dimensional spatial model. Our numerical simulation demonstrates that the fear effect in a diffusive predator-prey system with mutual interference between predators may exhibit more complicated dynamics.

In the **Chapter 6**, we proposed and analyzed a mathematical model for carbon dioxide, phytoplankton and zooplankton in a marine environment. Over the last 250 years, anthropogenic activity has increased atmospheric carbon dioxide by nearly 40%. This increase is mainly caused by human fossil fuel combustion and deforestation, which are the main causes of global warming. Phytoplankton are the free floating and autotrophic organism in the ocean. Phytoplankton of world's ocean synthesizes half of the carbon dioxide of the total Earth's photosynthetic activity. Thus phytoplankton plays a crucial role in controlling Earth's climate. In this study, we proposed and analyzed a mathematical model for the carbon-phytoplankton-zooplankton interaction dynamics. Positivity and boundedness of the model are investi-

gated. Existence and stability of the biologically feasible equilibrium points are studied. We define the conditions for the Hopf bifurcation of the proposed model around the coexisting equilibrium point and the system shows Hopf bifurcation with respect to the carbon capturing coefficient. Complex spatiotemporal dynamics and patchy pattern formation are observed in the spatially explicit model. The proposed carbon-phytoplankton-zooplankton system incorporates the effect of global warming, and our simulation shows shifts in plankton seasonal dynamics.

Finally, in the **Chapter 7**, we included conclusion with the overall concluding observations of this study along with a brief discussion on the scope for future research work.

Chapter 2

Rich dynamics of a predator - prey system with the impact of fear effect on growth of prey [†]

2.1 Introduction

Predator-prey interplay is a dominant theme in ecology studies that has been investigated by many scientists over the last few decades. Mathematical models have played a key role in better understanding these complex interactions. A large number of studies have been focused on the predator–prey interaction which is governed by direct killing of prey by the predators for their food. The intake rate of predators as a function of prey is known as functional response. C. S. Holling [74] has proposed different types of functional responses, namely, type-I, type-II and type-III, which are functions of prey density only. One of the widely studied functional responses is Holling type-II response function, which is characterized by the decelerating intake rate. The rate of predation rises as prey density increases, but after a certain time the rate of predation becomes saturated although prey density increases. Later it is recognized that the response function is also depends on predator density. In the year 1975, Beddington & DeAngelis [75, 76] introduced a response function, which is similar to Holling type-II response function but holds an additional term that represents the mutual interaction between the predators.

Apart from natural death of prey, traditionally, it has been considered in

---

ecological studies that the density of prey population reduces due to direct killing of prey by predators. At the same time, the mere presence of predators, prey population may significantly change their behavior in a state of psychological stress that influences the prey population more effectively than direct predation [7, 88]. Based on the field observations, some ecologist have understood that a predator-prey system should include not only the direct killing but also include the effect of fear [7].

In this chapter, we investigated a predator-prey system with different types of functional responses. Also, we introduce the effect of fear in the predator-prey system with Holling type-II functional response. The quantitative analysis carried out for the predator-prey system with and without fear effect that includes positivity, boundedness, uniform persistence, local stability, global stability and bifurcations. Extensive numerical simulations are carried out to validate our analytical findings. The aim of this chapter has two-folds:

(i) To study the effect of different type of functional responses in a predator-prey system.

(ii) To study the effect of fear in the growth of prey in a predator-prey system.

2.2 Model formulation

The interaction between prey and predator species are represented by the following system of a coupled differential equations [98, 99]:

$$\frac{dN}{dt} = Nf(N) - g(N, P)P,$$
$$\frac{dP}{dt} = P(-\delta_2 + \theta g(N, P)),$$

where $P(t)$ and $N(t)$ represents the predator and prey population, respectively, at any time t and $f(N)$ stands the birth rate of prey species in exclusion of any predator population as well as death rate and the intra-specific competition between the prey species. Here, δ_2 denotes the natural death rate for predator species and θ stands the conversion coefficient of prey's biomass to predator's biomass, and $g(N, P)$ indicates the prey-dependent response function.

Our proposed model consists of two population, namely, prey population and predator population. Concentration of prey and predator species at

time t can be represented by $N(t)$ and $P(t)$, respectively. Both the prey and predator population are continuous in time t. The predator-prey interaction with response function $g(N, P)$ can be expressed by the following system of coupled differential equations:

$$
\begin{aligned}
\frac{dN}{dt} &= r_0 N - \delta_1 N - \gamma N^2 - g(N, P)P, \\
\frac{dP}{dt} &= P(-\delta_2 + \theta g(N, P)),
\end{aligned}
\tag{2.1}
$$

with initial values

$$
N(0) = N_0 \geq 0 \text{ and } P(0) = P_0 \geq 0,
$$

all the model parameters r_0, δ_1, γ, δ_2, θ are positive constants and can be interpreted as follows: r_0 represents the birth rate of prey species in absence of predators, δ_1 represents the death rate for prey population, γ denotes the intra-specific competition of prey species, δ_2 represents the death rate for predator population and θ represents the conversion coefficient of prey's biomass to predator's biomass. The dimensions of all the parameters are presented in Table 2.1. In exclusion of predator species, the prey population obeys the logistic growth with an intrinsic growth rate $(r_0 - \delta_1) > 0$.

2.2.1 Functional response

In ecology, the functional responses are the intake rate of predator population as a function of prey population. C. S. Holling [74] proposed three types of response function, namely, Holling type-I, II and III. In our model formulation, we consider Holling type-II response function in the following form:

$$
g(N, P) = \frac{\beta N}{1 + \xi N},
$$

where β represents the attack rate and ξ is the handling time to capture the prey population; both β and ξ are positive constants. The dimensions of β and ξ are are presented in Table 2.1. Predation rate increases as the prey density increases, but after a certain stage, rate of predation becomes constant although prey density increases. The functional response depends on prey density but not on predator's density. By using the functional form of $g(N, P)$ the system (2.1), leads to

$$
\begin{aligned}
\frac{dN}{dt} &= r_0 N - \delta_1 N - \gamma N^2 - \frac{\beta N P}{1 + \xi N} \equiv F_1(N, P), \\
\frac{dP}{dt} &= \frac{\theta \beta N P}{1 + \xi N} - \delta_2 P \equiv F_2(N, P).
\end{aligned}
\tag{2.2}
$$

23

Table 2.1: *Description of the model parameters, variables and their units/dimensions.*

Symbols	Description	Units/Dimension
N	Density of prey population	No. per unit area
P	Density of predator population	No. per unit area
r_0	Birth rate of prey population	Time^{-1}
δ_1	Natural death rate of prey population	Time^{-1}
γ	Decay rate due to intra-species competition	[No. per unit area]$^{-1}$Time^{-1}
β	Rate of predation	[No. per unit area]$^{-1}$Time^{-1}
ξ	Handling time	[No. per unit area]$^{-1}$
θ	Conversion rate of prey biomass to predator biomass	Dimensionless
δ_2	Death rate of predator	Time^{-1}
η	Cost of minimum fear	Dimensionless
α	Level of fear	No. per unit area

2.3 Qualitative behavior of the model

2.3.1 Positivity, boundedness and uniform persistence

Right side of the system (2.2) is a continuous function of t. Hence, after integration on both sides of the system (2.2), we get

$$N(t) = N(0) \exp\left(\int_0^t \left[r_0 - \delta_1 - \gamma N(s) - \frac{\beta P(s)}{1 + \xi N(s)}\right] ds\right) > 0 \ \ \forall \ \ t \geq 0,$$

$$P(t) = P(0) \exp\left(\int_0^t \left[\frac{\theta \beta N(s)}{1 + \xi N(s)} - \delta_2\right] ds\right) > 0 \ \ \forall \ \ t \geq 0.$$

From the above expressions of $N(t)$ and $P(t)$, it is clear that both $N(t)$ and $P(t)$ remains non-negative for all finite time, that is, $t > 0$. Hence, $\Re_2^+ = \{[N(t), P(t)] : N(t) \geq 0, P(t) \geq 0\}$ is a positively invariant set of (2.2). To prove the boundedness of the prey-predator model (2.2), we consider the function

$$\phi(t) = N(t) + \frac{1}{\theta} P(t).$$

Differentiation with respect to t gives

$$\frac{d\phi(t)}{dt} = \frac{dN(t)}{dt} + \frac{1}{\theta}\frac{dP(t)}{dt},$$

$$= (r_0 - \delta_1)N(t) - \gamma N^2(t) - \frac{\delta_2}{\theta}P(t).$$

Now for each $\phi(t) > 0$, we get

$$\frac{\phi(t)}{dt} + \rho\phi(t) \leq r_0 N - \gamma N^2,$$

where $\rho = \min\left\{\delta_1, \frac{\delta_2}{\theta}\right\}$. The maximum value of $r_0 N - \gamma N^2$ is $\frac{r_0^2}{4\gamma}$. Therefore,

$$\frac{\phi(t)}{dt} + \rho\phi(t) \leq \frac{r_0^2}{4\gamma} = m \quad (\text{say}).$$

Due to the theory of differential inequality, we have

$$0 \leq \phi(t) \leq \frac{m}{\rho}\left(1 - e^{-\rho t}\right) + \phi(0)e^{-\rho t},$$

for $t \to \infty$, we have $0 \leq \phi(t) \leq \frac{m}{\rho}$. Therefore, $\phi(t)$ is bounded. Thus, all the solution of (2.2) are confined in

$$\Omega = \left\{(N, P) : 0 \leq N(t) + \frac{1}{\theta}P(t) \leq \frac{m}{\rho} + \epsilon \ \forall \ \epsilon \geq 0\right\}.$$

This implies that the solution of the system (2.2) is bounded. Thus, we have the following theorem.

Theorem 2.3.1. *For any initial value $(N_0, P_0) \in \Re_2^+$, all the solutions of (2.2) are non-negative and bounded.*

From the ecological perspective, the positivity of the prey-predator system (2.2) interprets that prey and the predators never be negative. The boundedness for the solutions of the prey-predator model (2.2) implies that neither the prey population nor the predator population will grow unboundedly or abruptly for a finite time.

Definition 2.3.1. *System (2.2) is said to be uniformly persistence if there exist two constants κ, τ where $0 \leq \kappa \leq \tau$ such that $\max\left\{\limsup\limits_{t\to\infty} N(t), \ \limsup\limits_{t\to\infty} P(t))\right\} \leq \tau$ and $\min\left\{\liminf\limits_{t\to\infty} N(t), \ \liminf\limits_{t\to\infty} P(t))\right\} \geq \kappa$, where κ and τ are independent of the initial conditions.*

Theorem 2.3.2. *System (2.2) is uniformly persistent if $r_0 > \delta_1 + \beta\bar{P}$, where $\bar{P}$ is the upper bound of $P(t)$.*

Proof. From the proof of Theorem 2.3.1, we have $\limsup_{t\to\infty} N(t) \leq m/\rho$ and $\limsup_{t\to\infty} P(t) \leq m\theta/\rho$. We choose $\tau = \max\{m/\rho, m\theta/\rho\}$. Hence, there exists $\tau > 0$ such that $\max\left\{\limsup_{t\to\infty} N(t), \ \limsup_{t\to\infty} P(t))\right\} \leq \tau$. Now, from the first equation of (2.2), we have

$$\frac{dN}{dt} = r_0 N - \delta_1 N - \gamma N^2 - \frac{\beta N P}{1 + \xi N}$$
$$\geq r_0 N - \delta_1 N - \gamma N^2 - \beta N \bar{P},$$
$$= (r_0 - \delta_1 - \beta\bar{P})N - \gamma N^2,$$

where $\bar{P}$ is upper limit of P in Ω.

Thus, we can conclude that $\liminf_{t\to\infty} N(t) \geq (r_0 - \delta_1 - \beta\bar{P})/\gamma$ with $r_0 > \delta_1 + \beta\bar{P}$. Again, from the second equation of (2.2), we have

$$\frac{dP}{dt} = \frac{\beta\theta N P}{1 + \xi N} - \delta_2 P \geq -\delta_2 P.$$

Hence, we have $\liminf_{t\to\infty} P(t) \geq 0$. Thus, if we choose $\kappa = \min\left\{0, (r_0 - \delta_1 - \beta\bar{P})/\gamma\right\} = 0$ with $r_0 > \delta_1 + \beta\bar{P}$, then $\min\left\{\liminf_{t\to\infty} N(t), \ \liminf_{t\to\infty} P(t))\right\} \geq \kappa$. Therefore, the system (2.2) will be uniformly persistent if $r_0 > \delta_1 + \beta\bar{P}$. $\square$

2.3.2 Equilibria and their existence

The singular points for the model (2.2) are non-negative solutions of $F_1(N, P) = 0$ and $F_2(N, P) = 0$ in $\Re^2_+$; that is, the equilibrium points of (2.2) are the intersection of zero growth of prey and predator isoclines. The prey isoclines are given by $N = 0$, and $P = (r_0 - \delta_1 - \gamma N)(1 + \xi N)/\beta$ with predator isoclines are stated as $P = 0$ and the vertical straight line $N = \delta_2/(\beta\theta - \xi\delta_2)$. The proposed system (2.2) possesses three biologically meaningful singular points, namely,

(i) Trivial steady state $\hat{E}_0(0,0)$.

(ii) Boundary singular point $\hat{E}_1(\bar{N}_e, 0)$, where $\bar{N}_e = \frac{r_0 - \delta_1}{\gamma}$, which is feasible only when $r_0 > \delta_1$; that is, growth of prey population is higher than the death rate for prey population.

(iii) The positive interior equilibrium point $\hat{E}^*(N_e^*, P_e^*)$, where $N_e^* = \frac{\delta_2}{\beta\theta - \xi\delta_2}$ and $P_e^* = (r_0 - \delta_1 - \gamma N_e^*)(\frac{1}{\beta} + \frac{\xi}{\beta}N_e^*)$.

The shape and position of the curve $P = (r_0 - \delta_1 - \gamma N)(1 + \xi N)/\beta$ depends upon multiple parameters. For different values of ξ, the zero growth prey isoclines are convex curve joining the boundary equilibrium $\hat{E}_1(\bar{N}_e, 0)$ and $(0, (r_0 - \delta_1)/\beta)$ (see Fig. 2.1(a)). As ξ increases, the predator isocline shifted towards N increasing. For different values of β, zero growth prey isocline become a convex curve, which meets at boundary equilibrium $\hat{E}_1(\bar{N}_e, 0)$ (see Fig. 2.1(b)). As β increases, the vertical predator isocline shifted towards N decreasing and the prey isocline shifted towards P decreasing. Also for different values of r_0, the zero growth prey isoclines are convex curve, but the zero growth predator isoclines do not change their position. As r_0 increases, the zero growth prey isocline shifted towards P increasing. In all this situations, the interior equilibrium point $\hat{E}^*(N_e^*, P_e^*)$ exists only if $\beta\theta - \xi\delta_2 > 0$ (see Fig. 2.1(c)).
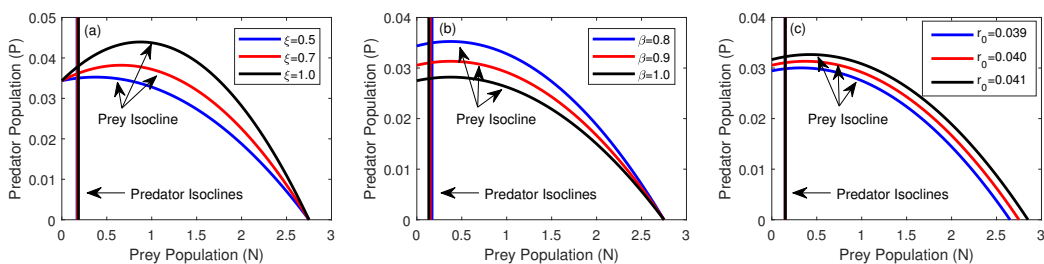
Figure 2.1: Isoclines of the predator-prey system (2.2) for three different cases with the following set of parameters: $r_0 = 0.04, \delta_1 = 0.0125, \gamma = 0.01, \beta = 0.8, \xi = 0.5, \theta = 0.4$, and $\delta_2 = 0.05$. (a) for different ξ, (b) for different β, and (c) for different values of r_0 as shown in the inset.

2.3.3 Local stability analysis

In this section, we analyzed the linear stability for the predator-prey system (2.2). Using linearization techniques, the local behavior of the nonlinear predator-prey system can be investigated. Generally, the predator-prey system is linearized around the biologically feasible singular points, and the model is perturb by a small quantity and observed whether the model returns to its original state of singular point or converges to another state of singular point. Analysis of local stability leads to investigate qualitative dynamics for the model system under consideration. For local stability analysis of the considered model (2.2) around every singular point, first calculate the

Jacobian matrix obtained from each of the equilibrium point. The variational matrix of the model (2.2) at (N, P) is

$$J = \begin{bmatrix} \hat{F}_N & \hat{F}_P \\ \hat{G}_N & \hat{G}_P \end{bmatrix}, \tag{2.3}$$

where

$$\hat{F}_N = r_0 - \delta_1 - 2\gamma N - \frac{\beta P}{(1 + \xi N)^2}, \quad \hat{F}_P = -\frac{\beta N}{1 + \xi N},$$

$$\hat{G}_N = \frac{\beta \theta P}{(1 + \xi N)^2}, \quad \hat{G}_P = \frac{\beta \theta N}{1 + \xi N} - \delta_2.$$

Theorem 2.3.3. *If $r_0 < \delta_1$, then the trivial singular point $\hat{E}_0(0, 0)$ of (2.2) becomes locally asymptotically stable and otherwise unstable.*

Proof. The eigenvalues of the Jacobian matrix (2.3) of (2.2) at the trivial equilibrium point $\hat{E}_0(0, 0)$ are $r_0 - \delta_1$ and $-\delta_2$. Here, $\delta_2 > 0$; therefore, the trivial equilibrium point $\hat{E}_0(0, 0)$ of the model (2.2) will be locally asymptotically stable if $r_0 < \delta_1$; that is, the growth rate of prey species is less than the natural death rate of prey species. It can be noted that if the trivial equilibrium point $\hat{E}_0(0, 0)$ becomes asymptotically stable, then the boundary singular point $\hat{E}_1(\bar{N}_e, 0)$ does not exit. For $r_0 = \delta_1$, the trivial equilibrium point $\hat{E}_0(0, 0)$ has eigenvalues 0 and $-\delta_2$. So $\hat{E}_0(0, 0)$ is a non-hyperbolic equilibrium point [100]. □

Theorem 2.3.4. *If $\delta_1 < r_0 < \delta_1 + \frac{\gamma \delta_2}{\beta \theta - \xi \delta_2}$, then the boundary equilibrium point $\hat{E}_1(\bar{N}_e, 0)$ of the model (2.2) becomes locally asymptotically stable and otherwise unstable.*

Proof. The eigenvalues of the Jacobian matrix (2.3) of (2.2) at the equilibrium point $\hat{E}_1(\bar{N}_e, 0)$ are $\lambda_1 = -(r_0 - \delta_1)$ and $\lambda_2 = \frac{\beta \theta (r_0 - \delta_1)}{\gamma + \xi (r_0 - \delta_1)} - \delta_2$. The boundary equilibrium point $\hat{E}_1(\bar{N}_e, 0)$ will be locally asymptotically stable if $\lambda_1 < 0$ and $\lambda_2 < 0$, and this condition implies $\delta_1 < r_0 < \delta_1 + \frac{\gamma \delta_2}{\beta \theta - \xi \delta_2}$. Biologically, $r_0 > \delta_1$ implies that the rate of growth of prey population is higher than the natural rate of death of the prey. Also, $r_0 < \delta_1 + \frac{\gamma \delta_2}{\beta \theta - \xi \delta_2}$ implies that the prey growth rate cannot be unbounded. It is to be noted that if the boundary equilibrium state $\hat{E}_1(\bar{N}_e, 0)$ becomes locally asymptotically stable, then the trivial equilibrium state $\hat{E}_0(0, 0)$ is unstable. □

Theorem 2.3.5. *If $r_0 - \delta_1 - 2\gamma N_e^* - \frac{\beta P_e^*}{(1 + \xi N_e^*)^2} < 0$, then the positive interior singular point $\hat{E}^*(N_e^*, P_e^*)$ of (2.2) will be asymptotically stable and otherwise unstable.*

28

Proof. The variational matrix around the co-existing singular point $\hat{E}^*(N_e^*, P_e^*)$ for the system (2.2) is given by

$$J^* = \begin{bmatrix} r_0 - \delta_1 - 2\gamma N_e^* - \frac{\beta P_e^*}{(1+\xi N_e^*)^2} & -\frac{\beta N_e^*}{1+\xi N_e^*} \\ \frac{\beta \theta P_e^*}{(1+\xi P_e^*)^2} & 0 \end{bmatrix}. \tag{2.4}$$

The characteristic equation of the above matrix J^* can be expressed as

$$\lambda^2 - \left[r_0 - \delta_1 - 2\gamma N_e^* - \frac{\beta P_e^*}{(1+\xi N*_e)^2} \right] \lambda + \frac{\beta \delta_2 P_e^*}{(1+\xi N_e^*)^2} = 0,$$

$$\text{or,} \quad \lambda^2 - K_{11}\lambda + K_{22} = 0, \tag{2.5}$$

where $K_{11} = r_0 - \delta_1 - 2\gamma N_e^* - \frac{\beta P_e^*}{(1+\xi N*_e)^2}$ and $K_{22} = \frac{\beta \delta_2 P_e^*}{(1+\xi N_e^*)^2}$.

Due to well-known Routh-Hurwitz criterion, the characteristic equation (2.5) will have negative real roots if $K_{11} < 0$ and $K_{22} > 0$. Hence, $r_0 - \delta_1 - 2\gamma N_e^* - \frac{\beta P_e^*}{(1+\xi N*_e)^2} < 0$ and $\frac{\beta \delta_2 P_e^*}{(1+\xi N_e^*)^2} > 0 \implies P_e^* > 0$ since $\beta, \delta_2, (1+\xi N_e^*)^2 > 0$. It is obvious that $P_e^* > 0$ because $\hat{E}^*(N_e^*, P_e^*)$ will be positive interior singular point of (2.2). Therefore, the positive interior steady state $\hat{E}^*(N_e^*, P_e^*)$ of (2.2) will be asymptotically stable if $r_0 - \delta_1 - 2\gamma N_e^* - \frac{\beta P_e^*}{(1+\xi N_e^*)^2} < 0$ and otherwise unstable. $\qquad \square$

Fig. 2.2 shows the stability region of different singular points of (2.2) in $r_0 - \xi$ parameter-space. The growth rate of prey species r_0 varies from 0 to 0.1, and the half saturation constant ξ varies from 0 to 1; other parameters are fixed as $\delta_1 = 0.0125$, $\gamma = 0.01$, $\beta = 0.8$, $\theta = 0.4$ and $\delta_2 = 0.05$. For a very small value of r_0, that is, when $r_0 < \delta_1$, the trivial equilibrium $\hat{E}_0$ is locally asymptotically stable. The stability region of $\hat{E}_0$ is shown by blue-shaded region in the $r_0 - \xi$ plane. In this blue-shaded region, the boundary equilibrium $\hat{E}_1$ and the interior equilibrium $\hat{E}^*$ are unstable. The boundary equilibrium $\hat{E}_1$ is locally asymptotically stable in the green-shaded region. But the trivial equilibrium $\hat{E}_0$ and the interior equilibrium $\hat{E}^*$ are unstable in this green-shaded region. The red-shaded region of the Fig. 2.2 shows locally asymptotically stable behavior of the interior equilibrium $\hat{E}^*$; that is, both the prey and predator population can exists together in the red-shaded region. For higher value of r_0 (such as $r_0 > 0.06$) and for higher value of ξ (such as $\xi > 0.5$), the co-existing equilibrium $\hat{E}^*$ loses its stability. The trivial equilibrium $\hat{E}_0$ and the boundary equilibrium $\hat{E}_1$ are unstable in the red-shaded region. All the equilibrium loses their stability in the white-shaded region.
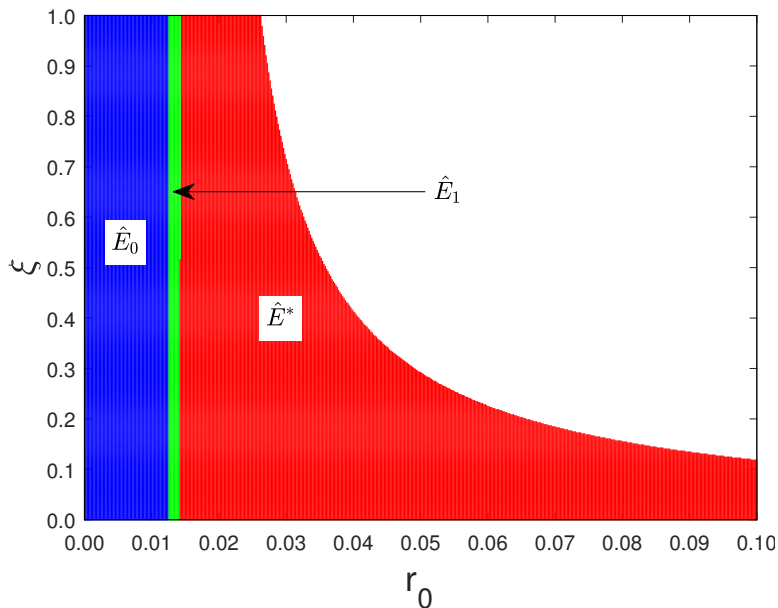
Figure 2.2: The stability region of the trivial singular state $\hat{E}_0$, boundary singular state $\hat{E}_1$ and the co-existing singular state $\hat{E}^*$ of (2.2), in the $(r_0 - \xi)$ parameter-space where $r_0 \in (0, 0.1)$ and $\xi \in (0, 1.0)$. Other parameter values are $\delta_1 = 0.0125$, $\gamma = 0.01$, $\beta = 0.8$, $\theta = 0.4$ and $\delta_2 = 0.05$. In the figure, (i) within the blue colored region, the equilibrium point $\hat{E}_0$ is locally asymptotically stable, but boundary singular point $\hat{E}_1$ and the interior equilibrium $\hat{E}^*$ are unstable; (ii) within the green colored region, the equilibrium point $\hat{E}_1$ is locally asymptotically stable, but trivial equilibrium $\hat{E}_0$ and interior equilibrium $\hat{E}^*$ are unstable and (iii) within the red colored region, the interior equilibrium point $\hat{E}^*$ is locally asymptotically stable, but the trivial equilibrium $\hat{E}_0$ and boundary equilibrium $\hat{E}_1$ are unstable.

2.3.4 Comparative study with different types of response function

Mainly, three types of response functions (Holling type-I, II, III) and Beddington-DeAngelis are widely investigated by the researchers in the predator-prey system [101–103]. Here, we also investigate the role of different kind of functional responses on the dynamics for the predator-prey system (2.1). To exemplify this matter, we performed a relative study for (2.1) with reference to three kinds of response functions, namely Beddington-DeAngelis, Holling type-I, and Holling type-II (already used in the model (2.2)). Holling type response functions are the function of prey population only; that is, the response functions are independent of predator population.

But, in nature, response functions are also the function of predator population. Widely studied Beddington-DeAngelis [75, 76] type response function considered the density of predators also. In our study, we have also study the stability of the system by considering Beddington-DeAngelis functional responses and two types of response function. The Beddington-DeAngelis response function is of the form:

$$g(N, P) = \frac{\beta N}{1 + \xi N + \varphi P},$$

where the parameters β, ξ and φ are non-negative and have their usual biological meanings. The Beddington-DeAngelis response function is a similar kind of Holling type-II response function but contains an additional term φP at the denominator. The term φP indicates the mutual interaction between the predator population. Thus, when the prey density $N(t)$ is constant and predator density $P(t)$ is minimum, then the value of the response function $g(N, P)$ is maximum; when predator density $P(t)$ is maximum, then the value of the response function $g(N, P)$ is minimum. This is more realistic because the number of predator species are less than their prey, consumption due to predators per unit time will be more, but when predator density is more, then the prey consumption due to predators per unit time will be less due to mutual interaction of predator population. But, when $\varphi = 0$, then the Beddington-DeAngelis functional response is same as Holling type-II functional response. Again, for $\xi = 0$ and $\varphi = 0$, then Beddingon-DeAngelis response function is same as Holling type-I response function. Hence, we may conclude that Bedington-DeAngelis response function is more generalized form of Holling type-II & type-I functional responses. By considering Bedington-DeAngelis response function, the system (2.1) becomes

$$\begin{aligned}
\frac{dN}{dt} &= r_0 N - \delta_1 N - \gamma N^2 - \frac{\beta NP}{1 + \xi N + \varphi P}, \\
\frac{dP}{dt} &= \frac{\theta \beta NP}{1 + \xi N + \varphi P} - \delta_2 P.
\end{aligned} \tag{2.6}$$

The predator-prey system (2.6) with Bedington-DeAngelis functional response has three ecologically relevant singular points, namely, trivial singular point $E_{BD}^0(0, 0)$, boundary singular point $E_{BD}^1(\hat{N}, 0)$ and an interior steady state $E_{BD}^*(\hat{N}^*, \hat{P}^*)$. Here, $\hat{N} = \frac{r_0 - \delta_1}{\gamma}$ and $\hat{N}^*$ is the positive root for the following second degree equation:

$$\theta \gamma \varphi \hat{N}^{*2} - [(r_0 - \delta_1)\theta\varphi - (\beta\theta - \xi\delta_2)] \hat{N}^* - \delta_2 = 0,$$

31

$$\hat{P}^* = \frac{1}{\varphi\delta_2}\left[(\theta\beta - \xi\delta_2)\hat{N}^* - \delta_2\right].$$

We have made a relative investigation of the predator-prey model (2.1), by considering three different functional responses, which are Type-I (model (2.6) with $\xi = 0, \varphi = 0$), Holling Type-II (already used in model (2.2) with $\varphi = 0$) and Beddington-DeAngelis. We are not showing detailed analysis of the model (2.1) for the different functional responses; rather, we have presented the stability scenarios for these three types of response function in the Table 2.2. The parameters r_0, θ and γ are varied to observe the stability behavior of the system. The detailed numerical study and graphical illustrations have shown in the numerical Section 2.7.

Table 2.2: *Stability conditions for different equilibrium points of the system (2.6). M_1, M_2, M_3 and M_4 are the components of the variational matrix around interior singular point $E_{BD}^*(\hat{N}^*, \hat{P}^*)$ where $M_1 = -\gamma\hat{N}^* - \frac{\beta\xi\hat{N}^*\hat{P}^*}{(1+\xi\hat{N}^*+\varphi\hat{P}^*)^2}$, $M_2 = -\frac{\beta\hat{N}^*(1-\varphi\hat{P}^*)}{(1+\xi\hat{N}^*+\varphi\hat{P}^*)^2}$, $M_3 = \frac{\beta\theta\hat{P}^*(1-\xi\hat{N}^*)}{(1+\xi\hat{N}^*+\varphi\hat{P}^*)^2}$ and $M_4 = \frac{\beta\theta\hat{N}^*(1-\varphi\hat{P}^*)}{(1+\xi\hat{N}^*+\varphi\hat{P}^*)^2} - \delta_2$.*

Equilibria	Holling Type-I $(\xi = 0, \varphi = 0)$	Holling Type-II $(\varphi = 0)$	Beddington-DeAngelis
$E_{BD}^0(0,0)$	$r_0 < \delta_1$	$r_0 < \delta_1$	$r_0 < \delta_1$
$E_{BD}^1(\hat{N}, 0)$	$r_0 > \delta_1$ and $\beta\theta(r_0 - \delta_1) < \delta_2$	$r_0 > \delta_1$ and $\frac{\beta\theta\gamma(r_0-\delta_1)}{\{\gamma+\xi(r_0-\delta_1)\}^2} < \delta_2$	$r_0 > \delta_1$ and $\frac{\beta\theta\gamma(r_0-\delta_1)}{\{\gamma+\xi(r_0-\delta_1)\}^2} < \delta_2$
$E_{BD}^*(\hat{N}^*, \hat{P}^*)$	$M_1 + M_4 < 0$ and $M_1M_4 - M_2M_3 > 0$ with $\xi = 0, \varphi = 0$	$M_1 + M_4 < 0$ and $M_1M_4 - M_2M_3 > 0$ with $\varphi = 0$	$M_1 + M_4 < 0$ and $M_1M_4 - M_2M_3 > 0$

2.3.5 Global stability analysis around $\hat{E}^*(N_e^*, P_e^*)$

In this subsection, we investigate the sufficient condition for global asymptotic stability of the positive co-existing singular point $\hat{E}^*(N_e^*, P_e^*)$ by establishing appropriate Lyapunov function.

Theorem 2.3.6. *The positive interior steady state $\hat{E}^*(N_e^*, P_e^*)$ of the system (2.2) is globally asymptotically stable if $\frac{\gamma}{\beta\xi} > P_e^*$.*

Proof. The interior steady state $\hat{E}^*(N_e^*, P_e^*)$ of the prey-predator model (2.2) fulfills the following conditions:

$$r_0 - \delta_1 = \gamma N_e^* + \frac{\beta P_e^*}{1 + \xi N_e^*},$$

$$\delta_2 = \frac{\beta \theta N_e^*}{1 + \xi N_e^*}.$$

With the help of the above two equations, the model (2.2) leads to

$$\frac{dN}{dt} = N \left(-\gamma(N - N_e^*) + \frac{\beta P_e^*}{1 + \xi N_e^*} - \frac{\beta P}{1 + \xi N} \right),$$

$$\frac{dP}{dt} = P \left(\frac{\beta \theta N}{1 + \xi N} - \frac{\beta \theta N_e^*}{1 + \xi N_e^*} \right).$$

We define the Lyapunov functional $V(N, P) : \Re_2^+ \to \Re$ such that

$$V(N, P) = V_1(N, P) + V_2(N, P), \tag{2.7}$$

where $V_1(N, P) = N - N_e^* - N_e^* \ln(\frac{N}{N_e^*})$ and $V_2(N, P) = K(P - P_e^* - P_e^* \ln(\frac{P}{P_e^*}))$. Here, K is a positive constant and is defined as $K = \frac{1}{\theta}(1 + \xi N_e^*)$. This particular type of Lyapunov function is widely used to study the stability of the interior equilibrium [102, 104–106]. The Lyapunov function $V(N, P)$ is continuous on $Int(\Re_2^+)$ and vanishes at $\hat{E}^*(N_e^*, P_e^*)$. Also, $V(N, P)$ is positive definite in $Int(\Re_2^+)$. Furthermore, $\frac{\partial V_1}{\partial N} > 0$ when $N > N_e^*$, $\frac{\partial V_1}{\partial N} < 0$ when $N < N_e^*$, $\frac{\partial V_2}{\partial P} > 0$ when $P > P_e^*$, and $\frac{\partial V_2}{\partial P} < 0$ when $P < P_e^*$. Hence, $\hat{E}^*(N_e^*, P_e^*)$ has a global minimum of $V(N, P)$. The time derivative of $V_1(N, P)$ and $V_2(N, P)$ along the solution for (2.2) is

$$\frac{dV_1}{dt} = \frac{N - N_e^*}{N} \frac{dN}{dt} = (N - N_e^*) \left[-\gamma(N - N_e^*) + \frac{\beta P_e^*}{1 + \xi N_e^*} - \frac{\beta P}{1 + \xi N} \right],$$

$$\frac{dV_2}{dt} = K \frac{P - P_e^*}{P} \frac{dP}{dt} = K\beta\theta(P - P_e^*) \left[\frac{N}{1 + \xi N} - \frac{N_e^*}{1 + \xi N_e^*} \right].$$

Now, differentiating (2.7) with respect to t and using the values of $\frac{dV_1}{dt}$ and $\frac{dV_2}{dt}$, we obtain

$$\frac{dV}{dt} = \frac{dV_1}{dt} + \frac{dV_2}{dt}$$

$$= -\gamma(N - N_e^*)^2 - \frac{\beta(N - N_e^*)\{(P - P_e^*) + \xi(N_e^* P - N P_e^*)\}}{(1 + \xi N)(1 + \xi N_e^*)}$$

$$+ \frac{K\beta\theta(N - N_e^*)(P - P_e^*)}{(1 + \xi N)(1 + \xi N_e^*)}.$$

33

Using the relation $N_e^* P - N P_e^* = N_e^*(P - P_e^*) - P^*(N - N_e^*)$, we obtain

$$\frac{dV}{dt} = -\gamma(N - N_e^*)^2 + \frac{\beta\xi P_e^*(N - N_e^*)^2}{(1 + \xi N)(1 + \xi N_e^*)}$$
$$- \frac{\beta(1 + \xi N_e^* - K\theta)}{(1 + \xi N)(1 + \xi N_e^*)}(N - N_e^*)(P - P_e^*).$$

Putting the value of K, we obtain

$$\frac{dV}{dt} = -\gamma(N - N_e^*)^2 + \frac{\beta\xi P_e^*(N - N_e^*)^2}{(1 + \xi N)(1 + \xi N_e^*)},$$
$$\leq -(\gamma - \beta\xi P_e^*)(N - N_e^*)^2.$$

Hence, $\frac{dV}{dt} < 0$ along the trajectories in $\Re_2^+$ excluding at $\hat{E}^*(N_e^*, P_e^*)$ if $\gamma - \beta\xi P_e^* > 0$, that is, if $\frac{\gamma}{\beta\xi} > P_e^*$. Thus, if $\frac{\gamma}{\beta\xi} > P_e^*$, then the co-existing singular point $\hat{E}^*(N_e^*, P_e^*)$ is globally asymptotically stable. $\square$

2.3.6   Hopf bifurcation analysis

In our study, the growth rate r_0 of prey population is one of the most important parameters. In this section, we investigate how predator-prey model alters their behavior when r_0 crosses the threshold value through Hopf bifurcation. We start with a theorem to study the analysis of Hopf bifurcation.

Theorem 2.3.7. *When the prey birth rate r_0 crosses a threshold value $r_0 = r_0^* = (\delta_1 + 2\gamma N_e^*)(1 + \frac{1}{\xi N_e^*}) - \frac{1}{\xi N_e^*}(\delta_1 + \gamma N_e^*)$, the predator-prey model (2.2) experiences Hopf bifurcation around the interior singular point E_e^*. Necessary and sufficient conditions of Hopf bifurcation to occur is that there exist $r_0 = r_0^*$ such that the transversality condition holds:*

$$\frac{d}{dr_0}(Re(\lambda(r_0))) \mid_{r_0 = r_0^*} = \frac{\xi N_e^*}{1 + \xi N_e^*} \neq 0.$$

Proof. A necessary condition for change in dynamics of the co-existing singular point $\hat{E}^*(N_e^*, P_e^*)$ of the prey-predator model (2.2) is that the characteristic polynomial (2.5) should have purely complex eigenvalues. The characteristic roots of the equation (2.5) will have purely complex roots if and only if $K_{11} = 0$ and $K_{22} > 0$. For $K_{11} = 0$, gives $r_0 = r_0^* = (\delta_1 + 2\gamma N_e^*)(1 + \frac{1}{\xi N_e^*}) - \frac{1}{\xi N_e^*}(\delta_1 + \gamma N_e^*)$, where $N_e^* = \frac{\delta_2}{\beta\theta - \xi\delta_2}$. Due to the Theorem 2.3.5, we can conclude that the positive co-existing singular point $\hat{E}^*(N_e^*, P_e^*)$ of the predator-prey model (2.2) will be stable

34

asymptotically if $r_0 - \delta_1 - 2\gamma N_e^* - \frac{\beta P_e^*}{(1+\xi N_e^*)^2} < 0$ and the model (2.2) experiences Hopf bifurcation at $r_0 = r_0^*$.

Let, the roots of the characteristic equation (2.5) are of the form $\lambda_{1,2} = \phi(r_0) \pm i\psi(r_0)$. Then $\lambda_1 + \lambda_2 = 2\phi(r_0) = K_{11}$; that is, $Re(\lambda(r_0)) = \phi(r_0) = \frac{1}{2}K_{11}$. To prove the transversality condition, we need to verify the following condition:

$$\frac{d}{dr_0}(Re(\lambda(r_0))) \mid_{r_0=r_0^*} = \frac{\xi N_e^*}{1 + \xi N_e^*} \neq 0 \ \text{ if } \ \xi \neq 0.$$

Hence, the transversality condition hold and the system (2.2) experiences Hopf bifurcation at $r_0 = r_0^*$. □

2.4 Direction and stability of Hopf bifurcation

To study the stability of bifurcating limit cycle appearing through Hopf bifurcation, we use the theorem of center manifold. Center manifold theorem is an essential tool to reduce the dimension of a differential equation system in a neighborhood of a coexisting steady state (see the book by Guckenheimer & Holmes, 1983, [107]). For the predator-prey system (2.2), we obtain the variational matrix J^* has a pair of complex conjugate eigenvalues for Hopf bifurcation [36].

To investigate the center manifold theory, first interpret the origin for the coordinate system to an interior singular point $\hat{E}^*(N_e^*, P_e^*)$ by expressing $\hat{N} = N - N_e^*$ and $\hat{P} = P - P_e^*$. For simplicity $\hat{N}$ and $\hat{P}$ denoted by N and P, respectively and the system (2.2) leads to

$$\begin{aligned}
\frac{dN}{dt} &= (r_0 - \delta_1)(N + N_e^*) - \gamma(N + N_e^*)^2 - \frac{\beta(N + N_e^*)(P + P_e^*)}{1 + \xi(N + N_e^*)}, \\
\frac{dP}{dt} &= \frac{\beta\theta(N + N_e^*)(P + P_e^*)}{1 + \xi(N + N_e^*)} - \delta_2(P + P_e^*).
\end{aligned} \tag{2.8}$$

The system of equations (2.8) can be rewritten as

$$\begin{bmatrix} N_t \\ P_t \end{bmatrix} = J^*(r_0) \begin{bmatrix} N \\ P \end{bmatrix} + \begin{bmatrix} f_1(N, P, r_0) \\ f_2(N, P, r_0) \end{bmatrix}, \tag{2.9}$$

where $J^*(r_0)$ is defined in (2.4), and

$$\begin{aligned}
f_1(N, P, r_0) &= a_1 N^2 + a_2 NP + a_3 P^2 + ..., \\
f_2(N, P, r_0) &= -(a_1 + \gamma)\theta N^2 - a_2\theta NP + a_3 P^2 + ...,
\end{aligned}$$

where $a_1 = -\gamma + \frac{\beta\xi P_e^*}{(1+\xi N_e^*)^3}$, $a_2 = -\frac{\beta}{(1+\xi N_e^*)^2}$, and $a_3 = 0$.

Let, the characteristic roots of the Jacobian matrix $J^*(r_0)$ are of the form $\lambda_{1,2} = \phi(r_0) \pm i\psi(r_0)$, where $\phi(r_0) = \frac{1}{2}tr(J^*)$ and $\psi(r_0) = \sqrt{\det(J^*) - \phi^2(r_0)}$. Here, the characteristics roots $\lambda_{1,2}$ are complex conjugate if $\det(J^*) - \phi^2(r_0) > 0$ and the characteristic roots $\lambda_{1,2}$ are purely imaginary; that is, $\lambda_{1,2} = \pm i\psi(r_0)$ when $\phi(r_0) = 0$; that is, when $r_0 = r_0^*$. Now, set the following matrix to get the normal form of the predator-prey system (2.2):

$$D = \begin{bmatrix} 1 & 0 \\ R & Q \end{bmatrix},$$

where $\begin{bmatrix} 1 \\ R - iQ \end{bmatrix}$ is the eigenvector corresponding to $\lambda = \phi(r_0) + i\psi(r_0)$ with $R = \frac{1 + \xi N_e^*}{\beta N_e^*}\left[\frac{\beta\xi N_e^* P_e^*}{(1 + \xi N_e^*)^2} - \gamma N_e^* - \phi\right]$ and $Q = \frac{(1 + \xi N_e^*)\psi}{\beta N_e^*}$. Then, we have

$$D^{-1} = \begin{bmatrix} 1 & 0 \\ -\frac{Q}{R} & \frac{1}{Q} \end{bmatrix}.$$

By using the transformation

$$\begin{bmatrix} N \\ P \end{bmatrix} = D \begin{bmatrix} x \\ y \end{bmatrix},$$

the system (2.8) becomes

$$\begin{bmatrix} x_t \\ y_t \end{bmatrix} = L_0(r_0) \begin{bmatrix} x \\ y \end{bmatrix} + \begin{bmatrix} G(x, y, r_0) \\ H(x, y, r_0) \end{bmatrix}, \tag{2.10}$$

where

$$L_0(r_0) = \begin{bmatrix} \phi & -\psi \\ \psi & \phi \end{bmatrix},$$

with

$$G(x, y, r_0) = \frac{\phi - \xi\gamma N_e^{*2}}{(1 + \xi N_e^*)N_e^*}x^2 - \frac{\phi}{(1 + \xi N_e^*)N_e^*}xy + 0 \times y^2 - \frac{\xi(\gamma N_e^* + \phi)}{(1 + \xi N_e^*)^2 N_e^*}x^3$$

$$+ \frac{\xi\phi}{(1 + \xi N_e^*)^2 N_e^*}x^2 y + 0 \times xy^2 + 0 \times y^3 + ...,$$

$$H(x, y, r_0) = -\frac{R}{Q}G(x, y, r_0) + \frac{1}{Q}g_2(x, y, r_0),$$

36

$$g_2(x, y, r_0) = \beta\theta \left[\frac{R}{(1+\xi N_e^*)^2} - \frac{\xi P_e^*}{(1+\xi N_e^*)^3} \right] x^2 + 0 \times y^2 + \frac{\beta\theta Q}{(1+\xi N_e^*)^2} xy$$
$$- \beta\xi\theta \left[\frac{R}{(1+\xi N_e^*)^3} - \frac{\xi P_e^*}{(1+\xi N_e^*)^4} \right] x^3$$
$$- \frac{\beta\xi\theta Q}{(1+\xi N_e^*)^3} x^2 y + 0 \times xy^2 + 0 \times y^3 + ...$$

Now, rewriting the expression (2.10) in polar coordinate (r, ζ) and then expand in Taylor series around $r_0 = r_0^*$, we obtain

$$r_t = \phi(r_0)r + a(r_0)r^3 + ... = \phi'(r_0^*)(r_0 - r_0^*)r + a(r_0^*)r^3 + ...,$$
$$\zeta_t = \psi(r_0) + c(r_0)r^2 + ... = \psi(r_0^*) + \psi'(r_0)(r_0 - r_0^*) + c(r_0^*)r^2 + ... \quad (2.11)$$

To investigate the stability of Hopf bifurcating periodic solution, we must have to compute the sign of the coefficient of $a(r_0)$, where $a(r_0)$ is given by

$$a(r_0^*) = \frac{1}{16} \left[G_{xxx} + G_{xyy} + H_{xxy} + H_{yyy} \right] |_{(0,0,r_0^*)}$$
$$+ \frac{1}{16\psi(r_0^*)} \Big[G_{xy}(G_{xx} + G_{yy}) - H_{xy}(H_{xx} + H_{yy})$$
$$- G_{xx}H_{xx} + G_{yy}H_{yy} \Big] |_{(0,0,r_0^*)}.$$

The above expression of $a(r_0^*)$ is obtained by well-known Hopf bifurcation formula to transform (2.10) into Jordan form [107]. Here, the subscript denotes partial derivative, we have

$$G_{xxx}(0, 0, r_0^*) = -\frac{3\xi(\gamma N_e^* + \phi)}{(1+\xi N_e^*)^2},$$

$$G_{xyy}(0, 0, r_0^*) = H_{yyy}(0, 0, r_0^*) = G_{yy}(0, 0, r_0^*) = H_{yy}(0, 0, r_0^*) = 0,$$

$$H_{xxy}(0, 0, r_0^*) = -\frac{2R\xi\phi}{QN_e^*(1+\xi N_e^*)^2} - \frac{2\beta\xi\theta}{(1+\xi N_e^*)^3},$$

$$G_{xy}(0, 0, r_0^*) = -\frac{\phi}{(1+\xi N_e^*)N_e^*}, \quad G_{xx}(0, 0, r_0^*) = \frac{2(\phi - \xi\gamma N_e^{*2})}{(1+\xi N_e^*)N_e^*},$$

$$H_{xy}(0, 0, r_0^*) = \frac{R\phi}{Q(1+\xi N_e^*)N_e^*} + \frac{\beta\theta}{(1+\xi N_e^*)^2}$$

$$H_{xx}(0, 0, r_0^*) = -\frac{2R(\phi - \xi\gamma N_e^{*2})}{QN_e^*(1+\xi N_e^*)} + \frac{2\beta\theta}{Q} \left[\frac{R}{(1+\xi N_e^*)^2} - \frac{\xi P_e^*}{(1+\xi N_e^*)^3} \right].$$

Here, $\phi(r_0) = \frac{1}{2}tr(J^*) = \frac{1}{2} \left[\frac{\beta\xi N_e^* P_e^*}{(1+\xi N_e^*)^2} - \gamma N_e^* \right]$ and $\frac{d\phi}{dr_0} = \frac{\xi N_e^*}{2(1+\xi N_e^*)} > 0$.

We obtain that $\Lambda = -\frac{a(r_0)}{\phi'(r_0)}$.

From the above computation of $a(r_0{}^*)$, the theorem can be stated as follows.

Theorem 2.4.1. *(i) The direction of Hopf bifurcation is supercritical, and bifurcating periodic solutions are stable if $a(r_0{}^*) < 0$.*

(ii) The direction of Hopf bifurcation is subcritical, and bifurcating periodic solutions are unstable if $a(r_0{}^*) > 0$.

2.5 Impact of fear effect

Several field data and experimental observation demonstrates that the fear effect reduces the production of prey species, we thus modify the model (2.1) by multiplying the prey production term by a function $f(\alpha, \eta, P)$ that accounts for the cost of anti-predator dependence due to fear, and the system (2.1) becomes

$$\frac{dN}{dt} = r_0 N f(\alpha, \eta, P) - \delta_1 N - \gamma N^2 - g(N, P)P,$$
$$\frac{dP}{dt} = P(-\delta_2 + \theta g(N, P)),$$

where the parameter α stands the level of fear which implies the anti-predator dependent scenarios for the prey population and η represents the cost of minimum fear.

2.5.1 Fear function

In our study, we consider the following fear function to measure the cost of fear

$$f(\alpha, \eta, P) = \eta + \frac{\alpha(1 - \eta)}{\alpha + P}, \tag{2.12}$$

where α represents the level of fear and $\eta \in [0, 1]$ indicates the minimum cost of fear. The dimension of all the parameters are presented in Table 2.1. Due to biological significance of α, P and $f(\alpha, \eta, P)$, it is worthy to assume that $f(0, \eta, P) = \eta$, $f(\alpha, \eta, 0) = 1$, $\lim_{P \to \infty} f(\alpha, \eta, P) = \eta$ but $\lim_{\alpha \to \infty} f(\alpha, \eta, P) = 1$. Here, $f(0, \eta, P) = \eta$ means that the prey population always remains under minimum fear η and $f(\alpha, \eta, 0) = 1$ means that in absence of predator the fear function has no effect in the growth of prey population. $\lim_{P \to \infty} f(\alpha, \eta, P) = \eta$ means that even if predator population

increases infinitely large, the prey population will stress under minimum fear due to physiological impact when the prey populations are habituated with fear from predator species. $\lim_{\alpha \to \infty} f(\alpha, \eta, P) = 1$ indicates that after certain level of fear with prey population the fear function has no effect due to physiological impact when they are habituated.

Previous studies have considered $\lim_{\alpha \to \infty} f(\alpha, \eta, P) = 0$, but in our study we obtained $\lim_{\alpha \to \infty} f(\alpha, \eta, P) = 1$. Zanette et al. [7] experimentally observed the effect of fear on offspring songbirds and found that offspring songbirds reduces 40% reproduction per year due to the effect of fear. This experiment shows that prey population have not stopped the reproduction due to fear. Mondal et al. [92] has shown theoretically that prey population shows stable behavior from chaotic behavior as the level of fear increases. This result is biologically meaningful, because the prey population is aware and show signs of habituation after certain level of fear. After certain level of fear, fear has no effect on prey population as prey population is aware and show sign of habituation and therefore in our model we have considered $\lim_{\alpha \to \infty} f(\alpha, \eta, P) = 1$. Fig. 2.3 shows the graphical representation of fear function. As the number of predator increases the value of fear function decreases though the prey population remains under minimum level of fear η. Since the fear factor multiplied with prey growth rate in the model, so the growth of prey population becomes lower when the value of fear function is low, that is why the predator population becomes higher. Incorporating the cost of fear for prey species due to predator species and considering Holling type-II response function, the model depicting the interaction between predator-prey populations is given by the following system of nonlinear ordinary differential equations:

$$
\begin{aligned}
\frac{dN}{dt} &= r_0 N \left[\eta + \frac{\alpha(1-\eta)}{\alpha + P} \right] - \delta_1 N - \gamma N^2 - \frac{\beta N P}{1 + \xi N}, \\
\frac{dP}{dt} &= \frac{\theta \beta N P}{1 + \xi N} - \delta_2 P.
\end{aligned}
\tag{2.13}
$$

The model system (2.13) is subjected to the positive initial values $N(0) = N_0 \geq 0$, $P(0) = P_0 \geq 0$ of the population model.

The right hand side of (2.13) is a continuous functions of dependent variables, after integration of the first equation of (2.13), we have

$$
N(t) = N(0) \exp \left(\int_0^t \left[r_0 \left\{ \eta + \frac{\alpha(1-\eta)}{\alpha + P(s)} \right\} - \delta_1 - \gamma N(s) - \frac{\beta P(s)}{1 + \xi N(s)} \right] ds \right).
$$
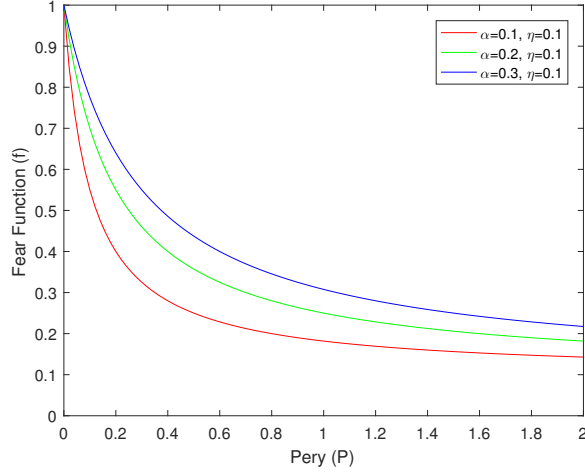
Figure 2.3: The figure represents the value of fear function decreases as the level of fear increases. The fear function has been plotted for different value of α as explained in the inset.

Similarly, from the second equation of (2.13), we have

$$P(t) = P(0) \exp\left(\int_0^t \left[\frac{\theta\beta N(s)}{1+\xi N(s)} - \delta_2\right] ds\right).$$

From the above expressions it is clear that $N(t)$ and $P(t)$ remain non-negative for infinite time if they initiate in the interior point of

$$\mathbf{R}_+^2 = \{(N(t), P(t)) : N(t) \geq 0, P(t) \geq 0\}.$$

Hence, $\mathbf{R}_+^2$ is a positively invariant set for the predator-prey model (2.13).

To prove the boundedness of the system (2.13), we consider the function

$$\psi(t) = N(t) + \frac{1}{\theta}P(t).$$

The time derivative along the solution trajectories for the model (2.13) is

$$\begin{aligned}
\frac{d\psi(t)}{dt} &= \frac{dN(t)}{dt} + \frac{1}{\theta}\frac{dP(t)}{dt} \\
&= r_0 N\left[\eta + \frac{\alpha(1-\eta)}{\alpha+P}\right] - \delta_1 N - \gamma N^2 - \frac{\delta_2}{\theta}P \\
&\leq r_0 N(\eta + (1-\eta)) - \delta_1 N - \gamma N^2 - \frac{\delta_2}{\theta}P.
\end{aligned}$$

Now, for each $\psi(t) > 0$, we get

$$\frac{d\psi(t)}{dt} + \rho\psi(t) \leq r_0 N(t) - \gamma N^2,$$

where $\rho = \min\{\delta_1, \frac{\delta_2}{\theta}\}$. The maximum value of $r_0 N(t) - \gamma N^2$ is $\frac{r_0^2}{4\gamma}$. Therefore,

$$\frac{d\psi(t)}{dt} + \rho\psi(t) \leq \frac{r_0^2}{4\gamma} = \lambda \text{ (say)}.$$

Now, applying the theory of differential inequality for $\psi(t)$, we have

$$0 < \psi(N, P) \leq \frac{\lambda}{\rho}(1 - e^{-\rho t}) + \psi(N(0), P(0))e^{-\rho t},$$

and for $t \to +\infty$, we obtain $0 < \psi \leq \frac{\lambda}{\rho}$. Hence, all the solutions for the system (2.13), which initiating in R_+^2 are confined in the region

$$\Omega = \left\{ (N, P) \in R_+^2 : \psi = \frac{\lambda}{\rho} + \epsilon, \text{ for any } \epsilon > 0 \right\}.$$

This shows that the solutions of the system represented by the equation (2.13) is bounded. We can now summarized our results in the following Lemma.

Lemma 2.5.1. *All the solutions of (2.13) with non-negative initial conditions (N_0, P_0), which initiate in R_+^2 are uniformly bounded.*

Note: From the ecological view point, the boundedness of the solutions implies that none of the interacting population grow abruptly or exponentially for a long period of time. The number of each of the population is bounded due to limited resource or source of food/nutrient.

2.5.2 Permanence of the system

The permanence of the model system plays a key role in ecology or evolutionary biology since the conditions of permanence for ecological models are guaranteed the long-term survival of all the interacting species. From the mathematical view point its mean that the solutions of the system under consideration are away from zero. Here, we prove the permanence result directly by using average Lyapunov functional [108], as our system (2.13) is uniformly bounded.

Theorem 2.5.1. *The system (2.13) is permanent if $r_0 > r_0^{[c]}$ with $\theta > \frac{\delta_2 \xi}{\beta}$.*

Proof. To prove the theorem, we consider the average Lyapunov functional for the system (2.13) as follows

$$\mathcal{L}(N, P) \quad = \quad N^{\rho_1} P^{\rho_2},$$

where ρ_1 and ρ_2 are non-negative constants. In the interior of positive quadrant, we have

$$
\begin{aligned}
\triangle(N, P) \quad &= \quad \frac{\dot{\mathcal{L}}(N, P)}{\mathcal{L}(N, P)} = \rho_1 \frac{\dot{N}}{N} + \rho_2 \frac{\dot{P}}{P} \\
&= \quad \rho_1 \left[r_0 \left\{ \eta + \frac{\alpha(1 - \eta)}{\alpha + P} \right\} - \delta_1 - \gamma N - \frac{\beta P}{1 + \xi N} \right] \\
&\qquad + \rho_2 \left[\frac{\theta \beta N}{1 + \xi N} - \delta_2 \right].
\end{aligned}
$$

To investigate the permanence of the solution for the model (2.13), we must have to verify $\triangle(N, P) > 0$ at the axial equilibrium point E_1. After some algebraic manipulations, we obtain that the condition $\triangle(N, P) > 0$ holds if $r_0 > r_0^{[c]}$, where $r_0^{[c]} = \delta_1 + \frac{\delta_2 \gamma}{\theta \beta - \delta_2 \xi}$ with $\theta > \frac{\delta_2 \xi}{\beta}$, that is, the birth rate for prey population is higher than a threshold value and the conversion rate of predator population is higher than the ratio of natural decay rate for predator species and the search rate for predator population. This completes the Theorem.

□

Note: In absence of the fear effect for prey species due to predator population does not influence the permanence of the model system under consideration.

2.6   Equilibria and their stability

2.6.1   Existence of steady states

Biologically feasible singular points are the points of intersection of the zero growth isoclines $r_0 N \left[\eta + \frac{\alpha(1 - \eta)}{\alpha + P} \right] - \delta_1 N - \gamma N^2 - \frac{\beta N P}{1 + \xi N} = 0$ and $\frac{\theta \beta N P}{1 + \xi N} - \delta_2 P = 0$, in the non-negative quadrant $\mathbf{R}_+^2 = \{(N(t), P(t)) : N(t) \geq 0, P(t) \geq 0\}$. The prey nullcline is a straight line that is parallel to P-axis and the equation of the prey nullcline is $N = \frac{\delta_2}{\theta \beta - \xi \delta_2}$ and also it lies in the first quadrant with parameter restriction $\theta > \frac{\delta_2 \xi}{\beta}$. Irrespective of the system parameters for the model (2.13) possesses three biologically meaningful singular points on the boundary of $\mathbf{R}_+^2$, namely

(i) trivial singular point $E_0(0,0)$,

(ii) axial singular point $E_1(\bar{N}, 0)$, where $\bar{N} = \frac{r_0 - \delta_1}{\gamma}$, which is feasible if $r_0 > \delta_1$, that is, the birth rate of prey is higher than the natural death rate of prey population. Otherwise, E_1 become the extinct equilibrium point E_0, and

(iii) the co-existing singular point $E^*(N^*, P^*)$, where

$$N^* = \frac{\delta_2}{\theta\beta - \xi\delta_2},$$

and P^* is the nonnegative root(s) of the quadratic equation

$$\sigma_1 P^{*2} + \sigma_2 P^* + \sigma_3 = 0, \tag{2.14}$$

where

$$\sigma_1 = \beta,$$

$$\sigma_2 = \alpha\beta + \gamma\xi N^{*2} + \delta_1\xi N^* + \gamma N^* + \delta_1 - r_0\eta - r_0\xi\eta N^*,$$

$$\sigma_3 = \alpha\gamma\xi N^{*2} + \alpha\delta_1\xi N^* + \alpha\gamma N^* + \alpha\delta_1 - r_0\alpha - r_0\alpha\xi N^*.$$

Now, for the existence of P^*, we consider the following two cases:

Case I: If $\sigma_3 < 0$, then the quadratic equation (2.14) has a unique non-negative root given by

$$P^* = \frac{-\sigma_2 + \sqrt{\sigma_2^2 - 4\sigma_1\sigma_3}}{2\sigma_1}.$$

For $\sigma_3 < 0$ gives the simplified form as $r_0 > \delta_1 + \gamma N^*$, with $N^* = \delta_2/(\theta\beta - \xi\delta_2)$. For $\theta > \xi\delta_2/\beta$ gives the positiveness of N^*. Explicit expression for a unique root of P^* is given by

$$P^* = \frac{-l_1 + \sqrt{\alpha^2\beta^2 + l_2 + (1 + \xi N^*)^2(\delta_1 + \gamma N^* - r_0\eta)^2}}{2\beta},$$

where $l_1 = \alpha\beta + (1 + \xi N^*)(\delta_1 + \gamma N^* - r_0\eta)$ and $l_2 = 2\alpha\beta(1 + \xi N^*)[2r_0 - (\delta_1 + \gamma N^* + r_0\eta)]$. Numerical results of mutual position of the prey and predator zero growth isoclines are plotted in the Figs. 2.4((a), (b)) for unique positive root with prey growth rate $r_0 = 0.7$ and 0.8, respectively. In the Figs. 2.4((a), (b)), the black dotted line represents the prey isocline and the

43

corresponding solid blue line represents the predator isocline for $r_0 > \delta_1 + \gamma N^*$ and $\theta > \xi\delta_2/\beta$.

Case II: If $\sigma_2 < 0$ and $\sigma_3 > 0$, then the quadratic equation (2.14) will have two non-negative roots are given by (provided $\sigma_2^2 > 4\sigma_1\sigma_3$)

$$P^* = \frac{-\sigma_2 \pm \sqrt{\sigma_2^2 - 4\sigma_1\sigma_3}}{2\sigma_1}.$$

For $\sigma_3 > 0$ gives the simplified version as $r_0 < \delta_1 + \gamma N^*$, where $N^* = \delta_2/(\theta\beta - \xi\delta_2)$. For $\theta > \xi\delta_2/\beta$ gives the positiveness of N^*. For $\sigma_2 < 0$ gives $\frac{1}{\eta}\left[(\delta_1 + \gamma N^*) + \frac{\alpha\delta_2}{\theta N^*}\right] < r_0$. Combining the cases for $\sigma_3 > 0$ and $\sigma_2 < 0$, we obtain $\frac{1}{\eta}\left[(\delta_1 + \gamma N^*) + \frac{\alpha\delta_2}{\theta N^*}\right] < r_0 < \delta_1 + \gamma N^*$.

Numerical simulations of mutual positions of the prey and predator zero growth isoclines are plotted in the Fig. 2.4(c), for two positive roots with prey growth rate $r_0 = 0.9$. In the Fig. 2.4(c), the black dotted line represents the prey isocline and the corresponding solid blue line represents the predator isocline for $\frac{1}{\eta}\left[(\delta_1 + \gamma N^*) + \frac{\alpha\delta_2}{\theta N^*}\right] < r_0 < \delta_1 + \gamma N^*$ and $\theta > \xi\delta_2/\beta$. The Fig. 2.4(d) represents that there is no mutual position for the prey and predator zero growth isocline with prey growth rate $r_0 = 1.4$. For the Case I and Case II, the model system (2.13) will have positive interior equilibrium point.

2.6.2   Local stability analysis

In this subsection, we shall study the local asymptotic stability of the biologically feasible singular points and Hopf bifurcation criterion of the co-existing singular point $E^*(N^*, P^*)$ for the system (2.13). To investigate the local asymptotic stability, we compute the variational matrix for the model system (2.13) at any point (N, P) is given by

$$J_E = \begin{bmatrix} F_N & F_P \\ G_N & G_P \end{bmatrix},$$

where

$$F_N = \frac{\partial F}{\partial N} = r_0\left[\eta + \frac{\alpha(1-\eta)}{\alpha + P}\right] - \delta_1 - 2\gamma N - \frac{\beta P}{1 + \xi N} + \frac{\beta\xi NP}{(1 + \xi N)^2},$$

$$F_P = \frac{\partial F}{\partial P} = -\frac{\alpha(1-\eta)r_0 N}{(\alpha + P)^2} - \frac{\beta N}{1 + \xi N},$$
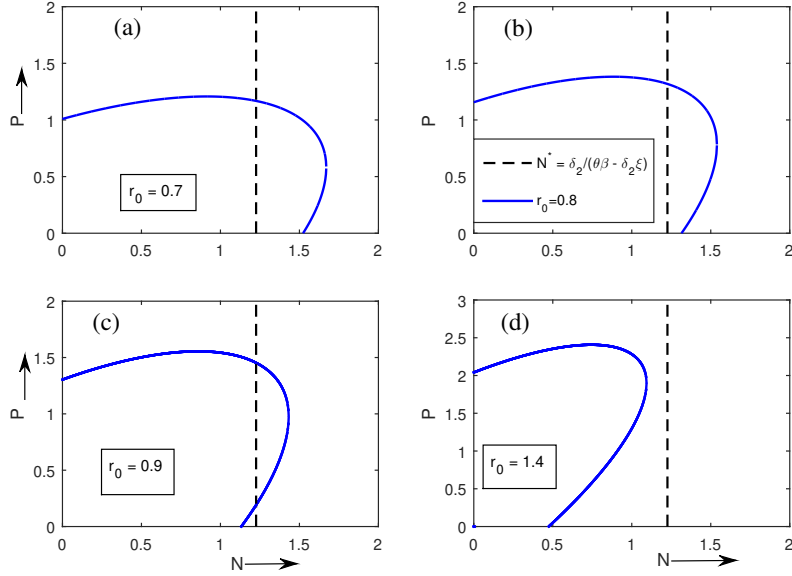
Figure 2.4: Mutual position of the nullclines for the predator-prey system (2.13) with cost of fear and Holling type-II response function. We fixed the parameters value $\eta = 0.10$, $\alpha = 0.20$, $\delta_1 = 0.015$, $\gamma = 0.01$, $\beta = 0.50$, $\xi = 0.60$, $\theta = 0.40$, $\delta_2 = 0.05$. The figure (a) depicts a unique interior equilibrium point for the model (2.13) with $r_0 = 0.7$; (b) depicts a unique interior equilibrium point for the model (2.13) with $r_0 = 0.8$; (c) depicts two interior equilibrium points for the model (2.13) with $r_0 = 0.9$; (d) depicts the non-existence of interior singular point for the model (2.13) with $r_0 = 1.4$.

$$
G_N = \frac{\partial G}{\partial N} = \frac{\theta\beta P}{1 + \xi N} - \frac{\theta\beta\xi NP}{(1 + \xi N)^2},
$$

$$
G_P = \frac{\partial G}{\partial P} = \frac{\theta\beta N}{1 + \xi N} - \delta_2.
$$

At the critical point $E_0(0,0)$, the eigenvalues of the variational matrix J_{E_0} of (2.13) are given by $r_0 - \delta_1$ and $-\delta_2 < 0$. The trivial singular point E_0 is locally asymptotically stable if $r_0 < \delta_1$. This indicates that the death rate of prey is larger than the growth rate of prey population. Thus, if the trivial equilibrium point E_0 is stable asymptotically, then the boundary singular point E_1 does not exist. In reality, the death rate of prey population can not be higher than the growth rate of prey population. The results can be stated in the following theorem.

Theorem 2.6.1. *The trivial singular point $E_0(0,0)$ is locally asymptotically stable if $r_0 < \delta_1$, otherwise unstable.*

Evaluating the Jacobian matrix for the system (2.13) at the boundary singular point $E_1(\frac{r_0 - \delta_1}{\gamma}, 0)$, we obtain the eigenvalues are $\lambda_1 = -\gamma\bar{N} = \delta_1 - r_0$ and $\lambda_2 = \frac{\theta\beta\bar{N}}{1+\xi\bar{N}} - \delta_2 = \frac{\theta\beta(r_0-\delta_1)}{\gamma+\xi(r_0-\delta_1)} - \delta_2$. The boundary singular point E_1 will be locally asymptotically stable if $\lambda_1 < 0$ and $\lambda_2 < 0$, that is, $r_0 > \delta_1$ and $r_0 < \delta_1 + \frac{\delta_2\gamma}{\theta\beta-\delta_2\xi}$, respectively. Biologically, $r_0 > \delta_1$ implies that the birth rate of prey population is higher than the death rate of prey species. The region of stability of E_1 has been shown in the Fig. 2.20 (red shaded region). The following theorem describes the local asymptotic stability of the boundary equilibrium point E_1.

Theorem 2.6.2. *The semi-trivial equilibrium point $E_1(\frac{r_0-\delta_1}{\gamma}, 0)$ is locally asymptotically stable if $\delta_1 < r_0 < \delta_1 + \frac{\delta_2\gamma}{\theta\beta-\delta_2\xi}$ with $\theta > \frac{\delta_2\xi}{\beta}$.*

From the biological view point, it is more important to study the local asymptotic stability of the positive interior equilibrium point $E^*(N^*, P^*)$ in which all the interacting species are co-exists. In order to study the stability of the singular point $E^*(N^*, P^*)$, we analyze the characteristic equation of the Jacobian matrix for the model (2.13) is given by

$$\lambda^2 + \left(\gamma N^* - \frac{\beta\xi N^* P^*}{(1+\xi N^*)^2}\right)\lambda + \frac{\theta\beta P^*}{(1+\xi N^*)^2}\left(\frac{\beta N^*}{1+\xi N^*} + \frac{r_0\alpha N^*(1-\eta)}{(\alpha+P^*)^2}\right) = 0,$$

which can be written as

$$\lambda^2 + \rho_{11}\lambda + \rho_{22} = 0, \tag{2.15}$$

where $\rho_{11} = \gamma N^* - \frac{\beta\xi N^* P^*}{(1+\xi N^*)^2}$ and $\rho_{22} = \frac{\theta\beta P^*}{(1+\xi N^*)^2}\left(\frac{\beta N^*}{1+\xi N^*} + \frac{r_0\alpha N^*(1-\eta)}{(\alpha+P^*)^2}\right)$. From these expressions it is quite difficult to explain the outcomes in terms of ecological system. Thus, we explore this results numerically. Due to Routh-Hurwitz criteria a set of necessary and sufficient conditions for the characteristic roots of (2.15) will have negative real parts if $\rho_{11} > 0$ and $\rho_{22} > 0$, which gives $\frac{\beta\xi P^*}{\gamma} < (1+\xi N^*)^2$ and $(1+\xi N^*) < \frac{\beta(\alpha+P^*)^2}{r_0\alpha(\eta-1)}$, respectively. The region of stability of E^* has been shown in Fig. 2.20 (blue shaded region). Therefore, we have the following theorem.

Theorem 2.6.3. *The necessary condition for the model (2.13) to be locally asymptotically stable around the co-existing singular point $E^*(N^*, P^*)$ is that $(1 + \xi N^*) \in \left(\sqrt{\frac{\beta\xi P^*}{\gamma}}, \frac{\beta(\alpha+P^*)^2}{r_0\alpha(\eta-1)}\right)$.*

2.6.3 Existence and uniqueness of limit cycle

Existence and stability of a limit cycle in the dynamics of a predator-prey relationship, is related to the existence and stability of biologically feasible singular point(s). We have already shown that our model system (2.13) exhibits at most two positive interior equilibrium points, otherwise the predator species tend to extinction. If the singular point is stable asymptotically, there may exist limit cycles, the innermost of which must be unstable from the inside and the outermost of which must be stable from the outside or vice-versa. In this case, we will show that if the limit cycle does not exist, the interior singular point is stable globally. If the non-negative singular point exists and is unstable, there must occur at least one limit cycle. We will employ the approach of Kuang & Freedman [109] to verify the existence and uniqueness of limit cycles for the model (2.13), without cost of fear for prey species due to predator population. In order to do that we rewrite the model (2.13) without cost of fear as

$$
\begin{aligned}
\frac{dN}{dt} &= Ng(N) - PH(N), \quad \text{with} \quad N(0) \geq 0, \\
\frac{dP}{dt} &= P(-\delta_2 + Q(N)), \quad \text{with} \quad P(0) \geq 0,
\end{aligned}
\tag{2.16}
$$

where, $g(N) = (r_0 - \delta_1) - \gamma N = \rho - \gamma N$, $H(N) = \frac{\beta N}{1+\xi N}$ and $Q(N) = \frac{\theta \beta N}{1+\xi N}$. The following assumptions are consistent with the model (2.13) of our predator-prey system with $N, P \geq 0$.

(A1) $g(0) > 0$; there exists a real number $K > 0$ in such a way that $g(N) > 0$ on the interval $0 \leq N < K$.

(A2) $H(0) = 0$, $H'(N) > 0$.

(A3) $Q(0) = 0$, $Q'(N) > 0$.

Theorem 2.6.4. *Suppose the model system (2.16)* $\frac{d}{dN}\left[\frac{Ng'(N)+g(N)-Ng(N)\frac{H'(N)}{H(N)}}{-\delta_2+Q(N)}\right] \leq 0$, *in the interval* $0 \leq N < N^*$ *and* $N^* < N \leq K$. *Then the model system (2.16) admits exactly one limit cycle which is stable globally with respect to the set* $\{(N,P) : N > 0, P > 0\}$ $\{E^*(N^*, P^*)\}$.

To study the existence and uniqueness of limit cycle and the stability of limit cycle, we use the above Theorem 2.6.4 of our proposed model (2.16) without any cost of fear for the prey species due to predator population.

Theorem 2.6.5. *Suppose that* $r_0 \geq \delta_1 + \gamma\left(2N^* + \frac{1}{\xi}\right)$, *then the model system (2.16) admits exactly one limit cycle which is stable globally.*

Proof. To prove the theorem, we employ the Theorem 2.6.4 by Kuang & Freedman [109], we have

$$\frac{d}{dN}\left[\frac{Ng'(N) + g(N) - Ng(N)\frac{H'(N)}{H(N)}}{-\delta_2 + Q(N)}\right] \leq 0$$

$$\Leftrightarrow \quad \frac{d}{dN}\left[\frac{N(-\gamma) + (\rho - \gamma N) - N(\rho - \gamma N)\cdot\frac{\beta}{(1+\xi N)^2}\cdot\frac{(1+\xi N)}{\beta N}}{-\delta_2 + \frac{\theta\beta N}{1+\xi N}}\right] \leq 0$$

$$\Leftrightarrow \quad \frac{d}{dN}\left[\frac{N(-\gamma) + (\rho - \gamma N) - \frac{(\rho - \gamma N)}{1+\xi N}}{-\delta_2 + \frac{\theta\beta N}{1+\xi N}}\right] \leq 0$$

$$\Leftrightarrow \quad \frac{d}{dN}\left[\frac{N(-\gamma) + (\rho - \gamma N)\frac{\xi N}{1+\xi N}}{-\delta_2 + \frac{\theta\beta N}{1+\xi N}}\right] \leq 0$$

$$\Leftrightarrow \quad \frac{d}{dN}\left[\frac{\xi N(\rho - \gamma N) + (1 + \xi N)(-N\gamma)}{\theta\beta N - \delta_2(1 + \xi N)}\right] \leq 0$$

$$\Leftrightarrow \quad \frac{d}{dN}\left[\frac{\xi N(\gamma N - \rho) + N\gamma(1 + \xi N)}{\theta\beta N - \delta_2(1 + \xi N)}\right] \geq 0$$

$$\Leftrightarrow \quad \frac{d}{dN}\left[\frac{\xi N(\gamma N - \rho) + N\gamma(1 + \xi N)}{(\theta\beta - \delta_2\xi)(N - \Delta)}\right] \geq 0, \text{where } \Delta = \frac{\delta_2}{\theta\beta - \delta_2\xi} = N^*$$

$$\Leftrightarrow \quad \frac{d}{dN}\left[\frac{\xi\gamma}{(\theta\beta - \delta_2\xi)}\cdot\frac{N\left(2N + \frac{1}{\xi} - \frac{\rho}{\gamma}\right)}{N - \Delta}\right] \geq 0$$

$$\Leftrightarrow \quad \frac{d}{dN}\left[\frac{N\left(2N + \frac{1}{\xi} - \frac{\rho}{\gamma}\right)}{N - \Delta}\right] \geq 0$$

$$\Leftrightarrow \quad \left(2N + \frac{1}{\xi} - \frac{\rho}{\gamma} + 2N\right)(N - \Delta) - N\left(2N + \frac{1}{\xi} - \frac{\rho}{\gamma}\right) \geq 0$$

$$\Leftrightarrow \quad 2N^2 - 4N\Delta - \Delta\left(\frac{1}{\xi} - \frac{\rho}{\gamma}\right) \geq 0$$

$$\Leftrightarrow \quad (N - \Delta)^2 + \frac{\Delta}{2}\left(\frac{\rho}{\gamma} - \frac{1}{\xi}\right) - \Delta^2 \geq 0$$

$$\Leftrightarrow \quad \left(\frac{\rho}{\gamma} - \frac{1}{\xi}\right) \geq 2\Delta$$

$$\Leftrightarrow \quad \rho \geq \gamma\left(2\Delta + \frac{1}{\xi}\right),$$

that is, $r_0 \geq \delta_1 + \gamma\left(\frac{2\delta_2}{\theta\beta - \delta_2\xi} + \frac{1}{\xi}\right)$. The equality holds if and only if $r_0 =$

48

$\delta_1 + \gamma \left(\frac{2\delta_2}{\theta\beta - \delta_2\xi} + \frac{1}{\xi} \right)$, which implies that the the existence and uniqueness of limit cycle and the global stability depends on the value of prey population and which also measured by the growth rate of prey population. From which we can conclude that the introduction of the cost of fear for prey species play an important role on the co-existence of predator-prey species. By using the Theorem 2.6.4, we investigate that for $r_0 \geq \delta_1 + \gamma \left(\frac{2\delta_2}{\theta\beta - \delta_2\xi} + \frac{1}{\xi} \right)$, the model system (2.16) admits only one limit cycle which is stable globally. This completes the proof of the Theorem. $\qquad\square$

Note: It can be observed that whenever the non-trivial singular point for (2.16) is unstable, then the entire solutions for (2.16) initiating in the interior of the non-negative octant of the N-P plane, except at the singular point, approaches a unique limit cycle eventually.

2.6.4 Analysis of Hopf bifurcation

The possibility of the Hopf bifurcation at an interior singular point $E^*(N^*, P^*)$ has been analyzed here by taking prey birth rate r_0, as a bifurcation parameter and keeping rest of the parameters are constant. To investigate the nature of the interior singular point $E^*(N^*, P^*)$ we required to investigate the sign of the real parts for the characteristic roots of the equation (2.15). A necessary condition for the change of stability for the singular point E^* is that at the characteristic polynomial (2.15) should have purely complex roots. Roots for the polynomial (2.15) will be purely complex if $\rho_{11} = 0$ and $\rho_{22} > 0$.

At $\rho_{11} = 0$ gives $P^* = \frac{\gamma(1+\xi N^*)^2}{\xi\beta}$ and (N^*, P^*) satisfies the characteristic equation (2.15). Putting this value of P^* into the characteristic equation (2.15), we get the threshold value of $r_0 = r_0^* = \left(\delta_1 + \frac{\gamma}{\xi} + 2\gamma N^* \right) \left[\frac{\alpha\beta\xi + \gamma(1+N^*)^2}{\alpha\beta\xi + \eta\gamma(1+N^*)^2} \right]$ where $N^* = \frac{\delta_2}{\theta\beta - \xi\delta_2}$.

Let $\lambda(r_0) = \pi_1(r_0) + i\pi_2(r_0)$ be the eigenvalues for the characteristic polynomial (2.15). Putting this expression into (2.15) and separating the real and complex parts, we have

$$\begin{aligned} \pi_1^2 - \pi_2^2 + \rho_{11}\pi_1 + \rho_{22} &= 0, \\ 2\pi_1\pi_2 + \rho_{11}\pi_2 &= 0. \end{aligned} \qquad (2.17)$$

Setting $r_0 = r_0^*$ in such a way that $\pi_1(r_0^*) = 0$ and substitute into the

equations (2.17), we have

$$\begin{aligned} -\pi_2^2 + \rho_{22} &= 0, \\ \rho_{11}\pi_2 &= 0, \quad \text{with} \quad \pi_2 \neq 0. \end{aligned} \tag{2.18}$$

From the above expressions (2.18), we have $\rho_{11}(r_0^*) = 0$ and $\pi_2(r_0^*) = \sqrt{\rho_{22}(r_0^*)}$, which implies $\lambda(r_0^*) = -i\sqrt{\rho_{22}(r_0^*)}$.

Theorem 2.6.6. *The necessary and sufficient conditions for the system (2.13) undergoes Hopf bifurcation from the interior singular point $E^*(N^*, P^*)$ is that there exists $r_0 = r_0^*$ such that*

$$\begin{aligned} (i) \quad & \pi_1(r_0^*) = 0, \\ (ii) \quad & \left[\frac{dRe(\lambda(r_0))}{dr_0}\right]_{r_0=r_0^*} \neq 0. \end{aligned}$$

Proof. The eigenvalues of the characteristic polynomial (2.15) are given by

$$\lambda_{1,2} = \frac{-\rho_{11} \pm \sqrt{\rho_{11}^2 - 4\rho_{22}}}{2},$$

where ρ_{11} and ρ_{22} are the functions of the birth rate of prey population r_0, in which all other parameters are fixed. Furthermore, we assume that there exists parameter $r_0 = r_0^*$ in such a way that $\rho_{11}(r_0^*) = 0$ and $\rho_{22}(r_0^*) > 0$. Thus, the non-negative real roots of these eigenvalues alter the sign when r_0 crosses through the critical value r_0^*. Consequently, the model system (2.13) switches its stability provided that the transversality condition is assured.

Differentiating both the expressions of (2.17), with respect to r_0 and then substitute $\pi_1(r_0) = 0$, we get

$$\begin{aligned} \rho_{11}\frac{d\pi_1(r_0)}{dr_0} - 2\pi_2\frac{d\pi_2(r_0)}{dr_0} &= -\frac{d\rho_{22}(r_0)}{dr_0}, \\ 2\pi_2\frac{d\pi_1(r_0)}{dr_0} + \rho_{11}\frac{d\pi_2(r_0)}{dr_0} &= -\pi_2\frac{d\rho_{11}(r_0)}{dr_0}. \end{aligned} \tag{2.19}$$

Solving the above system of equations (2.19), we get

$$\left[\frac{dRe(\lambda(r_0))}{dr_0}\right]_{r_0=r_0^*} = -\left[\frac{\rho_{11}\frac{d\rho_{22}}{dr_0} + 2\pi_2^2\frac{d\rho_{11}}{dr_0}}{\rho_{11}^2 + 4\pi_2^2}\right]_{r_0=r_0^*} \neq 0,$$

provided $\rho_{11}\frac{d\rho_{22}}{dr_0} + 2\pi_2^2\frac{d\rho_{11}}{dr_0} \neq 0$. This completes the proof. $\square$

2.6.5 Direction and stability of Hopf bifurcation

In the previous subsection, we derived the conditions under which the model (2.13) experiences Hopf bifurcation. Now, we shall employ center manifold theorem and normal form theory to investigate the direction of Hopf bifurcation and sufficient conditions for the stability of bifurcating periodic solutions arising through Hopf bifurcation. Center manifold theorem is a viable tool in reducing the dimension of a system of differential equations in the neighborhood of co-existing singular point [107, 110].

For our present system, given by the equations (2.13), we obtained that the variational matrix $J(N^*, P^*)$ has a pair of purely complex eigenvalues at the Hopf bifurcation point $r_0 = r_0{}^*$. Thus, we can analyze the model under consideration on a two dimensional center manifold. The flow transverse to the center manifold is relatively simple, that is, exponentially contracting. To investigate the center manifold and investigate the flow theorem, first we translate the non-negative interior singular point $E^*(N^*, P^*)$ to the origin by using the transformation $\hat{N} = N - N^*$ and $\hat{P} = P - P^*$. For simplicity, we denote $\hat{N}$ and $\hat{P}$ again by N and P, respectively. We can rewrite the system of equations (2.13), by Taylor series expansion about (N^*, P^*) as follows

$$
\begin{aligned}
\frac{dN}{dt} &= r_0(N + N^*)\left(\eta + \frac{\alpha(1 - \eta)}{\alpha + P + P^*}\right) - \delta_1(N + N^*) \\
&\quad - \gamma(N + N^*)^2 - \frac{\beta(N + N^*)(P + P^*)}{1 + \xi(N + N^*)}, \\
\frac{dP}{dt} &= \frac{\theta\beta(N + N^*)(P + P^*)}{1 + \xi(N + N^*)} - \delta_2(P + P^*).
\end{aligned} \tag{2.20}
$$

The system (2.20) can be written as

$$
\begin{bmatrix} \frac{dN}{dt} \\ \frac{dP}{dt} \end{bmatrix} = J^*(N^*, P^*)\begin{bmatrix} N \\ P \end{bmatrix} + \begin{bmatrix} \phi(N, P) \\ \psi(N, P) \end{bmatrix}, \tag{2.21}
$$

where

$$
\begin{aligned}
\phi(N, P) &= a_1 N^2 + a_2 NP + a_3 P^2 + \cdots, \\
\psi(N, P) &= b_1 N^2 + b_2 NP + b_3 P^2 + \cdots,
\end{aligned}
$$

51

with

$$a_1 = -\gamma + \frac{\beta\xi P^*}{(1+\xi N^*)^2} - \frac{\beta\xi N^* P^*}{(1+\xi N^*)^2},$$

$$a_2 = \frac{r_0\alpha(1-\eta)}{(\alpha+P^*)^2} - \frac{\beta}{(1+\xi N^*)} + \frac{\beta\xi N^*}{(1+\xi N^*)^2},$$

$$a_3 = \frac{r_0\alpha N^*(1-\eta)}{(\alpha+P^*)^3}, \ldots,$$

$$b_1 = \frac{\theta\beta\xi P^*}{(1+\xi N^*)^2} + \frac{\theta\beta\xi^2 N^* P^*}{(1+\xi N^*)^3},$$

$$b_2 = \frac{\theta\beta}{1+\xi N^*} - \frac{\theta\beta\xi N^*}{(1+\xi N^*)^2}, \quad b_3 = 0, \ldots.$$

The characteristic roots of $J^*(N^*, P^*)$ are of the form $\lambda_{1,2} = L \pm iM$, where $L = \frac{1}{2}(tr(J^*))$ and $M = \sqrt{\det(J^*) - L^2}$. Here, the eigenvalues λ_1 and λ_2 will be complex conjugate if $\det(J^*) - L^2 > 0$ and λ_1, λ_2 will be purely imaginary at $r_0 = r_0^*$, that is, $L(r_0^*) = 0$ and then $\lambda_{1,2} = \pm iM(r_0^*)$.

The eigenvectors of $J^*(N^*, P^*)$ corresponding to the eigenvalues of $\lambda = L + iM$ are given by

$$X = \begin{bmatrix} 1 \\ Y - iZ \end{bmatrix},$$

where

$$Y = \frac{\theta(\alpha+P^*)^2}{r_0\alpha\theta(1-\eta)N^* + \delta_2(\alpha+P^*)^2} \left(\gamma N^* - \frac{\beta\xi N^* P^*}{(1+\xi N^*)^2} + M \right),$$

$$Z = -\frac{\theta(\alpha+P^*)^2 L}{r_0\alpha(1-\eta)\theta N^* + \delta_2(\alpha+P^*)^2}.$$

We set the matrix as follows

$$D = \begin{bmatrix} 1 & 0 \\ Y & Z \end{bmatrix}.$$

By using the transformation

$$\begin{bmatrix} N \\ P \end{bmatrix} = D \begin{bmatrix} x \\ y \end{bmatrix},$$

that is, $N = x$ and $P = xY + yZ$. Using the above transformation, the model system (2.21) becomes

$$\begin{bmatrix} \frac{dx}{dt} \\ \frac{dy}{dt} \end{bmatrix} = J^*(N^*, P^*) \begin{bmatrix} x \\ y \end{bmatrix} + \begin{bmatrix} Q(x, y) \\ R(x, y) \end{bmatrix}, \qquad (2.22)$$

where

$$J^*(N^*, P^*) = \begin{bmatrix} L & -M \\ M & L \end{bmatrix},$$

and

$$
\begin{aligned}
Q(x, y) &= \left[-\gamma + \frac{r_0\alpha(1-\eta)N^*Y^2}{(\alpha + P^*)^3} - \frac{r_0\alpha(1-\eta)Y}{(\alpha + P^*)^3} - \frac{\beta\xi^2 N^* P^*}{(1 + \xi N^*)^3} \right. \\
&\quad \left. + \frac{\beta\xi P^*}{(1 + \xi N^*)^2} - \frac{\beta\xi N^* Y}{(1 + \xi N^*)^2} - \frac{\beta Y}{1 + \xi N^*} \right] x^2 \\
&\quad + \left[\frac{r_0\alpha(1-\eta)N^* Z^2}{(\alpha + P^*)^3} \right] y^2 + \left[-\frac{\beta Z}{1 + \xi N^*} + \frac{r_0\alpha(1-\eta)N^* Y Z}{(\alpha + P^*)^3} \right. \\
&\quad \left. + \frac{r_0\alpha(1-\eta)Z}{(\alpha + P^*)^2} + \frac{\beta\xi N^* Z}{(1 + \xi N^*)^2} \right] xy + \left[-\frac{r_0\alpha(1-\eta)N^* Y^3}{(\alpha + P^*)^4} \right. \\
&\quad + \frac{r_0\alpha(1-\eta)Y^2}{(\alpha + P^*)^3} + \frac{\beta\xi^3 N^* P^*}{(1 + \xi N^*)^4} - \frac{\beta\xi P^{*2}}{(1 + \xi N^*)^3} \\
&\quad \left. - \frac{\beta\xi^2 N^* Y}{(1 + \xi N^*)^3} + \frac{\beta\xi Y}{(1 + \xi N^*)^2} \right] x^3 + \cdots
\end{aligned}
$$

$$
\begin{aligned}
R(x, y) &= \frac{1}{Z} \left[\frac{\theta\beta\xi^2 N^* P^*}{(1 + \xi N^*)^3} - \frac{\theta\beta\xi P^*}{(1 + \xi N^*)^2} - \frac{\theta\beta\xi N^* Y}{(1 + \xi N^*)^2} - \frac{r_0\alpha(1-\eta)N^* Y^3}{(\alpha + P^*)^3} \right. \\
&\quad + \frac{r_0\alpha(1-\eta)Y^2}{(\alpha + P^*)^2} + \gamma Y + \frac{\beta Y^2}{1 + \xi N^*} - \frac{\beta\xi P^* Y}{(1 + \xi N^*)^2} \\
&\quad \left. + \frac{\beta\xi N^* Y^2}{(1 + \xi N^*)^2} + \frac{\beta\xi^2 N^* P^* Y}{(1 + \xi N^*)^3} + \frac{\theta\beta Y}{1 + \xi N^*} \right] x^2 \\
&\quad - \left[\frac{r_0\alpha(1-\eta)Y Z}{(\alpha + P^*)^3} \right] y^2 + \left[\frac{\beta Y}{1 + \xi N^*} + \frac{\theta\beta}{1 + \xi N^*} - \frac{\theta\beta\xi N^*}{(1 + \xi N^*)^2} \right. \\
&\quad \left. + \frac{r_0\alpha(1-\eta)Y}{(\alpha + P^*)^2} - \frac{2r_0\alpha(1-\eta)N^* Y}{(\alpha + P^*)^3} - \frac{\beta\xi N^* Y}{(1 + \xi N^*)^2} \right] xy + \cdots
\end{aligned}
$$

The model system (2.22) can be written in the polar form as

$$\frac{dr}{dt} = L(r_0)r + a(r_0)r^3 + \dots,$$
$$\frac{d\theta}{dt} = M(r_0) + c(r_0)r^2 + \dots. \tag{2.23}$$

The Taylor's series expansion of (2.23) at $r_0 = r_0{}^*$ gives

$$\frac{dr}{dt} = L'(r_0{}^*)(r_0 - r_0{}^*)r + a(r_0{}^*)r^3 + \dots,$$
$$\frac{d\theta}{dt} = M(r_0{}^*) + M'(r_0{}^*)(r_0 - r_0{}^*) + c(r_0{}^*)r^2 + \dots,$$

where

$$
\begin{aligned}
a(r_0{}^*) \;=\;& \frac{1}{16}\left[Q_{xxx} + Q_{xyy} + R_{xxy} + R_{yyy}\right]_{(0,0,r_0{}^*)} \\
&+ \frac{1}{16M(r_0{}^*)}\left[Q_{xy}(Q_{xx} + Q_{yy}) - R_{xy}(R_{xx} + R_{yy})\right. \\
&\left. - Q_{xx}R_{xx} + Q_{yy}R_{yy}\right]_{(0,0,r_0{}^*)}
\end{aligned}
$$

with

$$
\begin{aligned}
Q_{xxx}(0,0,r_0{}^*) \;=\;& 6\left[-\frac{r_0{}^*\alpha(1-\eta)N^*Y^3}{(\alpha + P^*)^4} + \frac{r_0{}^*\alpha(1-\eta)Y^2}{(\alpha + P^*)^3} + \frac{\beta\xi^3 N^* P^*}{(1 + \xi N^*)^4} \right. \\
&\left. -\frac{\beta\xi P^{*2}}{(1 + \xi N^*)^3} - \frac{\beta\xi^2 N^* Y}{(1 + \xi N^*)^3} + \frac{\beta\xi Y}{(1 + \xi N^*)^2} \right], \\
Q_{xyy}(0,0,r_0{}^*) \;=\;& 2\left[-\frac{3r_0{}^*\alpha(1-\eta)N^*YZ^2}{(\alpha + P^*)^4} + \frac{r_0{}^*\alpha(1-\eta)Z^2}{(\alpha + P^*)^3} \right],
\end{aligned}
$$

$$
\begin{aligned}
R_{xxy}(0,0,r_0{}^*) \;=\;& 2\left[-\frac{\theta\beta\xi}{(1 + \xi N^*)^2} - \frac{\beta\xi Y}{(1 + \xi N^*)^2} + \frac{\theta\beta\xi^2 N^*}{(1 + \xi N^*)^3} \right. \\
&\left. + \frac{3r_0{}^*\alpha(1-\eta)N^*Y^3}{(\alpha + P^*)^4} - \frac{2r_0{}^*\alpha(1-\eta)Y^2}{(\alpha + P^*)^3} + \frac{\beta\xi^2 N^* Y}{(1 + \xi N^*)^3} \right], \\
R_{yyy}(0,0,r_0{}^*) \;=\;& \frac{r_0{}^*\alpha(1-\eta)N^*YZ^2}{(\alpha + P^*)^4},
\end{aligned}
$$

54

$$Q_{xy}(0,0,r_0{}^*) = -\frac{\beta Z}{1+\xi N^*} + \frac{2r_0{}^*\alpha(1-\eta)N^*YZ}{(\alpha+P^*)^3} - \frac{r_0{}^*\alpha(1-\eta)Z}{(\alpha+P^*)^2}$$
$$+ \frac{\beta\xi N^*Z}{(1+\xi N^*)^2},$$

$$Q_{xx}(0,0,r_0{}^*) = 2\left[-\gamma + \frac{r_0{}^*\alpha(1-\eta)N^*Y^2}{(\alpha+P^*)^3} - \frac{r_0{}^*\alpha(1-\eta)Y}{(\alpha+P^*)^3}\right.$$
$$\left. - \frac{\beta\xi^2 N^*P^*}{(1+\xi N^*)^3} + \frac{\beta\xi P^*}{(1+\xi N^*)^2} - \frac{\beta\xi N^*Y}{(1+\xi N^*)^2} - \frac{\beta Y}{1+\xi N^*}\right],$$

$$Q_{yy}(0,0,r_0{}^*) = \frac{2r_0{}^*\alpha(1-\eta)N^*Z^2}{(\alpha+P^*)^3},$$

$$R_{xy}(0,0,r_0{}^*) = \frac{\beta Y}{1+\xi N^*} + \frac{\theta\beta}{1+\xi N^*} - \frac{\theta\beta\xi N^*}{(1+\xi N^*)^2} + \frac{r_0{}^*\alpha(1-\eta)Y}{(\alpha+P^*)^2}$$
$$- \frac{2r_0{}^*\alpha(1-\eta)N^*Y}{(\alpha+P^*)^3} - \frac{\beta\xi N^*Y}{(1+\xi N^*)^2},$$

$$R_{yy}(0,0,r_0{}^*) = -\frac{2r_0{}^*\alpha(1-\eta)N^*YZ}{(\alpha+P^*)^3},$$

$$R_{xx}(0,0,r_0{}^*) = \frac{2}{Z}\left[\frac{\theta\beta\xi^2 N^*P^*}{(1+\xi N^*)^3} - \frac{\theta\beta\xi P^*}{(1+\xi N^*)^2} - \frac{\theta\beta\xi N^*Y}{(1+\xi N^*)^2}\right.$$
$$- \frac{r_0{}^*\alpha(1-\eta)N^*Y^3}{(\alpha+P^*)^3} + \frac{r_0{}^*\alpha(1-\eta)Y^2}{(\alpha+P^*)^2} + \gamma Y$$
$$+ \frac{\beta Y^2}{1+\xi N^*} - \frac{\beta\xi P^*Y}{(1+\xi N^*)^2} - \frac{\beta\xi N^*Y^2}{(1+\xi N^*)^2}$$
$$\left. + \frac{\beta\xi^2 N^*P^*Y}{(1+\xi N^*)^3} + \frac{\theta\beta Y}{1+\xi N^*}\right].$$

The sign of the coefficient of $a(r_0{}^*)$ determines the stability of Hopf bifurcating periodic solution. Thus, we have

$$\left[\frac{\partial L}{\partial r_0}\right]_{r_0=r_0{}^*} = \left[\text{Derivative of real part of the eigenvalue}\right.$$
$$\left.\text{with respect to } r_0\right]_{r_0=r_0{}^*}$$
$$= -\left[\frac{\rho_{11}\frac{d\rho_{22}}{dr_0} + 2\pi_2^2\frac{d\rho_{11}}{dr_0}}{\rho_{11}^2 + 4\pi_2^2}\right]_{r_0=r_0^*} \neq 0,$$

provided $\rho_{11}\frac{d\rho_{22}}{dr_0} + 2\pi_2^2\frac{d\rho_{11}}{dr_0} \neq 0$. Thus,

$$\Lambda = -\frac{a(r_0{}^*)}{L'(r_0{}^*)}.$$

From the above calculations for $a(r_0{}^*)$, we have the following theorem.

Theorem 2.6.7. *Let* $\rho_{11}\frac{d\rho_{22}}{dr_0} + 2\pi_2^2\frac{d\rho_{11}}{dr_0} \neq 0$, *then*

(i) *the interior equilibrium point* $E^*(N^*, P^*)$ *for (2.13) is locally asymptotically stable when* $r_0 < r_0{}^*$ *and unstable when* $r_0 > r_0{}^*$. *The system (2.13) experiences a Hopf bifurcation at the non-negative singular point* $E^*(N^*, P^*)$ *for* $r_0 = r_0{}^*$.

(ii) *If* $L'(r_0{}^*) > 0$ *and* $a(r_0{}^*) < 0$, *the Hopf bifurcated periodic solutions are stable and the direction of Hopf bifurcation become supercritical.*

(iii) *If* $L'(r_0{}^*) > 0$ *and* $a(r_0{}^*) > 0$, *the Hopf bifurcated periodic solutions are unstable and the direction of Hopf bifurcation become subcritical.*

2.7 Numerical simulations

In this section, we performed extensive numerical simulations to check the feasibility of analytical findings for the predator-prey models (2.2) and (2.13). A hypothetical set of parameters value is used to solve numerically the system of nonlinear ordinary differential equations (2.2) and (2.13) by the fourth order Runge-Kutta method. Firstly, analytical findings of system (2.2) will be validated numerically and then the analytical findings of system (2.13) will be validated.

2.7.1 Numerical simulations for the predator-prey system (2.2)

The hypothetical set of parameters for the system (2.2) are $r_0 = 0.01$, $\delta_1 = 0.02$, $\gamma = 0.01$, $\beta = 0.9$, $\xi = 0.5$, $\theta = 0.4$ and $\delta_2 = 0.05$. For this parameter set, the stability condition $r_0 < \delta_1$ for the trivial singular point E_0 of system (2.2) is satisfied, and hence, $\hat{E}_0(0,0)$ is locally asymptotically stable. From the time series solution shown in the Fig. 2.5(a), it can be noticed that both prey and predator populations $N(t)$ and $P(t)$ initiating from the initial values $(0.5, 0.3)$ and goes to extinct; hence, the trivial steady state $\hat{E}_0$ is stable asymptotically. Again, we have chosen the parameters value as $r_0 = 0.03$, $\delta_1 = 0.01$, $\gamma = 0.15$, $\beta = 0.9$, $\xi = 0.5$, $\theta = 0.4$ and

$\delta_2 = 0.05$. The condition of locally asymptotic stability $\delta_1 < r_0 < \delta_1 + \frac{\gamma \delta_2}{\theta \beta - \xi \delta_2}$ of the boundary equilibrium point $\hat{E}_1(\bar{N}_e, 0)$ of (2.2) is satisfied, and hence, $\hat{E}_1(\bar{N}_e, 0)$ is locally asymptotically stable. Time series solution demonstrated in the Fig. 2.5(b) represents that both predator and prey population $N(t)$ and $P(t)$ initiate from an initial value $(0.5, 0.3)$ and go to their boundary equilibrium state, and hence the boundary steady state $\hat{E}_1(0.1333, 0)$ is stable asymptotically. Also, we have chosen the parameter set as $r_0 = 0.03$, $\delta_1 = 0.02$, $\gamma = 0.01$, $\beta = 0.9$, $\xi = 0.5$, $\theta = 0.4$ and $\delta_2 = 0.05$. The condition of local asymptotic stability $r_0 - \delta_1 - 2\gamma N^* - \frac{\beta P^*}{(1+\xi N^*)^2} = -0.0009 < 0$ of the co-existing singular point $\hat{E}^*(N^*, P^*)$ is satisfied and hence, $\hat{E}^*(N^*, P^*)$ is locally asymptotically stable. From the time series analysis shown in the Fig. 2.5(c), it can be demonstrated that both prey and predators $N(t)$ and $P(t)$ initiating from the initial value $(0.5, 0.3)$ and goes to their interior singular point; and hence the co-existing steady state $\hat{E}^*(0.1493, 0.0102)$ is locally asymptotically stable.
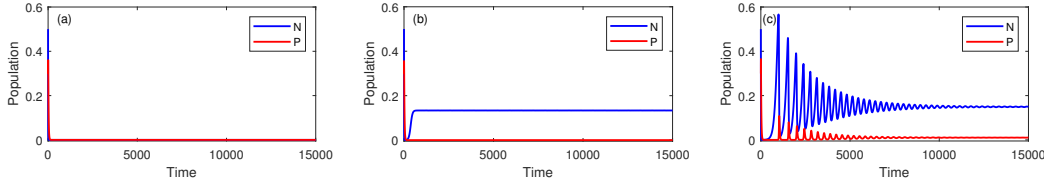
Figure 2.5: The time series evolution of prey population $N(t)$ and predator population $P(t)$ for the model system (2.2) with parameters is defined in numerical section. The subplot (a) shows that trivial singular point $\hat{E}_0(0,0)$ is locally asymptotically stable, (b) boundary singular point $\hat{E}_1(0.1333, 0)$ is locally asymptotically stable, and (c) the co-existing steady state $\hat{E}^*(0.1493, 0.0102)$ is stable asymptotically.

The dynamical behavior around the co-existing steady state $\hat{E}^*(N_e^*, P_e^*)$ of the system (2.2) have shown in the phase diagram (Fig. 2.6). The system (2.2) is integrated by using fourth order Runge-Kutta scheme with the parameter set $\delta_1 = 0.01$, $\gamma = 0.01$, $\beta = 0.9$, $\xi = 0.5$, $\delta_2 = 0.05$, $\theta = 0.4$ and varies the prey birth rate r_0. For $r_0 = 0.018$, the positive interior singular point is given by $\hat{E}^*(0.1493, 0.0078)$. To verify the Theorem 2.3.5, we find $K_{11} = r_0 - \delta_1 - 2\gamma N_e^* - \frac{\beta P_e^*}{(1+\beta N^*_e)^2} = -0.1113 < 0$ and $K_{22} = 0.0003 > 0$, which ensure that the asymptotic stability of co-existing state $\hat{E}^*(N_e^*, P_e^*)$. Phase portrait diagram (see Fig. 2.6(a)) demonstrates that the predator-prey model (2.2) is stable asymptotically at co-existing equilibrium state $\hat{E}^*(N_e^*, P_e^*)$ as we have chosen an initial point $(0.5, 0.3)$

and both the species moves around interior steady state $\hat{E}^*(0.1493, 0.0078)$ and ultimately goes to $\hat{E}^*$. The system (2.2) enter into the limit cycle behavior from stable one, for the value of prey birth rate r_0 gradually increases, which means that, for increasing the size of prey population, the predator have taken more time to handle the prey species. Thus, the magnitude of the prey species oscillation increases due to increasing size of the prey species. The Fig. 2.6(b) demonstrate the limit cycle oscillations around co-existing state $\hat{E}^*(0.1493, 0.0400)$ for $r_0 = 0.045$ and the other parameters value are same as in Fig. 2.6(a). In this case, the values of the coefficients of the characteristic equation (2.5) are $K_{11} = 0.000834 > 0$ and $K_{22} = 0.001559 > 0$, which does not satisfy the conditions for local asymptotically stability of $\hat{E}^*$ in the Theorem 2.3.5. As the values of K_{11} and K_{22} are both positive for $r_0 = 0.045$, the solutions of the system (2.2) are unstable, and this ensure the limit cycle oscillation around the co-existing equilibrium $\hat{E}^*(0.1493, 0.0400)$.
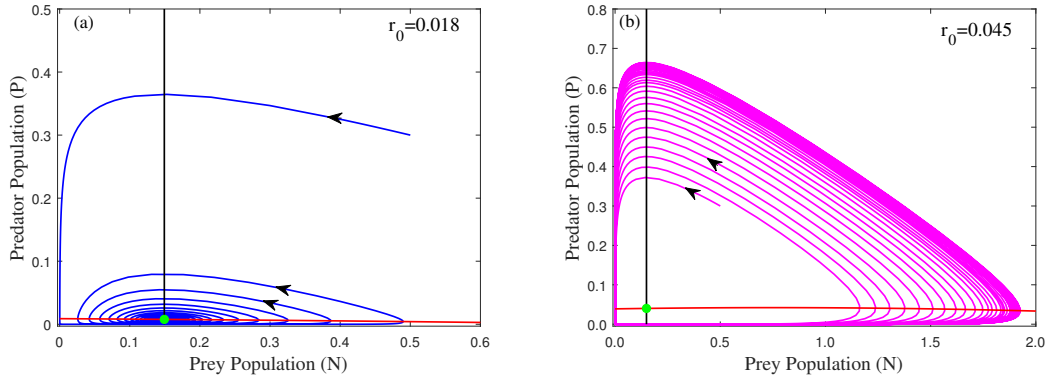
Figure 2.6: The phase portrait diagram of (2.2) around the co-existing singular point $\hat{E}^*$ (green filled circle) with initial values $[N(0), P(0)] = [0.5, 0.3]$. Black line represents the predator isocline, and the red curve represents the prey isocline. The subplot (a) shows the phase portrait diagram is stable asymptotically at $\hat{E}^*(0.1493, 0.0078)$ for $r_0 = 0.018$, and (b) the phase portrait diagram shows the limit cycle oscillation around $\hat{E}^*(0.1493, 0.0400)$ for $r_0 = 0.045$; the other parameters value are $\delta_1 = 0.01, \gamma = 0.01, \beta = 0.9, \xi = 0.5, \theta = 0.4$ and $\delta_2 = 0.05$.

Analytically, we have shown that the co-existing state $\hat{E}^*(N^*, P^*)$ for the system (2.2) experiences Hopf bifurcation with respect to the prey birth rate r_0. By numerical simulations, Fig. 2.7 exhibits that the predator-prey system (2.2) experiences Hopf bifurcation around the threshold values $r_0^* = 0.0330$. For the set of parameters value specified in this section, we ob-

tain $\frac{d}{dr_0}(Re(\lambda(r_0)))\mid_{r_0=r_0*} = 0.0694 > 0$. This indicates that the transvesality condition for Hopf bifurcation is verified. Hence, the co-existence steady state $\hat{E}^*(N_e^*, P_e^*)$ of the predator-prey system (2.2) is asymptotically stable for $r_0 < r_0^*$ and unstable for $r_0 > r_0^*$. It can also be noticed that the system (2.2) exhibits oscillatory behavior from the stable one, when the value of prey birth rate r_0 is increased gradually, and the high amplitude oscillation may leads to the crash of the species [111, 112]. Hence, the prey growth rate (r_0) has a critical role for the stability of the system (2.2).
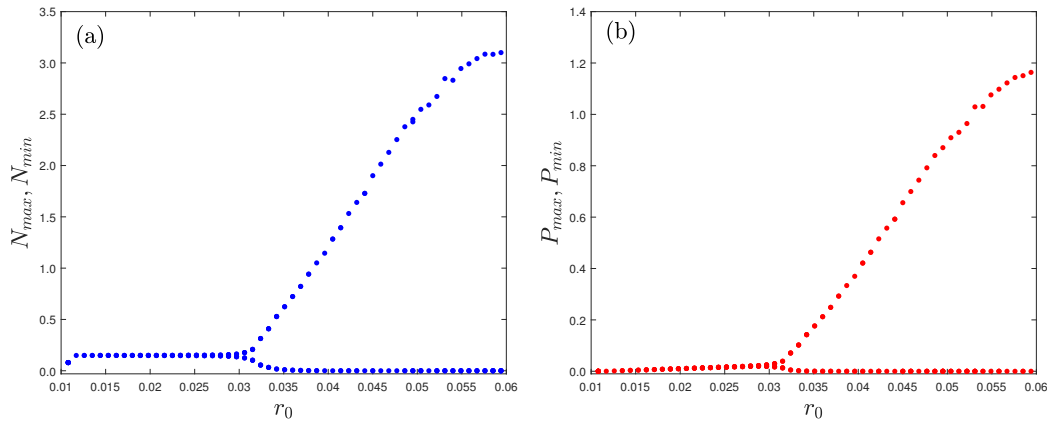
Figure 2.7: Bifurcation diagram with respect to the prey birth rate r_0 of the predator-prey system (2.2) with Holling type-II response function. Other parameters value are $\delta_1 = 0.01$,$\gamma = 0.01$, $\beta = 0.9$, $\xi = 0.5$, $\delta_2 = 0.05$ and $\theta = 0.4$.

In our study, we have not shown analytically that the bifurcation for the predator-prey system (2.2) with respect to the conversion coefficient θ and the intra-specific coefficient γ; here, we have numerically plotted the bifurcation figure for (2.2) with reference to the parameters θ and γ. The bifurcation figure for (2.2) with respect to θ have shown in the Fig. 2.8. Here, r_0 is predetermined at 0.07, and the rest of parameters are same as in the Fig. 2.7. The system (2.2) shows the limit cycle oscillation from equilibrium state as the bifurcation parameter θ increases. The system (2.2) experiences Hopf bifurcation around $\theta \approx 0.055$. The bifurcation diagram for the system (2.2) with reference to the intra-specific competition coefficient γ have shown in the Fig. 2.9. Here, r_0 is predetermined at 0.07, and the rest of parameters are same as in the Fig. 2.7. This bifurcation diagram shows that the model alter the stability from limit cycle behavior to equilibrium state as bifurcation parameter γ increases.
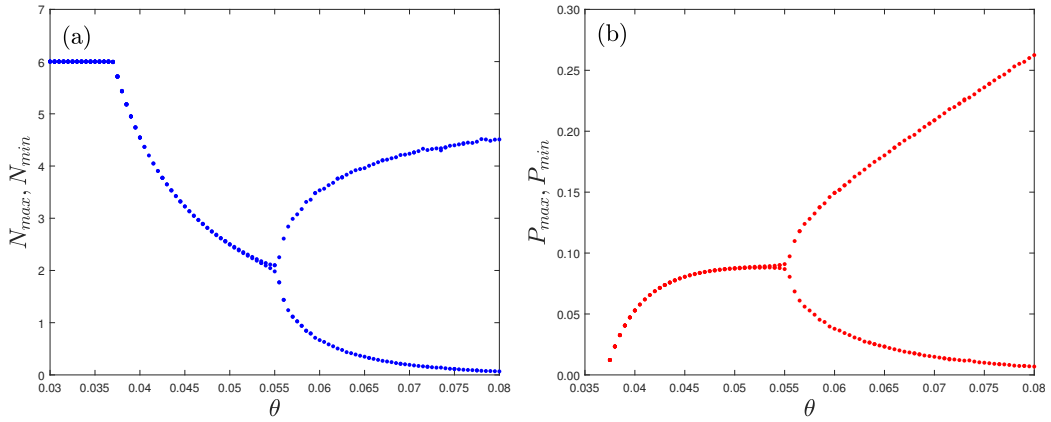
Figure 2.8: Bifurcation diagram with respect to conversion term θ for the predator-prey model (2.2) with Holling type-II response function. Rest of parameters: $r_0 = 0.07$, $\delta_1 = 0.01$,$\gamma = 0.01$, $\beta = 0.9$, $\xi = 0.5$ and $\delta_2 = 0.05$.
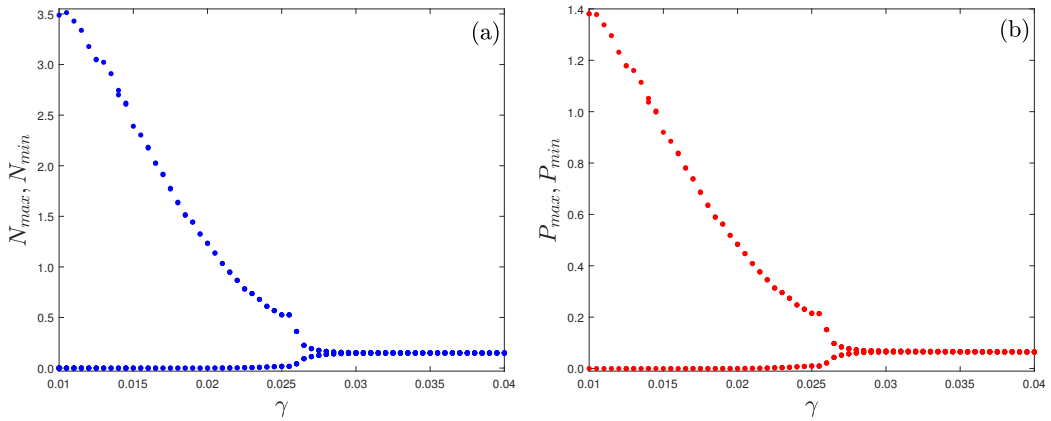
Figure 2.9: Bifurcation diagram with respect to intra-specific competition between prey species γ of predator-prey system (2.2) with Holling type-II response function. Rest of the parameters: $r_0 = 0.07$, $\delta_1 = 0.01$,$\beta = 0.9$, $\xi = 0.5$, $\theta = 0.4$ and $\delta_2 = 0.05$.

Again, the dynamics around the interior singular point of the Beddington-DeAngelis type predator-prey system (2.6) have shown in the Fig. 2.10. The system (2.6) is integrated using Runge-Kutta scheme with parameter set $\delta_1 = 0.01$,$\gamma = 0.01$, $\beta = 0.9$, $\xi = 0.5$, $\delta_2 = 0.05$, $\theta = 0.4$, $\varphi = 0.3$ and varies the prey birth rate r_0. For $r_0 = 0.018$, the predator-prey system (2.6) has one interior positive singular point $E_{BD}^*(0.1496, 0.0078)$. As shown in Table 2.2, we compute the value of $M_1 + M_4 = -0.0056$ and $M_1 M_4 - M_2 M_3 = 0.0002659$; therefore, $M_1 + M_4 < 0$ and $M_1 M_4 - M_2 M_3 > 0$.

This ensure the stability for the interior singular point for the predator-prey system (2.6). Phase portrait diagram for the Beddington-DeAngelis type prey-predator system (2.6) shown in the Fig. 2.10(a) demonstrate that the co-existing steady state is locally asymptotically stable. The Beddington-DeAngelis type prey-predator system (2.6) enter into the limit cycle behavior from stable one for increasing value of r_0. Also, the phase portrait Fig. 2.10(b) shows the limit cycle oscillation at an interior singular state $E_{BD}^*(0.1511, 0.0405)$ for $r_0 = 0.045$.
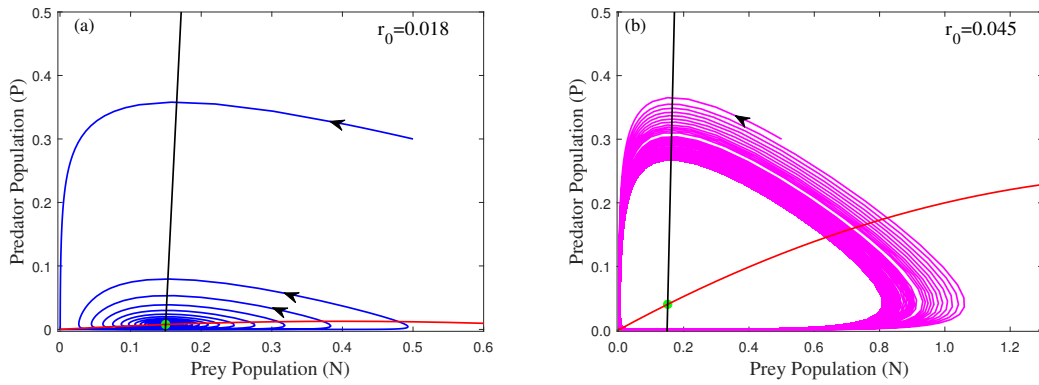
Figure 2.10: Phase portrait diagram of the predator-prey system (2.6) with Bedington-DeAngelis type response function at the coexisting singular point E_{BD}^* (green filled circle) with initial values $[N(0), P(0)] = [0.5, 0.3]$. Black line is the predator isocline and the red curve is the prey isocline. (a) $r_0 = 0.018$; (b) for $r_0 = 0.045$, and rest of the parameters are specified as $\delta_1 = 0.01$, $\gamma = 0.01$, $\beta = 0.9$, $\xi = 0.5$, $\theta = 0.4$, $\delta_2 = 0.05$, and $\xi = 0.30$.

The bifurcation diagram of the Beddington-DeAngelis type predator-prey system (2.6) with respect to growth rate r_0 for prey species, the conversion rate θ of prey biomass to predator biomass and the intra-specific competition rate γ are plotted numerically in the Figs. 2.11 - 2.13, respectively. From the bifurcation diagram of the Holling Type-II predator-prey system (2.2) and Baddington-DeAngelis type predator-prey system (2.6), it can be observed that we obtained similar kind of dynamics of the prey and predator species except the changes in the bifurcation point. The bifurcation diagram in the Fig. 2.11 represents that the predator-prey system (2.6) is asymptotically stable for lower critical value of prey birth rate r_0, and if r_0 crosses threshold value $r_0^c \approx 0.035$ the Beddington-DeAngelis type predator-prey system (2.6) shows limit cycle behavior or oscillating behavior. The bifurcation diagram for the Baddington-DeAngelis type predator-prey system (2.6) is shown in the Fig. 2.12 with respect to conversion parameter θ. Fig. 2.12 exhibits that

the system alter the stability from equilibrium state to limit cycle behavior as the bifurcation parameter θ increases. The bifurcation diagram shown in Fig. 2.13 of the Baddington-DeAngelis type predator-prey system (2.6) with respect to the intra-specific competition rate γ shows that the model alter the stability from limit cycle behavior to equilibrium state for increasing bifurcation term γ.
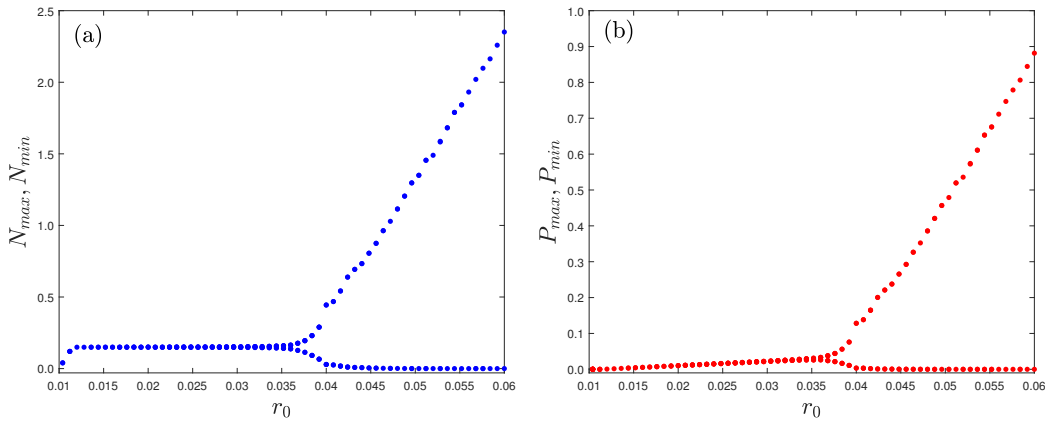
Figure 2.11: Bifurcation diagram with respect to birth rate of prey species r_0 of the predator-prey system (2.6) with Bedington-DeAngelis type response function. Other parameters value are specified as $\delta_1 = 0.01$, $\gamma = 0.01$, $\beta = 0.9$, $\xi = 0.5$, $\delta_2 = 0.05$, $\theta = 0.4$ and $\varphi = 0.30$.
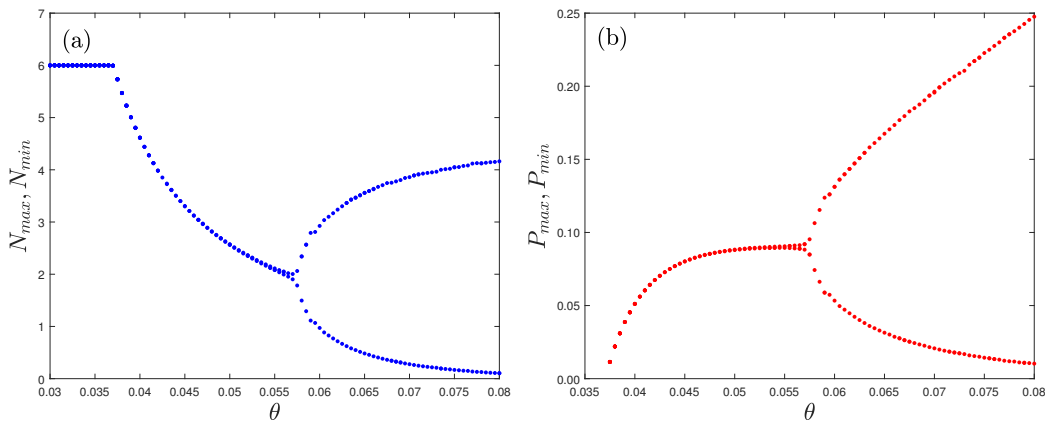
Figure 2.12: Bifurcation diagram with respect to conversion term θ for predator-prey system (2.6) with Bedington-DeAngelis type response function. Rest of parameters are $r_0 = 0.07$, $\delta_1 = 0.01$, $\gamma = 0.01$, $\beta = 0.9$, $\xi = 0.5$, $\delta_2 = 0.05$ and $\varphi = 0.30$.
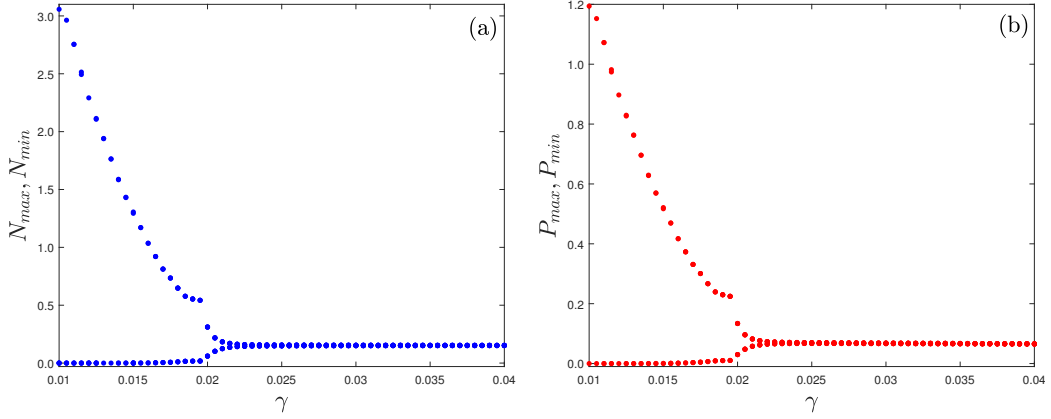
Figure 2.13: Bifurcation diagram with respect to intra-specific competition between prey species γ for predator-prey system (2.6) with Bedington-DeAngelis response function. Rest of parameters are specified as $r_0 = 0.07$, $\delta_1 = 0.01$, $\beta = 0.9$, $\xi = 0.5$, $\theta = 0.4$, $\delta_2 = 0.05$ and $\varphi = 0.30$.

Our predator-prey system (2.2) with Holling type-II response function undergoes transcritical bifurcation with respect to the prey growth rate r_0, which is plotted in the bifurcation diagram (in the Fig. 2.14), and the other parameters value are $\delta_1 = 0.01$, $\gamma = 0.01$, $\beta = 0.9$, $\xi = 0.5$, $\theta = 0.4$ and $\delta_2 = 0.05$. The bifurcating parameter r_0 varied from 0 to 0.04 and is plotted r_0 along $x-$axis equilibrium prey (left panel in Fig. 2.14) and predator (right panel in Fig. 2.14) density along the $y-$ axis. Black line represents the stable branch of the trivial equilibrium point $\hat{E}_0(0,0)$, blue dotted line represents the stable branch of the boundary equilibrium point $\hat{E}_1(\bar{N}_e, 0)$, and the green line represents the unstable branch of the boundary equilibrium point $\hat{E}_1(\bar{N}_e, 0)$. The red horizontal line (left panel) and the red oblique line (right panel) indicate the stable branch of the interior equilibrium point $\hat{E}^*(N_e^*, P_e^*)$, and the magenta line indicates the unstable branch of the interior steady state $\hat{E}^*(N_e^*, P_e^*)$. There is no stable branch of the boundary steady state $\hat{E}_1(\bar{N}_e, 0)$ in the plot of predator density (right panel in Fig. 2.14) as there is no predator density in the boundary equilibrium $\hat{E}_1(\bar{N}_e, 0)$. Both the prey and predator population oscillate in the blue shaded region.

Our predator-prey system (2.6) with Beddington-DeAngelis response function also undergoes transcritical bifurcation with respect to the prey growth rate r_0, which has been plotted in the bifurcation diagram (in the Fig. 2.15), and the other parameters value are $\delta_1 = 0.01$, $\gamma = 0.01$, $\beta = 0.9$, $\xi = 0.5$, $\theta = 0.4$, $\delta_2 = 0.05$ and $\varphi = 0.30$. The bifurcating parameter r_0 varied from 0 to 0.04 and is plotted r_0 along $x-$axis and equilibrium prey (left panel in Fig. 2.15) and predator (right panel in Fig. 2.15) density along

63
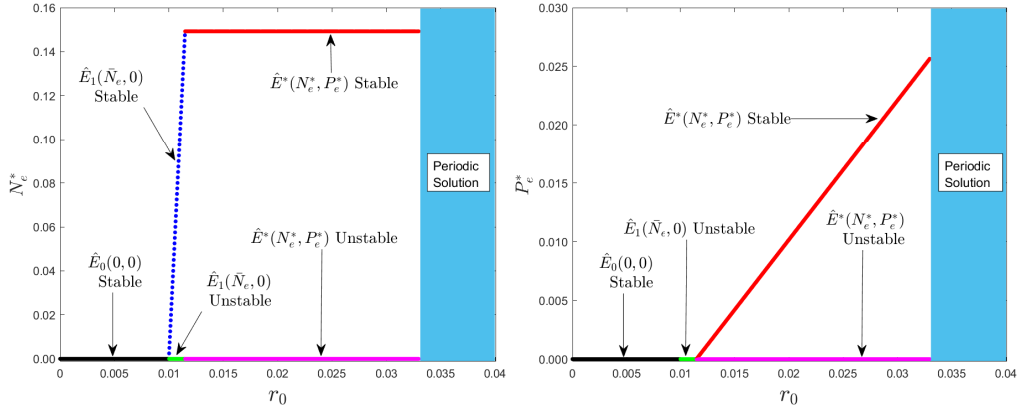
Figure 2.14: The transcritical bifurcation diagram with respect to the prey birth rate r_0 for the predator-prey system (2.2) with Holling type-II response function. Other parameters value are specified as $\delta_1 = 0.01$, $\gamma = 0.01$, $\beta = 0.9$, $\xi = 0.5$, $\theta = 0.4$, and $\delta_2 = 0.05$.

the $y-$ axis. Black line represents the stable branch of the trivial equilibrium point $E_{BD}^0(0,0)$, blue-dotted curve represents the stable branch of the boundary equilibrium point $E_{BD}^1(\hat{N}, 0)$, and the green line represents the unstable branch of the boundary equilibrium point $E_{BD}^1(\hat{N}, 0)$. Red curve indicates the stable branch of the interior equilibrium point $E_{BD}^*(\hat{N}^*, \hat{P}^*)$, and the magenta line indicates the unstable branch of the interior steady state $E_{BD}^*(\hat{N}^*, \hat{P}^*)$. There is no stable branch of the boundary steady state $E_{BD}^1(\hat{N}, 0)$ in the plot of the predator density (right panel in Fig. 2.15) as there is no predator density in the boundary equilibrium $E_{BD}^1(\hat{N}, 0)$. Both the prey and predator population oscillate in the blue shaded region. From the transcritical bifurcation for Holling type-II and Beddington DeAngelis type response function, we can conclude that density of prey species increases (see the read curve of Fig. 2.14 and Fig. 2.15) for Beddington-DeAngelis type response function. The red curve (left panel in Fig. 2.15) is increasing as the value of r_0 is increasing; that is, the density of prey species is increasing as the prey growth rate r_0 is increasing. To better understand the increasing pattern of prey species for Beddington-DeAngelis type response function, we put a portion of the red curve in the dash dotted box, which has been zoomed and plotted in the inset (left panel of Fig. 2.15).

By constructing suitable Lyapunov function, we have analytically shown that (see the Section 2.3.5) the co-existing steady state $\hat{E}^*(N_e^*, P_e^*)$ for the predator-prey system (2.2) is globally asymptotically stable for $\frac{\gamma}{\beta\xi} > P_e^*$. For the following parameters value $r_0 = 0.045$, $\delta_1 = 0.01$, $\gamma = 0.15$, $\beta = 0.9$,

64
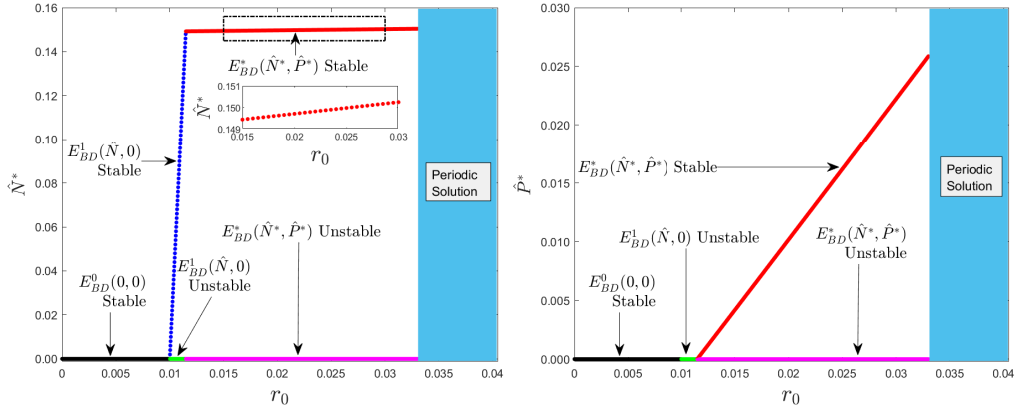
Figure 2.15: Bifurcation diagram with respect to the growth rate r_0 of the prey species for predator-prey model system (2.6) with Bedington-DeAngelis response function. Other parameters value are specified as $\delta_1 = 0.01$, $\gamma = 0.01$, $\beta = 0.9$, $\xi = 0.5$, $\theta = 0.4$, $\delta_2 = 0.05$ and $\varphi = 0.30$. The dash dotted box zoomed in the inset, which shows the increasing trend of the stable branch of the interior steady state $E^*_{BD}(\hat{N}^*, \hat{P}^*)$.

$\xi = 0.5$, $\theta = 0.4$ and $\delta_2 = 0.05$, we obtain the interior equilibrium is $\hat{E}^*(0.1493, 0.0151)$. Here, $\frac{\gamma}{\beta\xi} = 0.3333$ and $P^*_e = 0.0151$, so it can be verified that $\frac{\gamma}{\beta\xi} > P^*_e$ for the assumed set of parameters value. Therefore, the interior steady state $\hat{E}^*(0.1493, 0.0151)$ is globally asymptotically stable. Now, we have numerically integrated the predator-prey system (2.2) using Runge-Kutta scheme with the assumed parameters value and considered different initial values $(0.4, 0.1)$, $(0.2, 0.2)$, $(0.4, 0.1)$ and $(0.1, 0.3)$. The phase diagram of this solution is plotted in Fig. 2.16. All the solution trajectories for different initial values converges to an interior singular point $\hat{E}^*(0.1493, 0.0151)$. This numerically ensure that the interior steady state $\hat{E}^*$ for the model (2.2) is globally asymptotically stable.

2.7.2 Numerical simulations for the predator-prey system (2.13)

To obtain a better visualization of how different set of parameters value influence the dynamics of the system (2.13), we check the feasibility of our theoretical analysis regarding the existence of singular points and the corresponding stability conditions numerically, we also solve the model (2.13) to demonstrate different types of behavior. Most of the parameters value are obtained from Wang et al. [88]; Wang & Zou [90], and the rest of
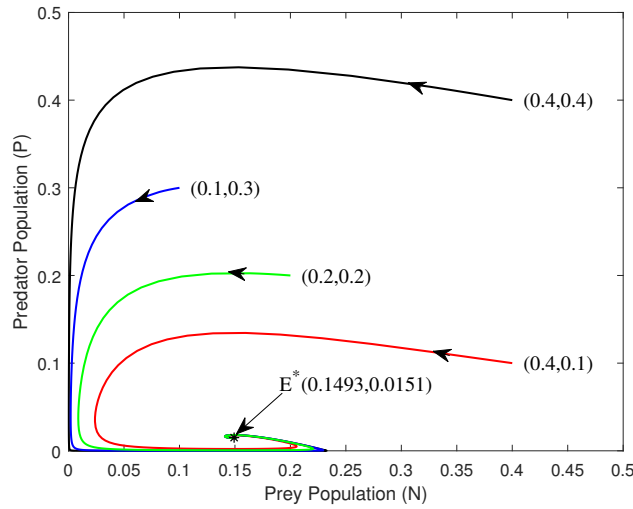
Figure 2.16: Interior singular point $\hat{E}^*(0.1493, 0.0151)$ for predator-prey system (2.2) is globally asymptotically stable with the parameters are specified as $r_0 = 0.045$, $\delta_1 = 0.01$, $\gamma = 0.15$, $\beta = 0.9$, $\xi = 0.5$, $\theta = 0.4$ and $\delta_2 = 0.05$. The initial values are shown within the bracket.

system parameters are hypothetical/estimated. Fig. 2.4 exhibits how the mutual position of the nullclines for the predator-prey model (2.13) affected by the birth rate r_0 of prey species.

Fig. 2.17 demonstrates the effect of fear due to predator population on the co-existing equilibrium point E^*. Fig. 2.17 represents the dependence of the level of fear α and the minimum cost of fear η due to predator species on the birth rate of the prey species r_0, when computed at an interior singular point E^*. It can be observed that the prey species get more fear of the spreading of predator population due to a higher level of the cost of fear, this leads to the larger equilibrium value of the total prey population N which, in turn, results in a maximum level of application of resources, which shows to the decrease in a equilibrium level of the prey birth rate r_0 and a lower level of the minimum cost of fear η. It must be observed, however, that this fear effect is only important for lower level of α and more increase in the level of fear stemming from perceiving predator population does not result in any important changes in the birth rate of prey species. To gain a better perception into the effects of fear on the interior equilibrium E^*, we plot the Fig. 2.18 for the equilibrium values of the prey and predator species depending on the prey birth rate r_0 and the conversion coefficient θ. As anticipated, for larger values of r_0 and θ corresponding to the larger

values of the equilibrium state of prey species, and a lower value of the predator species. For a specific choice of parameters value in this diagram, the interior equilibrium state become stable for any combination of r_0 and θ values observed.
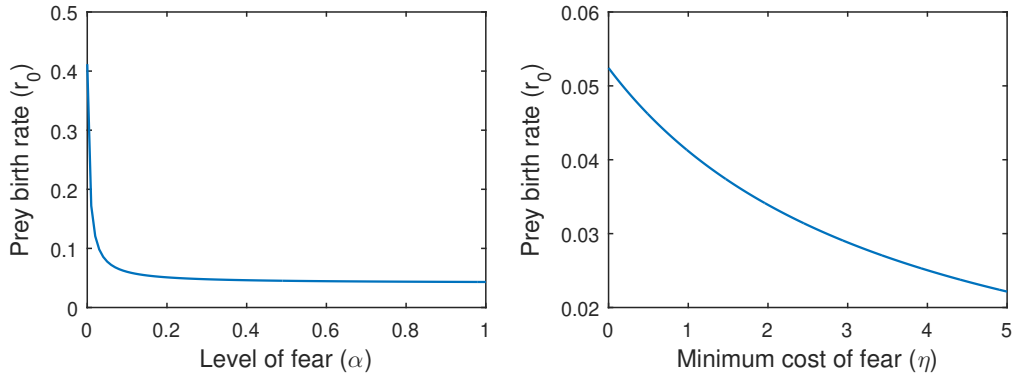
Figure 2.17: The figure shows the dependence of the level of fear α and the minimum cost of fear η on the birth rate r_0 of prey population at the interior singular point $E^*(N^*, P^*)$. The set of parameters value are the same as in Fig. 2.4.

Fig. 2.19 shows the variability of equilibrium densities of prey and predator species in presence of fear effect. In Fig. 2.19, we have plotted four subfigures to better understand the change of equilibrium densities with respect to prey growth rate r_0 and the conversion coefficient θ between prey and predator population. From the Figs. 2.19(a) and 2.19(b) it can be noticed that for lower birth rate r_0 of prey population does not alter the steady state density of prey population N^* (see Fig. 2.19(a)), however it increases the steady state density of P^* (see Fig. 2.19(b)). It can be noted that the expression of the equilibrium density of prey is $\delta_2/(\theta\beta - \xi\delta_2)$, which is independent of prey species growth rate r_0. Thus, the prey equilibrium density N^* remain constant with respect to r_0. This scenario can be interpreted as the well-known top-down control of prey species due to predator species, in which the prey steady state density does not depend on the birth rate of prey species. From Figs. 2.19(c) and 2.19(d) it can be noticed that the conversion coefficient θ plays a crucial role for the equilibrium densities of prey and predator population. The Fig. 2.19(c) shows that the prey equilibrium density N^* decreases continuously due to increasing value of the conversion coefficient θ whereas the Fig. 2.19(d) represents that the predator equilibrium density P^* increases and become a
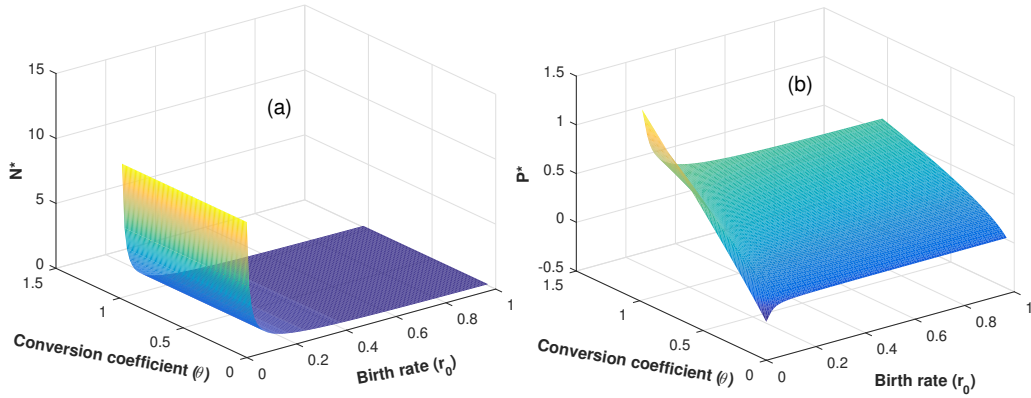
Figure 2.18: The figure shows the dependence of the equilibrium state values of the prey and predator population on the birth rate r_0 of prey populations and the conversion coefficient θ. The set of parameters value are specified in the Fig. 2.4.

predator steady state for increasing value of of the conversion coefficient θ.

Fig. 2.20 shows how stability of the biologically feasible equilibrium state depends on the relation among r_0 and two rates of positive constants, namely death rate of predators δ_2 and the Michaelis-Menten constant ξ. One observes that for very small value of r_0, the extinct steady state E_0 is locally asymptotically stable for $r_0 < \delta_1$, which has been observed in the green shaded region. The red colored region designates the local asymptotic stability of the predator extinct equilibrium point E_1. Form the Fig. 2.20 it can be noticed that for larger value of death rate δ_2 of predator species can be extinct, which is a good agreement with the reality as the higher mortality rate always harmful for any kind of species. The blue colored region designates the stability region for E^* in which all the two populations can exist together. The black shaded region designates the instability of all the three biologically feasible equilibrium points. Here the black shaded region is denoted by $E_0^u \cup E_1^u \cup E^{*u}$ in which the three equilibrium points E_0, E_1 and E^* loses their stability. The parameters value for this simulations are same as in the Fig. 2.4.

The most important parameters characterizing the dynamics of predator-prey relationship is the growth rate r_0 of prey population and the predators natural mortality rate δ_2, Fig. 2.21 and Fig. 2.22 represents the Hopf bifurcation diagram for an interior equilibrium state E^* depending on r_0

68
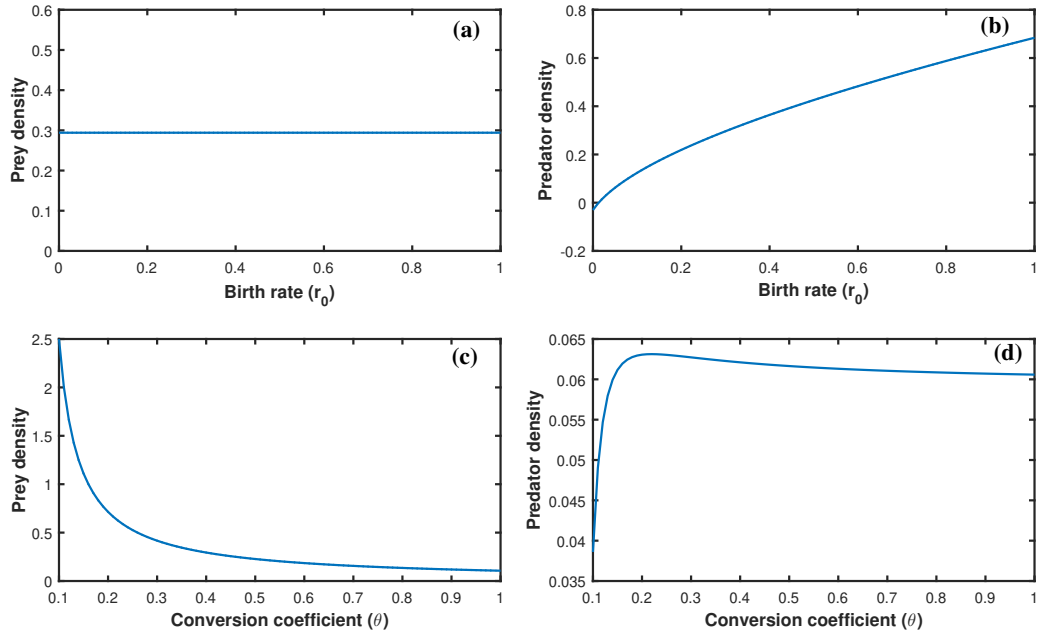
Figure 2.19: Change of the equilibrium points for the system (2.13) with respect to the birth rate r_0 of prey population and conversion coefficient θ. The set of parameters are the same as in the Fig. 2.4.

and δ_2, respectively. For very small values of r_0, and in agreement with the Theorem 2.6.1, the trivial singular point E_0 is stable and the predator extinct singular point E_1 is not biologically feasible. In agreement with Theorem 2.6.2, if E_1 is locally asymptotically stable then E_0 is unstable and the interior singular point E^* is biologically meaningful. If we increase the value of r_0, the trivial singular point E_0 loses its stability and a stable interior equilibrium state occurs. For higher values of r_0, E^* becomes unstable via Hopf bifurcation shows a stable periodic behavior. Fig. 2.21 also demonstrates minima and maxima of this solution, indicating the amplitude of oscillations itself increases for r_0, with the lower values for the species on a periodic orbit being very near to zero. From Fig. 2.21 it can be noticed that, when r_0 crosses the threshold value $r_0^{[c]} \approx 0.036$, steady state values of prey and predator populations are divided into maximum and minimum of periodic solution and interior steady state become unstable in nature. It can be noted that for sufficiently lower values for the prey growth rate r_0, it is possible to attain the situation in which the prey species can live without fear from predators. Fig. 2.22 represent the Hopf bifurcation diagram for the system (2.13) with respect to natural mortality rate of predator species δ_2 and other parameters are same as in the Fig. 2.4. We
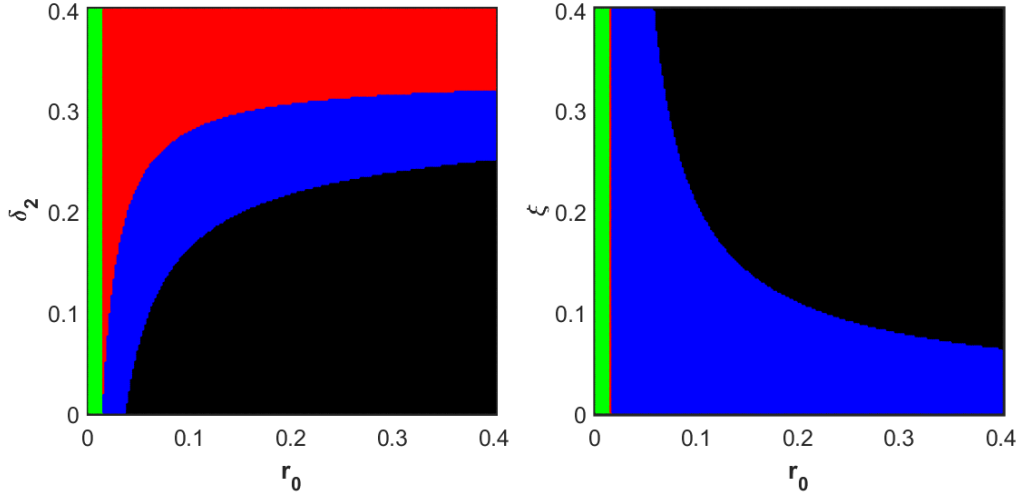
Figure 2.20: The figure shows the stability regions for the extinct singular point $E_0(0,0)$, predator-free singular point $E_1(3.5,0)$ and the co-existing singular point $E^*(0.0294, 0.0531)$ in the parameter spaces $r_0 - \delta_2$ and $r_0 - \xi$, respectively. The green shaded region is the stability region for the trivial singular point E_0, the red shaded region represents the stability region for the axial singular point E_1, the blue shaded region designates the stability region for the interior singular point E^*, whereas the black shaded region is the unstable region for the union of all the equilibrium points, which can be denoted by $E_0^u \cup E_1^u \cup E^{*u}$. We varied the parameters r_0, δ_2 and ξ from 0 to 0.4 with the initial conditions $[N(0), P(0)] = [0.5, 0.3]$ and other parameters are same as in the Fig. 2.4.

noticed that the model (2.13) alters the stability from limit cycle behavior to the equilibrium state as the bifurcating parameter increase through the bifurcation point ($\delta_2^{[c]} \approx 0.085$). For $\delta_2 < 0.085$, the model (2.13) exhibits limit cycle oscillations and the system enter into the stable equilibrium state with $\delta_2 > 0.085$ through Hopf bifurcation. Both the Fig. 2.21 and 2.22 clearly demonstrates that the prey growth rate r_0 and predators death rates acts as the control parameter.

Fig. 2.23 represents various dynamical regimes which can be demonstrated for the system (2.13), beginning with a stable predator free equilibrium state for sufficiently lower value of prey growth rate r_0. For sufficiently larger prey growth rate r_0, we notice that the alteration to a stable interior equilibrium state, with oscillatory approach to this equilibrium state, demonstrating that the maximal characteristic eigenvalues are actually a

Figure 2.21: The figure represents the Hopf bifurcation diagram for the interior singular point E^* of the system (2.13) considering r_0 as a bifurcation parameter and other parameters are specified in the Fig. 2.4. We plotted the steady state values of the predator-prey population and the maximum/minimum of the periodic solutions whenever it exists.

pair of imaginary eigenvalues with real part negative, that is increasing with r_0. As r_0 passes the critical value for a Hopf bifurcation stated in the Theorem 2.6.6, the model system (2.13) undergoes on a stable periodic solution. The corresponding phase diagram also plotted in the Fig. 2.23(c) for locally asymptotic stable (at $r_0 = 0.03$ in blue color), Fig. 2.23(d) for periodic solution (at $r_0 = 0.05$ in red color) and Fig. 2.23(e) for periodic solution with large amplitude (at $r_0 = 0.07$ in black color). Fig. 2.24 demonstrates various dynamical regimes which can be demonstrated by the system (2.13), beginning with a large periodic solution for the interior steady for sufficiently small value of predator mortality rate δ_2. For sufficiently larger predators death rate δ_2, we notice that the transition to a periodic solution for interior equilibrium state, with a stable approach to this equilibrium point, indicating the maximal characteristic eigenvalues are actually a pair of imaginary eigenvalues with real part negative become a stable steady state, which is increasing with δ_2. The corresponding phase diagram also plotted in the Fig. 2.24(c) for large periodic oscillations (at $\delta_2 = 0.03$ in black color), Fig. 2.24(d) for periodic oscillation (at $\delta_2 = 0.06$ in red color) and Fig. 2.24(e) for locally asymptotically stable solution (at $r_0 = 0.09$ in blue color).

Considering the parameters value as specified in the Fig. 2.4, we have computed the values of $L'(r_0{}^*)$ and $a(r_0{}^*)$ with $r_0{}^* = 0.5$ and we get $\Lambda = 0.4718 > 0$ and $a(r_0{}^*) = -0.02210 < 0$. So, according to the Theorem 2.6.7, the direction of Hopf bifurcation is supercritical. The phase portrait with the same parameters value have been plotted in Fig. 2.25 with three different initial points. Two initial points are inside the limit cycle and one
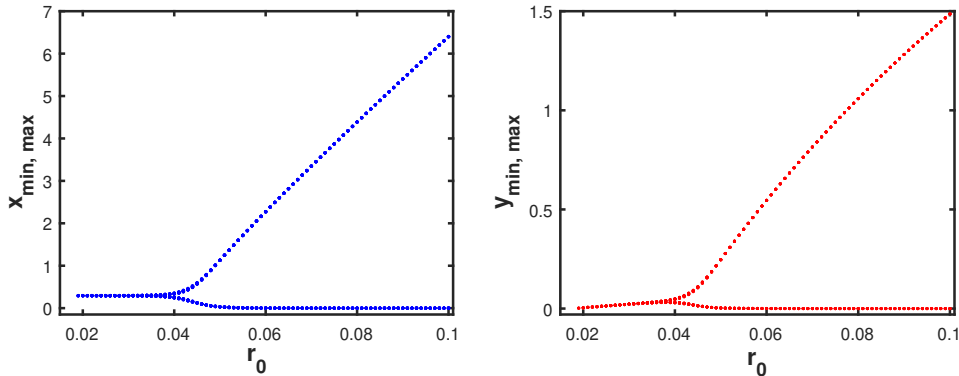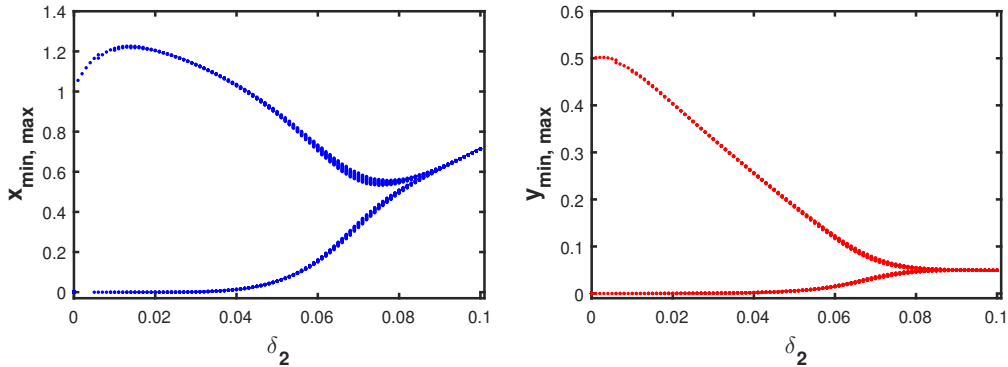
Figure 2.22: The figure represents the Hopf bifurcation diagram for the interior singular point E^* of the model (2.13) considering δ_2 as a bifurcation parameter and other parameters are specified in the Fig. 2.4. We plotted the steady state values of the predator-prey population and the maximum/minimum of the periodic solutions whenever it exists.

initial point from the outside of the limit cycle. For all the initial points, the periodic solutions converges to the limit cycle. Hence the direction of the Hopf bifurcation is supercritical.

2.8   Discussion

In this chapter, we investigate a very simple mathematical model for predator-prey system with three different types of functional response and then introduced the effect of fear for prey population due to predator population. First, a comparative study have been made in this chapter by considering Holling type-I, Holling type-II and Beddington-DeAngelis type response function of the predator-prey system (2.1). The stability conditions for different biologically feasible equilibrium points by considering three different types of response function is presented in the Table 2.2. Our results demonstrate that birth suppression of prey population by predator population lower the density of equilibrium point of predator population. Moreover, we noticed that above the critical value of prey birth rate r_0^* of the interplay between prey and predator population, the system produces limit cycle oscillations. Thus, the prey growth rate play a critical role to destabilize the predator-prey dynamics through Hopf bifurcation (see Fig. 2.7). Analytically, we have computed the global asymptotic stability condition for the interior equilibrium point of the prey-predator system (2.2) by formulating an appropriate Lyapunov functional. The co-existing singular point is glob-
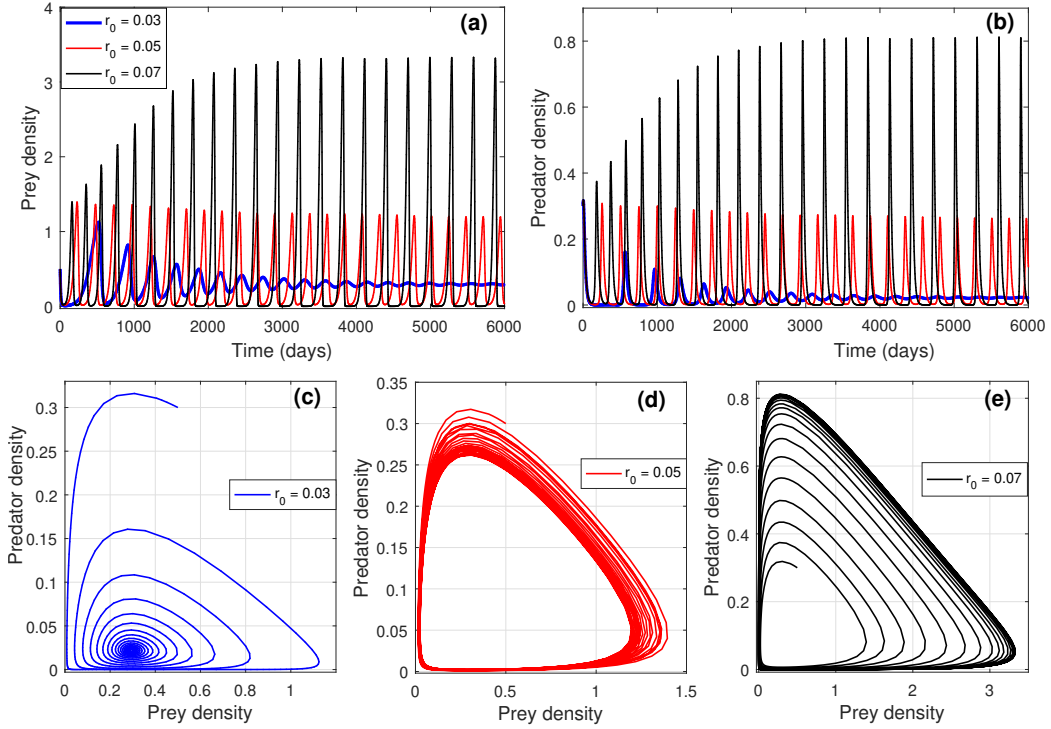
Figure 2.23: Numerical solution for the model (2.13) with parameters value as specified in the Fig. 2.4: a locally asymptotically stable interior steady state ($r_0 = 0.03$, blue color); periodic solutions around interior equilibrium state ($r_0 = 0.05$, red) and periodic oscillations with large amplitude around the interior equilibrium state ($r_0 = 0.07$, black).

ally asymptotically stable if $\frac{\gamma}{\alpha\beta} > P_e^*$, that is, the predator species is lower than the ratio of intra-specific competition between prey population and the product of attack rate and handling time to capture the prey population by predator population. For the hypothetical parameter set, we have shown numerically the condition for global asymptotic stability of the co-existing singular point E^*. Thus, the Theorem 2.3.6 is verified numerically.

We have explored the bifurcation scenario of the system (2.2) and (2.6) by varying the birth rate r_0 of prey species, the conversion coefficient θ of prey biomass to predator biomass, and the intra-specific competition γ between prey species. Analytically, we have shown that the system (2.2) experiences a Hopf bifurcation around $\hat{E}^*(N_e^*, P_e^*)$ with respect to the prey birth rate at $r_0 = r_0^*$. Bifurcation diagram with respect to another two parameters θ and γ have been plotted by numerical simulations and found that both the system (2.2) and (2.6) undergoes from limit cycle oscillations to equilibrium
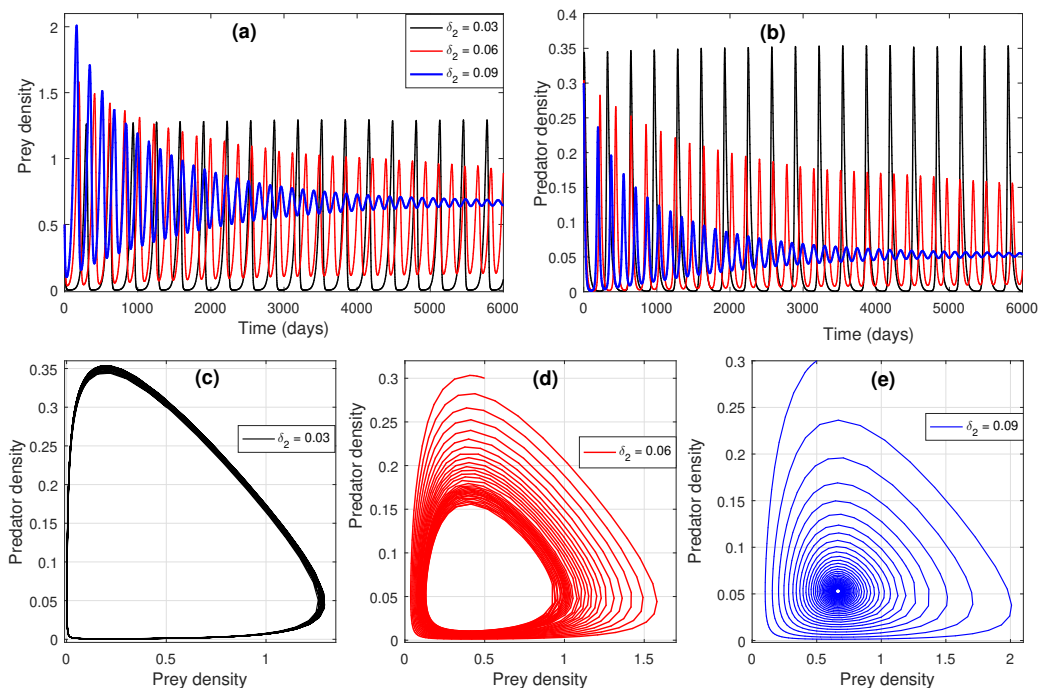
Figure 2.24: Numerical solution for the model (2.13) with parameters value as specified in the Fig. 2.4: periodic oscillations with large amplitude around the interior equilibrium state ($\delta_2 = 0.03$, black color); periodic solutions around interior equilibrium state ($\delta_2 = 0.06$, red) and a stable solution around the interior equilibrium state ($\delta_2 = 0.09$, black).

state situation as the parameter γ increases. Again both the system (2.2) and (2.6) undergoes equilibrium state to limit cycle oscillation as the conversion coefficient θ increases. Thus, the dynamical behavior of (2.6) remains same as the system (2.2) only the position of the bifurcation points has been changed. We performed direction and stability for Hopf bifurcation of the predator-prey system (2.2). The main result of the direction of Hopf bifurcation is presented in the Theorem 2.4.1.

Again, we have investigated the dynamics of predator-prey system by introducing the affect of fear for predator population on prey population with Holling type II functional response. Theoretically, we performed local asymptotic stability analysis of the biologically meaningful singular points, Hopf bifurcation analysis, existence and uniqueness of limit cycle, direction and stability of Poincare-Andronov Hopf bifurcation. Analytical findings demonstrate that there exists a locally asymptotically stable non-negative steady state if the growth rate r_0 of prey population is not high enough to maintain fluctuations. Thus, in this situation both the prey and predator
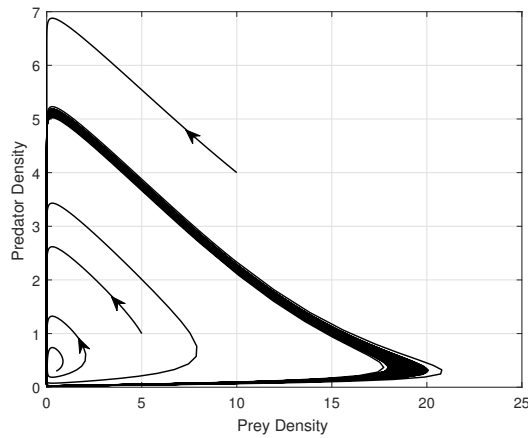
Figure 2.25: Numerical solutions for the model (2.13) with parameters value as specified in the Fig. 2.4 and $r_0 = 0.5$. Periodic solution around the interior equilibrium $E^*(0.2941, 0.4181)$ shows supercritical Hopf bifurcation.

species eventually tend to produce non-negative constants, no matter how sensitive the prey population is to potential dangers the predator population. For larger prey growth rate r_0, we investigate that the transition to a locally asymptotically stable interior equilibrium, with oscillatory approach to this equilibrium point, indicating that the maximum characteristics eigenvalues are actually a pair of imaginary eigenvalues with real part negative, which is increasing with high level of fear (see Fig. 2.21). Therefore, the cost of fear has an impact to stabilize the predator-prey interactions by ruling out periodic oscillatory behavior. This suggests a new interesting technique to ignore the "paradox of enrichment" in ecological system. It is biologically as well as ecologically meaningful and in good agreement with the reality, because after certain level of fear, the prey population become perceive and show sign of habituation. The model system under consideration exhibits that the periodic oscillations can persist for the low level of prey birth rate r_0 (see the bifurcation Fig. 2.21, the time series solution and phase-portrait diagram Fig. 2.23). We investigate the situations for the occurrence of Hopf bifurcation and the conditions for investigating the direction of Poincare-Andronov Hopf bifurcation, which demonstrate that the cost of fear will not only influence the occurrence of Hopf bifurcation but also alter the direction of Poincare-Andronov Hopf bifurcation, in agreement with Theorem 2.6.7. We have verified that the Hopf bifurcation in the model introducing the cost of fear can be both subcritical or supercritical according to the sign of the coefficient of $a(r_0^*)$ (see the Theorem 2.6.7).

We performed some numerical simulations to investigate the potentiality that the cost of fear can play a pivotal role in predator-prey system. We observed that the prey growth rate r_0 and natural mortality rate for predators δ_2 can exhibit bistability situation by creating multiple limit cycles via subcritical Hopf bifurcation. By increasing the prey growth rate r_0 may cause the alter in the direction of Poincare-Andronov Hopf bifurcation, according to the sign of the coefficient of $a(r_0^*)$ from supercritical to subcritical. From the bifurcation diagram (see Fig. 2.22) and the numerical solution (see Figs. 2.24(a)-(e)) it can be observed that for increasing the predator mortality rate δ_2 there is a transition to a stable periodic oscillation from a stable interior singular point, indicating the characteristic eigenvalues are actually a pair of imaginary roots with real part negative from the eigenvalues are real and negative, which is increasing with δ_2. Due to fear, the prey birth rate r_0 develops rich dynamical behavior including bi-stability, in which the solutions tend to a periodic oscillatory behavior from stable steady state depending on the initial size of the population. Similarly, due to fear the predator mortality rate δ_2 develops rich dynamical behavior including bi-stability, in which the solutions tend to a stable equilibrium state from periodic oscillatory behavior depending on the initial size of the population. Model simulations also exhibit that the prey species are less sensitive to perceive predation risk when the prey growth rate r_0 become larger, irrespective of how other parameters value alter. Furthermore, the prey species would be more willing to exhibit anti-predator defence when the rate of predation become larger. Model simulations regarding the cost of fear represent that the outcomes we have obtained in this manuscript, sincerely hope that it will be helpful for further study/investigation.

Chapter 3

An eco-epidemiological model with the impact of fear [†]

3.1 Introduction

In mathematical biology, the study of ecological and epidemiological issues simultaneously known as eco-epidemiology. The ecological and epidemiological fields were merged and formulated a predator–prey model by Anderson and May [15] in the year 1986. After this pioneering research work, the study of the prey-predator system with infected prey has grown enormously in the last three decades [16, 18–20, 101]. The predation of prey by the predator population is omnipresent in nature and in presence of the predators the system alters physiology and behavior of the prey population [2, 113].

Thus, in presence of predators, the prey population becomes more vigilant and moves away from suspected predator population. Prey population assesses predation risk, and they choose to abandon the original high-risk habitat though it is rich in food and the prey population relocate to low-risk habitats [4]. Such a foraging activity of the prey reduces the chance of infection among susceptible prey by lowering the contact with the infected prey. Thus, the fear for predators on the prey population has a high impact on the dynamics in an eco-epidemiological model. As far as knowledge goes, nobody has experimentally studied the effect of fear in an eco-epidemiological system. Thus, theoretical studies have drawn attention to study the impact of fear in controlling infection in a predator-prey system but limited studies of an eco-epidemiological model with disease in prey populations has incorporated the effect of fear [29, 30, 114].

[†]A considerable part of this chapter has been published in **Chaos**, Volume 32, Article ID 083126, 2022.

In this chapter, we investigated a eco-epidemiological system with disease in prey and incorporated the effect of fear on prey due to predator population. We assumed that the prey population can only be infected by a disease, and the predator population will not be infected by the disease through feeding on the infected prey population. Infected prey cannot reproduce, and the infected prey will not recover. We also assumed that due to the effect of fear, the reproduction of the prey population reduces and lowers the foraging activity of prey. The lower forging activity will reduce the contact between the infected and susceptible prey, which consequently reduces the rate of infection. The quantitative analysis is carried out for the eco-epidemiological system which includes positivity, boundedness, uniform persistence, local stability and bifurcation analysis. Extensive numerical simulations are carried out to validate our analytical findings.

3.2   The model

In this section, we have formulated a three species predator-prey system with fear effect. The prey population is assumed to be susceptible to disease and the total prey population is divided into two classes, namely susceptible prey (N) and infected prey (I). We assumed that in absence of any infection and predator population, the susceptible prey population follows a logistic growth. The logistic growth of susceptible prey population has been divided into three parts, which are the birth rate r_0, the natural death rate δ_1 and the decay rate γ due to intra-species competition. Thus, the growth of susceptible prey population (N) can be expressed as

$$\frac{dN}{dt} = r_0 N - \delta_1 N - \gamma N^2.$$ (3.1)

The pioneering work by Zanette et al. [7] shows that the effect of fear can reduces the growth of the prey population. Thus, we have modified our predator-prey system (3.1) by multiplying the reproduction term by fear function $f(\alpha_f, \eta_f, P)$ to account the effect of fear and the system (3.1) leads to the following form:

$$\frac{dN}{dt} = r_0 f(\alpha_f, \eta_f, P) N - \delta_1 N - \gamma N^2,$$ (3.2)

where P is the density of predator, α_f and η_f represents the level of fear and the minimum level of fear, respectively. Now, we assumed that the disease spreads only among the prey population through the law of mass action and the disease is not genetically inherited. In presence of the disease, the

prey population is classified into two distinct classes, namely susceptible prey population (N) and infected prey population (I). At any time t, total prey biomass is $T(t) = N(t) + I(t)$. We assumed that the susceptible prey populations are capable of reproducing with logistic growth, while the infected prey population are unable to reproduce [115] and the infected prey population do not recover or become immune. Predator populations are not infected though feeding on infected prey populations. We also assumed that fear has no effect on infected prey population as the infected prey populations are vulnerable. Then the system (3.2) leads to the following form:

$$\frac{dN}{dt} = r_0 f(\alpha_f, \eta_f, P)N - \delta_1 N - \gamma N^2 - a_1 NI,$$

$$\frac{dI}{dt} = a_1 NI - \delta_2 I,$$

where a_1 is the rate of infection from susceptible prey to infected prey and δ_2 is the natural mortality rate of infected prey population. Now, we assumed that the predator population cannot be differentiated into the susceptible and infected prey and they consumed both susceptible and infected prey populations at the rates $g(N)$ and $h(I)$, respectively where $g(N)$ and $h(I)$ are known as functional responses. Using the above assumptions, we can express the following eco-epidemiological model as

$$\begin{aligned}
\frac{dN}{dt} &= r_0 f(\alpha_f, \eta_f, P)N - \delta_1 N - \gamma N^2 - a_1 NI - g(N)P, \\
\frac{dI}{dt} &= a_1 NI - h(I)P - \delta_2 I, \\
\frac{dP}{dt} &= \theta_1 h(I)P + \theta_2 g(N)P - \delta_3 P,
\end{aligned} \tag{3.3}$$

where θ_2 is the conversion rate of susceptible prey to predator biomass, θ_1 is the conversion rate of infected prey to predator biomass and δ_3 is the natural mortality rate of predator population. The interaction among the population of our proposed model is depicted in Fig. 3.1. Since the infected prey population is vulnerable to the diseases, the handling time can be neglected to capture the infected prey population, but the predator population needs sufficient handling time to capture healthy susceptible prey species. These phenomena are introduced in system (3.3) by using Holling type I and II response functions [16]. We have considered $h(I) = a_2 I$ and $g(N) = \beta N/(1 + \xi N)$, where a_2, β and ξ are non-negative constants. Here, $h(I) = a_2 I$ is a monotonic increasing function and $g(N) = \beta N/(1 + \xi N)$ is a monotonic increasing and bounded function. Sarkar & Khajanchi [116] have introduced a fear function of the form $f(\alpha_f, \eta_f, P) = \left[\eta_f + \frac{\alpha_f(1 - \eta_f)}{\alpha_f + P}\right]$,

which gives significant results in terms of ecology, and also used the same fear function in our present study. Here, α_f represents the level of fear, η_f indicates the minimum level of fear, $\eta_f \in [0,1]$ and $f(0, \eta_f, P) = \eta_f$, that is, the susceptible prey (N) population always remains under a minimum level of fear (η_f) in presence of predator species. Again, $f(\alpha_f, \eta_f, 0) = 1$; that is, in absence of predator population the fear function has no effect on the growth of susceptible prey species. Since $\lim_{P \to \infty} f(\alpha_f, \eta_f, P) = \eta_f$, which implies that even if predator populations infinitely increase, the susceptible prey populations are habituated with the fear of predators and the susceptible prey will stress under a minimum level of fear η_f. Also, $\lim_{\alpha_f \to \infty} f(\alpha_f, \eta_f, P) = 1$, which implies that after a certain level of fear on prey species, it has no effect due to the physiological impact when the susceptible prey is habituated with the fear of predators. The ecological description of the parameters and their numerical values used for numerical simulations are given in Table 3.1. By incorporating all model assumptions and putting the functional responses, we obtain the following system of ordinary differential equations:

$$
\begin{aligned}
\frac{dN}{dt} &= r_0 N \left[\eta_f + \frac{\alpha_f(1 - \eta_f)}{\alpha_f + P} \right] - \delta_1 N - \gamma N^2 - a_1 NI - \frac{\beta NP}{1 + \xi N}, \\
\frac{dI}{dt} &= a_1 NI - a_2 IP - \delta_2 I, \\
\frac{dP}{dt} &= \theta_1 a_2 IP + \frac{\theta_2 \beta NP}{1 + \xi N} - \delta_3 P,
\end{aligned}
\tag{3.4}
$$

with non-negative initial conditions: $N(0) = N_0 \geq 0$, $I(0) = I_0 \geq 0$ and $P(0) = P_0 \geq 0$.

3.3 Positivity, boundedness and uniformly persistent

3.3.1 Positive invariance

The biomass of a population cannot be negative at any time t. Thus, in this section, we investigate the positivity of the solutions of system (3.4) with non-negative initial conditions. From the ecological perspective, the positivity of the predator-prey system (3.4) interprets that the prey and the predators are biologically well-behaved. To do this, we use the following proposition.

Proposition 3.3.1. *The solutions of (3.4) with non-negative initial conditions remain non-negative for all finite time.*
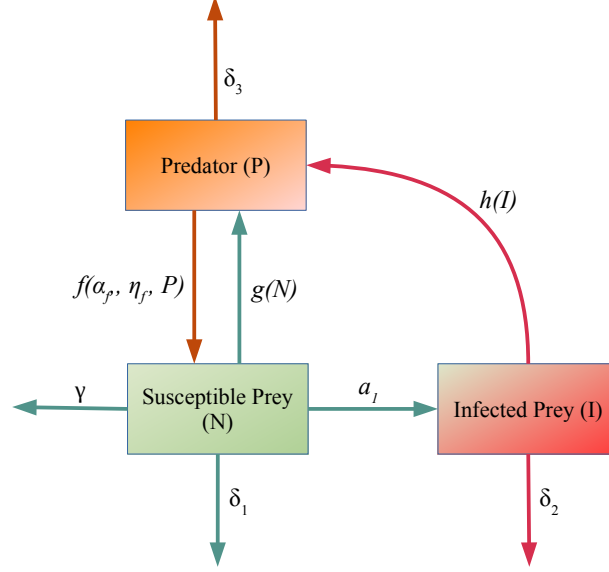
Figure 3.1: Schematic diagram represents the biological mechanism of the predator-prey system with disease in prey that influences the formulation of the model (3.3), where $P(t)$, $N(t)$ and $I(t)$ indicates the predator biomass, prey biomass and infected prey biomass, respectively.

Proof. The right-hand side of the system of equations (3.4) is continuous function of dependent variable t. After integration, we obtain

$$
\begin{aligned}
N(t) &= N(0) \exp \left(\int_0^t \left[r_0 \left\{ \eta_f + \frac{\alpha_f (1 - \eta_f)}{\alpha_f + P(s)} \right\} - \delta_1 \right. \right. \\
&\quad \left. \left. - \gamma N(s) - a_1 I(s) - \frac{\beta P(s)}{1 + \xi N(s)} \right] ds \right), \\
I(t) &= I(0) \exp \left(\int_0^t \left[a_1 N(s) - a_2 P(s) - \delta_2 \right] ds \right), \\
P(t) &= P(0) \exp \left(\int_0^t \left[\theta_1 a_2 I(s) + \frac{\theta_2 \beta N(s)}{1 + \xi N(s)} - \delta_3 \right] ds \right).
\end{aligned}
$$

From the above expressions, it is obvious that $N(t)$, $I(t)$ and $P(t)$ remains positive for all future time if they initiate from an interior initial point of

$$
\mathbf{R}_+^3 = \{ [N(t), I(t), P(t)] : N(t) > 0, I(t) > 0, P(t) > 0 \} .
$$

Therefore, $\mathbf{R}_+^3$ is the positive invariant for the system (3.4). $\qquad \square$

3.3.2 Boundedness

The boundedness for the solutions of (3.4) implies that none of the population will grow unboundedly or exponentially at any time t. Due to the limited resources, the biomass of each population remains bounded.

Proposition 3.3.2. *All the solutions of (3.4) with non-negative initial conditions $(N_0, I_0, P_0) \in \mathbf{R}_+^3$ are uniformly bounded.*

Proof. We assume that $\theta_1 \leq \theta_2$ and define a function

$$W(t) = N(t) + I(t) + \frac{1}{\theta_2}P(t). \tag{3.5}$$

Taking the time derivative of (3.5) along the solution trajectory of (3.4) is given by

$$\frac{dW(t)}{dt} = r_0 N \left[\eta_f + \frac{\alpha_f(1 - \eta_f)}{\alpha_f + P} \right] - \delta_1 N - \gamma N^2$$

$$- a_2 \left(1 - \frac{\theta_1}{\theta_2} \right) IP - \delta_2 I - \frac{\delta_3}{\theta_2}P,$$

$$\leq r_0 N \left[\eta_f + (1 - \eta_f) \right] - \delta_1 N - \gamma N^2 - \delta_2 I - \frac{\delta_3}{\theta_2}P,$$

$$= r_0 N - \delta_1 N - \gamma N^2 - \delta_2 I - \frac{\delta_3}{\theta_2}P.$$

By assuming $0 < \rho < \min\left\{ \delta_1, \delta_2, \frac{\delta_3}{\theta_2} \right\}$, we have

$$\frac{dW(t)}{dt} + \rho W(t) \leq r_0 N - (\delta_1 - \rho)N - \gamma N^2 - (\delta_2 - \rho)I - \left(\frac{\delta_3}{\theta_2} - \rho \right) P,$$

$$\leq r_0 N - \gamma N^2,$$

$$\leq \frac{r_0^2}{4\gamma},$$

where $r_0^2/4\gamma$ is the maximum value of $r_0 N - \gamma N^2$. Consider $\phi = \frac{r_0^2}{4\gamma} > 0$, the above equation becomes

$$\frac{dW(t)}{dt} + \rho W(t) \leq \phi.$$

Due to the theory of differential inequality for $W(t)$, we have

$$0 < W(N, I, P) \leq \frac{\phi}{\rho} \left(1 - e^{-\rho t} \right) + W(N(0), I(0), P(0))e^{-\rho t},$$

and if $t \to \infty$, then $0 < W < \frac{\phi}{\rho}$. Hence, all the solutions of (3.4), which initiated in $\mathbf{R}_+^3$, are confined in the region $S = \{(N, I, P) \in \mathbf{R}_+^3 : W = \frac{\phi}{\rho} + \epsilon, \text{ for } \epsilon > 0\}$. $\qquad \square$

3.3.3 Uniformly persistent

In terms of ecology, the uniform persistency of a system ensure the long-term survival of the population without depending on the initial population size. Analytically, uniform persistency of (3.4) is defined in the following definition.

Definition 3.3.1. *System (3.4) is said to be uniformly persistent if there exist positive constants m_1, m_2, m_3, M_1, M_2 and M_3 that do not depend on the initial conditions, and any solution $[N(t), I(t), P(t)]$ of (3.4) satisfies the following inequality:*

$$m_1 \leq \liminf_{t \to \infty} N(t) \leq \limsup_{t \to \infty} N(t) \leq M_1,$$

$$m_2 \leq \liminf_{t \to \infty} I(t) \leq \limsup_{t \to \infty} I(t) \leq M_2,$$

$$m_3 \leq \liminf_{t \to \infty} P(t) \leq \limsup_{t \to \infty} P(t) \leq M_3.$$

Theorem 3.3.1. *System (3.4) is uniformly persistent if $\gamma \delta_3 > \theta_2 \beta (r_0 - \delta_1) > 0$ and $r_0(\alpha_f + \eta_f M_3) > (\alpha_f + M_3)(a_1 \delta_1 + a_1{}^2 M_2 + \gamma a_2 M_3 + \gamma \delta_2)$ where M_2 and M_3 are defined in the proof.*

Proof. From (3.4), we have

$$\frac{dN}{dt} \leq N(r_0 - \delta_1 - \gamma N),$$

$$\frac{dI}{dt} \leq I(a_1 N - a_2 P),$$

$$\frac{dP}{dt} \leq P(\theta_1 a_2 I + \theta_2 \beta N - \delta_3).$$

Let M_1, M_2 and M_3 be the positive roots of the system of equations,

$$N(r_0 - \delta_1 - \gamma N) = 0, \ I(a_1 N - a_2 P) = 0,$$
$$P(\theta_1 a_2 I + \theta_2 \beta N - \delta_3) = 0.$$

Then

$$M_1 = \frac{r_0 - \delta_1}{\gamma}, \ M_2 = \frac{\gamma \delta_3 - \theta_2 \beta (r_0 - \delta_1)}{\gamma \theta_1 a_2} \text{ and}$$

$$M_3 = \frac{a_1(r_0 - \delta_1)}{\gamma a_2}.$$

Due to the standard comparison theorem [37, 117], we have from the above inequalities

$$\limsup_{t\to\infty} N(t) \le M_1, \ \limsup_{t\to\infty} I(t) \le M_2, \ \limsup_{t\to\infty} P(t) \le M_3. \qquad (3.6)$$

Here, M_1 and M_3 will be positive if $r_0 - \delta_1 > 0$ and M_2 will be positive if $\gamma\delta_3 > \beta\theta_2(r_0 - \delta_1)$. Hence, M_1, M_2 and M_3 will be positive if $\gamma\delta_3 > \beta\theta_2(r_0 - \delta_1) > 0$. Similarly, from the system of equations (3.4), we have

$$\frac{dN}{dt} \ge N\left[r_0\left\{\eta_f + \frac{\alpha_f(1-\eta_f)}{\alpha_f + M_3}\right\} - \delta_1 - a_1 M_2 - \beta P - \gamma N\right],$$

$$\frac{dI}{dt} \ge I(a_1 N - a_2 M_3 - \delta_2),$$

$$\frac{dP}{dt} \ge P(\theta_1 a_2 I - \delta_3).$$

Let m_1, m_2 and m_3 be the positive roots of the system of equations,

$$N\left[r_0\left\{\eta_f + \frac{\alpha_f(1-\eta_f)}{\alpha_f + M_3}\right\} - \delta_1 - a_1 M_2 - \beta P - \gamma N\right] = 0,$$
$$I(a_1 N - a_2 M_3 - \delta_2) = 0, \ P(\theta_1 a_2 I - \delta_3) = 0.$$

Then

$$m_1 = \frac{a_1(r_0 - \delta_1) + \gamma\delta_2}{\gamma a_1}, \ m_2 = \frac{\delta_3}{\theta_1 a_2},$$

$$m_3 = \frac{r_0(\alpha_f + \eta_f M_3) - (\alpha_f + M_3)(a_1\delta_1 + a_1{}^2 M_2 + \gamma a_2 M_3 + \gamma\delta_2)}{\beta a_1(\alpha_f + M_3)}.$$

Due to the standard comparison theorem [37, 117], we have from the above inequalities,

$$\liminf_{t\to\infty} N(t) \ge m_1, \ \liminf_{t\to\infty} I(t) \ge m_2, \ \liminf_{t\to\infty} P(t) \ge m_3. \qquad (3.7)$$

Here, m_1 and m_2 will be positive if $r_0 - \delta_1 > 0$ and m_3 will be positive if $r_0(\alpha_f + \eta_f M_3) > (\alpha_f + M_3)(a_1\delta_1 + a_1{}^2 M_2 + \gamma a_2 M_3 + \gamma\delta_2)$. Hence, from (3.6) and (3.7), we obtain that the system (3.4) is uniformly persistent. $\square$

3.4 Equilibria and their stability

3.4.1 Existence of equilibria

Biologically feasible equilibrium points of (3.4) are the non-negative solutions $(\tilde{N}, \tilde{I}, \tilde{P})$ of the system

$$r_0 N \left[\eta_f + \frac{\alpha_f(1 - \eta_f)}{\alpha_f + P} \right] - \delta_1 N - \gamma N^2 - a_1 N I - \frac{\beta N P}{1 + \xi N} = 0,$$

$$a_1 N I - a_2 I P - \delta_2 I = 0,$$

$$\theta_1 a_2 I P + \frac{\theta_2 \beta N P}{1 + \xi N} - \delta_3 P = 0,$$

in the non-negative octant $\mathbf{R}^3_+ = \big\{ [N(t), I(t), P(t)] : N(t) \geq 0, I(t) \geq 0, P(t) \geq 0 \big\}$. System (3.4) possesses five biologically feasible equilibrium points in $\mathbf{R}^3_+$, namely

(i) the trivial equilibrium $E_0(0, 0, 0)$;

(ii) the equilibrium point in which only susceptible prey exists $E_1(N_1, 0, 0)$, where $N_1 = \frac{r_0 - \delta_1}{\gamma}$; the equilibrium $E_1(N_1, 0, 0)$ is feasible for $r_0 > \delta_1$;

(iii) predator-free equilibrium $E_2(N_2, I_2, 0)$, where $N_2 = \frac{\delta_2}{a_1}$ and $I_2 = \frac{a_1(r_0 - \delta_1) - \gamma \delta_2}{a_1^2}$; the equilibrium $E_2(N_2, I_2, 0)$ is feasible for $r_0 > \delta_1 + \frac{\gamma \delta_2}{a_1}$;

(iv) infected prey-free equilibrium $E_3(N_3, 0, P_3)$, where $N_3 = \frac{\delta_3}{\theta_2 \beta - \xi \delta_3}$ and P_3 is the positive root(s) of

$$l_1 P^2 + l_2 P + l_3 = 0,$$

where

$$l_1 = \frac{\beta}{1 + \xi N_3},$$

$$l_2 = \delta_1 - r_0 \eta_f + \gamma N_3 + \frac{\alpha_f \beta}{1 + \xi N_3},$$

$$l_3 = \alpha_f(\delta_1 + \gamma N_3 - r_0),$$

and $P_3 = \frac{-l_2 + \sqrt{l_2^2 - 4 l_1 l_3}}{2 l_1}$. The equilibrium $E_3(N_3, 0, P_3)$ is feasible for $0 < \theta_2 \beta - \xi \delta_3 < \frac{\gamma \delta_3}{r_0 - \delta_1}$ with $\xi < \frac{\theta_2 \beta}{\delta_3}$ and $r_0 > \delta_1$; and

(v) interior equilibrium $E^*(N^*, I^*, P^*)$ where $N^* = \frac{\delta_2 + a_2 P^*}{a_1}$, $I^* = \frac{\delta_3}{\theta_1 a_2} - \frac{\beta\theta_2}{\theta_1 a_2}\left[\frac{\delta_2 + a_2 P^*}{a_1 + \xi(\delta_2 + a_2 P^*)}\right]$ and P^* is the positive root of the equation

$$P^3 + \tau_1 P^2 + \tau_2 P + \tau_3 = 0, \tag{3.8}$$

where $\tau_1 = K_1/K_0$, $\tau_2 = K_2/K_0$ and $\tau_3 = K_3/K_0$ with

$$
\begin{aligned}
K_0 &= \gamma\xi a_2{}^3\theta_1, \\
K_1 &= \gamma\theta_1 a_2\left(\xi a_2\delta_2 + \alpha_f\xi a_2{}^2 + a_1 a_2 + \xi a_2\delta_2\right) \\
&\quad + \xi a_1 a_2{}^2\theta_1\delta_1 + \xi a_1{}^2 a_2\delta_3 + \beta a_1{}^2 a_2\theta_1 \\
&\quad - \xi\eta_f r_0 a_1 a_2{}^2\theta_1 - \beta a_1{}^2 a_2\theta_2, \\
K_2 &= a_1 a_2\theta_1\delta_1\left(\alpha_f\xi a_2 + a_1 + \xi\delta_2\right) + \gamma a_2\theta_1\left(a_1\delta_2 + \xi\delta_2{}^2\right. \\
&\quad \left. + \alpha_f a_1 a_2 + 2\alpha_f\xi a_2\delta_2\right) + a_1{}^2\delta_3\left(\alpha_f\xi a_2 + a_1 + \xi\delta_2\right) \\
&\quad + \alpha_f\beta a_1{}^2 a_2\theta_1 - \beta a_1{}^2\theta_2\left(\alpha_f a_2 + \delta_2\right) \\
&\quad - r_0 a_1 a_2\theta_1\left(\alpha_f\xi a_2 + \eta_f a_1 + \xi\eta_f\delta_2\right), \\
K_3 &= \left(a_1 + \xi\delta_2\right)\left(a_1 a_2\theta_1\delta_1\alpha_f + a_2\theta_1\gamma\alpha_f\delta_2 + \alpha_f a_1{}^2\delta_3\right. \\
&\quad \left. - r_0 a_1 a_2\theta_1\alpha_f\right) - \alpha_f\beta a_1{}^2\theta_2\delta_2.
\end{aligned}
$$

The number of positive roots of (3.8) can be determined by the sign of the coefficients of τ_1, τ_2 and τ_3 and the sign of the quantities of Π_1, Π_2, Π_3 obtained from Sturm's sequence, where $\Pi_1 = \tau_2\tau_1 - 9\tau_3$, $\Pi_2 = 2\tau_1{}^2 - 6\tau_2$ and $\Pi_3 = 2\tau_1\left(\frac{\Pi_1}{\Pi_2}\right) - 3\left(\frac{\Pi_1}{\Pi_2}\right)^2 - \tau_2$ [118].

Theorem 3.4.1. *System (3.4) will have at least one interior equilibrium point $E^*(N^*, I^*, P^*)$ if $N^* < \frac{\delta_3}{\beta\theta_2 - \xi\delta_3}$, $a_1 > 0$, a_2 and δ_2 both cannot be zero.*

Proof. If $E^*(N^*, I^*, P^*)$ is the interior equilibrium point, then $N^* = \frac{\delta_2 + a_2 P^*}{a_1}$, $I^* = \frac{\delta_3}{\theta_1 a_2} - \frac{\beta\theta_2}{\theta_1 a_2}\left[\frac{\delta_2 + a_2 P^*}{a_1 + \xi(\delta_2 + a_2 P^*)}\right]$ and P^* is the positive root of equation (3.8). The number of positive root(s) of the equation (3.8) depends on the sign of τ_1, τ_2 and τ_3 and the sign of quantities Π_1, Π_2 and Π_3. Table 3.2 gives the details of the existence of positive roots of the cubic equation (3.8).

Now, assuming the existence of at least one positive root of (3.8), the interior equilibrium $E^*(N^*, I^*, P^*)$ will be feasible if $N^* > 0$ and $I^* > 0$. Here, $N^* = \frac{\delta_2 + a_2 P^*}{a_1}$ and $P^* > 0$; therefore $N^* > 0$ if $a_1 > 0$, a_2 and δ_2 both can not be zero. Again, $I^* > 0$ implies $N^* > \frac{\delta_3}{\beta\theta_2 - \xi\delta_3}$. Here $a_1 > 0$ interprets that the rate of infection must be positive to exist in the endemic (or interior) equilibrium. $\square$

The nullclines of (3.4) are the surfaces

$$f_1 \equiv r_0 \left[\eta_f + \frac{\alpha_f(1 - \eta_f)}{\alpha_f + P} \right] - \delta_1 - \gamma N - a_1 I - \frac{\beta N P}{1 + \xi N} = 0,$$

$$f_2 \equiv a_1 N - a_2 P - \delta_2 = 0,$$

$$f_3 \equiv \theta_1 a_2 I + \frac{\theta_2 \beta N}{1 + \xi N} - \delta_3 = 0,$$

and the $I - P$ coordinate plane (that is, $N = 0$), the $N - P$ coordinate plane (that is, $I = 0$) and the $N - I$ coordinate plane (that is, $P = 0$) in the NIP-space. The nullcline surfaces $f_1 = 0$, $f_2 = 0$ and $f_3 = 0$ are plotted in Fig. 3.2 by red, blue and green color, respectively. The equilibrium points of (3.4) are the point of intersections of the nullcline surfaces. Coordinate planes are also the nullcline surfaces of the system (3.4). To show the interior equilibrium point, we have plotted the nullcline surfaces, which are not in the coordinate planes. The red surface is the susceptible prey nullcline, the blue surface is the infected prey nullcline and the green surface is the predator nullcline. The parameters value used to plot Fig. 3.2(a) are listed in Table 3.1. The parameters value for Fig. 3.2(b) are the same as in Fig. 3.2(a) except $\delta_3 = 0.3$. Here, we are mainly interested to find the non-negative equilibrium points and therefore, the nullcline surfaces are limited to positive octant only. The surfaces $f_1 = 0$ and $f_2 = 0$ intersect along the red curve, the surfaces $f_2 = 0$ and $f_3 = 0$ intersect along the green curve and the black curve is the intersection of the surfaces $f_1 = 0$ and $f_3 = 0$. The interior equilibrium $E^*(1.1247, 0.2452, 0.1718)$ is the point of intersection of the red, green and black curves. The interior equilibrium E^* has been shown by the solid red circle in Fig. 3.2(a). The trivial equilibrium $E_0(0, 0, 0)$ is shown by the solid black circle in Fig. 3.2(a). The susceptible prey only equilibrium $E_1(3.6420, 0.0, 0.0)$ lies on the N-axis and shown by the solid green circle in Fig. 3.2(a). The predator-free equilibrium $E_2(0.1429, 2.4994, 0)$ lies on the $N - I$ plane and is shown by a solid blue circle in Fig. 3.2(a). The infected prey-free equilibrium $E_3(0.0811, 0.0, 0.0268)$ lies on the $N - P$ plane and is shown by a solid cyan circle in Fig. 3.2(b).
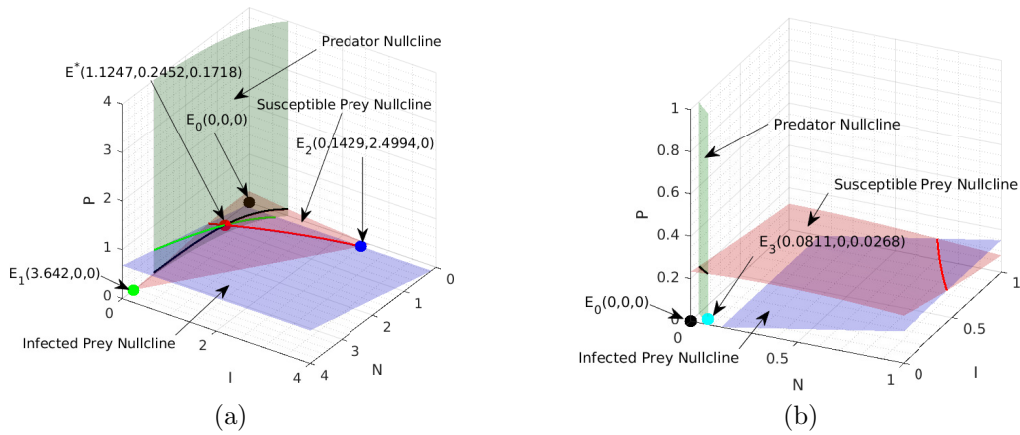
Figure 3.2: The biologically feasible equilibrium points of (3.4) are the point of intersections of the nullcline surfaces in the N-I-P-space. To show the interior equilibrium point, we have plotted the nullcline surfaces that are not in the coordinate planes. In the phase plot, the red surface represents the susceptible prey nullcline, the blue surface indicates the infected prey nullcline and the green surface determines the predator nullcline. The susceptible prey nullcline surface and the infected prey nullcline surface intersect along the red curve, the infected prey nullcline surface and the predator nullcline surface intersect along the green curve and the black curve determines the intersection of the susceptible prey nullcline surface and the predator nullcline surface. Interior equilibrium point $E^*(1.1247, 0.2452, 0.1718)$ is the intersection of the red, green and black curves (shown by a solid red circle), respectively. The parameters value for subfigure (a) are listed in Table 3.1; for subfigure (b), $\delta_3 = 0.3$ and other parameters value are the same as in subfigure (a).

Table 3.1: *Biological description of system parameters with their units/dimension and numerical values for the system (3.4).*

Par.	Biological meaning	Units/dimension	Values	Source
N	Density of susceptible prey population	No. per unit area	2.00	Assumed
I	Density of infected prey population	No. per unit area	1.50	Assumed
P	Density of predator population	No. per unit area	1.25	Assumed
r_0	Natural growth rate of susceptible prey	Time^{-1}	1.836	Assumed
δ_1	Natural mortality rate of susceptible prey	Time^{-1}	0.015	[116]
γ	Decay rate of susceptible prey due to intra-species competition	[No. per unit area]$^{-1}$Time^{-1}	0.5	Assumed
a_1	Force of infection between susceptible and infected prey	[No. per unit area]$^{-1}$Time^{-1}	0.7	[119]
β	Rate of predation of susceptible prey	[No. per unit area]$^{-1}$Time^{-1}	4.0	[119]
ξ	Handling time	[No. per unit area]$^{-1}$	1.0	[119]
a_2	Rate of predation of infected prey	[No. per unit area]$^{-1}$Time^{-1}	4.0	[119]
δ_2	Natural mortality rate of infected prey	Time^{-1}	0.1	[119]
θ_1	Conversion rate of susceptible prey to predator biomass	Dimensionless	0.9	[119]
θ_2	Conversion rate of infected prey to predator biomass	Dimensionless	1.0	[119]
δ_3	Natural mortality rate of predator	Time^{-1}	3.0	[119]
η_f	Cost of minimum fear	Dimensionless	0.1	[116]
α_f	Level of fear	No. per unit area	0.2	[116]

3.4.2 Local stability analysis

In this section, we shall investigate the local asymptotic stability of all the biologically feasible steady states. To study the local stability of (3.4), we computed the Jacobian matrix around each of the steady states. The Jacobian matrix at any point (N, I, P) is given by

$$J_E = \begin{bmatrix} F_N & F_I & F_P \\ G_N & G_I & G_P \\ H_N & H_I & H_P \end{bmatrix},$$

where

$$F_N = r_0 \left[\eta_f + \frac{\alpha_f(1 - \eta_f)}{\alpha_f + P} \right] - \delta_1 - 2\gamma N - a_1 I - \frac{\beta P}{(1 + \xi N)^2},$$

$$F_I = -a_1 N, \quad F_P = -\frac{r_0 \alpha_f(1 - \eta_f)N}{(\alpha_f + P)^2} - \frac{\beta N}{1 + \xi N},$$

$$G_N = a_1 I, \quad G_I = a_1 N - a_2 P - \delta_2, \quad G_P = -a_2 I,$$

$$H_N = \frac{\beta \theta_2 P}{(1 + \xi N)^2}, \quad H_I = \theta_1 a_2 P,$$

$$H_P = \theta_1 a_2 I + \frac{\theta_2 \beta N}{1 + \xi N} - \delta_3.$$

Theorem 3.4.2. *The trivial equilibrium point $E_0(0,0,0)$ is always unstable.*

Proof. The eigenvalues of the Jacobian matrix around $E_0(0,0,0)$ are $r_0 - \delta_1$, $-\delta_2$ and $-\delta_3$. The equilibrium point $E_0(0,0,0)$ is locally asymptotically stable if $r_0 - \delta_1 < 0$; that is, $r_0 < \delta_1$ as the other two eigenvalues are negative. In terms of ecology, $r_0 < \delta_1$ implies that the growth rate of susceptible prey is less than the natural death rate of the susceptible prey, which is impossible. Hence, the trivial equilibrium $E_0(0,0,0)$ is always unstable. $\square$

Theorem 3.4.3. *The equilibrium $E_1(N_1, 0, 0)$ is locally asymptotic stable if* $0 < \frac{r_0 - \delta_1}{\gamma} < \min\left\{ \frac{\delta_2}{a_1}, \frac{\delta_3}{\theta_2\beta - \xi\delta_3} \right\}.$

Proof. The eigenvalues of the Jacobian matrix at the equilibrium $E_1(N_1, 0, 0)$ are $\lambda_1 = \delta_1 - r_0$, $\lambda_2 = \frac{a_1(r_0 - \delta_1) - \gamma\delta_2}{\gamma}$ and $\lambda_3 = \{\theta_2\beta(r_0 - \delta_1) - \gamma\delta_3 - \xi\delta_3(r_0 - \delta_1)\} / \{\gamma + \xi(r_0 - \delta_1)\}$. Now, $E_1(N_1, 0, 0)$ will be locally asymptotically stable if all the eigenvalues are negative or have negative real parts. Thus, $\lambda_1 < 0$, $\lambda_2 < 0$ and $\lambda_3 < 0$ implies that $0 < \frac{r_0 - \delta_1}{\gamma} < \min\left\{ \frac{\delta_2}{a_1}, \frac{\delta_3}{\theta_2\beta - \xi\delta_3} \right\}$ with $r_0 > \delta_1$ and $\xi < \frac{\theta_2\beta}{\delta_3}$. $\square$

Note: If $E_1(N_1, 0, 0)$ is locally asymptotically stable, then the predator-free equilibrium $E_2(N_2, I_2, 0)$ does not exist.

Theorem 3.4.4. *The predator-free equilibrium $E_2(N_2, I_2, 0)$ is locally asymptotically stable if $\phi_1 > 0$, $\phi_3 > 0$ and $\phi_1\phi_2 - \phi_3 > 0$, where ϕ_1, ϕ_2 and ϕ_3 are defined in the proof.*

Proof. To investigate the local asymptotic stability of the predator-free equilibrium point $E_2(N_2, I_2, 0)$, we compute the Jacobian matrix around the equilibrium $E_2(N_2, I_2, 0)$ is given by

$$\lambda^3 + \phi_1\lambda^2 + \phi_2\lambda + \phi_3 = 0, \tag{3.9}$$

where

$$
\begin{aligned}
\phi_1 &= \delta_1 + \delta_2 + \delta_3 + 2\gamma N_2 + a_1 I_2 - r_0 - a_1 N_2 \\
&\quad - \theta_1 a_2 I_2 - \frac{\theta_2 \beta N_2}{1 + \xi N_2}, \\
\phi_2 &= a_1{}^2 I_2 N_2 + \left(r_0 + a_1 N_2 - \delta_1 - \delta_2 - a_1 I_2 \right. \\
&\quad \left. - 2\gamma N_2 \right)\left(\theta_1 a_2 I_2 + \frac{\theta_2 \beta N_2}{1 + \xi N_2} - \delta_3 \right) \\
&\quad + (a_1 N_2 - \delta_2)(r_0 - \delta_1 - 2\gamma N_2 - a_1 I_2), \\
\phi_3 &= \left(\delta_3 - \theta_1 a_2 I_2 - \frac{\theta_2 \beta N_2}{1 + \xi N_2} \right)\left[a_1{}^2 I_2 N_2 \right. \\
&\quad \left. + (a_1 N_2 - \delta_2)(r_0 - \delta_1 - 2\gamma N_2 - a_1 I_2) \right].
\end{aligned}
$$

According to the Routh-Hurwitz criteria, we get that the system (3.4) is locally asymptotically stable around $E_2(N_2, I_2, 0)$ if $\phi_1 > 0$, $\phi_3 > 0$ and $\phi_1\phi_2 - \phi_3 > 0$. $\qquad \square$

Theorem 3.4.5. *The infected prey-free equilibrium $E_3(N_3, 0, P_3)$ is locally asymptotically stable if $\psi_1 > 0$, $\psi_3 > 0$ and $\psi_1\psi_2 - \psi_3 > 0$, where ψ_1, ψ_2 and ψ_3 are defined in the proof.*

Proof. The characteristic equation of the Jacobian matrix around the infected prey-free equilibrium point $E_3(N_3, 0, P_3)$ is given by

$$\lambda^3 + \psi_1\lambda^2 + \psi_2\lambda + \psi_3 = 0, \tag{3.10}$$

where

$$\psi_1 = \delta_1 + \delta_2 + \delta_3 + 2\gamma N_3 + a_2 P_3 - a_1 N_3 + \frac{\beta P_3}{(1 + \xi N_3)^2}$$

$$- \frac{\theta_2 \beta N_3}{1 + \xi N_3} - \frac{r_0(\alpha_f + \eta_f P_3)}{\alpha_f + P_3},$$

$$\psi_2 = (a_1 N_3 - a_2 P_3 - \delta_2) \left(\frac{\theta_2 \beta N_3}{1 + \xi N_3} - \delta_3 \right)$$

$$+ \left[\frac{r_0(\alpha_f + \eta_f P_3)}{\alpha_f + P_3} - \delta_1 - 2\gamma N_3 \right.$$

$$\left. - \frac{\beta P_3}{(1 + \xi N_3)^2} \right] \left[a_1 N_3 - a_2 P_3 - \delta_2 - \delta_3 + \frac{\theta_2 \beta N_3}{1 + \xi N_3} \right]$$

$$+ \frac{\beta \theta_2 P_3}{(1 + \xi N_3)^2} \left\{ \frac{r_0 \alpha_f (1 - \eta_f) N_3}{(\alpha_f + P_3)^2} + \frac{\beta N_3}{1 + \xi N_3} \right\},$$

$$\psi_3 = -(a_1 N_3 - a_2 P_3 - \delta_2) \left[\frac{\beta \theta_2 P_3}{(1 + \xi N_3)^2} \left(\frac{r_0 \alpha_f (1 - \eta_f) N_3}{(\alpha_f + P_3)^2} \right. \right.$$

$$\left. + \frac{\beta N_3}{1 + \xi N_3} \right) + \left(\frac{\theta_2 \beta N_3}{1 + \xi N_3} - \delta_3 \right) \left(\frac{r_0(\alpha_f + \eta_f P_3)}{\alpha_f + P_3} - \delta_1 \right.$$

$$\left. \left. - 2\gamma N_3 - \frac{\beta P_3}{(1 + \xi N_3)^2} \right) \right].$$

Hence, from Routh-Hurwitz criteria, we get that the system (3.4) is locally asymptotically stable around $E_3(N_3, 0, P_3)$ if $\psi_1 > 0$, $\psi_3 > 0$ and $\psi_1 \psi_2 - \psi_3 > 0$. $\qquad \square$

Theorem 3.4.6. *The interior equilibrium $E^*(N^*, I^*, P^*)$ of (3.4) is locally asymptotically stable if $\Omega_1 > 0$, $\Omega_3 > 0$ and $\Omega_1 \Omega_2 - \Omega_3 > 0$, where Ω_1, Ω_2 and Ω_3 are defined in the proof.*

Proof. The characteristic equation of the Jacobian matrix around the interior equilibrium point $E^*(N^*, I^*, P^*)$ is given by

$$\lambda^3 + \Omega_1 \lambda^2 + \Omega_2 \lambda + \Omega_3 = 0, \tag{3.11}$$

where

$$\Omega_1 = -(F_N{}^* + G_I{}^* + H_P{}^*),$$
$$\Omega_2 = (G_I{}^* H_P{}^* - G_P{}^* H_I{}^*) + (F_N{}^* H_P{}^* - F_P{}^* H_N{}^*)$$
$$+ (F_N{}^* G_I{}^* - F_I{}^* G_N{}^*),$$
$$\Omega_3 = -\left[F_N{}^* (G_I{}^* H_P{}^* - G_P{}^* H_I{}^*) - F_I{}^* (G_N{}^* H_P{}^* - G_P{}^* H_N{}^*) \right.$$
$$\left. + F_P{}^* (G_N{}^* H_I{}^* - G_I{}^* H_N{}^*) \right],$$

$$F_N{}^* = r_0 \left[\eta_f + \frac{\alpha_f (1 - \eta_f)}{\alpha_f + P^*} \right] - \delta_1 - 2\gamma N^* - a_1 I^* - \frac{\beta P^*}{(1 + \xi N^*)^2},$$

$$F_I{}^* = -a_1 N^*, F_P{}^* = -\frac{r_0 \alpha_f (1 - \eta_f) N^*}{(\alpha_f + P^*)^2} - \frac{\beta N^*}{1 + \xi N^*},$$

$$G_N{}^* = a_1 I^*, G_I{}^* = a_1 N^* - a_2 P^* - \delta_2, \quad G_P{}^* = -a_2 I^*,$$

$$H_N{}^* = \frac{\beta \theta_2 P^*}{(1 + \xi N^*)^2}, H_I{}^* = \theta_1 a_2 P^*,$$

$$H_P{}^* = \theta_1 a_2 I^* + \frac{\theta_2 \beta N^*}{1 + \xi N^*} - \delta_3.$$

The interior equilibrium point $E^*(N^*, I^*, P^*)$ will be locally asymptotically stable if all the eigenvalues of the characteristic equation (3.9) are negative or have negative real parts. Hence, from Routh-Hurwitz criteria, we get that the system (3.4) will be locally asymptotically stable around $E^*(N^*, I^*, P^*)$ if $\Omega_1 > 0$, $\Omega_3 > 0$ and $\Omega_1 \Omega_2 - \Omega_3 > 0$. The interior equilibrium point $E^*(N^*, I^*, P^*)$ will be unstable if the coefficients of (3.9) fail to satisfy these conditions. $\qquad\square$

The coefficients of the characteristic equations (3.9), (3.10) and (3.11) for the variational matrix of (3.4) at different equilibrium points are very complicated. Thus, it is quite difficult to find the conditions for the stability of the equilibrium points in terms of a_1, which is the force of infection from susceptible prey to infected prey. Hence, we will study the stability of the equilibrium points of (3.4) with respect to the parameter a_1 by plotting coefficients of the characteristic equations (3.9), (3.10) and (3.11) in terms of a_1. Parameter a_1 varies from 0 to 3.0 and the values of the coefficients of the characteristic equations are plotted in Fig. 3.3. Other parameters value are listed in Table 3.1. Fig. 3.3(a) shows that the coefficients of ψ_1, ψ_3 and $\psi_1 \psi_2 - \psi_3$ in terms of a_1 of the characteristic equation (3.10) for the variational matrix of (3.4) at the infected prey-free equilibrium (E_3). Fig. 3.3(b) demonstrates that the coefficients of Ω_1, Ω_3 and $\Omega_1 \Omega_2 - \Omega_3$ in terms of a_1 of the characteristic equation (3.11) for the variational matrix of (3.4) at the coexisting equilibrium (E^*). Also, Fig. 3.3(c) exhibits the coefficients of ϕ_1, ϕ_3 and $\phi_1 \phi_2 - \phi_3$ in terms of a_1 of the characteristic equation (3.9) for the variational matrix of system (3.4) at the predator-free equilibrium (E_2).

Fig. 3.3(a) shows that the expressions of ψ_1, ψ_3 and $\psi_1 \psi_2 - \psi_3$ are positive for $a_1 \in (0, 0.09)$ (gray shaded region). Therefore, the infection-free equilibrium point (E_3) is locally asymptotically stable for $a_1 \in (0, 0.09)$ and unstable for $a_1 > 0.09$. Again, Fig. 3.3(b) demonstrates that the expressions of Ω_1, Ω_3 and $\Omega_1 \Omega_2 - \Omega_3$ are positive for $a_1 \in (0.09, 0.55)$ (brown shaded region). Thus, the co-existing equilibrium point (E^*) is locally asymptotically stable
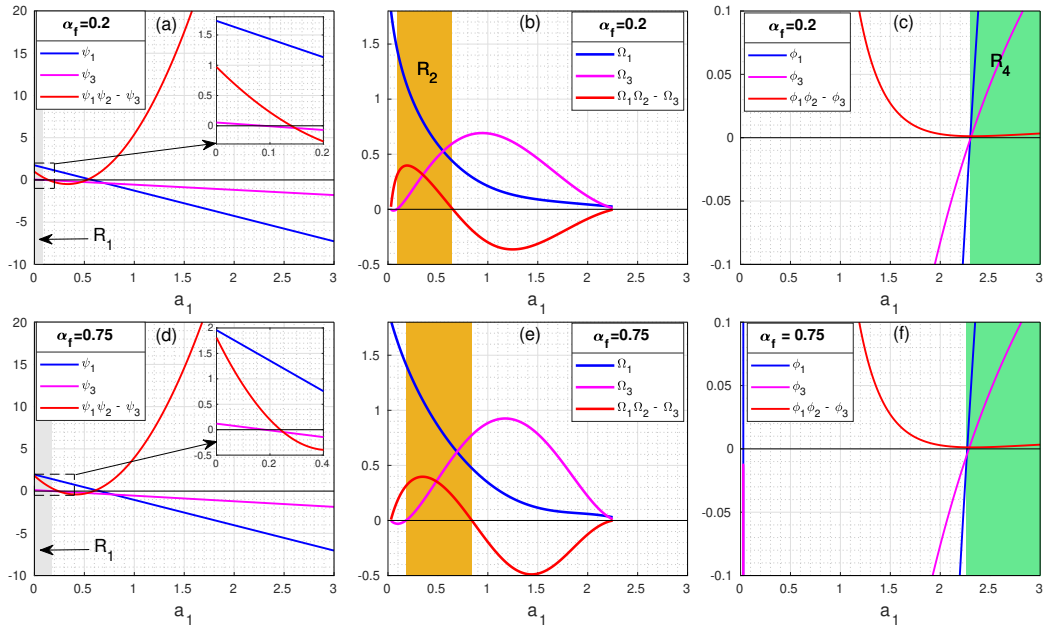
Figure 3.3: The graph represents the coefficients of the characteristic equations (3.10), (3.11) and (3.9) of the variational matrix for the system (3.4) at the equilibrium points; (a) the infection-free equilibrium point (E_3), (b) the interior equilibrium point (E^*) and (c) the predator-free equilibrium point (E_2), respectively for $\alpha_f = 0.2$. Again, for $\alpha_f = 0.75$, coefficients of characteristic equations (3.10), (3.11) and (3.9) of the variational matrix for (3.4) at the equilibrium points are plotted; (d) infection-free equilibrium point (E_3), (e) interior equilibrium point (E^*) and (f) the predator-free equilibrium point (E_2), respectively. Other parameters value are listed in Table 3.1. In (a) and (d), the regions in the black box are zoomed and plotted in the inset.

for $a_1 \in (0.09, 0.55)$, otherwise unstable. Fig. 3.3(c) exhibits that ϕ_1, ϕ_3 and $\phi_1\phi_2 - \phi_3$ are positive for $a_1 \in (2.29, 3.0)$ (green shaded region). Hence, the predator-free equilibrium point (E_2) is locally asymptotically stable for $a_1 \in (2.29, 3.0)$ and unstable for $a_1 < 2.29$. To demonstrate these scenarios of our system (3.4), the bifurcation diagram for each population with respect to parameter a_1 is presented in Fig. 3.4(a). The region $0 < a_1 < 0.09$ is shaded by gray color in Fig. 3.3(a) and Fig. 3.4, for $a_1 \in (0, 0.09)$, ψ_1, ψ_3 and $\psi_1\psi_2 - \psi_3$ are all positive, which are the stability conditions for the infected prey-free equilibrium point E_3. The bifurcation diagram shown in Fig. 3.4(a) demonstrates that the equilibrium point E_3 is stable for $a_1 \in (0, 0.09)$. From an ecological point of view, this explains that for the lower threshold value of a_1, that is, for the low value of the force of infection from susceptible

prey to infected prey, the infected population remains stable in our system.
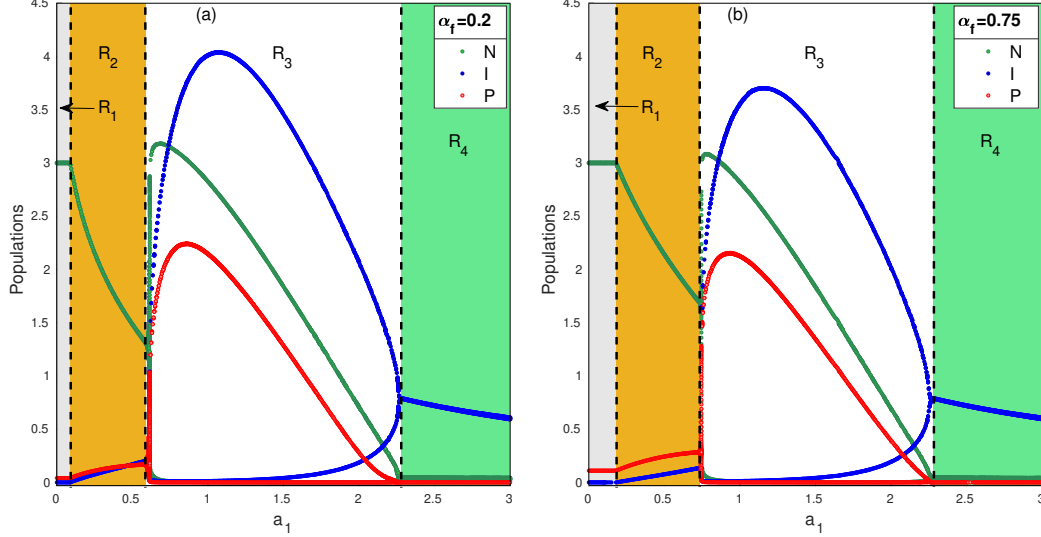
Figure 3.4: Bifurcation diagram for the system (3.4) with respect to the force of infection a_1 from susceptible to infected population. The bifurcation parameter a_1 varies from 0 to 3 and other parameters value are listed in Table 3.1. The value of α_f is 0.2 for (a) and 0.75 for (b). The green, blue and red curves represents the susceptible prey (N), infected prey (I) and predator (P) population, respectively. The gray colored region R_1 represents the stability of the susceptible prey and predator population; the brown colored region R_2 demonstrates the stability of the interior steady state E^*; the white colored region R_3 exhibits the oscillatory behavior of the interior steady state E^*; and the green colored region R_4 represents the stability of the susceptible prey and infected prey population.

The region $0.09 < a_1 < 0.55$ shaded by brown color has been shown in Fig. 3.3(b) and Fig. 3.4(a). Fig. 3.3(b) shows that Ω_1, Ω_3 and $\Omega_1\Omega_2 - \Omega_3$ are positive in the interval $a_1 \in (0.09, 0.55)$, which delineates the stability conditions for the co-existing equilibrium point E^*. The bifurcation diagram Fig. 3.4(a) also demonstrates that the co-existing equilibrium point E^* is stable for $a_1 \in (0.09, 0.55)$. In terms of ecology, this explains that as the value of a_1 is increased, the infected prey population starts to grow and the co-existing equilibrium (E^*) is stable for $a_1 \in (0.09, 0.55)$. System (3.4) experiences a Hopf bifurcation around $a_1 \approx 0.55$ and the system demonstrates the oscillatory behavior for all the populations in region $0.55 < a_1 < 2.29$. The region $2.29 < a_1 < 3.0$ shaded by green color has been shown in Fig. 3.3(c) and Fig. 3.4(a). Fig. 3.3(c) demonstrates that ϕ_1, ϕ_3 and $\phi_1\phi_2 - \phi_3$ are positive

in the region $a_1 \in (2.29, 3.0)$, which describes the stability conditions for the predator-free equilibrium point (E_2). The bifurcation diagram Fig. 3.4(a) also shows that the predator-free equilibrium point (E_2) is stable in region $a_1 \in (2.29, 3.0)$. Hence, for the higher value of a_1, that is, for the high rate of infection from susceptible prey to infected prey population, the predator population becomes extinct from the system.

To investigate the influence of fear on our system (3.4), we have increased the level of fear α_f from 0.2 to 0.75 and plotted the bifurcation diagram (see Fig. 3.4(b)) with respect to the same parameter a_1 and the coefficients (see Figs. 3.3(d)-(f)) for the characteristic equations (3.9), (3.10) and (3.11). The parameters value for Figs. 3.3(d)-(f) are the same as in Fig. 3.3(a) except $\alpha_f = 0.75$. Also, the parameters value of the Fig. 3.4(b) are the same as in Fig. 3.4(a) except $\alpha_f = 0.75$. It can be observed that, if the level of fear increased, the dynamics of (3.4) remains similar, but the position of the bifurcation point has been altered. The infected prey-free equilibrium point (E_3) is stable in the range $a_1 \in (0, 0.18)$ for $\alpha_f = 0.75$, but E_3 is stable in the range $a_1 \in (0, 0.09)$ for $\alpha_f = 0.2$. This can be interpreted that if the level of fear is increased, then the infection-free equilibrium point (E_3) will be stable for a higher value of the infection rate a_1.

3.4.3 Stability region

To explore the complicated dynamics of (3.4), the stability regions for different equilibrium points of the system (3.4) have been demonstrated in the $a_1 - \gamma$ plane (see Fig. 3.5 and Fig. 3.6) for different values of the level of fear α_f. Both parameters a_1 (force of infection from susceptible to infected population) and γ (decay rate due to intra-specific competition) varies from 0 to 2 and other parameters value are listed in Table 3.1. The stability region has been plotted in Fig. 3.5 for the level of fear $\alpha_f = 0.20$ and in Fig. 3.6 for the level of fear $\alpha_f = 0.50$. The stability regions for different equilibrium points have been shown by different colors and keep the same color for each equilibrium point in both figures. The phase portrait diagrams for each regions have also shown for four initial values, namely (2.0, 1.5, 1.25), (3.0,2.0,1.5), (1.0, 2.0, 0.5) and (3.0, 2.0, 0.25).

The stability region and the corresponding phase diagram have been plotted in Fig. 3.5 in the plane $a_1 - \gamma$ with the level of fear $\alpha_f = 0.2$ and the other parameters are listed in Table 3.1. The colored regions corresponding to the phase diagram are marked as R_1, R_2, R_3, R_4 and R_5, respectively. In region R_1 (Orange), system (3.4) has a stable limit cycle oscillation. The corresponding phase portrait for region R_1, initiating from the initial points, converges to the limit cycle oscillation around the co-existing equilibrium

point E^*. Hence, the system (3.4) is unstable in the R_1 region. In region R_2 (Red), the co-existing equilibrium E^* is stable. The corresponding phase portrait for region R_2 shows that the solution trajectories initiating from the initial points converge to the co-existing equilibrium point E^*. In region R_3 (green), predator species dies out and two prey populations are stable. The solution trajectories initiating from the initial points converge to the predator-free equilibrium point E_2 on the $N - I$ plane. In region R_4 (pink), only susceptible prey exist and the solution trajectories initiating from the initial points converge to the susceptible prey only equilibrium E_1, which lies on the N-axis. Also, in region R_5 (sky blue), the infected prey population dies out and other two populations are stable. The solution trajectories initiating from the initial points converge to the infected prey-free equilibrium point E_3, which lies on the $N - P$ plane.

The stability region and the corresponding phase diagram have been plotted in Fig. 3.6 in the plane $a_1 - \gamma$ with the level of fear $\alpha_f = 0.5$ and the rest of parameters are specified in Table 3.1. The colored regions corresponding to the phase plane are marked as R_1, R_2, R_3, R_4 and R_5, respectively. The area of the region R_1 has reduced and the area of region R_2 has increased in comparison with the regions for $\alpha_f = 0.2$ (see Fig. 3.5 and Fig. 3.6). This observation indicates that if the value of the level of fear α_f is increased, then the stability region for the co-existing equilibrium point E^* is increased and the unstable region for E^* is reduced. In the region R_1 (orange), system (3.4) has a stable limit cycle oscillation and the phase portrait for the region R_1, initiating from the initial points, converges to the limit cycle oscillation around the co-existing equilibrium E^*. Hence, system (3.4) is unstable in the R_1 region. In the region R_2 (red), the co-existing equilibrium E^* is stable. The phase portrait for region R_2 shows that the solution trajectories initiating from the initial points converge to the co-existing equilibrium point E^*. In the region R_3 (green), predator species dies out and the susceptible and infected prey populations are stable. The solution trajectories initiating from the initial points converge to the predator-free equilibrium E_2 on the $N - I$ plane. In region R_4 (pink), only susceptible prey exists and the solution trajectories initiating from the initial points converge to the susceptible prey only at equilibrium point E_1, which lies on the N-axis. Also, in the region R_5 (sky blue), infected prey dies out and other two populations are stable. The solution trajectories initiating from the initial points converge to the infected prey-free equilibrium E_3, which lies on the $N - P$ plane.

3.4.4 Analysis of Hopf bifurcation

In this section, we have analytically computed the Hopf bifurcation of the system (3.4). For complex conjugate eigenvalues, the system (3.4) undergoes a Hopf bifurcation around the co-existing equilibrium point $E^*(N^*, I^*, P^*)$ with respect to the level of fear α_f. However, Section 3.5, we have also investigated the bifurcation with respect to the parameters γ, a_1 and a_2. The following theorem investigates the existence of the Hopf bifurcation with respect to the level of fear α_f as the bifurcating parameter.

Theorem 3.4.7. *The necessary and sufficient conditions for the existence of Hopf bifurcation around $\alpha_f = \alpha_f{}^*$ if the following conditions are satisfied*

(i) $\Omega_i(\alpha_f{}^*) > 0$, $i = 1, 2, 3$;

(ii) $\Omega_1(\alpha_f{}^*)\Omega_2(\alpha_f{}^*) - \Omega_3(\alpha_f{}^*) = 0$;

(iii) $\left[\frac{d}{d\alpha_f}(Re(\lambda_i))\right]_{\alpha_f = \alpha_f{}^*} \neq 0$, $i = 1, 2$.

Proof. Since $\Omega_i(\alpha_f) > 0$ for $\alpha_f = \alpha_f{}^*$ with $i = 1, 2, 3$, then there exists an interval containing $\alpha_f{}^*$, say, $(\alpha_f{}^* - \delta_i, \alpha_f{}^* + \delta_i)$, for some $\delta_i > 0$, $i = 1, 2, 3$. We choose, $0 < \delta \leq \min\{\delta_i : i = 1, 2, 3\}$ such that $\alpha_f{}^* - \delta > 0$ and $\Omega_i(\alpha_f) > 0$ for $\alpha_f \in (\alpha_f{}^* - \delta, \alpha_f{}^* + \delta)$, $i = 1, 2, 3$. Therefore, the characteristic equation (3.11) have no real positive root as explained in Table 3.2 for the existence of the positive real root of the cubic equation. For $\alpha_f = \alpha_f{}^*$, $\Omega_1(\alpha_f{}^*)\Omega_2(\alpha_f{}^*) - \Omega_3(\alpha_f{}^*) = 0$, and therefore, from (3.11), we have

$$(\lambda^2 + \Omega_2)(\lambda + \Omega_1) = 0.$$

The roots of the above equation are $\lambda_1 = i\sqrt{\Omega_2}$, $\lambda_2 = -i\sqrt{\Omega_2}$ and $\lambda_3 = -\Omega_1$. For any $\alpha_f \in (\alpha_f{}^* - \delta, \alpha_f{}^* + \delta)$, the roots of (3.11) are of the form

$$\lambda_1(\alpha_f) = \sigma_1(\alpha_f) + i\sigma_2(\alpha_f),$$
$$\lambda_2(\alpha_f) = \sigma_1(\alpha_f) - i\sigma_2(\alpha_f),$$
$$\lambda_3(\alpha_f) = -\Omega_1(\alpha_f).$$

Now, we shall verify the transversality condition $\left[\frac{d}{d\alpha_f}(Re(\lambda_i))\right]_{\alpha_f = \alpha_f{}^*} \neq 0$, $i = 1, 2$. Substituting $\lambda_1(\alpha_f) = \sigma_1(\alpha_f) + i\sigma_2(\alpha_f)$ in (3.11) and differentiating with respect to α_f, we have

$$\begin{aligned} A(\alpha_f)\sigma_1{}'(\alpha_f) - B(\alpha_f)\sigma_2{}'(\alpha_f) + C(\alpha_f) &= 0, \qquad (3.12)\\ B(\alpha_f)\sigma_1{}'(\alpha_f) + A(\alpha_f)\sigma_2{}'(\alpha_f) + D(\alpha_f) &= 0, \end{aligned}$$

where

$$A(\alpha_f) = 3{\sigma_1}^2(\alpha_f) - 3{\sigma_2}^2(\alpha_f) + 2\Omega_1(\alpha_f)\sigma_1(\alpha_f) + \Omega_2(\alpha_f),$$
$$B(\alpha_f) = 6\sigma_1(\alpha_f)\sigma_2(\alpha_f) + 2\Omega_1(\alpha_f)\sigma_2(\alpha_f),$$
$$C(\alpha_f) = {\Omega_1}'(\alpha_f){\sigma_1}^2(\alpha_f) - {\Omega_1}'(\alpha_f){\sigma_2}^2(\alpha_f)$$
$$\qquad\quad + {\Omega_2}'(\alpha_f)\sigma_1(\alpha_f) + {\Omega_3}'(\alpha_f),$$
$$D(\alpha_f) = 2{\Omega_1}'(\alpha_f)\sigma_1(\alpha_f)\sigma_2(\alpha_f) + {\Omega_2}'(\alpha_f)\sigma_2(\alpha_f).$$

Here, $\sigma_1({\alpha_f}^*) = 0$ and $\sigma_2({\alpha_f}^*) = \sqrt{\Omega_2({\alpha_f}^*)}$; therefore, we have $A({\alpha_f}^*) = -2\Omega_2({\alpha_f}^*)$, $\quad B({\alpha_f}^*) = 2\Omega_1({\alpha_f}^*)\sqrt{\Omega_2({\alpha_f}^*)}$, $\quad C({\alpha_f}^*) = -{\Omega_1}'({\alpha_f}^*)\Omega_2({\alpha_f}^*) + {\Omega_3}'({\alpha_f}^*)$ and $D({\alpha_f}^*) = {\Omega_2}'({\alpha_f}^*)\sqrt{\Omega_2({\alpha_f}^*)}$. From (3.12), we have

$$\left[\frac{d}{d\alpha_f}(Re(\lambda_i))\right]_{\alpha_f = {\alpha_f}^*} = {\sigma_1}'({\alpha_f}^*)$$

$$= -\left[\frac{A(\alpha_f)C(\alpha_f) + B(\alpha_f)D(\alpha_f)}{A^2(\alpha_f) + B^2(\alpha_f)}\right]_{\alpha_f = {\alpha_f}^*}$$

$$= -\frac{\Omega_1({\alpha_f}^*){\Omega_2}'({\alpha_f}^*) - {\Omega_3}'({\alpha_f}^*) + {\Omega_1}'({\alpha_f}^*)\Omega_2({\alpha_f}^*)}{2\left(\Omega_2({\alpha_f}^*) + {\Omega_1}^2({\alpha_f}^*)\right)} \neq 0,$$

provided $\Omega_1({\alpha_f}^*){\Omega_2}'({\alpha_f}^*) - {\Omega_3}'({\alpha_f}^*) + {\Omega_1}'({\alpha_f}^*)\Omega_2({\alpha_f}^*) \neq 0$ and $\lambda_3({\alpha_f}^*) = -\Omega_3({\alpha_f}^*) \neq 0$. Hence, the transversality condition holds and the Hopf bifurcation occurs at $\alpha_f = {\alpha_f}^*$. $\qquad\square$

3.5 Numerical simulation

Herein, we performed some numerical simulations to check the feasibility of our theoretical analysis regarding stability conditions with the hypothetical set of parameters. System of nonlinear ordinary differential equations (3.4) has been solved numerically by the fourth order Runge-Kutta method, with the aid of MATLAB version R2016a. The system of equation (3.4) numerically integrated using initial population size $[N(0), I(0), P(0)] = [2.0, 1.5, 1.25]$, the system parameters value as $\gamma = 1.3$, $a_1 = 0.79$ and other parameters are listed in Table 3.1. The time series solutions for each population and the corresponding phase portrait diagram are presented in Fig. 3.7 (the top panel of Figs. 3.7(a)-(c) for time series solutions and the bottom panel Figs. 3.7 (d)-(f) for phase portrait diagrams). From the time series solutions, it can be observed that initially, all the population shows oscillatory behavior and finally, all the population becomes stable and reaches their steady states. The phase portrait diagram [see Fig. 3.7(d)] exhibits

that the system converges asymptotically to the interior equilibrium point $E^*(0.5767, 0.4269, 0.0889)$. We have computed the numerical values of the co-efficients of the characteristic equation (3.11) using the assumed parameters value and obtained $\Omega_1 = 0.6672 > 0$, $\Omega_2 = 1.2361 > 0$ and $\Omega_3 = 0.6578 > 0$ with $\Omega_1\Omega_2 - \Omega_3 = 0.1670 > 0$. As stated in Theorem 3.4.6, the local asymptotical stability criteria for E^* is satisfied and our numerical simulation confirms the stability of the interior equilibrium point E^*.

Now, the system of equation (3.4) was numerically integrated with the same parameters value in Table 3.1 except parameters γ and a_1 with the same initial values. In this case, we have taken the lower values of γ and a_1, that is, 0.15 and 0.25, respectively. The time series solution for each population is presented by black curves in Fig. 3.7(a), Fig. 3.7(b) and Fig. 3.7(c). The corresponding phase portrait diagram is presented in Fig. 3.7(e). From the time series solutions, it can be observed that initially all the population exhibits oscillatory behavior and finally, all the population becomes stable and reaches their equilibrium states. The phase portrait diagram (see Fig. 3.7(e)) shows that the system converges asymptotically to the infected prey-free equilibrium point $E_3(3.0, 0, 0.3356)$. We have computed the numerical values of the coefficients of the characteristic equation (3.10) using the assumed parameters and obtained $\psi_1 = 0.8907 > 0$, $\psi_2 = 0.6790 > 0$ and $\psi_3 = 0.3751 > 0$ with $\psi_1\psi_2 - \psi_3 = 0.2297 > 0$. According to the Theorem 3.4.5, the local asymptotic stability criteria for E_3 is satisfied, and our numerical simulation confirms the stability of the infected prey-free equilibrium point E_3.

Again, the system of equations (3.4) is numerically integrated with assumed parameters in Table 3.1 except parameters γ and a_1 with the same initial values. In this case, we set parameters γ and a_1 as 0.55 and 0.7, respectively. The time series solutions for each population are presented by blue curves in the Fig. 3.7(a), Fig. 3.7(b) and Fig. 3.7(c). The corresponding phase portrait diagram is presented in Fig. 3.7(f). The time series solutions for each population are showing oscillatory behavior or limit cycle oscillations with the same magnitude for a long-time, which means system (3.4) undergoes Hopf bifurcation. We have computed the numerical values of the coefficients of the characteristic equation (3.11) using the assumed parameters value and obtained $\Omega_1 = 0.4255 > 0$, $\Omega_2 = 1.4616 > 0$ and $\Omega_3 = 0.6439 > 0$ with $\Omega_1\Omega_2 - \Omega_3 = -0.0220 < 0$, which does not satisfy the Routh-Hurwitz criteria. Thus the Theorem 3.4.6 fails to satisfy the criteria for local asymptotic stability for interior steady state E^* because $\Omega_1\Omega_2 - \Omega_3 < 0$ and therefore, the solutions are not asymptotically stable. Therefore, system (3.4) shows a limit cycle oscillation around the co-existing equilibrium point $E^*(1.0676, 0.2596, 0.1614)$.

In the Section 3.4.4, we established the conditions for Hopf bifurcation, and the Theorem 3.4.7 is satisfied. Therefore, the system (3.4) undergoes a Hopf bifurcation with respect to the level of fear α_f as a bifurcation parameter. We have plotted the bifurcation diagram (see Fig. 3.8(a)) by varying α_f from 0 to 1, and the other parameters value are listed in Table 3.1. From the bifurcation diagram, it can be noticed that if we gradually increase the level of fear α_f, the system (3.4) changes its stability from a limit cycle oscillation to locally asymptotically stable. System (3.4) changes its stability at $\alpha_f{}^* \approx 0.55$ (see Fig. 3.8(a)) and this threshold is known as the Hopf bifurcation point. We have analytically verified the transversality condition for a Hopf bifurcation and, thus the interior steady state E^* is locally asymptotically stable for $\alpha_f > \alpha_f{}^*$ and unstable for $\alpha_f < \alpha_f{}^*$. From the bifurcation plot [see Fig. 3.8(a)], the system shows a limit cycle oscillation for $0 \leq \alpha_f < 0.55$; the Hopf bifurcation occurs at $\alpha_f^* \approx 0.55$ and interior equilibrium E^* is locally asymptotically stable for $0.55 < \alpha_f \leq 1.0$. From an ecological point of view, it can be interpreted that as the level of fear α_f increases, the system enters into the stable steady state from a limit cycle oscillation.

Analytically, we have not shown the bifurcation of (3.4) with respect to the parameters γ and a_2, though we have shown numerically the bifurcation diagram with respect to the parameters γ and a_2. The bifurcation diagram of (3.4) with respect to the prey intra-species competition γ is presented in Fig. 3.8(b), and the value of $\alpha_f = 0.2$ and other parameters are the same as in Fig. 3.8(a). From the bifurcation diagram, it can be observed that the system (3.4) changes its stability from a limit cycle oscillation to local asymptotic stability of the interior steady state E^* as the value of γ is increased. The system (3.4) undergoes a Hopf bifurcation at the threshold value $\gamma^* \approx 0.63$ [see Fig. 3.8(b)]. The system shows a limit cycle oscillation for $0 \leq \gamma < 0.63$; there is occurrence of a Hopf bifurcation at $\gamma \approx 0.63$, and the interior equilibrium point E^* is locally asymptotically stable for $0.63 < \gamma \leq 1.0$. Hence, the interior equilibrium point E^* is locally asymptotically stable for $\gamma > \gamma^*$ and unstable for $\gamma < \gamma^*$.

The bifurcation diagram of (3.4) with respect to a_2 (predation rate of infected prey) is presented in Fig. 3.9. The parameters value are the same as in Fig. 3.8(a) with $\alpha_f = 0.2$, and the bifurcation parameter a_2 varies from 0 to 5.5. The bifurcation diagram (Fig. 3.9) is divided into three regions, namely, R_1, R_2 and R_3. In region R_1, the predator-free equilibrium point E_2 is locally asymptotically stable and the system (3.4) shows a limit cycle oscillation in region R_2. The interior equilibrium point E^* is locally asymptotically stable in region R_3. From the bifurcation diagram (Fig. 3.9), it can be observed that the predator-free equilibrium point (E_2) is locally asymptotically stable for $a_2 \in (0, 1.1)$, the interior equilibrium point E^* is locally asymptotically

stable for $a_2 \in (4.9, 5.5)$ and the system (3.4) is unstable for $a_2 \in (1.1, 4.9)$.

3.6   Discussion

In this chapter, we proposed and analyzed a three-tier eco-epidemiological model by introducing the effect of fear and infection on the prey population. We performed the qualitative properties of the predator-prey system (3.4), including positivity and boundedness of the solutions as the population cannot be negative and cannot grow unboundedly or exponentially. Through theoretical analysis, we find the criteria for the existence of five biologically feasible steady states, namely, the trivial equilibrium point, the axial equilibrium point (only susceptible prey exists), the predator-free equilibrium point, the infected prey-free equilibrium point and the co-existing equilibrium point. The local asymptotic stability of all these equilibria is investigated and our numerical simulations validate the stability of each of the equilibrium points. By considering the stability criteria for each of the equilibrium points, we have plotted the stability region in the $a_1 - \gamma$ parameter-space. Corresponding to each of the stability regions, we have plotted the three-dimensional phase portrait diagram to better understand the dynamics of the predator-prey system. From the stability region and the phase portrait diagram (see the Fig. 3.5), we observed in the $a_1 - \gamma$ parameter-space if the level of fear increases, then the stability region for the infected extinction equilibrium point (E_3) decreases and the stability region of the co-existing equilibrium point (E^*) increases.

To observe the impact of fear for prey species due to the predators in the eco-epidemiological system, we gradually increase the level of fear. We observed that the system (3.4) demonstrates a limit cycle oscillation around the interior equilibrium point (for the level of fear $\alpha_f = 0.3$) and further increased the value of the level of fear above a critical value (for the level of fear $\alpha_f^* = 0.6$) and then the system reaches an interior steady state. Thus, increasing the level of fear cannot eliminate/eradicate the disease from the system. The amplitude of the infected prey reduces as the level of fear increases [see the Fig. 3.8(a)]. We derived the conditions for the Hopf bifurcation of the proposed model with respect to the level of fear (α_f). To verify the Hopf bifurcation of (3.4), we have verified the transversality condition $\left[\frac{d}{d\alpha_f}(Re(\lambda_i))\right]_{\alpha_f = \alpha_f^*} \neq 0,\ i = 1, 2)$ for the critical value of $\alpha_f = \alpha_f^*$. The system is unstable for $\alpha_f \in (0, \alpha_f^*)$ and the system is locally asymptotically stable around the interior equilibrium point (E^*) for $\alpha_f > \alpha_f^*$.

Though we have not established the criteria for bifurcation with respect

to the parameters γ and a_2, numerically, we have plotted the bifurcation diagrams for the system (3.4) with respect to the parameters γ and a_2. These bifurcation diagrams shows that as the level of intra-species competition γ increases, population become asymptotically stable from oscillatory behavior. When the predator-free equilibrium point (E_2) is stable, we gradually increase parameter a_2, the system shows a limit cycle oscillation around the interior equilibrium point and finally, the interior equilibrium point become stable when a_2 crosses the critical value a_2^*. Thus, if the rate of predation of infected prey a_2 increases, initially the predator-free equilibrium point (E_2) become stable and finally, the interior equilibrium point (E^*) become stable. When the infection rate a_1 gradually increases (see Fig. 3.4) initially, the infected prey-free equilibrium point $(2.997, 0, 0.041)$ become stable, then the system (3.4) reaches a steady state at an interior equilibrium point as a_1 crosses a critical value $a_1 = 0.09$, the system (3.4) become unstable as a_1 crosses another critical value $a_1 = 0.55$ and finally, the predator-free equilibrium become stable as a_1 crosses another critical value $a_1 = 2.29$. Thus, if the rate of infection a_1 increases, the predator population may become extinct, though predators are not infected by the disease.

In summary, we can conclude that the effect of fear can reduce the spread of the diseases but cannot eliminate the disease from the system. System (3.4) shows similar dynamics as the rate of infection a_1 increases, but the bifurcation point changes as the level of fear changes. As no experimental data are available, we have conducted our study based on hypothetical data, but this study will be helpful to the researchers who are doing the research in the related field on the basis of observed/experimental data.

Table 3.2: *Number of positive roots of (3.8) based on the sign of the coefficients τ_1, τ_2 and τ_3 and the terms Π_1, Π_2 and Π_3. For example, if the signs of the coefficients τ_1, τ_2 and τ_3 are +, + and -, respectively and whatever be the sign of the terms Π_1, Π_2 and Π_3, equation (3.8) has an unique positive root.*

Number of positive roots	τ_1	τ_2	τ_3	Π_1	Π_2	Π_3
0	-	+	+	+	+	+
				+	-	-
				-	-	-
				+	-	+
				-	+	-
				-	-	+
	-	-	+	+	-	-
				-	-	+
	+	-	+	+	-	-
				-	-	+
	+	+	+	Any sign	Any sign	Any sign
1	+	+	-	Any sign	Any sign	Any sign
	+	-	-	Any sign	Any sign	Any sign
	-	-	-	Any sign	Any sign	Any sign
	-	+	-	+	+	+
				+	-	-
				-	-	-
				-	-	+
				+	-	+
				-	+	-
2	-	+	+	+	+	-
				-	+	+
	+	-	-	+	+	+
				+	+	-
				-	-	-
				-	+	+
				+	-	+
				-	+	-
	-	-	+	+	+	+
				+	+	-
				-	-	-
				-	+	+
				+	-	+
				-	+	-
3	-	+	-	-	+	+
				+	+	-

Figure 3.5: Stability region for different equilibrium points of the system (3.4) in the $a_1 - \gamma$ parameter-space. Both parameters a_1 and γ are varied from 0 to 2 with $\alpha_f = 0.2$ and other parameters value are listed in Table 3.1. The phase portrait plots for each regions shown with four different initial points are as follows: (2.0, 1.5, 1.25), (3.0,2.0,1.5), (1.0, 2.0, 0.5) and (3.0, 2.0, 0.25). The location of different initial points are marked by solid dots in the phase portrait plots, and the corresponding colored regions are marked as R_1, R_2, R_3, R_4 and R_5. In the orange colored region R_1, the system (3.4) shows a stable limit cycle oscillation. In the red colored region R_2, the system (3.4) demonstrates the stability of the interior equilibrium point E^*. In the green colored region R_3, the system (3.4) exhibits the stability of the steady state E_2 in which the predator species dies out and the susceptible prey and infected prey population exists together. In the pink colored region R_4, the system (3.4) represents the stability of the equilibrium point E_1 in which only the susceptible prey population exists, while the skyblue colored region R_5 delineates the stability of E_3 in which the infected prey population dies out and the other two population exists together.
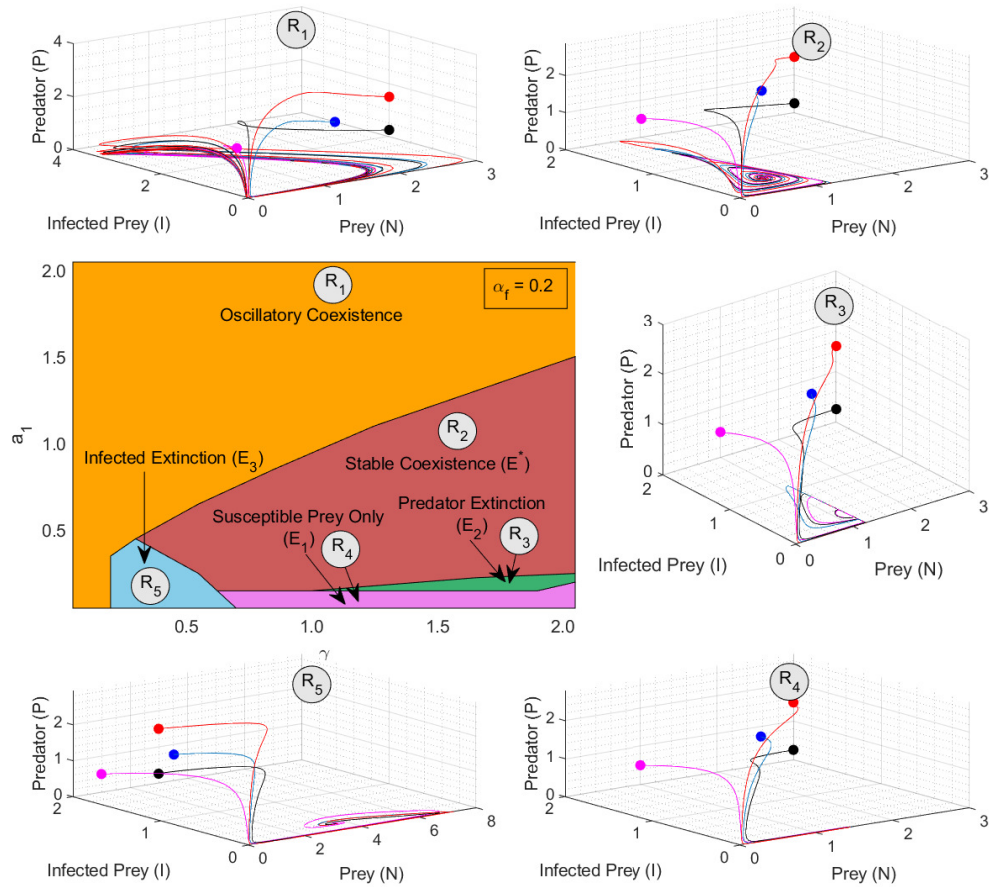
105
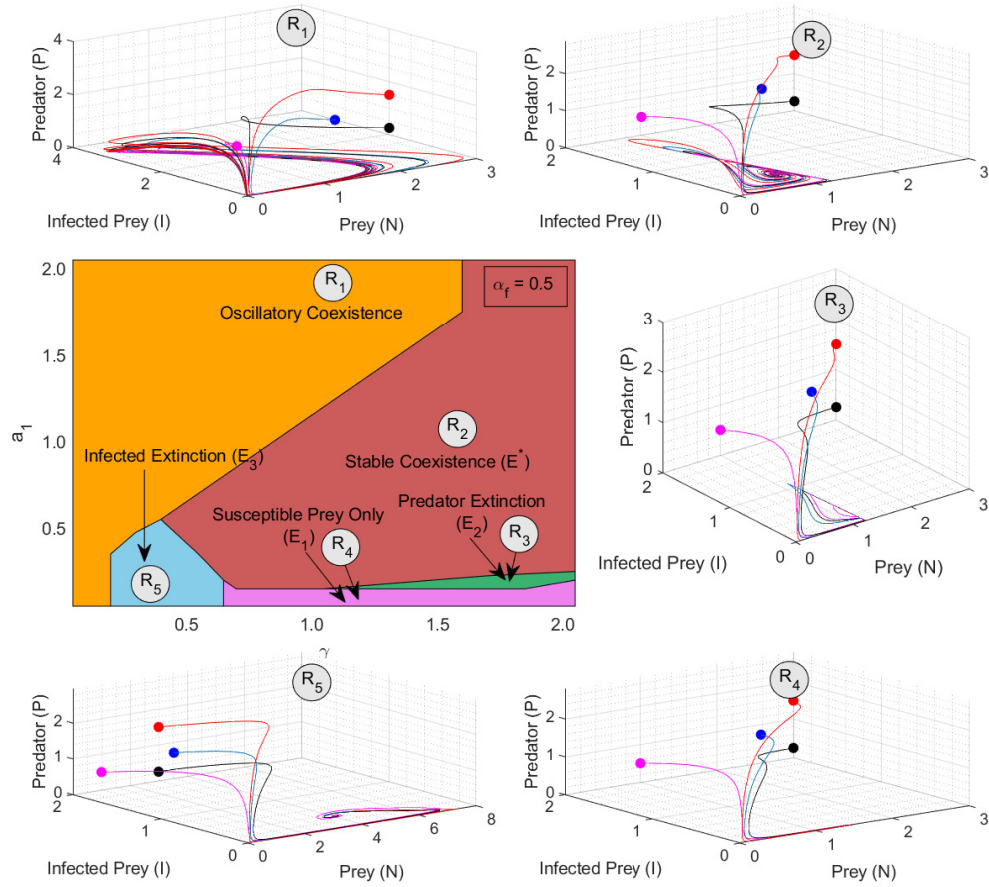
Figure 3.6: Stability region for different equilibrium points of the system (3.4) in the $a_1 - \gamma$ parameter-space. Both parameters a_1 and γ are varied from 0 to 2 with $\alpha_f = 0.5$ and other parameters value are listed in Table 3.1. The phase portrait plots for each regions are shown with four different initial points are as follows: (2.0, 1.5, 1.25), (3.0,2.0,1.5), (1.0, 2.0, 0.5) and (3.0, 2.0, 0.25). The location of different initial points are marked by solid dots in the phase portrait plots, and the corresponding colored regions are marked as R_1, R_2, R_3, R_4 and R_5. In the orange colored R_1, the system (3.4) shows stable limit cycle oscillation. In the red shaded region R_2, the system (3.4) exhibits the stability of the interior equilibrium point E^*. In the green shaded region R_3, the system (3.4) shows the stability of the steady state E_2 in which the predator species dies out and the susceptible prey and infected prey population exists together. In the pink colored region R_4, the system (3.4) demonstrates the stability of the equilibrium point E_1 in which only susceptible prey population exists, while skyblue colored region R_5 describes the stability of E_3 in which the infected prey population dies out and other two population exists together.

106
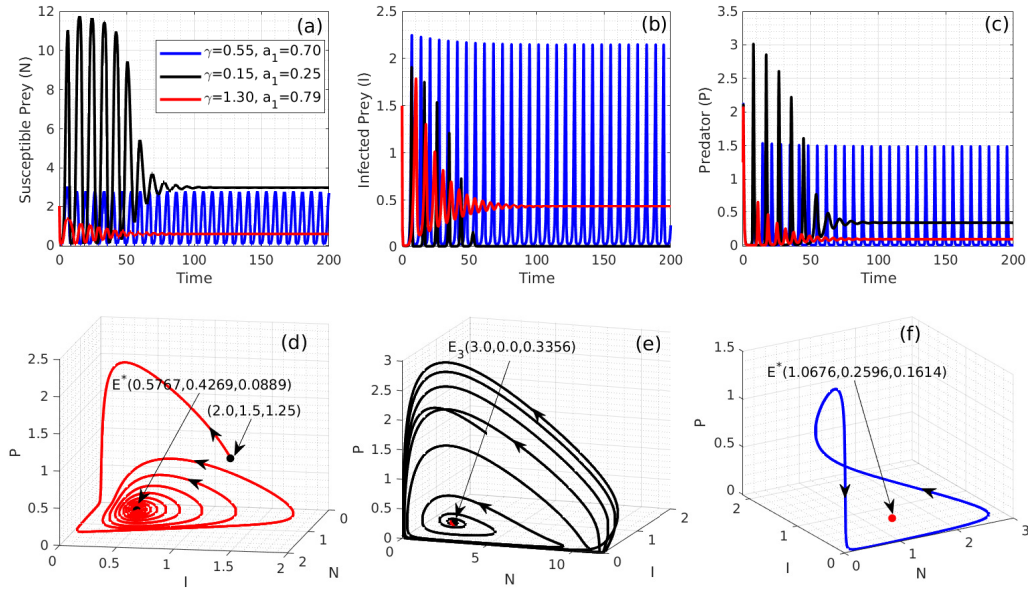
Figure 3.7: Numerical solutions of the system (3.4) with initial values $[N(0), I(0), P(0)] = [2.0, 1.5, 1.25]$ and parameters value are listed in Table 3.1. Stable time series solution of the system (3.4) around the interior equilibrium point $E^*(0.5767, 0.4269, 0.0889)$ shown by red color ($\gamma = 1.30$, $a_1 = 0.79$) and subfigure (d) shows the phase portrait of the time series solution. The stable time series solution of the system (3.4) around the infected prey-free equilibrium point $E_3(3.0, 0, 0.3356)$ is shown by black color ($\gamma = 0.15$, $a_1 = 0.25$) and subfigure (e) shows the phase portrait of the time series solution. The oscillatory time series solution is shown by blue color ($\gamma = 0.55$, $a_1 = 0.70$) and subfigure (f) shows the stable limit cycle around the co-existing equilibrium $E^*(1.0676, 0.2596, 0.1614)$.
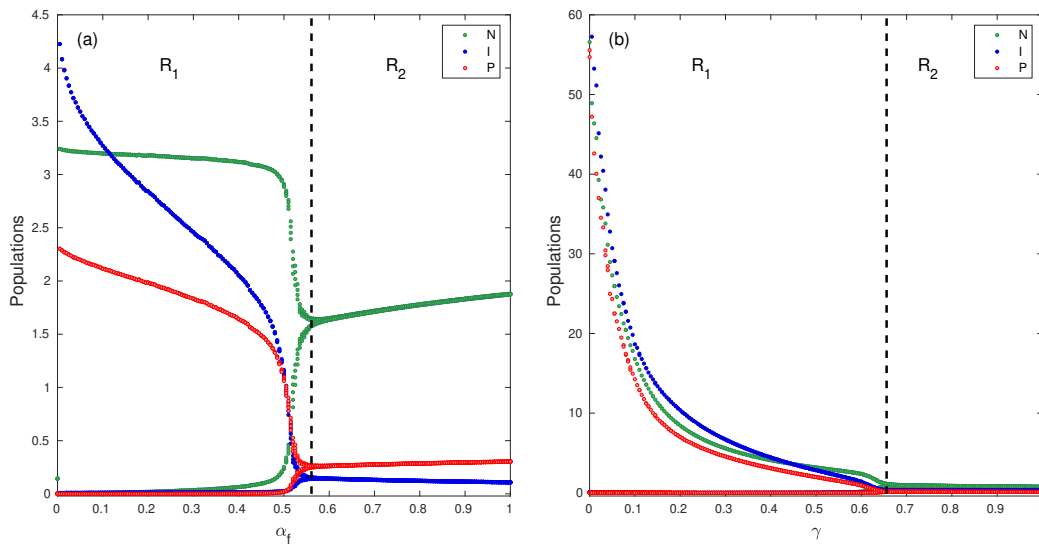
Figure 3.8: Bifurcation diagram for the interior equilibrium point $E^*(N^*, I^*, P^*)$ of the system (3.4) with respect to parameters α_f [subfigure (a)] and γ [subfigure (b)]. Both parameters α_f and γ varies from 0 to 1 and other parameters value are listed in Table 3.1. The maximum and minimum values of the oscillations are plotted: (i) green color is for susceptible prey (N), (ii) blue color is for infected prey (I) and (iii) red color is for predator (P) population. In the bifurcation diagram, region R_1 represents the oscillatory behavior of the interior steady state E^* and region R_2 demonstrates the local asymptotic stability of the interior steady state E^*. The bifurcation plots demonstrate that if both parameters α_f (the level of fear) and γ (the intra-species competition rate) increases, then the population becomes asymptotically stable from the oscillatory behavior.
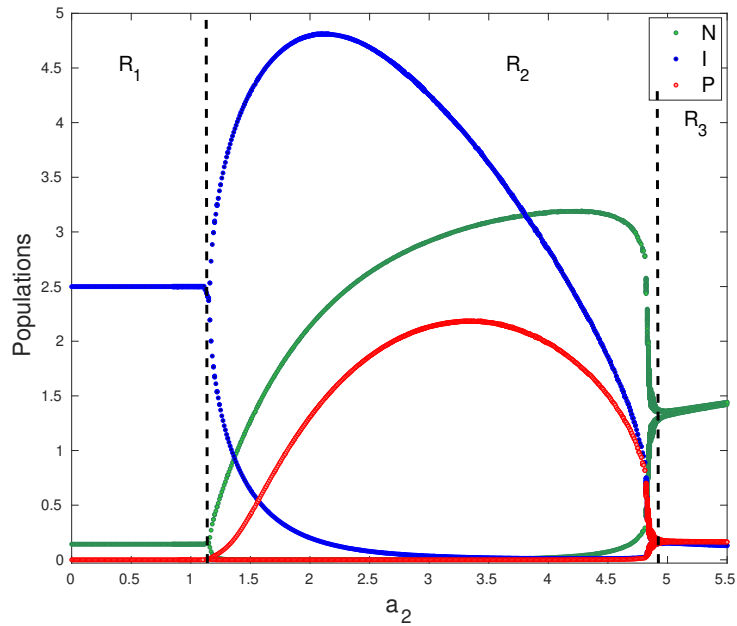
Figure 3.9: Bifurcation diagram for the interior equilibrium point $E^*(N^*, I^*, P^*)$ of the system (3.4) with respect to the parameter a_2. The bifurcation parameter a_2 varies from 0 to 5.5 and other parameters value are listed in Table 3.1. The maximum and minimum values of the oscillations are plotted: (i) green color is for susceptible prey (N), (ii) blue color is for infected prey (I) and (iii) red color is for predator (P) population. Region R_1 indicates the stability of the susceptible prey and predator population, region R_2 represents the oscillatory behavior of the interior steady state E^* and region R_3 demonstrates the local stability of the interior steady state E^*.

Chapter 4

A delayed eco-epidemiological model with weak Allee effect and disease in prey [†]

4.1 Introduction

The role of infectious diseases in ecological modeling is a significant issue from the view point of mathematics as well as ecology. The investigation on eco-epidemiological models are now ubiquitous after the pioneering work of Hadeler & Freedman [120]. Recently, an important attention has been paid on the concept of Allee effect named after W.C. Allee [78] that related to the non-negative correlation among individual size/density & per-capita proliferation rate at the density of low population [78–82]. Such non-negative correlation may give rise to a critical population size below which the population dies out [121]. If the population dies out below the critical level, then the Allee effect is known as strong Allee effect. In another way, the weak Allee effect happens where the proliferation rate diminishes but stays non-negative at low level of species density.

Alike Allee effect, the infection is another fundamental reason for which the population become extinct. The interaction among Allee effects and infection has a substantial biological connection with nature and needs to be investigated further [122]. As for illustrations, the combined role of diseases & Allee effect has been noticed in African wild dogs (Lycaon pictus) [123] and the island fox (Urocyon littoralis) [124]. The predator-prey system with Allee effect has been studied by numerous authors for comprehensive under-

---

standing the complicated dynamics [79–82, 125–129] as well as the interplay of Allee effects and disease on species's establishment and persistence [18–20, 31, 101, 120, 130, 131]. All these study suggests the intense role of Allee effects in population dynamics, especially when it couples with disease.

The main aim of this chapter is to investigate the role of weak Allee effect in a delayed eco-epidemiological model. We assume that the infection spread among prey population only and the prey population is divided into two categories, such as uninfected and infected prey population. The predator population are not infected by the disease though they consume infected prey. The transmission of the disease in the uninfected prey population is not an instantaneous process followed by some time lag. The proposed predator-prey system experiences a Hopf bifurcation as the value of the time delay increases and further increment of the time delay shows chaotic behavior of the proposed system. The system also shows chaotic behavior as the disease transmission rate increases.

4.2   The model

A mathematical model has been formulated to study the interactive dynamics of prey-predator interplays with disease in the prey species and the role of discrete time lag as well as the impact of the weak Allee effect. The following hypothesis are made to develop the basic eco-epidemiological model:

- In absence of disease and predation, the prey species grow logistically with proliferation rate $\alpha(> 0)$ and carrying capacity $K(> 0)$. So, we have $\frac{dS}{dT} = \alpha S \left(1 - \frac{S}{K}\right)$.

- Let the predator population (P) feed the prey population (S) with response function $f(S)$. We consider that the predator population attend Holling type-II response function, where $f(S) = \lambda S/(\eta + S)$, with λ is the search rate of prey by the predators and η is the half-saturation constant. Hence, the predator-prey system leads to the following form

$$
\begin{aligned}
\frac{dS}{dT} &= \alpha S \left(1 - \frac{S}{K}\right) - \frac{\lambda SP}{\eta + S}, \\
\frac{dP}{dT} &= \frac{\lambda \xi SP}{\eta + S} - \mu_2 P,
\end{aligned}
\tag{4.1}
$$

where ξ represents the conversion coefficient and μ_2 is the natural death rate of predator species.

111

- In presence of the infectious diseases, the total prey population (N) are classified into two different categories, namely uninfected (S) and infected (I) prey population. At any instant T, the total biomass of prey species is $N(T) = S(T) + I(T)$ and $P(T)$ describes the biomass for the predator species.

- It is assumed that the infection is spread among prey species only. The mode of infection transmission obey the law of mass action and spread among the prey species only and infection is not genetically inherited. The infected individuals do not recover or become life-long immune. The uninfected species (S) are able to reproduce with logistic growth and infected individual (I), died before having the ability of reproducing. Howbeit, infected individuals (I) still added with (S) to individuals proliferation towards the biotic capacity. Hence, we have the following system

$$
\begin{aligned}
\frac{dS}{dT} &= \alpha S \left(1 - \frac{S+I}{K} \right) - \gamma SI, \\
\frac{dI}{dT} &= \gamma SI - \mu_1 I,
\end{aligned}
\tag{4.2}
$$

where γ represents the force of infection among healthy and infected prey individuals and μ_1 is the natural decay rate of the infected prey population.

Therefore, we have two system, as for example, predator-prey system (4.1) and epidemic system (4.2). The system (4.1) and (4.2) have been rigorously examined as they have strong interplays among each of the components. The system (4.1) has three equilibrium points $E_0^{SP}(0,0)$, $E_1^{SP}(K,0)$ and $E_{SP}^*(S_{SP}^*, I_{SP}^*)$ where $S_{SP}^* = \eta\mu_2/(\lambda\xi - \mu_2)$ and $I_{SP}^* = \frac{\alpha}{\lambda}(\eta + S_{SP}^*)(1 - \frac{S_{SP}^*}{K})$. The trivial equilibrium $E_0^{SP}(0,0)$ of the system (4.1) always exists but unstable. The predator-free equilibrium $E_1^{SP}(K,0)$ of the model (4.1) always exists and stable if $\lambda\xi K < \mu_2(\eta + K)$. The co-existing equilibrium $E_{SP}^*(S_{SP}^*, I_{SP}^*)$ of the system (4.1) exists if $\xi > \mu_2/\lambda$ and $S_{SP}^* < K$ and stable if $\alpha/K > \lambda P_{SP}^*/(\eta + S_{SP}^*)^2$.

The system (4.2) has three feasible equilibrium points, namely $E_0^{SI}(0,0)$, $E_1^{SI}(K,0)$ and $E_{SI}^*(S_{SI}^*, I_{SI}^*)$ where $S_{SI}^* = \mu_1/\gamma$ and $I_{SI}^* = \alpha(\gamma K - \mu_1)/(\gamma K + \alpha)$. The trivial equilibrium $E_0^{SI}(0,0)$ of the model (4.2) always persists but unstable. The infection-free equilibrium $E_1^{SI}(K,0)$ of the model (4.2) always exists and stable if $\gamma < \mu_1/K$, that is, if the force of infection (γ) is less than a threshold value μ_1/K. The co-existing equilibrium point $E_{SI}^*(S_{SI}^*, I_{SI}^*)$ of the system (4.2) exists and become stable if $\gamma > \mu_1/K$, that is, when the force of infection is grater than the threshold value μ_1/K.

We amalgamate these two system to obtain a single system and this type of system is called eco-epidemiological system, in which both ecological & epidemiological cases are considered synchronously. Assuming that the predator population cannot recognize the infected and susceptible prey, they consume both infected and healthy prey species. The predator population are not infected though feed the infected prey population and the consumption of infected prey species added non-negative proliferation to the predators. Thus, incorporating an Allee effect into the predator population dynamics and based on the above assumptions, combining the system (4.1) and system (4.2) we can depicts the following eco-epidemiological interplays via a system of Ordinary Differential Equations (ODEs):

$$\frac{dS}{dT} = \alpha S \left(1 - \frac{S+I}{K} \right) - \gamma SI - \frac{\lambda SP}{\eta + S},$$
$$\frac{dI}{dT} = \gamma SI - \beta IP - \mu_1 I, \tag{4.3}$$
$$\frac{dP}{dT} = \left(c\beta IP + \frac{\xi \lambda SP}{\eta + S} \right) \frac{P}{\theta + P} - \mu_2 P,$$

where λ represents the search rate of healthy prey by the predators, β is the search rate of infected prey by the predator species, μ_2 is the natural decay rate of predator population, c and ξ represents the conversion coefficients and η is the half-saturation constant. All the model parameters are assumed to be positive from the biological view point. The term $P/(\theta + P)$ indicates Allee effect (which is familiar as weak Allee effect) that indicates the probability of obtaining a mate and θ represents the population finding efficiency [79–82]. The Allee effect will be stronger, if the value of θ is bigger and slower than the per-capita proliferation rate for predators.

To reduce the number of system parameters and non-dimensionalize the model (4.3), we use the transformations as $x = S/K$, $y = I/K$, $z = P/K$, $t = T$ and get the following dimensionless model

$$\frac{dx}{dt} = \alpha x \left[1 - (x+y) \right] - \gamma_x xy - \frac{\lambda xz}{\eta_x + x},$$
$$\frac{dy}{dt} = \gamma_x xy - \beta_y yz - \mu_1 y, \tag{4.4}$$
$$\frac{dz}{dt} = \left(\theta_1 yz + \frac{\theta_2 xz}{\eta_x + x} \right) \frac{z}{\theta_0 + z} - \mu_2 z,$$

where $\gamma_x = \gamma K$, $\eta_x = \eta/K$, $\beta_y = \beta K$, $\theta_0 = \theta/K$, $\theta_1 = c\beta K$ and $\theta_2 = \xi\lambda$.

In the system (4.4), the uninfected prey population become infected prey instantly in presence of the infectious diseases. But in reality there is a time

113

lag for the uninfected prey to become infected prey. Hence, we considered that the disease transmission from uninfected prey to infected prey population is not an immediate procedure, but mediated by some discrete time lag τ (> 0). Thus, the time delay is incorporated in the system (4.4) and we obtain the following system:

$$
\begin{aligned}
\frac{dx}{dt} &= \alpha x \left[1 - (x + y)\right] - \gamma_x xy - \frac{\lambda xz}{\eta_x + x}, \\
\frac{dy}{dt} &= \gamma_x \int_{-\infty}^{t} x(\tilde{k}) y(\tilde{k}) \mathbb{H}(t - \tilde{k}) \, d\tilde{k} - \beta_y yz - \mu_1 y, \\
\frac{dz}{dt} &= \left(\theta_1 yz + \frac{\theta_2 xz}{\eta_x + x}\right) \frac{z}{\theta_0 + z} - \mu_2 z.
\end{aligned}
\tag{4.5}
$$

The infected prey at time t is rising from the uninfected prey at time $t - \tilde{k}$. Here the probability distribution function of $\tilde{k}$ is $\mathbb{H}$ and the function $\mathbb{H}$ is known as the memory function (or delay kernel). The memory function is defined as

$$
\mathbb{H} = \frac{m^{i+1} \tilde{k}^i}{i!} \exp(-m\tilde{k}),
$$

where m is a positive constant and i is a non-negative integer, known as the order of delay. The average time delay is determined as follows [132]:

$$
\bar{T} = \int_0^{\infty} \tilde{k} \mathbb{H}(\tilde{k}) \, d\tilde{k} = \frac{i+1}{m}.
$$

Now, if the memory function takes the form of a delta function as

$$
\mathbb{H} = \delta(\tilde{k} - \tau),
$$

where τ is a non-negative constant, then the system (4.5) leads to

$$
\begin{aligned}
\frac{dx}{dt} &= \alpha x \left[1 - (x + y)\right] - \gamma_x xy - \frac{\lambda xz}{\eta_x + x}, \\
\frac{dy}{dt} &= \gamma_x x(t - \tau) y(t - \tau) - \beta_y yz - \mu_1 y, \\
\frac{dz}{dt} &= \left(\theta_1 yz + \frac{\theta_2 xz}{\eta_x + x}\right) \frac{z}{\theta_0 + z} - \mu_2 z.
\end{aligned}
\tag{4.6}
$$

Let $\bar{C} = C([-\tau, 0], \mathbb{R}_+^3)$ be the Banach space of continuous function in the range $[-\tau, 0]$ into $\mathbb{R}_+^3$, where $\mathbb{R}_+^3 = \{(x, y, z) : x > 0, y > 0, z > 0\}$. The initial history for our predator-prey system with disease in prey system (4.6) as follows:

$$
\begin{aligned}
x(\varphi) = \phi_1(\varphi) > 0, \quad y(\varphi) = \phi_2(\varphi) > 0, \quad z(\varphi) = \phi_3(\varphi) > 0, \\
\varphi \in [-\tau, 0], \quad \phi_1(0) > 0, \quad \phi_2(0) > 0, \quad \phi_3(0) > 0,
\end{aligned}
\tag{4.7}
$$

where $(\phi_1(0), \ \phi_2(0), \ \phi_3(0)) \ \in \ \bar{C}$ and the norm of ϕ in $\bar{C}$ is

$$\|\phi\| = \sup_{-\tau \ \leq \ \varphi \ \leq \ 0} \{|\phi_1(\varphi)|, \ |\phi_2(\varphi)|, \ |\phi_3(\varphi)|\}.$$

4.3 Theoretical analysis of the model (4.6) without delay $(\tau = 0)$

In this section, we investigate the predator-prey model (4.6) with infection in prey population without time delay (that is, $\tau = 0$). The model (4.6) without time lag $(\tau = 0)$ can be expressed as

$$
\begin{aligned}
\frac{dx}{dt} &= \alpha x \left[1 - (x+y)\right] - \gamma_x xy - \frac{\lambda xz}{\eta_x + x} \equiv F(x,y,z), \\
\frac{dy}{dt} &= \gamma_x xy - \beta_y yz - \mu_1 y \equiv G(x,y,z), \qquad\qquad (4.8) \\
\frac{dz}{dt} &= \left(\theta_1 yz + \frac{\theta_2 xz}{\eta_x + x}\right) \frac{z}{\theta_0 + z} - \mu_2 z \equiv H(x,y,z).
\end{aligned}
$$

4.3.1 Equilibria and their existence

Biologically meaningful equilibrium points are the point of intersections of zero-growth isoclines $\alpha x \left[1 - (x+y)\right] - \gamma_x xy - \frac{\lambda xz}{\eta_x + x} = 0, \quad \gamma_x xy - \beta_y yz - \mu_1 y = 0$ and $\left(\theta_1 yz + \frac{\theta_2 xz}{\eta_x + x}\right) \frac{z}{\theta_0 + z} - \mu_2 z = 0$ in the non-negative octant $\mathbf{R}^3_+ = \{[x(t), y(t), z(t)] : x(t) \geq 0, \ y(t) \geq 0, \ z(t) \geq 0\}$. The feasible equilibrium points of (4.8) are as follows:

(i) trivial equilibrium point $E_0(0,0,0)$,

(ii) only susceptible prey equilibrium point $E_1(1,0,0)$,

(iii) predator-free equilibrium point $E_2(x_2, y_2, 0)$ where $x_2 = \mu_1/\gamma_x$ and $y_2 = \alpha(1 - \frac{\mu_1}{\gamma_x})/(\alpha + \gamma_x)$, which is feasible if $\gamma_x > \mu_1$,

(iv) interior equilibrium point $E^*(x^*, y^*, z^*)$ where $y^* = \frac{\alpha(1-x^*)}{\alpha+\gamma_x} - \frac{\lambda(\gamma_x x^* - \mu_1)}{\beta_y(\eta_x + x^*)(\alpha+\gamma_x)}$, $z^* = \frac{\gamma_x x^* - \mu_1}{\beta_y}$ and x^* represents the positive root(s) of

$$x^3 + B_1 x^2 + B_2 x + B_3 = 0, \qquad\qquad (4.9)$$

115

where

$$B_1 = \frac{1}{\alpha\theta_1\gamma_x\beta_y}\left[\lambda\theta_1{\gamma_x}^2 + \gamma_x\beta_y(\alpha + \gamma_x)(\mu_2 - \theta_2)\right.$$
$$\left. -\alpha\theta_1\beta_y\{\mu_1 + \gamma_x(1 - \eta_x)\}\right],$$

$$B_2 = \frac{1}{\alpha\theta_1\gamma_x\beta_y}\left[\alpha\theta_1\mu_1\beta_y(1 - \eta_x) + \mu_1\theta_2\beta_y(\alpha + \gamma_x)\right.$$
$$+\mu_2\gamma_x\eta_x\beta_y(\alpha + \gamma_x) + \mu_2\beta_y(\alpha + \gamma_x)(\theta_0\beta_y - \mu_1)$$
$$\left. -\theta_1\gamma_x(\alpha\eta_x\beta_y + 2\lambda\mu_1)\right],$$

$$B_3 = \frac{1}{\alpha\theta_1\gamma_x\beta_y}\left[\theta_1\mu_1(\alpha\eta_x\beta_y + \lambda\mu_1) + \mu_2\eta_x\beta_y(\alpha + \gamma_x)(\theta_0\beta_y - \mu_1)\right].$$

4.3.2 Nullcline surfaces

The nullclines of the non-delayed predator-prey system (4.8) are the surfaces of $f_1 \equiv \alpha\left[1 - (x + y)\right] - \gamma_x y - \frac{\lambda z}{\eta_x + x} = 0$, $f_2 \equiv \gamma_x x - \beta_y z - \mu_1 = 0$ and $f_3 \equiv \left(\theta_1 yz + \frac{\theta_2 xz}{\eta_x + x}\right)\frac{1}{\theta_0 + z} - \mu_2 = 0$, with $x - y$ co-ordinate plane (that is, $z = 0$), $y - z$ co-ordinate plane (that is, $x = 0$) and $z - x$ co-ordinate plane (that is, $y = 0$). The nullcline surfaces are plotted in Fig. 4.1. The co-ordinate planes are shown by the dotted grid lines. The surfaces $f_1 = 0$, $f_2 = 0$ and $f_3 = 0$ are shown by red, green and blue color, respectively. Equilibrium points are the point of the intersections of these nullcline surfaces. Parameters value for the Fig. 4.1(a) are as follows: $\alpha = 1.0$, $\gamma_x = 0.6$, $\lambda = 0.07$, $\eta_x = 2.0$, $\beta_y = 0.01$, $\mu_1 = 0.1$, $\mu_2 = 0.1$, $\theta_0 = 0.1$, $\theta_1 = 0.75$, $\theta_2 = 0.07$ and for the Fig. 4.1(b) are as follows: $\beta_y = 0.1$ and all other parameters are same as in the subfigure 4.1(a). Nullcline surfaces are limited to the positive octant only as we are interested for non-negative equilibrium points only. The green surface represents $f_3 = 0$, which is the predator nullcline. The red surface represents $f_1 = 0$, which is the susceptible prey nullcline and the blue surface represents $f_2 = 0$, which is the infected prey nullcline. The red, black and green curves in the Fig. 4.1 are the intersection of the nullcline surfaces. The nullcline surfaces $f_1 = 0$ and $f_2 = 0$ intersect along the red curve, the nullcline surfaces $f_2 = 0$ and $f_3 = 0$ intersects along the green curve and the black curve is the intersection of the surfaces $f_1 = 0$ and $f_3 = 0$. The equilibrium points E_0, E_1, E_2 and E^* are shown by black, blue, green and red color solid circles, respectively.

The value of β_y is higher in the Fig. 4.1(b) than the Fig. 4.1(a). This high value of β_y indicates the more consumption of the infected prey species by the predator species. This leads to the lower biomass of the infected prey population. Fig. 4.1(b) shows the inclination of the infected prey nullcline surface whereas the Fig. 4.1(a) shows the infected prey nullcline surface is almost vertical, which is biologically meaningful. The interior equilibrium point in the Fig. 4.1(a) is $E^*(0.4007, 0.1187, 14.0404)$ and the interior equilibrium point in the Fig. 4.1(b) is $E^*(0.7334, 0.1122, 3.4003)$. From the nullcline plots, it can be observed that the predator biomass is reduced for the interior steady state (see the Fig. 4.1(b)) as the value of β_y is increased.
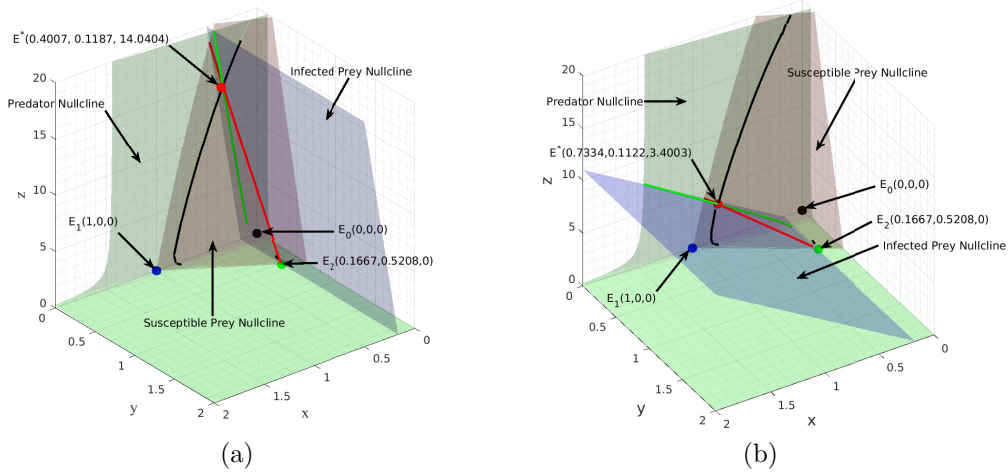
Figure 4.1: Nullcline surfaces of the non-delayed predator-prey system (4.8) in the $x - y - z$ plane. Red surface represents the susceptible prey nullcline, blue surface indicates the infected prey nullcline and the green surface designates the predator nullcline. Biologically feasible equilibrium points E_0, E_1, E_2 and E^* are marked in the figure. The parameters value for (a) are as follows: $\alpha = 1.0$, $\gamma_x = 0.6$, $\lambda = 0.07$, $\eta_x = 2.0$, $\beta_y = 0.01$, $\mu_1 = 0.1$, $\mu_2 = 0.1$, $\theta_0 = 0.1$, $\theta_1 = 0.75$, $\theta_2 = 0.07$ and for (b) $\beta_y = 0.1$ and all other parameters are same as in (a).

4.3.3 Local stability analysis

To determine the local asymptotic stability of the feasible steady states for non-delayed model (4.8), we calculate the Jacobian matrix at each of the singular points. The Jacobian matrix of non-delayed model (4.8) at any

point $E(x, y, z)$ is

$$J_{E(x,y,z)} = \begin{bmatrix} \frac{\partial F}{\partial x} & \frac{\partial F}{\partial y} & \frac{\partial F}{\partial z} \\ \frac{\partial G}{\partial x} & \frac{\partial G}{\partial y} & \frac{\partial G}{\partial z} \\ \frac{\partial H}{\partial x} & \frac{\partial H}{\partial y} & \frac{\partial H}{\partial z} \end{bmatrix}, \tag{4.10}$$

where

$$\frac{\partial F}{\partial x} = \alpha\left[1 - (x + y)\right] - \gamma_x y - \alpha x - \frac{\lambda \eta_x z}{(\eta_x + x)^2}, \quad \frac{\partial F}{\partial y} = -\alpha x - \gamma_x x,$$

$$\frac{\partial F}{\partial z} = -\frac{\lambda x}{\eta_x + x}, \quad \frac{\partial G}{\partial x} = \gamma_x y,$$

$$\frac{\partial G}{\partial y} = \gamma_x x - \beta_y z - \mu_1, \quad \frac{\partial G}{\partial z} = -\beta_y y,$$

$$\frac{\partial H}{\partial x} = \frac{\theta_2 \eta_x z^2}{(\eta_x + x)^2(\theta_0 + z)}, \quad \frac{\partial H}{\partial y} = \frac{\theta_1 z^2}{\theta_0 + z},$$

$$\frac{\partial H}{\partial z} = \left(\theta_1 y + \frac{\theta_2 x}{\eta_x + x}\right)\frac{z}{\theta_0 + z} + \left(\theta_1 y + \frac{\theta_2 x}{\eta_x + x}\right)\frac{\theta_0 z}{(\theta_0 + z)^2} - \mu_2.$$

Theorem 4.3.1. *The trivial equilibrium point $E_0(0,0,0)$ of the model (4.8) is always unstable.*

Proof. The eigenvalues of characteristics equation of the Jacobian matrix (4.10) of (4.8) around $E_0(0,0,0)$ are $\rho_1 = \alpha$, $\rho_2 = -\mu_1$ and $\rho_3 = -\mu_2$. Hence, the trivial equilibrium point $E_0(0,0,0)$ of the system (4.8) is always unstable. $\qquad\square$

Theorem 4.3.2. *The equilibrium point $E_1(1,0,0)$ in which only susceptible prey exists is asymptotically stable if $\gamma_x < \mu_1$.*

Proof. The eigenvalues of characteristic equation of the Jacobian matrix (4.10) of (4.8) around $E_1(1,0,0)$ are $\rho_1 = -\alpha$, $\rho_2 = \gamma_x - \mu_1$ and $\rho_3 = -\mu_2$. Hence, the equilibrium point $E_1(1,0,0)$ of (4.8) will be locally asymptotically stable if $\rho_2 < 0$, that is, if $\gamma_x < \mu_1$. $\qquad\square$

Theorem 4.3.3. *The predator-free equilibrium point $E_2(x_2, y_2, 0)$ is asymptotically stable if $C_1 > 0$, $C_3 > 0$ and $C_1 C_2 - C_3 > 0$, where C_1, C_2 and C_3 are defined in the proof.*

Proof. The characteristic equation for the Jacobian matrix (4.10) of (4.8) around $E_2(x_2, y_2, 0)$ is given by

$$\rho^3 + C_1\rho^2 + C_2\rho + C_3 = 0, \tag{4.11}$$

118

where

$$C_1 = \mu_2 + \alpha x_2,$$
$$C_2 = \alpha x_2(\gamma_x - \mu_1),$$
$$C_3 = \mu_2 x_2(\gamma_x - \mu_1).$$

According to the well-known Routh-Hurwitz criterion, we obtain that the model (4.8) is locally asymptotically stable at $E_2(x_2, y_2, 0)$ if $C_1 > 0$, $C_3 > 0$ and $C_1 C_2 - C_3 > 0$. If the coefficients C_1, C_2 and C_3 fails to satisfy this criteria then predator-free equilibrium point $E_2(x_2, y_2, 0)$ become unstable. □

Theorem 4.3.4. *The interior equilibrium point $E^*(x^*, y^*, z^*)$ is asymptotically stable if $D_1 > 0$, $D_3 > 0$ and $D_1 D_2 - D_3 > 0$, where D_1, D_2 and D_3 are defined in the proof.*

Proof. The characteristic equation of the Jacobian matrix (4.10) evaluated at the interior equilibrium point $E^*(x^*, y^*, z^*)$ is

$$\rho^3 + D_1\rho^2 + D_2\rho + D_3 = 0, \tag{4.12}$$

where

$$
\begin{aligned}
D_1 &= -\left[F_x(x^*, y^*, z^*) + G_y(x^*, y^*, z^*) + H_z(x^*, y^*, z^*)\right], \\
D_2 &= \left[F_x(x^*, y^*, z^*)G_y(x^*, y^*, z^*) - F_y(x^*, y^*, z^*)G_x(x^*, y^*, z^*)\right] \\
&\quad + \left[G_y(x^*, y^*, z^*)H_z(x^*, y^*, z^*) - G_z(x^*, y^*, z^*)H_y(x^*, y^*, z^*)\right] \\
&\quad + \left[F_x(x^*, y^*, z^*)H_z(x^*, y^*, z^*) - F_z(x^*, y^*, z^*)H_x(x^*, y^*, z^*)\right], \\
D_3 &= -F_x(x^*, y^*, z^*)\big[G_y(x^*, y^*, z^*)H_z(x^*, y^*, z^*) \\
&\qquad\qquad\qquad\qquad - G_z(x^*, y^*, z^*)H_y(x^*, y^*, z^*)\big] \\
&\quad + F_y(x^*, y^*, z^*)\big[G_x(x^*, y^*, z^*)H_z(x^*, y^*, z^*) \\
&\qquad\qquad\qquad\qquad - G_z(x^*, y^*, z^*)H_x(x^*, y^*, z^*)\big] \\
&\quad - F_z(x^*, y^*, z^*)\big[G_x(x^*, y^*, z^*)H_y(x^*, y^*, z^*) \\
&\qquad\qquad\qquad\qquad - G_y(x^*, y^*, z^*)H_x(x^*, y^*, z^*)\big].
\end{aligned}
$$

According to the Routh-Hurwitz criterion, we obtain that the non-delayed model (4.8) become locally asymptotically stable at $E^*(x^*, y^*, z^*)$ if $D_1 > 0$, $D_3 > 0$ and $D_1 D_2 - D_3 > 0$. If the coefficients D_1, D_2 and D_3 fails to satisfy this criteria then interior equilibrium point $E^*(x^*, y^*, z^*)$ become unstable. □

4.3.4 PRCC sensitivity analysis

To recognize the most effective parameters of the non-delayed model (4.8) with reference to each of the three populations, a sensitivity analysis is conducted by utilizing Partial Rank Correlation Coefficient (PRCC) method for all system parameters. The PRCC sensitivity analysis measures the relation among the state variables with system parameters. This leads to recognize the most sensitive system parameters, which contributes most to the system variability. The value of the PRCC chosen between -1.0 to $+1.0$ for the model simulation. Following the technique by Marino et al. [133] we conducted Latin hypercube sampling and created 3200 samples to calculate PRCC with reference to the uninfected prey (S), infected prey (I) and predator (P). The indices are assessed at three different time points 50, 100 and 150 days. The PRCC results have shown in the Fig. 4.2 for three different time points. Fig. 4.2(a) shows the highly positive correlated system parameters for the susceptible prey (S) are α, η_x, β_y, μ_1, θ_1 and the highly negative correlated parameters are γ_x, λ and μ_2. Fig. 4.2(b) shows the high positively correlated system parameters for the infected prey (I) is μ_2 and the highly negative correlated parameters are γ_x and θ_1. Fig. 4.2(c) shows the highly positive correlated system parameters for the predator (P) are α, γ_x, η_x, θ_1 and the highly negative correlated parameters are λ, β_y, μ_1 and μ_2. Thus, the PRCC analysis shows that the eight system parameters α, γ_x, λ, η_x, β_y, μ_1, θ_1 and μ_2 are the most sensitive parameters out of ten system parameters.

4.4 Mathematical analysis of the delayed system

Positivity and boundedness of the system (4.6), local stability analysis of the interior equilibrium point and the existence of switching stability studied in this section. The positivity and boundedness of the model system plays a key role in evolutionary biology since the conditions of positivity and boundedness for ecological models guarantees the long-term survival of all the population.

4.4.1 Positivity and boundedness

We determine the positivity and boundedness of (4.6) by the following theorem.

Theorem 4.4.1. *For any initial values $(x_0, y_0, z_0) \in \mathbf{R}_+^3$, all the solutions of (4.6) are positively invariant and uniformly bounded in the domain Γ, where*
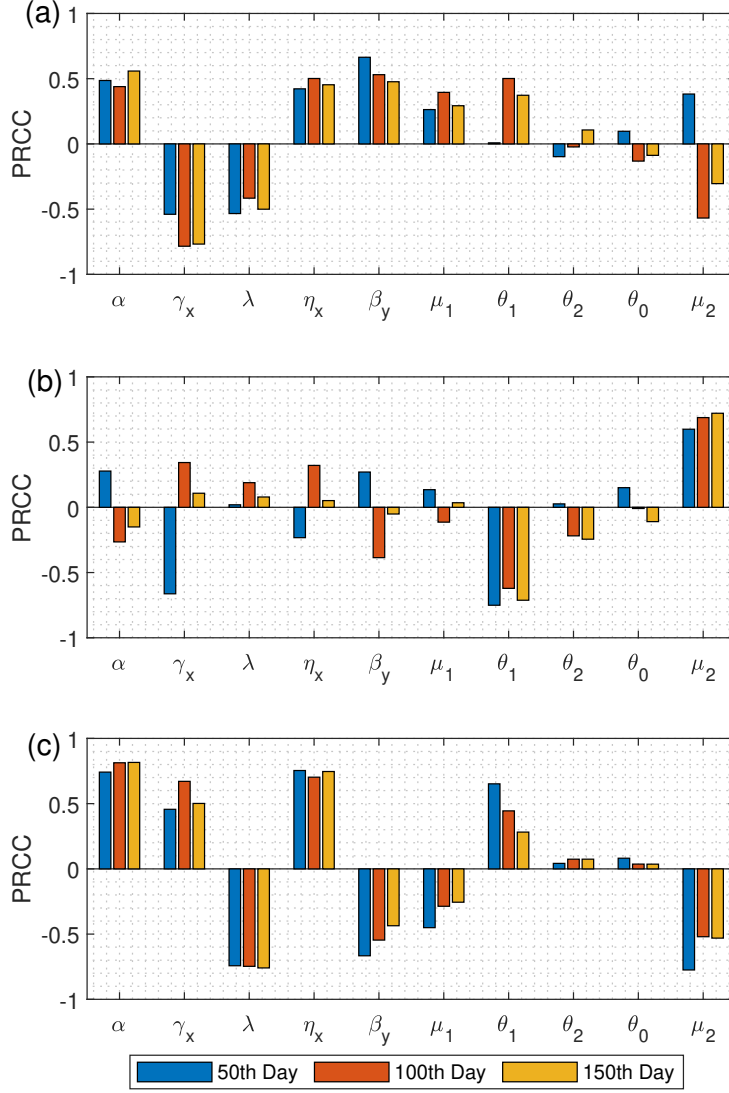
Figure 4.2: Partial rank correlation coefficients illustrating the sensitivity indices for the parameters of the system (4.8) with respect to the (a) susceptible prey, (b) infected prey and (c) predator population at different times with $p < 0.001$.

$$\Gamma = \left\{ (x, y, z) \in \mathbf{R}_+^3 : 0 < x(t) \leq 1, 0 < y(t) \leq 2\alpha/\alpha_1, 0 < z(t) \leq \alpha/(\lambda\alpha_2) \right\},$$

with $\alpha_1 = \min\{\alpha, \mu_1\}$ and $\alpha_2 = \min\{\alpha, (\alpha_1\theta_2\mu_1 - 2\alpha\theta_1)/\alpha_1\}$.

Proof. The first equation of the model (4.6) can be expressed as

$$\frac{dx}{x} = \left[\alpha(1 - x - y) - \gamma_x y - \frac{\lambda z}{\eta_x + x} \right] dt.$$

121

Integrating both sides leads to

$$x(t) = x(0)\exp\left(\int_0^t \left[\alpha\left\{1 - x(s) - y(s)\right\} - \gamma_x y(s)\right.\right.$$
$$\left.\left. - \frac{\lambda z(s)}{\eta_x + x(s)}\right]ds\right) > 0 \ \forall \ t \geq 0.$$

In similar way, the second and third equation of (4.6) gives

$$y(t) = y(0)\exp\left(\int_0^t \left[\gamma_x x(s-\tau)y(s-\tau)\frac{1}{y(s)} - \beta_y z(s) - \mu_1\right]ds\right) > 0,$$

$$z(t) = z(0)\exp\left(\int_0^t \left[\left\{\theta_1 y(s) + \frac{\theta_2 x(s)}{\eta_x + x(s)}\right\}\frac{z(s)}{\theta_0 + z(s)} - \mu_2\right]ds\right) > 0,$$

where $x(0) = x_0 > 0$, $y(0) = y_0 > 0$ and $z(0) = z_0 > 0$. Thus, from $x(t)$, $y(t)$ and $z(t)$, it is obvious that $x(t)$, $y(t)$ and $z(t)$ remains non-negative $\forall$ $t \geq 0$. Therefore, all the solutions of (4.6) are positively invariant.

Now, we shall determine that all the solutions of (4.6) are bounded in the region Γ. To do this, from the first equation of (4.6), we have

$$\frac{dx}{dt} \leq \alpha x(1-x), \qquad \Rightarrow \limsup_{t\to\infty} x \leq 1.$$

Let us consider, $\Upsilon_1 = x(t-\tau) + y$ and taking the derivative of Υ_1 along the solution of (4.6) gives

$$\dot{\Upsilon}_1 = \alpha x(t-\tau)\left[1 - x(t-\tau) - y(t-\tau)\right]$$
$$- \frac{\lambda x(t-\tau)z(t-\tau)}{\eta_x + x(t-\tau)} - \beta_y yz - \mu_1 y,$$
$$\leq 2\alpha x(t-\tau) - \left[\alpha x(t-\tau) + \mu_1 y\right],$$
$$\leq 2\alpha - \alpha_1 \Upsilon_1, \quad \text{where} \quad \alpha_1 = \min\{\alpha, \mu_1\}$$
$$\therefore \quad \lim_{t\to\infty} \Upsilon_1 \leq \frac{2\alpha}{\alpha_1} \implies \limsup_{t\to\infty} y \leq \frac{2\alpha}{\alpha_1}.$$

Again, we consider that $\Upsilon_2 = \frac{1}{\lambda}x + \frac{1}{\theta_2}z$, and taking time derivative of Υ_2

along the solution trajectory of (4.6) gives

$$
\begin{aligned}
\dot{\Upsilon}_2 &\leq \frac{\alpha}{\lambda}x(1-x) + \frac{\theta_1}{\theta_2}yz - \mu_2 z, \\
&\leq \frac{\alpha}{\lambda} - \frac{\alpha}{\lambda}x - \left(\mu_2 - \frac{2\alpha\theta_1}{\alpha_1\theta_2}\right)z, \\
&\leq \frac{\alpha}{\lambda} - \alpha_2\Upsilon_2, \quad \text{where} \quad \alpha_2 = \min\left\{\alpha, (\alpha_1\theta_2\mu_1 - 2\alpha\theta_1)/\alpha_1\right\}
\end{aligned}
$$

$$
\therefore \quad \lim_{t \to \infty} \Upsilon_2 \leq \frac{\alpha}{\lambda\alpha_2} \implies \limsup_{t \to \infty} z \leq \frac{\alpha}{\lambda\alpha_2}.
$$

Thus, all the solutions of the system (4.6) are confined in Γ, where

$$\Gamma = \{(x,y,z) \in \mathbf{R}^3_+ : 0 < x(t) \leq 1, 0 < y(t) \leq 2\alpha/\alpha_1, 0 < z(t) \leq \alpha/(\lambda\alpha_2)\}.$$

$\square$

4.4.2 Local stability analysis

Theorem 4.4.2. *The trivial equilibrium point $E_0(0,0,0)$ of the delayed system (4.6) is always unstable.*

Proof. The variational matrix of the delayed model (4.6) at $E_0(0,0,0)$ is

$$
J_{E_0(0,0,0)} = \begin{bmatrix} \alpha & 0 & 0 \\ 0 & -\mu_1 & 0 \\ 0 & 0 & -\mu_2 \end{bmatrix}.
$$

The eigenvalues of the Jacobian matrix $J_{E_0(0,0,0)}$ are α, $-\mu_1$ and $-\mu_2$. Here, $\alpha > 0$ and hence the trivial equilibrium point $E_0(0,0,0)$ of the delayed system (4.6) is always unstable. $\square$

Proposition 4.4.1. *Suppose $C_1 > 0$ and $C_2 > 0$ then we have the following:*

- *If $C_1 < C_2$, all the roots of $\rho + C_1 - C_2 e^{-\rho\tau} = 0$ have positive real parts for*

$$\tau < \frac{1}{\sqrt{C_2^2 - C_1^2}} \arccos\left(\frac{C_1}{C_2}\right).$$

- *If $C_1 > C_2$, all the roots of $\rho + C_1 - C_2 e^{-\rho\tau} = 0$ have negative real parts for any τ.*

Theorem 4.4.3. *The boundary equilibrium point $E_1(1,0,0)$ of the delayed system (4.6) is unstable if $\mu_1 < \gamma_x$ and*

$$\tau < \frac{1}{\sqrt{\gamma_x{}^2 - \mu_1{}^2}} \arccos \frac{\mu_1}{\gamma_x}.$$

Again if $\mu_1 > \gamma_x$, then $E_1(1,0,0)$ is stable for any τ.

Proof. The variational matrix of the delayed model (4.6) at $E_1(1,0,0)$ is

$$J_{E_1(1,0,0)} = \begin{bmatrix} -\alpha & -\alpha - \gamma_x & -\frac{\lambda}{1+\eta_x} \\ 0 & -\mu_1 + \gamma_x e^{-\rho\tau} & 0 \\ 0 & 0 & -\mu_2 \end{bmatrix}.$$

The characteristic equation is

$$(\rho + \mu_2)(\rho + \alpha)(\rho + \mu_1 - \gamma_x e^{-\rho\tau}) = 0.$$

The variational matrix $J_{E_1(1,0,0)}$ has two negative eigenvalues $-\alpha$ and $-\mu_2$. Due to the Proposition 4.4.1, if $\mu_1 < \gamma_x$ and $\tau < \frac{1}{\sqrt{\gamma_x{}^2-\mu_1{}^2}} \arccos \frac{\mu_1}{\gamma_x}$ then $J_{E_1(1,0,0)}$ has no eigenvalue ρ with $Re\ \rho \leq 0$. Thus, if $\mu_1 < \gamma_x$ and $\tau < \frac{1}{\sqrt{\gamma_x{}^2-\mu_1{}^2}} \arccos \frac{\mu_1}{\gamma_x}$ then $E_1(1,0,0)$ is unstable. Again if $\mu_1 > \gamma_x$, then all the roots of $\rho + \mu_1 - \gamma_x e^{-\rho\tau} = 0$ have negative real parts for any τ, that is, $E_1(1,0,0)$ is stable for any τ but $E_2(x_2, y_2, 0)$ does not exist. $\square$

Theorem 4.4.4. *The predator-free equilibrium point $E_2(x_2, y_2, 0)$ of the delayed model (4.6) is stable for sufficiently large τ.*

Proof. By using $\alpha [1 - (x_2 + y_2)] - \alpha x_2 = 0$, we have the Jacobian matrix of the delayed model (4.6) at $E_2(x_2, y_2, 0)$ is

$$J_{E_2(x_2,y_2,0)} = \begin{bmatrix} -\alpha x_2 & -(\alpha + \gamma_x)x_2 & -\frac{\lambda x_2}{1+\eta_x} \\ \gamma_x y_2 e^{-\rho\tau} & -\mu_1 + \gamma_x x_2 e^{-\rho\tau} & -\beta_y y_2 \\ 0 & 0 & -\mu_2 \end{bmatrix}.$$

The characteristic equation of $J_{E_2(x_2,y_2,0)}$ is

$$(\rho + \mu_2) \left[(\rho + \alpha x_2)(\rho + \mu_1 - \gamma_x x_2 e^{-\rho\tau}) + (\alpha + \gamma_x)\gamma_x x_2 y_2 e^{-\rho\tau} \right] = 0. \quad (4.13)$$

Here, $-\mu_2$ is a root of (4.13). Let $\rho = u + iv$ $(u \geq 0)$ is a root of (4.13). The imaginary part of (4.13) after substitution of $\rho = u + iv$ is

$$2u + (\mu_1 + \alpha x_2) \quad - \quad \gamma_x x_2 e^{-\tau u} \cos \tau v$$

$$+ \quad \gamma_x x_2 e^{-\tau u} \frac{\sin \tau v}{v} [u + \alpha x_2 - (\alpha + \gamma_x)y_2] > \mu_1 + \alpha x_2,$$

for large τ. Here $-\mu_2 < 0$, so for sufficiently large value of τ, $E_2(x_2, y_2, 0)$ will be stable. $\qquad\square$

To perform local stability of delayed model (4.6) at $E(x^*, y^*, z^*)$, we linearized the proposed model (4.6) at the co-existing equilibrium point $E(x^*, y^*, z^*)$ as follows

$$
\begin{aligned}
\frac{du}{dt} &= -\alpha x^*(u + v) + \alpha u[1 - (x^* + y^*)] - \gamma_x(x^* v + y^* u) \\
&\quad - \frac{\lambda}{\eta_x + x^*}(x^* w + z^* u) + \frac{\lambda x^* z^* u}{(\eta_x + x^*)^2}, \\
\frac{dv}{dt} &= \gamma_x \left[x^* v(t - \tau) + y^* u(t - \tau)\right] - \beta_y(y^* w + z^* v) - \mu_1 v, \qquad (4.14) \\
\frac{dw}{dt} &= \left[\theta_1(y^* w + z^* v) + \frac{\theta_2}{\eta_x + x^*}(x^* w + u z^*) - \frac{\theta_2 x^* z^* u}{(\eta_x + x^*)^2}\right]\frac{z^*}{\theta_0 + z^*} \\
&\quad + \left(\theta_1 y^* z^* + \frac{\theta_2 x^* z^*}{\eta_x + x^*}\right)\left[\frac{w}{\theta_0 + z^*} - \frac{z^* w}{(\theta_0 + z^*)^2}\right] - \mu_2 w.
\end{aligned}
$$

Then the corresponding characteristic equation of (4.6) evaluated at interior equilibrium $E^*(x^*, y^*, z^*)$ is

$$
\begin{aligned}
F(\rho, \tau) &\equiv \rho^3 + K_{11}\rho^2 + K_{21}\rho + K_{31} \\
&\quad - \left[K_{12}\rho^2 + K_{22}\rho + K_{32}\right]e^{-\rho\tau} = 0, \qquad (4.15)
\end{aligned}
$$

where

$$
K_{11} = \mu_1 + \alpha x^* + \beta_y z^* - \frac{\lambda x^* z^*}{(\eta_x + x^*)^2} - \frac{\mu_2 \theta_0}{\theta_0 + z^*}, \qquad K_{12} = \gamma_x x^*,
$$

$$
\begin{aligned}
K_{21} &= \alpha x^*(\mu_1 + \beta_y z^*) - \left[\mu_1 + \alpha x^* + \beta_y z^* - \frac{\lambda x^* z^*}{(\eta_x + x^*)^2}\right]\frac{\mu_2 \theta_0}{\theta_0 + z^*} \\
&\quad + \frac{\lambda \eta_x \theta_2 x^* z^{*2}}{(\theta_0 + z^*)(\eta_x + x^*)^3} + \frac{\theta_1 \beta_y y^* z^{*2}}{\theta_0 + z^*} - \frac{\lambda(\mu_1 + \beta_y z^*) x^* z^*}{(\eta_x + x^*)^2},
\end{aligned}
$$

$$
K_{22} = \gamma_x x^*\left[\alpha x^* - \frac{\lambda x^* z^*}{(\eta_x + x^*)^2} - \frac{\mu_2 \theta_0}{\theta_0 + z^*}\right] - \gamma_x(\alpha + \gamma_x)x^* y^*,
$$

$$
\begin{aligned}
K_{31} &= \beta_y y^*\left[\left\{\alpha x^* - \frac{\lambda x^* z^*}{(\eta_x + x^*)^2}\right\}\frac{\theta_1 z^{*2}}{\theta_0 + z^*} - \frac{\eta_x \theta_2(\alpha + \gamma_x) x^* z^{*2}}{(\theta_0 + z^*)(\eta_x + x^*)^2}\right] \\
&\quad + (\mu_1 + \beta_y z^*)\left[\frac{\lambda \eta_x \theta_2 x^* z^{*2}}{(\theta_0 + z^*)(\eta_x + x^*)^3} - \left\{\alpha x^* - \frac{\lambda x^* z^*}{(\eta_x + x^*)^2}\right\}\frac{\mu_2 \theta_0}{\theta_0 + z^*}\right],
\end{aligned}
$$

$$K_{32} = \gamma_x x^* \left[\frac{\lambda \eta_x \theta_2 x^* z^{*2}}{(\theta_0 + z^*)(\eta_x + x^*)^3} - \left\{ \alpha x^* - \frac{\lambda x^* z^*}{(\eta_x + x^*)^2} \right\} \frac{\mu_2 \theta_0}{\theta_0 + z^*} \right]$$
$$+ \gamma_x y^* \left[\frac{\mu_2 \theta_0 (\alpha + \gamma_x) x^*}{\theta_0 + z^*} - \frac{\lambda \theta_1 x^* z^{*2}}{(\eta_x + x^*)(\theta_0 + z^*)} \right].$$

The delay-induced system (4.6) will be stable asymptotically around $E^*(x^*, y^*, z^*)$ if the roots of (4.15) are negative or have negative real part. As the characteristic equation (4.15) is transcendental in nature, so the standard Routh-Hurwitz criteria never be utilized to analyze the stability of delay-induced model (4.6). To understand the behavior of stability we need to identify the sign of real part for the characteristic roots of (4.15).

Let us consider, $\rho(\tau) = \phi(\tau) + i\psi(\tau)$ be a root of the characteristic polynomial (4.15) and substituting $\rho(\tau) = \phi(\tau) + i\psi(\tau)$ in (4.15) and isolating real and complex parts leads to

$$\begin{aligned} \phi^3 - 3\phi\psi^2 \quad + \quad & K_{11}(\phi^2 - \psi^2) + K_{21}\phi + K_{31} \\ = \quad & \Big[\big\{ K_{12}(\phi^2 - \psi^2) + K_{22}\phi + K_{32} \big\} \cos\tau\psi \\ & + (2K_{12}\phi\psi + K_{22}\psi) \sin\tau\psi \Big] e^{-\tau\phi}, \qquad (4.16) \end{aligned}$$

$$\begin{aligned} 3\phi^2\psi - \psi^3 \quad + \quad & 2K_{11}\phi\psi + K_{21}\psi \\ = \quad & \Big[(2K_{12}\phi\psi + K_{22}\psi) \cos\tau\psi \\ & - \big\{ K_{12}(\phi^2 - \psi^2) + K_{22}\phi + K_{32} \big\} \sin\tau\psi \Big] e^{-\tau\phi}. \quad (4.17) \end{aligned}$$

The necessary condition in changing the of stability of E^* is that the characteristic polynomial (4.15) of (4.6) must have complex roots. We set $\phi = 0$ in (4.16) and (4.17), we have

$$K_{31} - K_{11}\psi^2 = (K_{32} - K_{12}\psi^2) \cos\tau\psi + K_{22}\psi \sin\tau\psi, \qquad (4.18)$$
$$K_{21}\psi - \psi^3 = K_{22}\psi \cos\tau\psi - (K_{32} - K_{12}\psi^2) \sin\tau\psi. \qquad (4.19)$$

Squaring and adding (4.18) and (4.19) and eliminating τ, we obtain the following algebraic equation of ψ as

$$\begin{aligned} \psi^6 \quad + \quad & (K_{11}{}^2 - 2K_{21} - K_{12}{}^2)\psi^4 \\ + \quad & (K_{21}{}^2 - 2K_{11}K_{31} + 2K_{12}K_{32} - K_{22}{}^2)\psi^2 \\ + \quad & (K_{31}{}^2 - K_{32}{}^2) = 0. \qquad (4.20) \end{aligned}$$

Substituting $\psi^2 = \xi$ in (4.20), we obtain cubic equation of ξ as

$$\xi^3 + \sigma_1 \xi^2 + \sigma_2 \xi + \sigma_3 = 0, \tag{4.21}$$

where

$$\begin{aligned}
\sigma_1 &= K_{11}{}^2 - 2K_{21} - K_{12}{}^2, \\
\sigma_2 &= K_{21}{}^2 - 2K_{11}K_{31} + 2K_{12}K_{32} - K_{22}{}^2, \\
\sigma_3 &= K_{31}{}^2 - K_{32}{}^2.
\end{aligned}$$

Equation (4.21) will have at least one positive root if $\sigma_3 < 0$. Switching the stability for E^* with reference to time lag τ are given in the following theorem.

Theorem 4.4.5. *If E^* exists and asymptotically stable for the delayed model (4.6) and $\xi_0 = \psi_0{}^2$ be a non-negative root of (4.21) then*

(i) *there exists $\tau = \tau^*$ in such a way that the co-existing equilibrium point E^* of (4.6) is asymptotically stable if $0 \leq \tau < \tau^*$ and unstable if $\tau > \tau^*$.*

(ii) *The delayed model (4.6) experiences Hopf bifurcation at E^* for $\tau = \tau^*$, gives $A(\psi)C(\psi) - B(\psi)D(\psi) \neq 0$,*

where $A(\psi)$, $C(\psi)$, $B(\psi)$ and $D(\psi)$ are stated in proof.

Proof. Since ψ_0 is a root of (4.20), so the characteristic equation (4.15) has a pair complex roots of the form $\pm i\psi_0$. From the expressions (4.18) and (4.19), we get $\tau_j{}^*$ is a function for ψ_0 with $j = 0, 1, 2, \ldots$ and $\tau_j{}^*$ is given by

$$\tau_j{}^* = \frac{1}{\psi_0} \arccos \left[\frac{\begin{aligned}(K_{11}K_{12} - K_{22})\psi_0{}^4 + K_{31}K_{32} \\ + (K_{21}K_{22} - K_{12}K_{31} - K_{11}K_{32})\psi_0{}^2\end{aligned}}{(K_{32} - K_{12}\psi_0{}^2)^2 + (K_{22}\psi_0)^2} \right] + \frac{2\pi j}{\psi_0}.$$

Due to Butler's lemma [134], the interior equilibrium point E^* is asymptotically stable if $\tau < \tau^*$ such that $\tau^* = \min_{j \geq 0} \tau_j{}^*$. Again, the interior equilibrium point E^* is unstable for $\tau > \tau^*$. We shall determine the transversality criteria $\frac{d}{d\tau}\left[Re\rho(\tau)\right]_{\tau=\tau^*} \neq 0$.

Differentiating the expressions (4.16) and (4.17) with reference to τ and substituting $\phi = 0$, we get

$$A(\tau)\frac{d\phi}{d\tau} + B(\tau)\frac{d\psi}{d\tau} = C(\tau), \tag{4.22}$$

$$-B(\tau)\frac{d\phi}{d\tau} + A(\tau)\frac{d\psi}{d\tau} = D(\tau), \tag{4.23}$$

127

where

$$A(\psi) = K_{21} - 3\psi^2 + \left\{(K_{32} - K_{12}\psi^2)\tau - K_{22}\right\}\cos\tau\psi$$
$$+ \psi(\tau K_{22} - 2K_{12})\sin\tau\psi,$$
$$B(\psi) = -2\psi K_{11} + \left\{(K_{32} - K_{12}\psi^2)\tau - K_{22}\right\}\sin\tau\psi$$
$$+ \psi(2K_{12} - \tau K_{22})\cos\tau\psi,$$
$$C(\psi) = \psi^2 K_{22}\cos\tau\psi - \psi(K_{32} - K_{12}\psi^2)\sin\tau\psi,$$
$$D(\psi) = -\psi^2 K_{22}\sin\tau\psi - \psi(K_{32} - K_{12}\psi^2)\cos\tau\psi.$$

Solving the equations (4.22) and (4.23), we have

$$\frac{d}{d\tau}\left[\phi(\tau)\right]_{\tau=\tau^*,\psi=\psi_0} = \left[\frac{A(\psi)C(\psi) - B(\psi)D(\psi)}{A^2(\psi) + B^2(\psi)}\right]_{\tau=\tau^*,\psi=\psi_0}$$

$$\implies \frac{d}{d\tau}\left[Re\psi(\tau)\right]_{\tau=\tau^*,\psi=\psi_0} = \left[\frac{A(\psi)C(\psi) - B(\psi)D(\psi)}{A^2(\psi) + B^2(\psi)}\right]_{\tau=\tau^*,\psi=\psi_0}$$

$$\implies \frac{d}{d\tau}\left[Re\psi(\tau)\right]_{\tau=\tau^*,\psi=\psi_0} \neq 0 \text{ if } \left[A(\psi)C(\psi) - B(\psi)D(\psi)\right]_{\tau=\tau^*,\psi=\psi_0} \neq 0.$$

Thus, the transversality condition is satisfied and the model (4.6) experiences Hopf bifurcation at $\tau = \tau^*$. This gives the proof. $\qquad\square$

4.4.3 Switching stability

We rewrite the characteristic equation (4.15) as

$$\Psi(\rho) + \Omega(\rho)e^{-\tau\rho} = 0,$$

where

$$\Psi(\rho) = \rho^3 + K_{11}\rho^2 + K_{21}\rho + K_{31},$$
$$\Omega(\rho) = -\left[K_{12}\rho^2 + K_{22}\rho + K_{32}\right].$$

Now, we can describe the results as follows:

(i) $\Psi(\rho)$ and $\Omega(\rho)$ have no common imaginary roots and are analytic for $Re(\rho) > 0$.

(ii) $\overline{\Psi(-iy)} = \Psi(iy)$, $\overline{\Omega(-iy)} = \Omega(iy)$ $\quad \forall\ y \in \mathbf{R}$.

(iii) $\Psi(0) + \Omega(0) = K_{31} - K_{32} \neq 0$.

(iv) $\limsup\limits_{|\rho|\to\infty}\left|\frac{\Omega(\rho)}{\Psi(\rho)}\right| = 0 < 1$.

(v) $\chi(y) =\mid \Psi(iy) \mid^2 - \mid \Omega(iy) \mid^2 = y^6 + \Theta_1 y^4 + \Theta_2 y^2 + \Theta_3,$

where

$$
\begin{aligned}
\Theta_1 &= K_{11}{}^2 - 2K_{21} - K_{12}{}^2, \\
\Theta_2 &= K_{21}{}^2 - 2K_{11}K_{31} + 2K_{12}K_{32} - K_{22}{}^2, \\
\Theta_3 &= K_{31}{}^2 - K_{32}{}^2.
\end{aligned}
$$

Here $\chi(y)$ is a cubic equation of y^2 and $\Theta_3 = \sigma_3 < 0$. So, $\chi(y) = 0$ must have at least one positive root. Hence, the system (4.6) has at most finite number of stability switches [49].

Table 4.1: *Interpretation of system variables and parameters and their units.*

Symbol	Interpretation	Units / Dimension
S	Density of uninfected prey species	No. per unit area
I	Density of infected prey species	No. per unit area
P	Density of predator species	No. per unit area
α	Growth rate of uninfected prey	Time^{-1}
K	Environmental prey carrying capacity	No. per unit area
γ	Rate of disease transmission	$[\text{No. per unit area}]^{-1}\text{Time}^{-1}$
λ	Search rate of healthy prey	Time^{-1}
η	Half-saturation constant	No. per unit area
β	Infected prey consumption rate	$[\text{No. per unit area}]^{-1}\text{Time}^{-1}$
μ_1	Decay rate for infected prey without predator consumption	Time^{-1}
c	Conversion coefficient of uninfected prey biomass to predator biomass	Dimensionless
ξ	Conversion coefficient of infected prey biomass to predator biomass	Dimensionless
μ_2	Decay rate for predator	Time^{-1}
θ	Individual searching efficiency	No. per unit area

4.4.4 Uniform persistence and global stability

This section, we establish the condition of uniform permanent of the model (4.6). We define $int(\mathbf{R}^3_+) = \{[x(t), y(t), z(t)] : x(t) > 0, \ y(t) > 0, \ z(t) > 0\}$ where $\mathbf{R}^3_+$ is defined in Section 4.3.1. Before starting the main theorem, we recall some useful definitions.

Definition 4.4.1. *The system (4.6) is known as uniform permanent if there exists a compact domain $D \subset int(\mathbf{R}^3_+)$ in such a way that every solutions of (4.6) with initial values (4.7) remains in the domain D.*

To establish the uniform permanent of (4.6), we describe the theory of uniform permanent for infinite dimensional system [135]. Let U be a complete metric space and U^0 is open and dense in U with $U^0 \cup U_0 = U$ and $U^0 \cap U_0 = \phi$. We also consider that $H(x)$ is a C^0 semigroup in U and $H(x)$ satisfies

$$
\begin{aligned}
H(t) &: U^0 \longrightarrow U^0, \\
H(t) &: U_0 \longrightarrow U_0.
\end{aligned}
\tag{4.24}
$$

Let G_b be the global attractor for $H_b(t)$ where $H_b(t) = H(t)|_{U_0}$.

Lemma 4.4.1. *[136] If $a > 0$, $b > 0$ and $\dot{u}(t) \geq (\leq)u(t)\left[b - au^c(t)\right]$, where c is a positive constant, $t \geq 0$ and $u(0) > 0$, then*

$$
u(t) \geq (\leq) \left(\frac{b}{a}\right)^{1/c} \left[1 + \left(\frac{bu^{-c}(0)}{a} - 1\right)e^{-bct}\right]^{-1/c}.
\tag{4.25}
$$

Lemma 4.4.2. *[117] If $A, B, \tau > 0$ and $\dot{u}(t) = Au(t - \tau) - Bu(t)$, $u(t) > 0$ when $-\tau \leq t \leq 0$, then*

(i) $\lim_{t \to +\infty} u(t) = 0$ *if $A < B$;*

(ii) $\lim_{t \to +\infty} u(t) = +\infty$ *if $A > B$.*

Lemma 4.4.3. *[135] If $H(t)$ satisfies (4.24) and the following conditions*

(i) $H(t)$ *is compact of $t \geq t_0$ where $t_0 > 0$,*

(ii) $H(t)$ *is point-wise dissipative in U,*

(iii) $\hat{G}_b = \bigcup_{x \in G_b} \vartheta(x)$ *is isolated & $\hat{S}$ is an open covering of $\hat{G}_b$, where $\hat{S} = \{S_1, S_2, \ldots, S_n\}$,*

(iv) $W^s(S_i) \cap U^0 = \phi$ *for $i = 1, 2, 3, \ldots, n$,*

holds, then U_0 is uniform repeller with reference to U^0. Hence, there exists $\epsilon > 0$ such that $\liminf_{t \to +\infty} d(H(t)x, U_0) \geq \epsilon$ for any $x \in U^0$, where d represents the distance of $H(t)x$ from U_0.

Now, from first expression of (4.6), we obtain

$$
\begin{aligned}
\frac{dx}{dt} &\geq \alpha x(1 - x - \frac{2\alpha}{\alpha_1}) - \frac{2\alpha\gamma_x}{\alpha_1}x - \frac{\alpha}{\alpha_2}x \\
&= x\left[\left(\alpha - \frac{2\alpha^2}{\alpha_1} - \frac{2\alpha\gamma_x}{\alpha_1} - \frac{\alpha}{\alpha_2}\right) - \alpha x\right].
\end{aligned}
$$

Using Lemma 4.4.1, we have $\liminf_{t \to +\infty} x(t) \geq m$, where $m = 1 - \frac{2\alpha}{\alpha_1} - \frac{2\gamma_x}{\alpha_1} - \frac{1}{\alpha_2}$.

Theorem 4.4.6. *The model (4.6) is permanent if $m > 0$, $(1 - \epsilon) - \dfrac{m\epsilon\gamma_x\alpha_2\theta_2 + \mu_2(1 + \eta_x)(\alpha + \lambda\theta_0\alpha_2)}{m\alpha\alpha_2\theta_2} > 0$ and $\gamma_x(1 - \epsilon') > \mu_1 + \dfrac{\alpha\beta_y}{\lambda\alpha_2}$ where ϵ, ϵ' are small positive numbers.*

Proof. To prove this theorem, we need to verify that the boundary of $\mathbf{R}_+^3$ repeal positive solutions of (4.6) uniformly. Let $C^+([-\tau, 0], \mathbf{R}_+^3)$ designate the space of continuous function from $[-\tau, 0]$ into $\mathbf{R}_+^3$. Define

$$
\begin{aligned}
C_1 &= \left\{(\nu_1, \nu_2, \nu_3) \in C^+([-\tau, 0], \mathbf{R}_+^3) : \nu_1(\phi) = 0, \phi \in [-\tau, 0]\right\}, \\
C_2 &= \left\{(\nu_1, \nu_2, \nu_3) \in C^+([-\tau, 0], \mathbf{R}_+^3) : \nu_1(\phi) \neq 0, \nu_2(\phi) = 0, \phi \in [-\tau, 0]\right\}, \\
C_3 &= \left\{(\nu_1, \nu_2, \nu_3) \in C^+([-\tau, 0], \mathbf{R}_+^3) : \nu_3(\phi) = 0, \nu_1(\phi)\nu_2(\phi) \neq 0, \phi \in [-\tau, 0]\right\}.
\end{aligned}
$$

Denote $C_0 = C_1 \bigcup C_2 \bigcup C_3$ and $C^0 = intC^+([-\tau, 0], \mathbf{R}_+^3)$, it is suffices to verify that there exists an $\epsilon_0 > 0$ such that for every solution u_t of (4.6) initiating from C^0, $\liminf_{t \to +\infty} d(u_t, C_0) \geq \epsilon_0$.

Now, we shall show that the criterion of the Lemma 4.4.3 are holds. Due to the definition of C_0 and C^0, it is simple to verify that C_0 & C^0 are positively invariant. Hence, the criterion (i) and (ii) of the Lemma 4.4.3 are holds. Then, we have to verify the criterion (iii) and (iv) of the Lemma 4.4.3 holds. There are three constant solutions E_0, E_1 and E_2 in C_0 associated to $(x(t) = 0, y(t) = 0, z(t) = 0)$, $(x(t) = 1, y(t) = 0, z(t) = 0)$ and $(x(t) = x_2, y(t) = y_2, z(t) = 0)$, respectively. If $(x(t), y(t), z(t))$ is the solution of (4.6) starting from C_1, then $dy(t)/dt \leq -\mu_1 y$, $dz(t)/dt \geq -\mu_2 z$. Hence, $y(t) \to 0$, $z(t) \to 0$ as $t \to \infty$. If $(x(t), y(t), z(t))$ is the solution of (4.6) starting from C_2 with $\nu_1(0) > 0$, then $dx(t)/dt \geq \alpha x(1 - x)$, $dz(t)/dt \geq -\mu_2 z$. Hence, $x(t) \to 1$, $z(t) \to 0$ as $t \to \infty$. If $(x(t), y(t), z(t))$ is a solution of (4.6)

starting from C_3 for $\nu_1(0)\nu_2(0) > 0$, then it gives $x(t) \to x_2$, $y(t) \to y_2$ as $t \to \infty$.

This exhibits that if invariant sets E_0, E_1 and E_2 are isolated invariant, then $\{E_0, E_1, E_2\}$ is an isolated as well as an acyclic covering, obeying the criterion (iii) of Lemma 4.4.3.

Now, we shall verify that $W^s(E_0) \cap C^0 = \phi$, $W^s(E_1) \cap C^0 = \phi$ and $W^s(E_2) \cap C^0 = \phi$. The proof of the first expression is very easy, here we shall proof the second and third expressions only. We shall proof the second expression by contradiction, that is, we assume that $W^s(E_1) \cap C^0 \neq \phi$, then there exists a non-negative solution $(x(t), y(t), z(t))$ of (4.6) in such a way that $(x(t), y(t), z(t)) \to (1, 0, 0)$ as $t \to +\infty$. We choose $\epsilon > 0$, sufficiently small enough

$$(1 - \epsilon) - \frac{m\epsilon\gamma_x\alpha_2\theta_2 + \mu_2(1 + \eta_x)(\alpha + \lambda\theta_0\alpha_2)}{m\alpha\alpha_2\theta_2} > 0, \ m > 0 \text{ and } 0 < y(t) < \epsilon,$$

for large $t > t_1$, with t_1 is large enough. From first and third equation of (4.6) we get, for $t > t_1$

$$
\begin{aligned}
\frac{dx}{dt} &\geq x\left[\alpha(1 - x - \epsilon) - \gamma_x\epsilon - \lambda z\right], \\
\frac{dz}{dt} &\geq z\left[\frac{m\lambda\alpha_2\theta_2 z}{(1 + \eta_x)(\alpha + \lambda\theta_0\alpha_2)} - \mu_2\right].
\end{aligned}
\tag{4.26}
$$

Let us consider

$$
\begin{aligned}
\frac{dx_1}{dt} &= x_1\left[\alpha(1 - x_1 - \epsilon) - \gamma_x\epsilon - \lambda x_2\right], \\
\frac{dx_2}{dt} &= x_2\left[\frac{m\lambda\alpha_2\theta_2 x_2}{(1 + \eta_x)(\alpha + \lambda\theta_0\alpha_2)} - \mu_2\right].
\end{aligned}
\tag{4.27}
$$

Let $v = (v_1, v_2)$ be a very small number $\varrho > 0$ such that $\varrho v_1 < x(t_1)$, $\varrho v_2 < z(t_1)$. If $(x_1(t), x_2(t))$ is a solution for (4.27) such that $x_1(t_1) = \varrho v_1$ and $x_2(t_1) = \varrho v_2$, then we obtain by using comparison theorem that $x(t) \geq x_1(t)$, $z(t) \geq x_2(t) \ \forall \ t > t_1$. We can easily obtain a unique positive equilibrium of the system (4.27) as

$$
\begin{aligned}
(x_1{}^*, x_2{}^*) &= \left((1 - \epsilon) - \frac{m\epsilon\gamma_x\alpha_2\theta_2 + \mu_2(1 + \eta_x)(\alpha + \lambda\theta_0\alpha_2)}{m\alpha\alpha_2\theta_2},\right. \\
&\left. \frac{\mu_2(1 + \eta_x)(\alpha + \lambda\theta_0\alpha_2)}{m\lambda\alpha_2\theta_2}\right).
\end{aligned}
$$

Now, $x(t) \geq x_1(t)$, $z(t) \geq x_2(t) \ \forall \ t > t_1$ and $\lim\limits_{t \to \infty} x_2(t) = x_2{}^*$. This leads to a contradiction. Therefore, $W^s(E_1) \cap C^0 = \phi$.

Again if possible let $W^s(E_2) \cap C^0 \neq \phi$. Then there exists a non-negative solution $(x(t), y(t), z(t))$ of (4.6) such that $(x(t), y(t), z(t)) \to (x_2, y_2, 0)$ as $t \to +\infty$. We choose $\epsilon' > 0$ small enough such that $x_1 - \epsilon' < x(t) < x_1 + \epsilon'$ and $\gamma_x(1 - \epsilon') > \mu_1 + \frac{\alpha\beta_y}{\lambda\alpha_2}$ for $t > t_2 - \tau$. From second equation of (4.6), we get for $t > t_2 - \tau$,

$$\frac{dy}{dt} \geq \gamma_x(x_1 - \epsilon')y(t - \tau) - \left(\frac{\alpha\beta_y}{\lambda\alpha_2} + \mu_1\right)y. \tag{4.28}$$

Let us consider

$$\frac{du}{dt} = \gamma_x(x_1 - \epsilon')u(t - \tau) - \left(\frac{\alpha\beta_y}{\lambda\alpha_2} + \mu_1\right)u(t). \tag{4.29}$$

Let $u_0 > 0$ is small enough, gives

$$u_0 < \vartheta(t_2 + \theta) \ for \ \theta \in [-\tau, 0]. \tag{4.30}$$

If $u(t)$ is a solution of (4.29) such that $u(t) = u_0$ for $t_2 - \tau \leq t \leq t_2$ and $\gamma_x(1 - \epsilon') > \mu_1 + \frac{\alpha\beta_y}{\lambda\alpha_2}$, using Lemma 4.4.2, we get $u(t) \to +\infty$ as $t \to +\infty$. Here, $y(t) \geq u(t)$ for $t \geq t_2$, hence $y(t) \to +\infty$ as $t \to +\infty$. This contradicts that $\limsup_{t \to \infty} y \leq \frac{2\alpha}{\alpha_1}$. Therefore, $W^s(E_2) \cap C^0 = \phi$ and we deduce from Lemma 4.4.3 that C_0 repels the non-negative solutions of (4.6) uniformly. Thus, the model (4.6) is permanent. This completes the proof. $\square$

4.4.5 Computation of the length of time lag

We determine the stability of Hopf bifurcating periodic orbit and estimated the magnitude of time lag that preserve the stability of period-1 limit cycle. We considered the model (4.6) and the space of real-valued functions specified in C_+ that satisfied the initial values (4.7) on $[-\tau, 0]$. The delayed system (4.6) is linearized about the co-existing singular point $E^*(x^*, y^*, z^*)$ in the sub-section 4.4.2 (see equations (4.14)). Considering Laplace transformation on both sides of (4.14) gives

$$\left[s - \alpha + 2\alpha x^* + (\alpha + \gamma_x)y^* + \frac{\lambda z^*}{\eta_x + x^*} - \frac{\lambda x^* z^*}{(\eta_x + x^*)^2}\right]U(s)$$

$$= u(0) - (\alpha + \gamma_x)x^* V(s) - \frac{\lambda x^*}{\eta_x + x^*}W(s),$$

$$(s + \mu_1 - \gamma_x x^* + \beta_y z^*)V(s) = v(0) + \gamma_x y^* U(s) - \beta_y y^* W(s)$$
$$+ \gamma_x e^{-s\tau}(y^* K_1 + x^* K_2),$$

$$\left[s + \mu_2 - \left(\theta_1 y^* + \frac{\theta_2 x^*}{\eta_x + x^*} \right) \frac{z^*}{\theta_0 + z^*} \right.$$
$$- \left(\theta_1 y^* z^* + \frac{\theta_2 x^* z^*}{\eta_x + x^*} \right) \left\{ \frac{1}{\theta_0 + z^*} - \frac{z^*}{(\theta_0 + z^*)^2} \right\} \left. \right] W(s)$$
$$= w(0) + \left\{ \frac{\theta_2 z^* U(s)}{\eta_x + x^*} - \frac{\theta_2 x^* z^* U(s)}{(\eta_x + x^*)^2} + \theta_1 z^* V(s) \right\} \frac{z^*}{\theta_0 + z^*},$$

where

$$K_1 = \int_{-\tau}^{0} e^{-st} u(t) dt,$$

$$K_2 = \int_{-\tau}^{0} e^{-st} v(t) dt,$$

and $U(s)$, $V(s)$ and $W(s)$ are Laplace transformation of $u(t)$, $v(t)$ and $w(t)$, respectively.

Due to lines of [134] and utilizing *Nyquist criterion* [137], we proved that the criteria for asymptotic stability of co-existing equilibrium $E^*(x^*, y^*, z^*)$ are as follows

$$\begin{aligned} ImT(i\zeta_0) &> 0, \\ ReT(i\zeta_0) &= 0, \end{aligned} \tag{4.31}$$

where $T(s) = s^3 + K_{11}s^2 + K_{21}s + K_{31} - e^{-\tau s} [K_{12}s^2 + K_{22}s + K_{32}]$ and ζ_0 is the smallest non-negative root for $ReT(i\zeta_0) = 0$.

We established that co-existing equilibrium $E^*(x^*, y^*, z^*)$ is stable due to absence of time lag. Due to continuity, all the eigenvalues will continue to have negative real parts for small $\tau > 0$, given one can assured that no eigenvalue of (4.15) have positive real part that bifurcates from infinity as τ increases from 0. Now, the conditions in (4.31) leads to the following form

$$K_{21}\zeta_0 - \zeta_0^3 > K_{22}\zeta_0 \cos(\tau\zeta_0) - (K_{32} - K_{12}\zeta_0^2) \sin(\tau\zeta_0), \tag{4.32}$$

$$K_{31} - K_{11}\zeta_0^2 = (K_{32} - K_{12}\zeta_0^2) \cos(\tau\zeta_0) + K_{22}\zeta_0 \sin(\tau\zeta_0). \tag{4.33}$$

If the conditions in (4.32) and (4.33) are simultaneously satisfied then the stability of the interior equilibrium $E^*(x^*, y^*, z^*)$ is ensured. We utilized them to get an approximate magnitude of τ. Main goal is to obtain an upper limit of ζ_+ on ζ_0 in such a way that ζ_+ is free from the time lag τ and then to calculate the magnitude of τ so that (4.32) satisfies $\forall$ values of ζ in $0 \le \zeta \le \zeta_+$ and thus in particular at $\zeta = \zeta_0$. We rewrite (4.33) as

$$K_{11}\zeta_0^2 = K_{31} - (K_{32} - K_{12}\zeta_0^2) \cos(\tau\zeta_0) - K_{22}\zeta_0 \sin(\tau\zeta_0).$$

We now maximize ζ_0^2 to obtain an upper value of ζ_+ on ζ_0:

Maximizing $K_{31} - (K_{32} - K_{12}\zeta_0^2)\cos(\tau\zeta_0) - K_{22}\zeta_0\sin(\tau\zeta_0)$.

Subject to $|\sin(\tau\zeta_0)| \leq 1$, $|\cos(\tau\zeta_0)| \leq 1$.

We obtain

$$|K_{11}|\zeta_0^2 \leq |K_{31}| + (|K_{32}| - K_{12}\zeta_0^2) + |K_{22}|\zeta_0. \tag{4.34}$$

Hence, if

$$\zeta_+ = \frac{1}{2(|K_{11}| + K_{12})}\left[-|K_{22}| + \sqrt{|K_{22}|^2 + 4\left(|K_{11}| + K_{12}\right)\left(|K_{31}| + |K_{32}|\right)}\right],$$

then clearly from (4.34), we have $\zeta_0 \leq \zeta_+$.

Now from the inequality (4.32), we obtain

$$\zeta_0^2 < K_{21} - K_{22}\cos(\tau\zeta_0) - K_{12}\sin(\tau\zeta_0) + \frac{K_{32}}{\zeta_0}\sin(\tau\zeta_0). \tag{4.35}$$

Since $E^*(x^*, y^*, z^*)$ is stable asymptotically if $\tau = 0$, hence, for small $\tau > 0$, (4.35) holds. Putting (4.33) in (4.35) and arranging leads to

$$(K_{11}K_{22} + K_{12}\zeta_0^2 - K_{32})\left[\cos(\tau\zeta_0) - 1\right] + \left[(K_{11}K_{12} - K_{22})\zeta_0\right.$$
$$\left. - \frac{K_{11}K_{32}}{\zeta_0}\right]\sin(\tau\zeta_0) < K_{11}K_{21} - K_{31} + K_{32} - K_{12}\zeta_0^2 - K_{11}K_{22}. \tag{4.36}$$

Using the bounds

$$
\begin{aligned}
(K_{11}K_{22} + K_{12}\zeta_0^2 \quad - \quad K_{32})\left[\cos(\tau\zeta_0) - 1\right] \\
= \quad (K_{11}K_{22} + K_{12}\zeta_0^2 - K_{32})2\sin^2\left(\frac{\tau\zeta_0}{2}\right) \\
\leq \quad \frac{1}{2}|K_{11}K_{22} + K_{12}\zeta_0^2 - K_{32}|\zeta_+^2\tau^2,
\end{aligned}
$$

and

$$\left[(K_{11}K_{12} - K_{22})\zeta_0 - \frac{K_{11}K_{32}}{\zeta_0}\right]\sin(\tau\zeta_0) \leq \left[|K_{11}K_{12} - K_{22}|\zeta_0^2 + |K_{11}||K_{32}|\right]\tau.$$

After simplification, we obtain from (4.36) that

$$P_1\tau^2 + P_2\tau < P_3,$$

where

$$P_1 = \frac{1}{2}|K_{11}K_{22} + K_{12}\zeta_+^2 - K_{32}|\zeta_+^2,$$
$$P_2 = |K_{11}K_{12} - K_{22}|\zeta_+^2 + |K_{11}||K_{32}|,$$
$$P_3 = K_{11}K_{21} - K_{31} + K_{32} - K_{12}\zeta_+^2 - K_{11}K_{22}.$$

Hence, if

$$\tau_+ = \frac{1}{2P_1}\left(-P_2 + \sqrt{P_2^2 + 4P_1P_3}\right),$$

then for $0 \le \tau \le \tau_+$, *Nyquist criteria* [137] satisfies and τ_+ calculates the maximum length of time lag that preserve the stability of limit cycle. Thus, we can summarize the results in the following theorem.

Theorem 4.4.7. *If there exists τ in $0 \le \tau \le \tau_+$ such that $P_1\tau^2 + P_2\tau < P_3$, then τ_+ is the maximum value (that is, the length of time lag) of τ for which $E^*(x^*, y^*, z^*)$ become asymptotically stable.*

4.4.6 Global stability

The global asymptotically stability of the co-existing equilibrium point E^* of the model (4.6) for $\tau > 0$ is studied in this section.

Theorem 4.4.8. *If*

$$\min\left\{\alpha + \frac{\gamma_x{}^2 x^*\delta\alpha_1\tau}{2\alpha} - \lambda z^* - \frac{2\alpha\gamma_x}{\delta\alpha_1} - \frac{\alpha\eta_x\theta_2(\theta_0 + z^*)}{\lambda\alpha_2}, \alpha + \gamma_x + \frac{(\gamma_x x^*)^2\alpha_1\tau}{2\alpha}\right.$$
$$\left. - \frac{(\gamma_x x^*)^2\tau}{\delta} - \frac{\alpha\theta_1(\theta_0 + z^*)}{\lambda\alpha_2}, \beta_y - \gamma_x\beta_y x^*\tau - \theta_0(\theta_2 x^* + \theta_1 y^*) - \lambda\right\} > 0,$$

then the interior singular point $E^*(x^*, y^*, z^*)$ is globally stable.

Proof. To prove the theorem, we consider

$$D = \{x, y, z : \delta < x < 1,\ \delta < y < 2\alpha/\alpha_1,\ \delta < z < \alpha/\lambda\alpha_2\}.$$

Then D is a compact bounded region in $\mathbf{R}^3_+$ that gives a distance from both the coordinates, then we get that there exists T^*, such that, for $t > T^*$, every positive solutions of (4.6) for $\tau > 0$, continually enters and stays in D. We consider the transformation as follows

$$x(t) = x^*e^{u(t)},\quad y(t) = y^*e^{v(t)},\quad z(t) = z^*e^{w(t)}.$$

The above transformation of variables alters the interior steady state E^* into trivial equilibrium $u(0) = v(0) = w(0) = 0$ for all $t > 0$. After changing the variables, the system (4.6) transforms to the following set of autonomous nonlinear system as

$$\frac{du}{dt} = \left(\frac{\lambda z^*}{(\eta_x + x)(\eta_x + x^*)} - \alpha \right) x^* \left(e^{u(t)} - 1 \right) - (\alpha + \gamma_x)y^* \left(e^{v(t)} - 1 \right)$$
$$- \frac{\lambda z^*}{\eta_x + x} \left(e^{w(t)} - 1 \right),$$

$$\frac{dv}{dt} = \frac{\gamma_x x^*}{y} y(t - \tau) \left(e^{u(t-\tau)} - 1 \right) + \frac{\gamma_x x^* y^*}{y} \left(e^{v(t-\tau)} - 1 \right) \qquad (4.37)$$
$$- \frac{\gamma_x x^* y^*}{y} \left(e^{v(t)} - 1 \right) - \beta_y z^* \left(e^{w(t)} - 1 \right),$$

$$\frac{dw}{dt} = \frac{1}{(\theta_0 + z)(\theta_0 + z^*)} \left[\frac{\theta_2 \eta_x x^* z(\theta_0 + z^*)}{(\eta_x + x)(\eta_x + x^*)} \left(e^{u(t)} - 1 \right) \right.$$
$$\left. + \theta_1 y^* z(\theta_0 + z^*) \left(e^{v(t)} - 1 \right) + \theta_0 z^* \left\{ \theta_1 y^* + \frac{\theta_2 x^*}{\eta_x + x^*} \right\} \left(e^{w(t)} - 1 \right) \right].$$

Let us consider $V_1(t) = |u(t)|$. Now, evaluating upper right derivative for $V_1(t)$ along the solution (4.6) leads to

$$D^+ V_1(t) \leq \left(\frac{\lambda z^*}{(\eta_x + x)(\eta_x + x^*)} - \alpha \right) x^* \mid e^{u(t)} - 1 \mid -(\alpha + \gamma_x)y^* \mid e^{v(t)} - 1 \mid$$
$$+ \frac{\lambda z^*}{\eta_x + x} \mid e^{w(t)} - 1 \mid,$$
$$\leq (\lambda z^* - \alpha) x^* \mid e^{u(t)} - 1 \mid -(\alpha + \gamma_x)y^* \mid e^{v(t)} - 1 \mid + \lambda z^* \mid e^{w(t)} - 1 \mid.$$

Now, using the relation

$$e^{v(t-\tau)} = e^{v(t)} - \int_{t-\tau}^{t} e^{v(s)} ds,$$

we obtain from the second equation of (4.37) as

$$\frac{dv}{dt} = \frac{\gamma_x x^*}{y} y(t - \tau) \left(e^{u(t-\tau)} - 1 \right) - \beta_y z^* \left(e^{w(t)} - 1 \right)$$
$$- \frac{\gamma_x x^* y^*}{y} \int_{t-\tau}^{t} e^{v(s)} \left\{ \frac{\gamma_x x^*}{y(s)} y(s - \tau) \left(e^{u(s-\tau)} - 1 \right) + \frac{\gamma_x x^* y^*}{y(s)} \left(e^{v(s-\tau)} - 1 \right) \right.$$
$$\left. - \frac{\gamma_x x^* y^*}{y(s)} \left(e^{v(s)} - 1 \right) - \beta_y z^* \left(e^{w(s)} - 1 \right) \right\} ds.$$

137

Now, let us consider $V_2(t) = |v(t)|$. Evaluating upper right derivative for $V_2(t)$ along the solution of (4.6) leads to

$$D^+V_2(t) \leq \frac{2\alpha\gamma_x x^*}{\delta\alpha_1} \mid e^{u(t-\tau)} - 1 \mid -\beta_y z^* \mid e^{w(t)} - 1 \mid$$

$$-\frac{\alpha_1\gamma_x x^* y^*}{2\alpha} \int_{t-\tau}^t e^{v(s)} \left\{ \frac{\delta\alpha_1\gamma_x x^*}{2\alpha} \mid e^{u(s-\tau)} - 1 \mid \right.$$

$$+ \frac{\alpha_1\gamma_x x^* y^*}{2\alpha} \mid e^{v(s-\tau)} - 1 \mid -\frac{\gamma_x x^* y^*}{\delta} \mid e^{v(s)} - 1 \mid -\beta_y z^* \mid e^{w(s)} - 1 \mid \left. \right\} ds.$$

We obtain that there exists $T > 0$, such that $y^* e^{v(t)} < 2\alpha/\alpha_1 \ \forall \ t > T$ and thus for $t > T + \tau$, we get

$$D^+V_2(t) \leq \frac{2\alpha\gamma_x x^*}{\delta\alpha_1} \mid e^{u(t-\tau)} - 1 \mid -\beta_y z^* \mid e^{w(t)} - 1 \mid$$

$$-\gamma_x x^* \int_{t-\tau}^t \left\{ \frac{\delta\alpha_1\gamma_x x^*}{2\alpha} \mid e^{u(s-\tau)} - 1 \mid + \frac{\alpha_1\gamma_x x^* y^*}{2\alpha} \mid e^{v(s-\tau)} - 1 \mid \right.$$

$$- \frac{\gamma_x x^* y^*}{\delta} \mid e^{v(s)} - 1 \mid -\beta_y z^* \mid e^{w(s)} - 1 \mid \left. \right\} ds. \qquad (4.38)$$

Again due to the structure of the above equation (4.38), we consider

$$V_{22}(t) = V_2(t) - \gamma_x x^* \int_{t-\tau}^t \int_h^t \left\{ \frac{\delta\alpha_1\gamma_x x^*}{2\alpha} \mid e^{u(s-\tau)} - 1 \mid \right.$$

$$+ \frac{\alpha_1\gamma_x x^* y^*}{2\alpha} \mid e^{v(s-\tau)} - 1 \mid -\frac{\gamma_x x^* y^*}{\delta} \mid e^{v(s)} - 1 \mid$$

$$- \beta_y z^* \mid e^{w(s)} - 1 \mid \left. \right\} ds dh$$

$$- \frac{(\gamma_x x^*)^2 \delta\alpha_1 \tau}{2\alpha} \int_{t-\tau}^t \mid e^{u(s)} - 1 \mid ds$$

$$- \frac{(\gamma_x x^*)^2 y^* \alpha_1 \tau}{2\alpha} \int_{t-\tau}^t \mid e^{v(s)} - 1 \mid ds$$

$$+ \frac{2\alpha\gamma_x x^*}{\delta\alpha_1} \int_{t-\tau}^t \mid e^{u(s)} - 1 \mid ds.$$

Now, evaluating upper right derivative for $V_{22}(t)$ along the solution of (4.6)

138

leads to

$$
\begin{aligned}
D^+V_{22}(t) \;=\;& D^+V_2(t) - \gamma_x x^* \tau \left[\frac{\delta \alpha_1 \gamma_x x^*}{2\alpha} \mid e^{u(t-\tau)} - 1 \mid \right. \\
& + \frac{\alpha_1 \gamma_x x^* y^*}{2\alpha} \mid e^{v(t-\tau)} - 1 \mid \\
& \left. - \frac{\gamma_x x^* y^*}{\delta} \mid e^{v(t)} - 1 \mid - \beta_y z^* \mid e^{w(t)} - 1 \mid \right] \\
& + \gamma_x x^* \int_{t-\tau}^{t} \left\{ \frac{\delta \alpha_1 \gamma_x x^*}{2\alpha} \mid e^{u(s-\tau)} - 1 \mid + \frac{\alpha_1 \gamma_x x^* y^*}{2\alpha} \mid e^{v(s-\tau)} - 1 \mid \right. \\
& \left. - \frac{\gamma_x x^* y^*}{\delta} \mid e^{v(s)} - 1 \mid - \beta_y z^* \mid e^{w(s)} - 1 \mid \right\} ds \\
& - \frac{(\gamma_x x^*)^2 \delta \alpha_1 \tau}{2\alpha} \left\{ \mid e^{u(t)} - 1 \mid - \mid e^{u(t-\tau)} - 1 \mid \right\} \\
& - \frac{(\gamma_x x^*)^2 y^* \alpha_1 \tau}{2\alpha} \left\{ \mid e^{v(t)} - 1 \mid - \mid e^{v(t-\tau)} - 1 \mid \right\} \\
& + \frac{2\alpha \gamma_x x^*}{\delta \alpha_1} \left\{ \mid e^{u(t)} - 1 \mid - \mid e^{u(t-\tau)} - 1 \mid \right\} \\
\leq\;& \mid e^{u(t)} - 1 \mid \left\{ \frac{2\alpha \gamma_x x^*}{\delta \alpha_1} - \frac{(\gamma_x x^*)^2 \delta \alpha_1 \tau}{2\alpha} \right\} \\
& + \mid e^{v(t)} - 1 \mid \left\{ \frac{(\gamma_x x^*)^2 y^* \tau}{\delta} - \frac{(\gamma_x x^*)^2 y^* \alpha_1 \tau}{2\alpha} \right\} \\
& + \mid e^{w(t)} - 1 \mid \left\{ \gamma_x \beta_y x^* z^* \tau - \beta_y z^* \right\}.
\end{aligned}
$$

Again, let us consider $V_3 = \mid w(t) \mid$. Evaluating the upper right derivative of $V_1(t)$ along the solution of (4.6) leads to

$$
\begin{aligned}
D^+V_3(t) \;\leq\;& \frac{\alpha \theta_2 \eta_x x^* (\theta_0 + z^*)}{\lambda \alpha_2} \mid e^{u(t)} - 1 \mid + \frac{\alpha \theta_1 y^* (\theta_0 + z^*)}{\lambda \alpha_2} \mid e^{v(t)} - 1 \mid \\
& + \theta_0 z^* (\theta_2 x^* + \theta_1 y^*) \mid e^{w(t)} - 1 \mid .
\end{aligned}
$$

Let us consider the Lyapunov functional $V(t)$ as

$$
V(t) = V_1(t) + V_{22}(t) + V_3(t) > \mid u(t) \mid + \mid v(t) \mid + \mid w(t) \mid .
$$

Evaluating upper right derivative for $V_1(t)$ along the solution of (4.6) leads to

$$
\begin{aligned}
D^+V(t) \;=\;& D^+V_1(t) + D^+V_{22}(t) + D^+V_3(t) \\
\leq\;& -p_1 x^* \mid e^{u(t)} - 1 \mid - p_2 y^* \mid e^{v(t)} - 1 \mid \\
& - p_3 w^* \mid e^{w(t)} - 1 \mid ,
\end{aligned}
$$

where

$$p_1 = \alpha + \frac{\gamma_x{}^2 x^* \delta \alpha_1 \tau}{2\alpha} - \lambda z^* - \frac{2\alpha\gamma_x}{\delta\alpha_1} - \frac{\alpha\eta_x\theta_2(\theta_0 + z^*)}{\lambda\alpha_2},$$

$$p_2 = \alpha + \gamma_x + \frac{(\gamma_x x^*)^2 \alpha_1 \tau}{2\alpha} - \frac{(\gamma_x x^*)^2 \tau}{\delta} - \frac{\alpha\theta_1(\theta_0 + z^*)}{\lambda\alpha_2},$$

$$p_3 = \beta_y - \gamma_x\beta_y x^*\tau - \theta_0(\theta_2 x^* + \theta_1 y^*) - \lambda.$$

Due to the Mean Value Theorem, leads to

$$x^* \mid e^{u(t)} - 1 \mid = x^* e^{\eta_1(t)} \mid u(t) \mid > \delta \mid u(t) \mid,$$
$$y^* \mid e^{v(t)} - 1 \mid = y^* e^{\eta_2(t)} \mid v(t) \mid > \delta \mid v(t) \mid,$$
$$z^* \mid e^{w(t)} - 1 \mid = z^* e^{\eta_3(t)} \mid w(t) \mid > \delta \mid w(t) \mid,$$

where $x^* e^{\eta_1(t)}$ lies between x^* and $x(t)$, $y^* e^{\eta_1(t)}$ lies between y^* and $y(t)$, $z^* e^{\eta_1(t)}$ lies between z^* and $z(t)$. Thus,

$$\begin{aligned} D^+ V(t) &\leq -p_1\delta \mid u(t) \mid -p_2\delta \mid v(t) \mid -p_3\delta \mid w(t) \mid \\ &\leq -\eta \left(\mid u(t) \mid + \mid v(t) \mid + \mid w(t) \mid \right), \end{aligned} \tag{4.39}$$

where $\eta = \min\{\delta p_1, \delta p_2, \delta p_3\}$. Note that $V(t) \geq \mid u(t) \mid + \mid v(t) \mid + \mid w(t) \mid$. Therefore, due global stability theorem and equation (4.39), it can be noticed that zero solution for (4.37) is globally asymptotically stable. So, the interior singular point E^* of (4.6) is globally asymptotically stable. $\square$

4.5 Numerical simulation

Numerical simulations are investigated to carry out our theoretical findings that has been performed in the previous sections. The dynamics of the delayed model (4.6) are observed for different values of τ. Local stability at each of the singular points are observed by using numerical simulation for both delayed and non-delayed system. Also, the limit cycle oscillations and high-periodic phenomena has been observed numerically for the delayed system (4.6). Our delayed predator-prey model with infection in prey undergoes Hopf bifurcation by examining τ as a bifurcation parameter.

To perform the model simulations, we consider the parameters set as follows: $\alpha = 1.0$, $\gamma_x = 0.6$, $\lambda = 0.07$, $\eta_x = 2.0$, $\beta_y = 0.01$, $\mu_1 = 0.1$, $\mu_2 = 0.1$, $\theta_0 = 0.1$, $\theta_1 = 0.75$ and $\theta_2 = 0.07$, with the following initial size of the population: $x(0) = 0.9$, $y(0) = 0.1$ and $z(0) = 10.0$. The initial size of the population are fixed for all the numerical simulations.

For this set of parameters, the interior singular point of the non-delayed system (4.8) is $E^*(0.4007, 0.1187, 14.0404)$ with eigenvalues -0.2733, $-0.0291 \pm 0.2122i$, which implies E^* is a stable focus. We also observed by numerical illustrations that for the hypothetical set of parameters value, the non-delayed system (4.8) shows local asymptotically stability at the co-existing steady state $E^*(0.4007, 0.1187, 14.0404)$ (see the black curves in Fig. 4.3). In the Fig. 4.3(d), the position of the co-existing steady state $E^*(0.4007, 0.1187, 14.0404)$ marked by solid red circle within the phase portrait plot for non-delayed model (4.8). The value of the coefficients of the characteristic equation (4.12) are $D_1 = 0.3316$, $D_2 = 0.0618$ and $D_3 = 0.0125$ for the hypothetical set of parameters. Here, $D_1 = 0.3316 > 0$, $D_3 = 0.0125 > 0$ and $D_1 D_2 - D_3 = 0.0080 > 0$, which ensure the local stability of the co-existing steady state $E^*(0.4007, 0.1187, 14.0404)$ of the non-delayed system (4.8).

To obtain a better visibility of how various model parameters affects the system dynamics, we plot the stability region of non-delayed model (4.8) by varying the parameters μ_1 (decay rate of the infected prey species) and γ_x (disease transmission rate) as these system parameters were found most effective due to PRCC sensitivity analysis. Fig. 4.4 shows the stability regions of the biologically meaningful singular points of non-delayed model (4.8) in the $\mu_1 - \gamma_x$ parameter space. Both the system parameters μ_1 and γ_x are varied from 0 to 1.0 and other parameters value are $\alpha = 1.0$, $\lambda = 0.07$, $\eta_x = 2.0$, $\beta_y = 0.01$, $\mu_2 = 0.1$, $\theta_0 = 0.1$, $\theta_1 = 0.75$ and $\theta_2 = 0.07$. We have checked the existence and stability criterion for each of the biologically feasible equilibrium points and the regions are plotted in the Fig. 4.4. The equilibrium point $E_1(1, 0, 0)$ in which only susceptible prey survive, is locally asymptotically stable if $\gamma_x < \mu_1$, which has been plotted in the red color region that has been denoted by the symbol (**A**). In this red-shaded region, the predator-free steady state does not exist. The predator-free equilibrium point $E_2(x_2, y_2, 0)$ is stable in the skyblue color region, which has been symbolized as (**B**). The steady state $E^*(x^*, y^*, z^*)$ where all population exists together, is stable in green color region and symbolized as (**C**). The non-delayed system (4.8) shows limit cycle oscillation in the orange color region, that is, when rate of infection ($\gamma_x = \gamma K$) is high and the death rate of infected prey is very low (μ_1) then the non-delayed system exhibits limit cycle oscillation, which has been shown in the orange color region and symbolized as (**D**).

Next, we explored the impact of discrete time delay for the delayed predator-prey interactions (4.6) by gradually increasing the value of delay
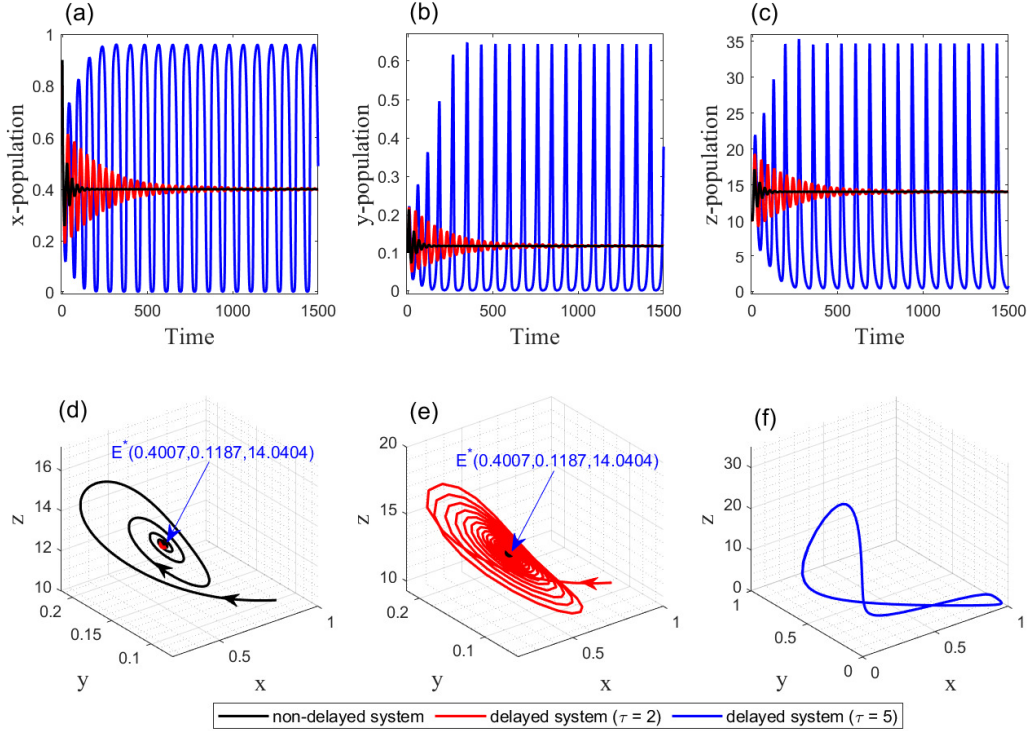
Figure 4.3: Time series evolution and phase portrait diagram of the non-delayed model (4.8) (black color), delayed system (4.6) with $\tau = 2$ (red color) and $\tau = 5$ (blue color). The system parameters value are $\alpha = 1.0$, $\gamma_x = 0.6$, $\lambda = 0.07$, $\eta_x = 2.0$, $\beta_y = 0.01$, $\mu_1 = 0.1$, $\mu_2 = 0.1$, $\theta_0 = 0.1$, $\theta_1 = 0.75$ and $\theta_2 = 0.07$ with initial size of the population are $[x(0), y(0), z(0)] = [0.9, 0.1, 10.0]$.

parameter τ. As the delay parameter τ increases, we investigate the rich dynamics of the delayed system including the existence of stability switching and the high periodic oscillatory dynamics. For $\tau = 2$, the delayed predator-prey model is stable at the interior equilibrium point $E^*(0.4007, 0.1187, 14.0404)$, which has been shown by red curves in the Fig. 4.3. In the time series solutions and phase diagram (see the Fig. 4.3(e)), the position of the interior equilibrium point E^* marked by the solid black circle within the phase portrait plot. In the phase diagram, it can be observed that the solution trajectory converge to the interior equilibrium point E^* implying the local asymptotic stability of E^*. Numerically, we have solved the delayed predator-prey system (4.6) to explore the dynamics at an co-existing equilibrium point E^* for $\tau = 5$ (blue curves in Fig. 4.3). Fig. 4.3(f) illustrates the limit cycle oscillation around E^* for $\tau = 5$.
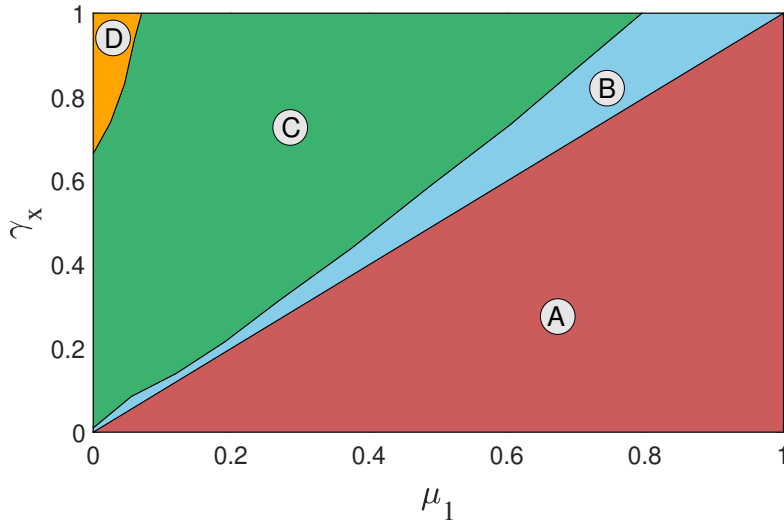
Figure 4.4: Stability region of the biologically feasible equilibrium points $E_1(1, 0, 0)$, $E_2(x_2, y_2, 0)$ and $E^*(x^*, y^*, z^*)$ of the non-delayed predator-prey system (4.8) in the $\mu_1 - \gamma_x$ parameter space. The region A (red) represents the boundary equilibrium $E_1(1, 0, 0)$ is stable. The region B (skyblue) represents the predator-free equilibrium $E_2(x_2, y_2, 0)$ is stable. The region C (green) represents the interior equilibrium point $E^*(x^*, y^*, z^*)$ is stable. The region D (orange) represents the limit cycle oscillation of $E^*(x^*, y^*, z^*)$.

As the value of delay parameter τ increases, the delayed system loses its stability via a Hopf bifurcation at the threshold value $\tau^* \approx 2.9951$. For larger values of delay parameter τ, the interior singular point E^* become unstable via a Hopf bifurcation, which gives a stable periodic behavior. The interior equilibrium point E^* experiences Hopf bifurcation and lose stability as time lag τ passes its critical point $\tau > \tau^*$. We have $\frac{d}{d\tau}[Re\psi(\tau)]_{\tau=\tau^*, \psi=\psi_0} \approx 0.0037 > 0$ that ensured the transversality criterion for Hopf bifurcation. The existence of Hopf bifurcation implies that at bifurcation point a limit cycle is occurred around co-existing steady state E^* and so resulting a periodic solution in time. The occurrence of periodic solution has a significance in ecosystem studies. Furthermore, we expand the magnitude of τ and the delayed model (4.6) exhibits 2-periodic oscillations around $\tau = 6$ and in this case $\tau > \tau^* = 2.9951$. Again, we expand the magnitude of the delay parameter τ and the delayed model demonstrates high periodic oscillating behavior for $\tau = 7$ and in this case also $\tau > \tau^* = 2.9951$ (see the Fig. 4.5). To comprehend the dynamical behavior of delayed model, we plot the bifurcation diagram for the system

(4.6) with reference to time lag τ in Fig. 4.6 for $0 < \tau < 60$ following the guides for plotting a proper bifurcation diagram [138]. As the value of the bifurcation parameter τ increases, the delayed model switches stability from stable to limit cycle behavior, limit cycle behavior to chaotic behavior. The delayed predator-prey system shows multiple periodic oscillation as the parameter τ gradually increases. The bifurcation plot (see Fig. 4.6) also demonstrates maxima and minima of the solution, resulting that the amplitude of oscillating behavior increases with bifurcation parameter τ, where the minimal values of individual on a periodic solution near to zero. The bifurcation diagram (see Fig. 4.6) demonstrates that the delayed model is stable at the interior singular point E^* for the range $\tau \in [0,\ 2.9951)$, the model (4.6) exhibits limit cycle behavior in the interval $\tau \in (2.9951,\ 6]$ and the predator-prey system shows high periodic oscillations in the interval $\tau \in (6,\ 60]$. For larger values of the time delay parameter τ, we observed that movement to a stable interior equilibrium point, with oscillatory behavior to this equilibrium point, resulting maximal characteristic eigenvalues are really a complex eigenvalues with negative real part, that is, increasing for delay parameter τ. An interesting phenomena can be observed that the predator population goes to extinction in the range $\tau \in (7.274,\ 60]$.

The Largest Lyapunov Exponent is an efficient tool to identify the chaos in a dynamical system. Positive Lyapunov exponent indicates the existence of chaos and local instability in a proposed model. Using well known Wolf algorithm [139], we have computed the Largest Lyapunov Exponent and plotted in the Fig. 4.6(d) with reference to the system parameter τ. Other system parameters value are same as in the Figs. 4.6(a)-(c). The Fig. 4.6(d) shows positive Largest Lyapunov Exponents when the system shows chaotic behavior as resulted in the bifurcation diagrams.

In our investigation, we have not explored theoretically the bifurcation of the delayed predator-prey system (4.6) with reference to disease transmission rate γ_x. One of the most influential parameter characterizing the kinetics of delayed predator-prey system is the disease transmission rate γ_x. Fig. 4.7 demonstrates the Hopf bifurcation plot for E^* depending on the parameter γ_x, where the time delay parameter τ is fixed at 30. The bifurcation plot of delayed predator-prey model with reference to the parameter γ_x has been plotted in the interval $0 \leq \gamma_x \leq 1$. The bifurcation diagram (Fig. 4.7) shows that the delayed system is stable at susceptible prey only equilibrium point E_1 for $\gamma_x \in [0,\ 0.099)$, the delayed system is stable at predator-free equilibrium point E_2 in the range $\gamma_x \in (0.099,\ 0.155)$, the delayed predator-prey system is stable around the interior equilibrium point
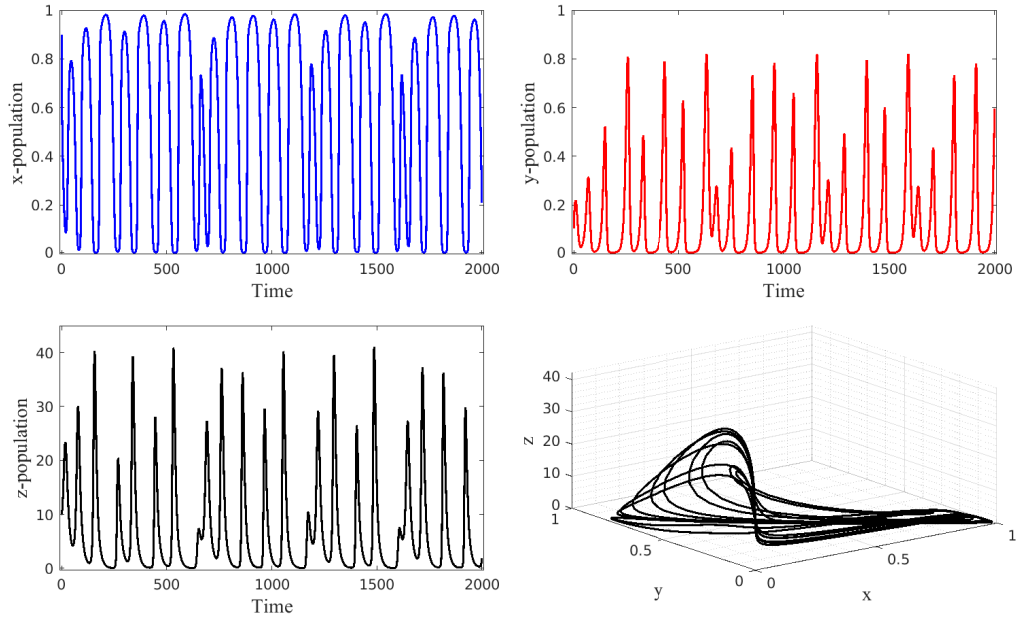
144

Figure 4.5: Time series evolution and phase diagram of the delayed model (4.6) shows the high periodic oscillations around the interior equilibrium point E^* with the time delay $\tau = 7$ ($> \tau^* = 2.7398$). The system parameters value are $\alpha = 1.0$, $\gamma_x = 0.6$, $\lambda = 0.07$, $\eta_x = 2.0$, $\beta_y = 0.01$, $\mu_1 = 0.1$, $\mu_2 = 0.1$, $\theta_0 = 0.1$, $\theta_1 = 0.75$ and $\theta_2 = 0.07$ with initial size of the populations are $[x(0), y(0), z(0)] = [0.9, 0.1, 10.0]$.

E^* for the interval $\gamma_x \in (0.155, \ 0.363)$ and the delayed system shows high periodic oscillating behavior for the range $\gamma_x \in (0.376, \ 1]$. For larger values of infection transmission coefficient γ_x, we observed that movement to a stable co-existing equilibrium point, with high periodic oscillatory behavior to this equilibrium point, implying that maximal eigenvalues are really an complex eigenvalues with negative real part, that is, increasing with the parameter γ_x with fixed time delay $\tau = 30$. Again the predator population goes to extinction for $\gamma_x \in (0.376, 1]$. The Largest Lyapunov Exponent is plotted in the Fig. 4.7(d) with respect to the system parameters γ_x using the Wolf algorithm [139]. Other system parameters value are same as in the Figs. 4.7(a)-(c). Fig. 4.7(d) shows positive Largest Lyapunov Exponents when the system exhibits chaotic behavior in the bifurcation diagrams.

Numerically, we have computed the magnitude of maximal length of $\tau_+ \approx 3.2892$ that preserve the stability for limit cycle. If $\tau < \tau_+$, then the stability of period-1 limit cycle is preserved. The value of τ_+ cannot

145
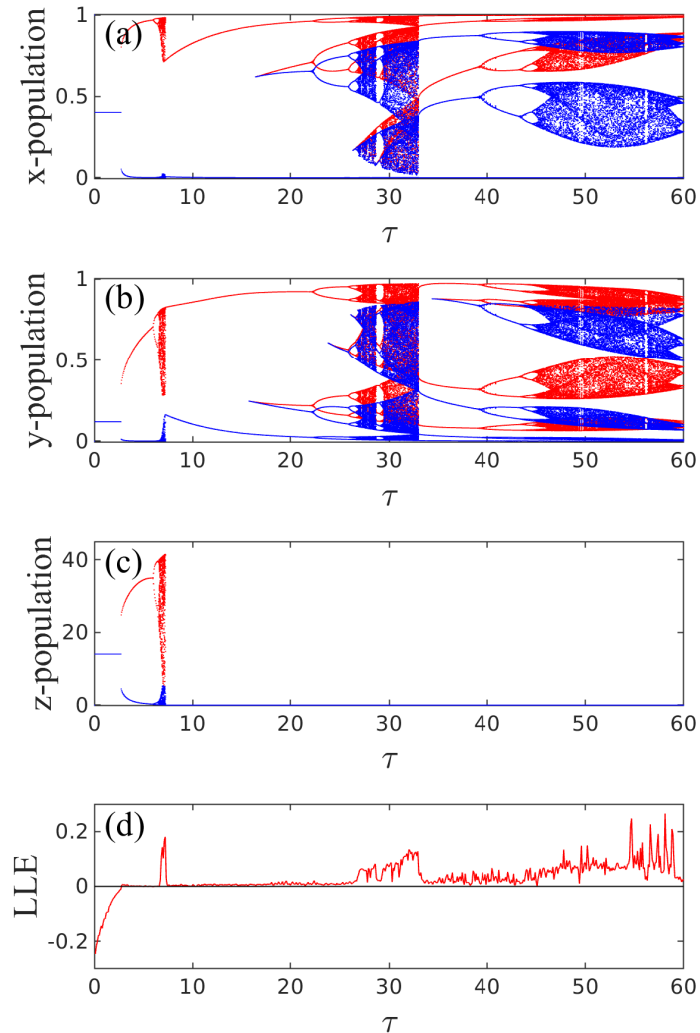
Figure 4.6: Bifurcation diagram of the delayed predator-prey model (4.6) considering time lag τ as a bifurcation parameter and the other system parameters value are $\alpha = 1.0$, $\gamma_x = 0.6$, $\lambda = 0.07$, $\eta_x = 2.0$, $\beta_y = 0.01$, $\mu_1 = 0.1$, $\mu_2 = 0.1$, $\theta_0 = 0.1$, $\theta_1 = 0.75$ and $\theta_2 = 0.07$. Here, (a) represents the bifurcation plot for the uninfected prey; (b) represents the bifurcation plot for infected prey; (c) represents bifurcation plot for predator population and (d) represents Largest Lyapunov Exponent (LLE) with respect to τ.

validate computed interval of values for τ as the estimated value obtained by using model parameters. Here, the model (4.6) is asymptotically stable at an interior singular point E^* if $\tau < \tau^* \approx 2.9951 < \tau_+ \approx 3.2892$ and Hopf

146

bifurcating periodic solution occurs at $\tau^* \approx 2.9951$ (see Figs. 4.6(a)-(c)).
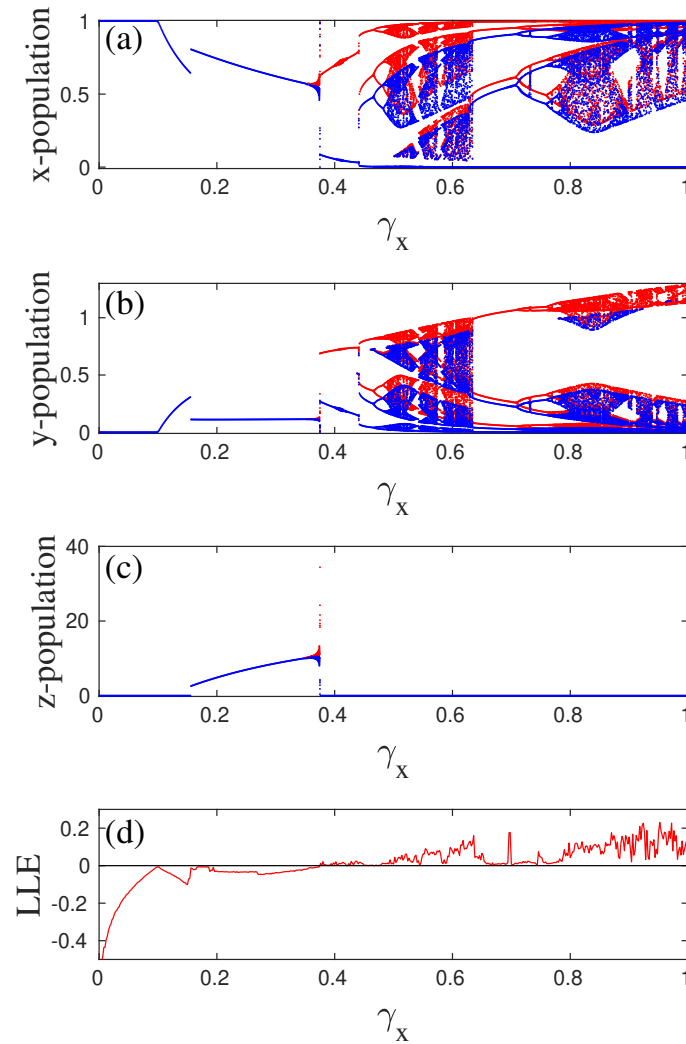
Figure 4.7: Bifurcation plot of the delayed predator-prey model (4.6) considering γ_x as bifurcation parameter and the other system parameters value are $\alpha = 1.0$, $\lambda = 0.07$, $\eta_x = 2.0$, $\beta_y = 0.01$, $\mu_1 = 0.1$, $\mu_2 = 0.1$, $\theta_0 = 0.1$, $\theta_1 = 0.75$, $\theta_2 = 0.07$ and time delay parameter $\tau = 30$. Here, (a) represents the bifurcation plot of the uninfected prey; (b) represents the bifurcation plot of infected prey; (c) represents bifurcation plot of predator population; and (d) represents Largest Lyapunov Exponent (LLE) with respect to γ_x.

4.6 Discussion

In this chapter, we proposed and analyzed the interactive dynamics of an eco-epidemiological predator-prey model with infection in prey species in existence of the incubation time lag τ, and the effect of weak Allee effect due to predators. At present time, Allee effect becomes the most salient research themes that gives a better comprehending towards the real-life ecological scenarios. The main aim of the proposed study is to investigate the kinetics of such eco-epidemiological model under the Allee effect and the influence of incubation time lag. Analytical criterion for the existence of feasible equilibrium points and their stability and bifurcations of an interior steady state have been elucidated by considering the role of incubation time lag τ. We performed extensive analytical computations for both the delayed and non-delayed model. Also, from our local stability analysis of the interior steady state, we can deduce that the individual searching efficiency parameter will never be large enough due to the weak Allee effect, that is, in the term $P/(\theta + P)$.

In our study, we have shown that the time lag τ due to the incubation delay plays a critical role. Incubation delay τ alter the stability of steady states from stable to unstable one, then there is a threshold τ^*, for $\tau^* > \tau$, non-negative interior equilibrium point E^* is locally stable, & it leaves stability as τ crosses via its threshold value τ^* from minimum to maximum values. We have observed that the model (4.6) experiences Hopf bifurcation while τ passes the critical value τ^*, that is, the Theorem 4.4.5 for Hopf bifurcation is verified. If we further increased the delay τ beyond the bifurcation value rise to highly complicated dynamics, incorporating high-periodic oscillations.

In terms of the various dynamical methods that can be demonstrated by our delayed system (4.6), our analytical calculations and numerical illustrations indicates that increasing the time delay parameter τ and infection transmission coefficient γ_x follows in an appearance of stable interior equilibrium point E^* that biologically associates a endured level of infection transmission in the species. Moreover, extend the time delay parameter τ and disease transmission coefficient γ_x gives a destabilization of this equilibrium point and occurrence of high-periodic oscillating behavior. The possible description of these periodic oscillating behavior can be explained as follows: higher disease transmission rate gives a chance to the proliferation of infected prey species; maximum number of infected prey species gives an extinction of the predator population, which in turn, outcomes in an expansion in the utilization of foods/nutrients that act to decrease the disease transmission

coefficient. Also, a higher disease transmission rate γ_x and time delay parameter τ actually destabilizes the interior steady state. We hope that our investigations in this chapter will definitely aid the ecologists and, as a result, it may enhance the theoretical ecology.

Chapter 5

Spatiotemporal dynamics of a predator-prey system with fear effect

5.1 Introduction

The non-uniform motion of the population over the space are omnipresent in nature. During the interplay between prey and predator species, predator species tend to diffuse due to search of prey species, and prey species migrate to circumvent predation, resulting in spatiotemporal variations [64]. This non-uniform motion resulting in a variety of interesting spatiotemporal pattern formation. The idea of Turing instability discovered by Alan Turing in the year 1952 [54] that came to light while a stable equilibrium state drops its stability due to existence of diffusion. The concept of Turing instability is used to explore the stationary and non-stationary patchy pattern formation, familiar as spatiotemporal pattern formation, due to interaction of prey and predator population while we include their randomness into our mathematical models. The reaction-diffusion system of interactive species are developed to incorporate randomness of the population into our mathematical modeling. The reaction part includes the inter and intra-species interplays while the randomness of the species within their habitat is modeled using the diffusion term. A significant number of research has been done on the basis of reaction-diffusion equations for interacting species with suitable initial and boundary restrictions that are able to generate spatiotemporal pattern due to Turing instability [56, 58, 64–66]. Other than the stationary Turing pattern, the non-stationary and chaotic spatial pattern formation are equally important to explore the patchy distribution of the interacting species [58, 67–72].

In this chapter, we studied a predator-prey system introducing the effect of fear on prey due to the presence of predator. A modified and more realistic fear function has been proposed in this chapter. We have extended our study in space by introducing diffusion terms in the proposed predator-prey system. The chapter is arranged in following manner: the mathematical model for predator-prey system with the effect of fear is formulated in Section 5.2. The mathematical form of fear function is modified in the subsection 5.2.2. Fundamental mathematical analysis has been discussed in Section 5.3. Existence of equilibria and their stability studied in Section 5.4, the bifurcation analysis also presented in this section. We considered spatiotemporal model and studied stability in Section 5.5. We conducted extensive numerical simulations in Section 5.6. The chapter ends with a brief discussion.

5.2 The model

We formulate a two species predator-prey system with the effect of fear. We assume that in absence of predation, prey population follows logistic growth. The logistic growth of prey population is divided into three part, namely natural birth rate r_0, natural death rate δ_1 and decay rate γ due to intra-species competition. Hence the prey population (u) can be expressed as follows:

$$\frac{du}{dt} = r_0 u - \gamma u^2 - \delta_1 u. \tag{5.1}$$

Experimental study is conducted to take into account the effect of fear on the growth of prey population and found that the fear of predation reduces the production (or growth) of prey population [7]. Hence, we modify the system (5.1) to account the effect of fear in prey population and we multiply the prey growth term by fear function $f(\alpha, \eta, v)$ and obtain the following expression of prey population:

$$\frac{du}{dt} = r_0 f(\alpha, \eta, v) u - \gamma u^2 - \delta_1 u, \tag{5.2}$$

where v is the density of predator population, α and η represents the level of fear and minimum level of fear, respectively. Here, α is a non-negative constant and the value of η lies between 0 and 1, that is, $0 < \eta \leq 1$. Now, we introduce the predation term $g(u)v$ into (5.2) and obtain the predator-prey system as follows:

$$\begin{aligned} \frac{du}{dt} &= r_0 f(\alpha, \eta, v) u - \gamma u^2 - \delta_1 u - g(u)v, \\ \frac{dv}{dt} &= \theta g(u)v - \delta_2 v, \end{aligned} \tag{5.3}$$

where $g(u)$ is the functional response of the predator to prey density, θ is the conversion coefficient for prey biomass to predator biomass and δ_2 is the natural death rate of predator population.

5.2.1 Functional response

The consumption rate of predator as a function of prey density is known as the functional response in ecology. Three types of functional response was proposed by Holling [140], namely Holling type-I, II and III. In this study, we considered the widely used Holling type-II functional response in the following form:

$$g(u) = \frac{\beta u}{1 + \xi u},\qquad(5.4)$$

where β and ξ are non-negative parameters.

5.2.2 Fear function

Fear induced on a single prey due to a single predator. If the prey is not scared in presence of predator then the level of fear is zero and predator population effects prey biomass only by direct killing. Predator population has no indirect effect on the growth of prey. In aquatic eco-system, zooplankton feed on the free floating phytoplankton and the phytoplankton has no indirect effect in presence of zooplankton. So, in this case the level of fear is zero.

Due to the fear of predators, the prey population become more vigilant and moves away from suspected predators even if prey population may compromise with their quality of food. In this way, predator affecting birth and survival in prey population. So, in this case the level of fear is positive and the presence of predator will decrease the growth of prey population.

Fear function is a monotonic decreasing function of predator density and the level of fear. This function multiplies with the growth term of prey population. The fear function $f(\alpha, \eta, v)$ is a dimensionless quantity and varies from 0 to 1. Considering the biological meaning of α, η and $f(\alpha, \eta, v)$ it is worthy in mentioning that the fear function $f(\alpha, \eta, v)$ satisfies the following properties:

(i) The fear function reduces the growth of prey but if $f(\alpha, \eta, v) = 1$, then the fear function has no effect on growth of prey. If $f(\alpha, \eta, v) = 0$, then the growth of prey population is 0 due to the fear of predators. This implies that the prey population decreases exponentially. To overcome this situation, we consider $f(\alpha, \eta, v) = \eta$ then the fear function has

maximum effect on the growth of prey species, that is, the growth of prey population will be minimum [116]. Hence, the value of the fear function $f(\alpha, \eta, v)$ lies between η and 1, that is, $\eta \leq f(\alpha, \eta, v) \leq 1$.

(ii) In absence of predators, fear has no effect on the growth of prey, that is, $f(\alpha, \eta, 0) = 1$.

(iii) If the level of fear is zero, then the fear function has no effect on the growth of prey, that is, $f(0, \eta, v) = 1$.

(iv) If the predator population becomes infinitely large, then the fear has maximum effect to reduce the growth of prey population, that is, $\lim_{v \to \infty} f(\alpha, \eta, v) = \eta$. The growth of prey population become minimum due to the effect of fear when the the predator population size become infinitely large but the growth of prey population will not become zero due to the effect of fear of predation as Zanette et al. [7] experimentally showed that 40% reduction in growth of prey due to fear. Till date, there is no experimental or observational study that showed that the growth of prey population become zero due the effect of fear. Hence, it is worth in mentioning that $\lim_{v \to \infty} f(\alpha, \eta, v) = \eta$.

(v) If the level of fear (α) become infinitely large, then the fear has maximum effect to reduce the growth of prey population. The growth of prey population will be minimum due to the infinitely large level of fear α. The growth of prey population will never become zero due to the effect of fear of predation as discussed in the fourth case. Hence, it is worthy in mentioning that $\lim_{\alpha \to \infty} f(\alpha, \eta, v) = \eta$.

(vi) If $\frac{\partial f(\alpha, \eta, v)}{\partial \alpha} < 0$, then the fear function $f(\alpha, \eta, v)$ is monotonic decreasing as the level of fear α is increased.

(vii) If $\frac{\partial f(\alpha, \eta, v)}{\partial v} < 0$, then the fear function $f(\alpha, \eta, v)$ is monotonic decreasing as the predator biomass v is increased.

Considering above properties of fear function and following the work of Wang et al. [88] and Sarkar & Khajanchi [116], we considered more realistic and modified fear function as follows:

$$f(\alpha, \eta, v) \; = \; \eta + \frac{1 - \eta}{1 + \alpha v} \; = \; \frac{1 + \eta \alpha v}{1 + \alpha v}, \qquad (5.5)$$

where η is the minimum level of fear and α is the level of fear which depicts the anti-predator behavior of the prey due to predator species. Fig. 5.1 shows the graphical representation of the fear function $f(\alpha, \eta, v)$
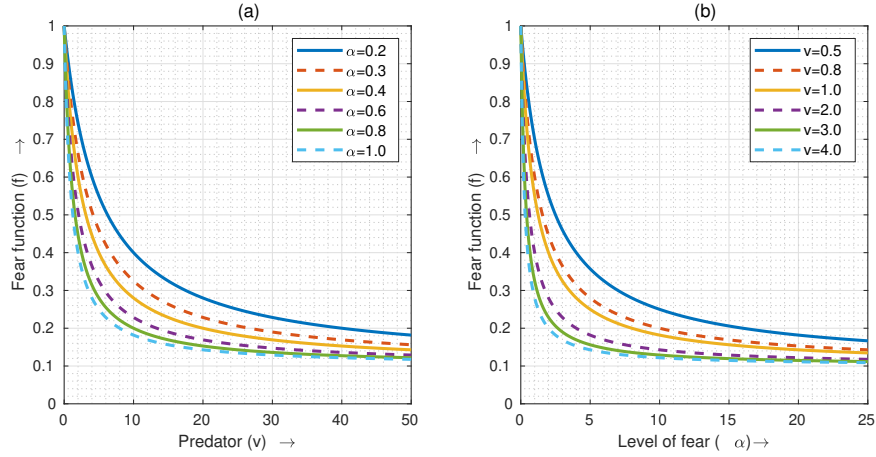
Figure 5.1: Graphical representation of fear function $f(\alpha, \eta, v)$ vs **(a)** predator density (v) for different values of the level of fear (α) and **(b)** level of fear (α) for different values of predator density (v).

with respect to level of fear α and predator density v. Fig. 5.1(a) shows that the fear function $f(\alpha, \eta, v)$ is a monotonic decreasing function of predator density v. The value of $f(\alpha, \eta, v)$ decreases as the value of α increases, that is, the prey growth rate become lower as α increases. Fig. 5.1(b) shows that the fear function $f(\alpha, \eta, v)$ is a monotonic decreasing function of the level of fear α. The value of $f(\alpha, \eta, v)$ decreases as the value of v increases, that is, prey growth rate become lower as v increases.

By considering the expressions of $g(u)$ in (5.4) and $f(\alpha, \eta, v)$ in (5.5), the predator-prey system (5.3) leads to the following form

$$
\begin{aligned}
\frac{du}{dt} &= r_0 u \left(\frac{1 + \alpha \eta v}{1 + \alpha v} \right) - \delta_1 u - \gamma u^2 - \frac{\beta u v}{1 + \xi u} \equiv F_1(u, v), \\
\frac{dv}{dt} &= \frac{\theta \beta u v}{1 + \xi u} - \delta_2 v \equiv F_2(u, v),
\end{aligned}
\tag{5.6}
$$

with non-negative initial conditions $u(0) = u_0 \geq 0$ and $v(0) = v_0 \geq 0$.

5.3 Basic properties of the model (5.6)

5.3.1 Positivity, boundedness and uniform persistent

Positivity of the solutions of (5.6) implies that the prey or predator population can not be negative at any time t for any non-negative initial values. To

proof this, we use the following proposition.

Proposition 5.3.1. *The solutions of (5.6) remains non-negative for any non-negative initial conditions.*

Proof. The system (5.6) can be written as

$$\frac{du}{dt} = \Phi_1(t)u,$$
$$\frac{dv}{dt} = \Phi_2(t)v, \tag{5.7}$$

where

$$\Phi_1(t) = r_0 \left(\frac{1 + \alpha \eta v}{1 + \alpha v} \right) - \delta_1 - \gamma u - \frac{\beta v}{1 + \xi u},$$
$$\Phi_2(t) = \frac{\theta \beta u}{1 + \xi u} - \delta_2.$$

Here, $\Phi_1(t)$ and $\Phi_2(t)$ both are continuous functions of t. Integration of (5.7) leads to

$$u(t) = u(0) \exp \left[\int_0^t \Phi_1(u(s), v(s))ds \right] \geq 0,$$
$$v(t) = v(0) \exp \left[\int_0^t \Phi_2(u(s), v(s))ds \right] \geq 0.$$

From the above expressions it is obvious that prey (u) and predator (v) population remains non-negative for all time t with non-negative initial conditions. $\square$

Proposition 5.3.2. *All the solutions of (5.6) are uniformly bounded for the non-negative initial conditions $(u(0), v(0)) \in \mathbb{R}_+^2$.*

Proof. We define a function

$$w(t) = u(t) + \frac{1}{\theta}v(t).$$

Differentiating with respect to t gives

$$\frac{dw}{dt} = \frac{du}{dt} + \frac{1}{\theta}\frac{dv}{dt}$$
$$= r_0 u \left(\frac{1 + \alpha \eta v}{1 + \alpha v} \right) - \delta_1 u - \gamma u^2 - \frac{\delta_2}{\theta}v$$
$$\leq r_0 u - \delta_1 u - \gamma u^2 - \frac{\delta_2}{\theta}v.$$

155

Assuming $0 < \varphi < \min\left\{\delta_1, \frac{\delta_2}{\theta}\right\}$, we have

$$\frac{dw}{dt} + \varphi w \;\leq\; r_0 u - \gamma u^2 \;\leq\; \frac{r_0^2}{4\gamma},$$

where $r_0^2/4\gamma$ is the maximum value of $r_0 u - \gamma u^2$. Now considering $\tilde{\varphi} = r_0^2/4\gamma$, the above equation becomes

$$\frac{dw}{dt} + \varphi w \;\leq\; \tilde{\varphi}.$$

Now using the theory of differential inequality for $w(t)$, we have

$$0 < w(u,v) \leq \frac{\tilde{\varphi}}{\varphi}(1 - e^{-\varphi t}) + w(u(0), v(0))e^{-\varphi t}.$$

So, if $t \to \infty$, then $0 < w < (\tilde{\varphi}/\varphi)$. Hence, $w(t)$ is bounded and therefore all the solutions of the system (5.6) are confined in the region $\boldsymbol{S} = \left\{(u,v) \in \mathbb{R}_+^2 : w = (\tilde{\varphi}/\varphi) + \epsilon \text{ for } \epsilon > 0\right\}$. $\qquad\square$

5.4 Equilibria and their existence

The equilibrium points are the intersection of the zero-growth prey and predator isoclines. The zero growth prey and predator isoclines are represented by $F_1(u,v) = 0$ and $F_2(u,v) = 0$, respectively. In other words, the biologically feasible equilibrium points of the system (5.6) are the non-negative solutions of $F_1(u,v) = 0$ and $F_2(u,v) = 0$ in $\mathbb{R}_+^2 = \{(u(t), v(t)) : u(t) \geq 0 \text{ and } v(t) \geq 0\}$. The prey isocline consists of the vertical line $u = \frac{\delta_2}{\theta\beta - \xi\delta_2}$ and the axis $u = 0$. Solving the coupled algebraic equations $F_1(u,v) = 0$ and $F_2(u,v) = 0$, we obtain the following biologically feasible equilibrium points:

(i) trivial equilibrium point $E_0(0,0)$,

(ii) axial equilibrium point $E_1(\hat{u}, 0)$, where $\hat{u} = \frac{r_0 - \delta_1}{\gamma}$, $E_1(\hat{u}, 0)$ exists only if $r_0 > \delta_1$,

(iii) co-existing equilibrium point $E^*(u^*, v^*)$, where $u^* = \frac{\delta_2}{\theta\beta - \xi\delta_2}$ and v^* is the positive root(s) of the equation

$$a_0 v^2 + a_1 v + a_2 = 0, \tag{5.8}$$

where

$$a_0 = \frac{\alpha\beta}{1 + \xi u^*},$$

$$a_1 = \frac{\beta}{1 + \xi u^*} + \alpha(\delta_1 + \gamma u^*) - r_0\alpha\eta,$$

$$a_2 = \delta_1 + \gamma u^* - r_0.$$

We state the following theorem for the existence of interior equilibrium point $E^*(u^*, v^*)$ of the system (5.6).

Theorem 5.4.1. *(a) The system (5.6) has no interior equilibrium if*

$$\beta^2 + \alpha^2(1 + \xi u^*)\left\{(\delta_1 + \gamma u^*)^2 + r_0^2\eta^2\right\} + 2\alpha\beta(1 + \xi u^*)(\delta_1 + \gamma u^* - r_0\eta)$$
$$< 2r_0\alpha^2\eta(1 + \xi u^*)^2(\delta_1 + \gamma u^*) + 4\alpha\beta(1 + \xi u^*)(\delta_1 + \gamma u^* - r_0).$$

(b) The system (5.6) has unique interior equilibrium $E^*(u^*, v^*)$ if $r_0 > \delta_1 + \gamma u^*$.

(c) The system (5.6) has two interior equilibrium $E^*(u^*, v^*)$ and $E_s^*(u_s^*, v_s^*)$ if

$$\frac{\beta}{\alpha\eta(1 + \xi u^*)} + \frac{\delta_1 + \gamma u^*}{r_0} < r_0 < \delta_1 + \gamma u^*,$$

where $u^* = \delta_2/(\theta\beta - \xi\delta_2) > 0$.

Proof. The quadratic equation (5.8) have no positive real root if $a_1^2 - 4a_0a_2 < 0$, which implies that

$$\beta^2 + \alpha^2(1 + \xi u^*)\left\{(\delta_1 + \gamma u^*)^2 + r_0^2\eta^2\right\} + 2\alpha\beta(1 + \xi u^*)(\delta_1 + \gamma u^* - r_0\eta)$$
$$< 2r_0\alpha^2\eta(1 + \xi u^*)^2(\delta_1 + \gamma u^*) + 4\alpha\beta(1 + \xi u^*)(\delta_1 + \gamma u^* - r_0).$$

Now if $a_2 < 0$, then the quadratic equation (5.8) has a unique non-negative root given by

$$v^* = \frac{-a_1 + \sqrt{a_1^2 - 4a_0a_2}}{2a_0}.$$

Here, $a_2 < 0$ gives $r_0 > \delta_1 + \gamma u^*$ with $u^* = \delta_2/(\theta\beta - \xi\delta_2)$ and the explicit expression of v^* is as follows:

$$v^* = \frac{\alpha(1 + \xi u^*)(r_0\eta - \delta_1 - \gamma u^*) - \beta}{\alpha\beta}$$
$$+ \frac{1}{\alpha\beta}\left[\beta^2 + \alpha^2(1 + \xi u^*)\left\{(\delta_1 + \gamma u^*)^2 + r_0^2\eta^2\right\}\right.$$
$$+ 2\alpha\beta(1 + \xi u^*)(\delta_1 + \gamma u^* - r_0\eta) - 2r_0\alpha^2\eta(1 + \xi u^*)^2(\delta_1 + \gamma u^*)$$
$$\left. - 4\alpha\beta(1 + \xi u^*)(\delta_1 + \gamma u^* - r_0)\right]^{1/2}.$$

Again, if $a_1 < 0$ and $a_2 > 0$ then the equation (5.8) have two non-negative roots provided $a_1^2 - 4a_0a_2 > 0$ and the roots are given by

$$v^*, v_s^* = \frac{-a_1 \pm \sqrt{a_1^2 - 4a_0a_2}}{2a_0}.$$

Now, if $a_1 < 0$ gives $\frac{\beta}{\alpha\eta(1+\xi u^*)} + \frac{\delta_1+\gamma u^*}{\eta} < r_0$ and $a_2 < 0$ gives $r_0 > \delta_1+\gamma u^*$ with $u^* = \delta_2/(\theta\beta - \xi\delta_2) > 0$. Hence, the system (5.6) has two interior equilibrium points if

$$\frac{\beta}{\alpha\eta(1 + \xi u^*)} + \frac{\delta_1 + \gamma u^*}{r_0} < r_0 < \delta_1 + \gamma u^*.$$

$\square$

5.4.1 Local stability analysis

To study the local asymptotic stability of the system (5.6), we compute the Jacobian matrix at any point $E(u, v)$ is given by

$$J_{E(u,v)} = \begin{bmatrix} \frac{\partial F_1}{\partial u} & \frac{\partial F_1}{\partial v} \\ \frac{\partial F_2}{\partial u} & \frac{\partial F_2}{\partial v} \end{bmatrix}, \tag{5.9}$$

where

$$\frac{\partial F_1}{\partial u} = r_0 \left(\frac{1 + \alpha\eta v}{1 + \alpha v} \right) - \delta_1 - 2\gamma u - \frac{\beta v}{1 + \xi u} + \frac{\beta\xi uv}{(1 + \xi u)^2},$$

$$\frac{\partial F_1}{\partial v} = -\frac{r_0\alpha u(1 - \eta)}{(1 + \alpha v)^2} - \frac{\beta u}{1 + \xi u},$$

$$\frac{\partial F_2}{\partial u} = \frac{\theta\beta v}{(1 + \xi u)^2}, \quad \frac{\partial F_2}{\partial v} = \frac{\theta\beta u}{1 + \xi u} - \delta_2.$$

Theorem 5.4.2. *The trivial equilibrium point $E_0(0,0)$ of the system (5.6) is always unstable.*

Proof. The eigenvalues of the characteristic equation of the Jacobian matrix (5.9) around $E_0(0,0)$ are $\lambda_1 = r_0 - \delta_1$ and $\lambda_2 = -\delta_2$. The trivial equilibrium $E_0(0,0)$ will be stable if $r_0 < \delta_1$, that is, the birth rate of prey is less than the death rate of prey, which is impossible in nature. Hence, the trivial equilibrium $E_0(0,0)$ is always unstable. $\square$

Theorem 5.4.3. *The axial equilibrium $E_1(\hat{u}, 0)$ will be locally asymptotically stable if $\delta_1 < r_0 < \frac{\gamma\delta_2}{\theta\beta - \xi\delta_2} + \delta_1$.*

Proof. The eigenvalues of the characteristic equation of the Jacobian matrix (5.9) around $E_1(\hat{u}, 0)$ are $\lambda_1 = r_0 - \delta_1 - 2\gamma\hat{u}$ and $\lambda_2 = \frac{\theta\beta\hat{u}}{1+\xi\hat{u}} - \delta_2$. The existence criterion of $E_1(\hat{u}, 0)$ is $r_0 > \delta_1$ and if $E_1(\hat{u}, 0)$ exist then $\lambda_1 < 0$. Again $\lambda_2 < 0$ if $r_0 < \frac{\gamma\delta_2}{\theta\beta-\xi\delta_2} + \delta_1$. Hence, the axial equilibrium point $E_1(\hat{u}, 0)$ will exists and become locally asymptotically stable if $\delta_1 < r_0 < \frac{\gamma\delta_2}{\theta\beta-\xi\delta_2} + \delta_1$. $\qquad\square$

Remark: Here $E_0(0,0)$ is locally asymptotically stable if $r_0 < \delta_1$ then the axial equilibrium point $E_1(\hat{u}, 0)$ does not exist. But the existence of $E_1(\hat{u}, 0)$ implies the instability (saddle) of the trivial equilibrium $E_0(0,0)$. It is worthy in mentioning that the local dynamics of $E_0(0,0)$ and $E_1(\hat{u}, 0)$ does not effected by the effect of fear. This indicates the occurrence of transcritical bifurcation around the trivial equilibrium point $E_0(0,0)$.

Theorem 5.4.4. *Necessary condition for the local asymptotic stability of the system (5.6) around the co-existing equilibrium point $E^*(u^*, v^*)$ is $0 < \eta \leq 1$ and $(1 + \xi u^*)^2 > \frac{\beta\xi v^*}{\gamma}$.*

Proof. The characteristic equation of the Jacobian matrix (5.9) around the interior equilibrium $E^*(u^*, v^*)$ is given by

$$\lambda^2 + \sigma_1\lambda + \sigma_2 = 0, \tag{5.10}$$

where

$$\sigma_1 = \gamma u^* - \frac{\beta\xi u^* v^*}{(1 + \xi u^*)^2},$$
$$\sigma_2 = \frac{\theta\beta v^*}{(1 + \xi u^*)^2}\left[\frac{r_0\alpha u^*(1 - \eta)}{(1 + \alpha v^*)^2} + \frac{\beta u^*}{1 + \xi u^*}\right].$$

Following the Routh-Hurwitz criterion, the eigenvalues of the characteristic equation (5.10) will have negative real part if $\sigma_1 > 0$ and $\sigma_2 > 0$. Here, $\sigma_1 > 0$ implies $(1 + \xi u^*)^2 > \frac{\beta\xi v^*}{\gamma}$ and from the expression of σ_2 it is obvious that $\sigma_2 > 0$ when $0 < \eta \leq 1$. Hence, the system (5.6) become asymptotically stable around the interior equilibrium $E^*(u^*, v^*)$ if $0 < \eta \leq 1$ and $(1+\xi u^*)^2 > (\beta\xi v^*/\gamma)$. $\qquad\square$

5.4.2 Existence of transcritical bifurcation

Theorem 5.4.5. *The system (5.6) undergoes a transcritical bifurcation around E_0 when the prey growth rate r_0 crosses the threshold parameter $r_0 = r_0^{tc} = \delta_1$.*

Proof. We use Sotomayor's theorem [141] to verify the transversality condition for the transcritical bifurcation. It can be easily verified that if $r_0 = r_0^{tc} = \delta_1$ then $\det\left[J_{E_0(0,0)}\right] = 0$ and therefore the Jacobian matrix $J_{E_0(0,0)}$ has a zero eigenvalue. Hence, the Sotomayor's theorem can be applied to verify the transcritical bifurcation. The eigenvalues of the Jacobian matrix $J_{E_0(0,0)}$ are $\lambda_1 = r_0 - \delta_1$ and $\lambda_2 = -\delta_2 < 0$. At $r_0 = r_0^{tc} = \delta_1$, the eigenvalue λ_1 vanishes and the other eigenvalue is $\lambda_2 = -\delta_2 < 0$. Let, M and N be two eigenvectors corresponding to zero eigenvalue of the matrix $J_{E_0(0,0)}$ and $J_{E_0(0,0)}^T$, respectively and the corresponding eigenvectors are as follows

$$
\begin{aligned}
M &= \begin{pmatrix} m_1 \\ m_2 \end{pmatrix} = \begin{pmatrix} 1 \\ 0 \end{pmatrix}, \\
N &= \begin{pmatrix} n_1 \\ n_2 \end{pmatrix} = \begin{pmatrix} 1 \\ 0 \end{pmatrix}.
\end{aligned}
$$

Now, we define

$$
\Psi(u,v) = \begin{pmatrix} F_1(u,v) \\ F_2(u,v) \end{pmatrix}.
$$

Therefore,

$$
\Psi_{r_0}(u,v) = \begin{pmatrix} \frac{\partial F_1(u,v)}{\partial r_0} \\ \frac{\partial F_2(u,v)}{\partial r_0} \end{pmatrix} = \begin{pmatrix} u\left[\frac{1+\alpha\eta v}{1+\alpha v}\right] \\ 0 \end{pmatrix}.
$$

Hence,

$$
N^T \Psi_{r_0}(u,v) = (1 \quad 0)\begin{pmatrix} u\left[\frac{1+\alpha\eta v}{1+\alpha v}\right] \\ 0 \end{pmatrix} = u\left[\frac{1+\alpha\eta v}{1+\alpha v}\right],
$$

and therefore $N^T \Psi_{r_0}(E_0(0,0); r_0^{tc}) = 0$.

Now,

$$
D\Psi_{r_0}(u,v) = \begin{pmatrix} \frac{\partial}{\partial u}\left(\frac{\partial F_1(u,v)}{\partial r_0}\right) & \frac{\partial}{\partial v}\left(\frac{\partial F_1(u,v)}{\partial r_0}\right) \\ \frac{\partial}{\partial u}\left(\frac{\partial F_2(u,v)}{\partial r_0}\right) & \frac{\partial}{\partial v}\left(\frac{\partial F_2(u,v)}{\partial r_0}\right) \end{pmatrix} = \begin{pmatrix} \frac{1+\alpha\eta v}{1+\alpha v} & \frac{\alpha(1-\eta)u}{(1+\alpha v)^2} \\ 0 & 0 \end{pmatrix}.
$$

Hence,

$$
N^T\left[D\Psi_{r_0}(E_0(0,0); r_0^{tc})\right]M = (1 \quad 0)\begin{pmatrix} 1 & 0 \\ 0 & 0 \end{pmatrix}\begin{pmatrix} 1 \\ 0 \end{pmatrix} = 1 \neq 0.
$$

160

Now we shall verify the transversality condition. To do this, we consider

$$D^2\Psi_{r_0}(u,v)(M,M) = \begin{pmatrix} \frac{\partial^2 F_1}{\partial u^2}m_1^2 + \frac{\partial^2 F_1}{\partial u \partial v}m_1 m_2 + \frac{\partial^2 F_1}{\partial v \partial u}m_2 m_1 + \frac{\partial^2 F_1}{\partial v^2}m_2^2 \\ \frac{\partial^2 F_2}{\partial u^2}m_1^2 + \frac{\partial^2 F_2}{\partial u \partial v}m_1 m_2 + \frac{\partial^2 F_2}{\partial v \partial u}m_2 m_1 + \frac{\partial^2 F_2}{\partial v^2}m_2^2 \end{pmatrix},$$

where

$$\left.\frac{\partial^2 F_1}{\partial u^2}\right|_{(0,0)} = -2\gamma < 0, \quad \left.\frac{\partial^2 F_1}{\partial v^2}\right|_{(0,0)} = 0,$$

$$\left.\frac{\partial^2 F_1}{\partial u \partial v}\right|_{(0,0)} = \left.\frac{\partial^2 F_1}{\partial v \partial u}\right|_{(0,0)} = -\beta - r_0\alpha(1-\eta) < 0,$$

$$\left.\frac{\partial^2 F_2}{\partial u^2}\right|_{(0,0)} = 0, \quad \left.\frac{\partial^2 F_2}{\partial v^2}\right|_{(0,0)} = 0,$$

$$\left.\frac{\partial^2 F_2}{\partial u \partial v}\right|_{(0,0)} = \left.\frac{\partial^2 F_2}{\partial v \partial u}\right|_{(0,0)} = \theta\beta.$$

Thus, we obtain

$$N^T D^2\Psi_{r_0}(E_0(0,0); r_0^{tc})(M,M) = \begin{pmatrix} 1 & 0 \end{pmatrix}\begin{pmatrix} -2\gamma \\ 0 \end{pmatrix} = -2\gamma < 0.$$

Hence, the system (5.6) experience a supercritical transcritical bifurcation at $E_0(0,0)$ when r_0 passes through $r_0 = r_0^{tc} = \delta_1$. $\square$

5.4.3 Analysis of Hopf bifurcation

In this section, we shall investigate the birth rate r_0 of prey population of the system (5.6) acts as a Hopf bifurcating parameter. The necessary condition to change the stability of (5.6) around the equilibrium $E^*(u^*, v^*)$ is that the characteristic equation (5.10) should have purely imaginary roots. The characteristic equation (5.10) will have purely imaginary roots if $\sigma_1 = 0$ and $\sigma_2 > 0$.

Here, $\sigma_1 = 0$ gives $v^* = \frac{\gamma(1+\xi u^*)^2}{\beta\xi}$ and putting this value of v^* in (5.8), we get the threshold value of r_0 as

$$r_0^* = \frac{1}{1+\alpha\eta v^*}\left[\frac{\alpha\beta v^{*2}}{1+\xi u^*} + \frac{\beta v^*}{1+\xi u^*} + \alpha(\delta_1 + \gamma u^*)v^* + (\delta_1 + \gamma u^*)\right],$$

where u^* is defined earlier.

Let $\lambda(r_0) = X_1(r_0) + iX_2(r_0)$ be the eigenvalue of the characteristic equation (5.10). Now, putting this value of λ in (5.10) and separating the real and imaginary parts, we obtain

$$\begin{aligned} X_1^2 - X_2^2 + \sigma_1 X_1 + \sigma_2 &= 0, \\ 2X_1 X_2 + \sigma_1 X_2 &= 0. \end{aligned} \qquad (5.11)$$

Setting $r_0 = r_0^*$ in such a way that $X_1(r_0^*) = 0$ and substituting in (5.11), we have

$$\begin{aligned} -X_2^2(r_0^*) + \sigma_2(r_0^*) &= 0, \\ \sigma_1(r_0^*)X_2(r_0^*) &= 0 \text{ with } X_2(r_0^*) \neq 0. \end{aligned}$$

From the above expressions, we have $\sigma_1(r_0^*) = 0$ and $X_2(r_0^*) = \sqrt{\sigma_2(r_0^*)}$ and hence $\lambda(r_0^*) = -i\sqrt{\sigma_2(r_0^*)}$.

Theorem 5.4.6. *The necessary and sufficient conditions for the system (5.6) undergoes Hopf bifurcation around $E^*(u^*, v^*)$ is that there exists $r_0 = r_0^*$ such that*

1. $X_1(r_0^*) = 0$,

2. $\left[\frac{d}{dr_0} Re\{\lambda(r_0)\} \right]_{r_0=r_0^*} \neq 0$.

Proof. The eigenvalues of the characteristic equation (5.10) are

$$\lambda_{1,2} = \frac{-\sigma_1 \pm \sqrt{\sigma_1^2 - 4\sigma_2}}{2}.$$

Both σ_1 and σ_2 are the functions of r_0, when other system parameters are fixed. Hence, the positive real part of these eigenvalues changes the sign when r_0 passes through r_0^*. Therefore, the system (5.6) switches its stability provided that the transversality condition is satisfied. Now, we shall verify the transversality condition $\left[\frac{d}{dr_0} Re\{\lambda(r_0)\} \right]_{r_0=r_0^*} \neq 0$. By differentiating both the equations of (5.11) with respect to r_0 and then substituting $X_1(r_0^*) = 0$, we obtain

$$\sigma_1(r_0^*)\frac{dX_1}{dr_0}\Big|_{r_0=r_0^*} - 2X_2(r_0^*)\frac{dX_2}{dr_0}\Big|_{r_0=r_0^*} = -\frac{d\sigma_2}{dr_0}\Big|_{r_0=r_0^*},$$

$$2X_2(r_0^*)\frac{dX_1}{dr_0}\Big|_{r_0=r_0^*} + \sigma_1(r_0^*)\frac{dX_2}{dr_0}\Big|_{r_0=r_0^*} = -X_2\frac{d\sigma_1}{dr_0}\Big|_{r_0=r_0^*}.$$

162

Solving the above two equations, we have

$$\left[\frac{d}{dr_0} Re\left\{\lambda(r_0)\right\}\right]_{r_0=r_0^*} = -\left[\frac{\sigma_1 \frac{d\sigma_2}{dr_0} + 2X_2^2 \frac{d\sigma_1}{dr_0}}{\sigma_1^2 + 4X_2^2}\right]_{r_0=r_0^*}.$$

Thus, the transversality condition is satisfied if $\left(\sigma_1 \frac{d\sigma_2}{dr_0} + 2X_2^2 \frac{d\sigma_1}{dr_0}\right) / (\sigma_1^2 + 4X_2^2) \neq 0$ at $r_0 = r_0^*$. Therefore, the system (5.6) undergoes Hopf bifurcation around $r_0 = r_0^*$. □

5.5   Spatiotemporal model

In this section, we shall analyzed the properties of the spatial predator-prey system with the effect of fear. We consider a bounded domain Ω in $\mathbb{R}^2$ with closed boundary $\partial\Omega$. The spatiotemporal model corresponding to the temporal model (5.6) is the following system of reaction-diffusion equations

$$\begin{aligned}
\frac{\partial u(t,x,y)}{\partial t} &= r_0 u\left(\frac{1+\alpha\eta v}{1+\alpha v}\right) - \delta_1 u - \gamma u^2 - \frac{\beta uv}{1+\xi u} + D_u \nabla^2 u, \\
\frac{\partial v(t,x,y)}{\partial t} &= \frac{\theta\beta uv}{1+\xi u} - \delta_2 v + D_v \nabla^2 v,
\end{aligned}$$
(5.12)

where D_u and D_v are the diffusion coefficients for prey and predator population respectively, with $\nabla^2 \equiv \partial^2/\partial x^2 + \partial^2/\partial y^2$ is the two-dimensional Laplacian operator and (x,y) is the position in space. The equations in (5.12) are subject to the non-negative initial conditions: $u(0,x,y) \equiv u_0(x,y) \geq 0$, $v(0,x,y) \equiv v_0(x,y) \geq 0$, for all $(x,y) \in \Omega$ with zero-flux boundary conditions: $\frac{\partial u}{\partial \hat{\varrho}} = 0 = \frac{\partial v}{\partial \hat{\varrho}}$, where $\hat{\varrho}$ is the outward drawn unit normal vector on the boundary $\partial\Omega$.

5.5.1   Stability analysis of the spatiotemporal model

Now, we shall linearize the system (5.12) about the co-existing equilibrium $E^*(u^*, v^*)$ by setting $u = u^* + U$, $v = v^* + V$ where $U \equiv U(t,x,y)$ and $V \equiv V(t,x,y)$ are small perturbations of u and v, respectively, such that the second and higher order terms can be neglected. We obtain the linearized system of equations as follows:

$$\begin{aligned}
\frac{\partial U(t,x,y)}{\partial t} &= a_{11}U + a_{12}V + D_u \nabla^2 U, \\
\frac{\partial V(t,x,y)}{\partial t} &= a_{21}U + a_{22}V + D_v \nabla^2 V,
\end{aligned}$$
(5.13)

where $a_{11} = \left.\frac{\partial F_1}{\partial u}\right|_{(u^*,v^*)}$, $a_{12} = \left.\frac{\partial F_1}{\partial v}\right|_{(u^*,v^*)}$, $a_{21} = \left.\frac{\partial F_2}{\partial u}\right|_{(u^*,v^*)}$ and $a_{22} = \left.\frac{\partial F_2}{\partial v}\right|_{(u^*,v^*)}$.

Let us consider the solutions of the system (5.13) in the following form

$$\begin{pmatrix} U \\ V \end{pmatrix} = \begin{pmatrix} U_k \\ V_k \end{pmatrix} e^{\zeta t + i(K_x x + K_y y)},$$

where ζ is the growth rate of perturbation in time t; $\sqrt{K_x^2 + K_y^2}$ is the wave number of the solution. The Jacobian matrix of the linearized system is as follows:

$$\tilde{J} = \begin{pmatrix} a_{11} - D_u(K_x^2 + K_y^2) & a_{12} \\ a_{21} & a_{22} - D_v(K_x^2 + K_y^2) \end{pmatrix}.$$

Substituting $K^2 = K_x^2 + K_y^2$, we obtain the characteristic equation as follows:

$$\lambda^2 + \tilde{\sigma}_1 \lambda + \tilde{\sigma}_2 = 0,$$

where $\tilde{\sigma}_1 = K^2(D_u + D_v) - (a_{11} + a_{22})$ and $\tilde{\sigma}_2 = D_u D_v K^4 - (a_{11} D_v + a_{22} D_u)K^2 + (a_{11}a_{22} - a_{12}a_{21})$. Hence, the stability condition due to the Routh-Hurwitz criteria is given in the following theorem.

Theorem 5.5.1. *In presence of diffusion, the co-existing equilibrium point E^* will be locally asymptotically stable if and only if $\tilde{\sigma}_1 > 0$ and $\tilde{\sigma}_2 > 0$.*

Here D_u, D_v and K^2 are always positive, so $\tilde{\sigma}_1 > 0$ only if $a_{11} < (D_u + D_v)K^2$. Hence, the relevant instability condition is given by

$$H(K^2) = D_u D_v K^4 - (a_{11} D_v + a_{22} D_u)K^2 + (a_{11}a_{22} - a_{12}a_{21}) < 0. \quad (5.14)$$

The above expression stating the condition of instability which shows only diffusion can loses the stability of the system with respect to the perturbation for some wave number. The graph of $H(K^2) = 0$ is a parabola as $H(K^2)$ is a quadratic function of K^2. The minimum value of $H(K^2)$ occurs at

$$K_{cr}^2 = \frac{a_{11}}{2D_u} > 0 \text{ if } a_{11} > 0. \quad (5.15)$$

Turing instability occurs when a stable homogeneous steady-state (which is stable under small amplitude of homogeneous perturbation) becomes unstable under small amplitude of inhomogeneous perturbation. First, we assumed that the homogeneous steady state E^* is locally asymptotically stable when $\tilde{\sigma}_1 > 0$ and $\tilde{\sigma}_2 > 0$.

The equation of Turing bifurcation boundary can be obtained by eliminating K^2 from $H(K^2) = 0$ with the help of $\frac{dH(K^2)}{dK^2} = 0$ as follows:

$$a_{12}a_{21} + \frac{a_{11}^2 D_v}{4D_u} = 0.$$

Thus the sufficient condition for instability is $H(K_{cr}^2) < 0$, which implies that

$$4a_{12}a_{21}D_u + a_{11}^2 D_v > 0.$$

The critical wave number K_{cr} of the growing perturbation is given by (5.15). On the other hand, a change of sign in $H(K^2)$ occurs when K^2 enters or leaves the interval (K_-^2, K_+^2), where

$$K_\pm^2 = \frac{a_{11}D_v \pm \sqrt{a_{11}^2 D_v^2 + 4a_{12}a_{21}D_u D_v}}{2D_u D_v}.$$

Hence, we have $H(K^2) < 0$ (that is instability) for $K_-^2 < K^2 < K_+^2$.

5.5.2 Instability condition: Higher-order analysis

We studied the Turing instability by linearizing the system around the co-existing equilibrium point. Hence, the prediction for pattern formation of the system far from the linear regime that cannot be ensured by the linear one. Linearization is unable to capture the effect of non-linearity considered in the proposed system. In this section, we used the method established in [142] to describe the stability condition by considering higher-order spatiotemporal perturbation techniques. The proposed predator-prey system (5.12) with reaction-diffusion can be re-written as follows:

$$
\begin{aligned}
u_t &= P(u,v) + D_u u_{xx} + D_u u_{yy}, \\
v_t &= Q(u,v) + D_v v_{xx} + D_v v_{yy},
\end{aligned}
\tag{5.16}
$$

where $P(u,v) = r_0 u \left(\frac{1+\alpha\eta v}{1+\alpha v}\right) - \delta_1 u - \gamma u^2 - \frac{\beta uv}{1+\xi u}$, $Q(x,y) = \frac{\theta \beta uv}{1+\xi u} - \delta_2 v$ with zero-flux boundary condition and known initial data. Here, $E^*(u^*, v^*)$ is the interior equilibrium point of the system without diffusion. The system (5.16) without diffusion is locally asymptotic stable around $E^*(u^*, v^*)$ if

$$
\begin{aligned}
&P_u + Q_v < 0 \text{ and} \\
&P_u Q_v - P_v Q_u > 0,
\end{aligned}
$$

where the partial derivatives P_u and P_v with respect to u and v, respectively, are evaluated at $E^*(u^*, v^*)$. Again, the partial derivatives of Q_u and Q_v with

respect to u and v, respectively, are evaluated at $E^*(u^*, v^*)$. Now consider the spatiotemporal perturbations of $U(t, x, y)$ and $V(t, x, y)$ around the equilibrium point $E^*(u^*, v^*)$ as $u = u^* + U(t, x, y)$ and $v = v^* + V(t, x, y)$; and expanding the temporal part in Taylor series expansion up to third order around $E^*(u^*, v^*)$ as follows

$$
\begin{aligned}
U_t &= P_u U + P_v V + \frac{P_{uu}}{2} U^2 + \frac{P_{vv}}{2} V^2 + P_{uv} UV + \frac{P_{uuu}}{6} U^3 \\
&\quad + \frac{P_{vvv}}{6} V^3 + \frac{P_{uuv}}{2} U^2 V + \frac{P_{uvv}}{2} UV^2 + D_u U_{xx} + D_u U_{yy}, \\
V_t &= Q_u U + Q_v V + \frac{Q_{uu}}{2} U^2 + \frac{Q_{vv}}{2} V^2 + Q_{uv} UV + \frac{Q_{uuu}}{6} U^3 \\
&\quad + \frac{Q_{vvv}}{6} V^3 + \frac{Q_{uuv}}{2} U^2 V + \frac{Q_{uvv}}{2} UV^2 + D_v V_{xx} + D_v V_{yy}.
\end{aligned}
$$

Considering the spatiotemporal perturbations of $U(t, x, y)$ and $V(t, x, y)$ in the following form

$$
\begin{aligned}
U(t, x, y) &= U_k(t) \cos K_x x \sin K_y y, \\
V(t, x, y) &= V_k(t) \cos K_x x \sin K_y y,
\end{aligned}
$$

and assuming $K^2 = K_x^2 + K_y^2$, we obtain

$$
\begin{aligned}
U_t &= P_u U + P_v V + \frac{P_{uu}}{2} U^2 + \frac{P_{vv}}{2} V^2 + P_{uv} UV + \frac{P_{uuu}}{6} U^3 + \frac{P_{vvv}}{6} V^3 \\
&\quad + \frac{P_{uuv}}{2} U^2 V + \frac{P_{uvv}}{2} UV^2 - D_u K^2 U, \\
V_t &= Q_u U + Q_v V + \frac{Q_{uu}}{2} U^2 + \frac{Q_{vv}}{2} V^2 + Q_{uv} UV + \frac{Q_{uuu}}{6} U^3 \\
&\quad + \frac{Q_{vvv}}{6} V^3 + \frac{Q_{uuv}}{2} U^2 V + \frac{Q_{uvv}}{2} UV^2 - D_v K^2 V.
\end{aligned}
\tag{5.17}
$$

From the above two equations, it can be observed that the growth or decay of U and V depends upon the higher order terms. In similar way, we compute the evolution of higher order terms. Multiply the first and second equations of (5.17) by $2U$ and $2V$, we obtain

$$
\begin{aligned}
(U^2)_t &= 2P_u U^2 + 2P_v UV + P_{uu} U^3 + P_{vv} UV^2 \\
&\quad + 2P_{uv} U^2 V - 2D_u K^2 U^2, \\
(V^2)_t &= 2Q_u UV + 2Q_v V^2 + Q_{uu} U^2 V + Q_{vv} V^3 \\
&\quad + 2Q_{uv} UV^2 - 2D_v K^2 V^2.
\end{aligned}
$$

166

Now multiplying the first equation of (5.17) by v and the second equation by u and adding, we obtain

$$(UV)_t = Q_u U^2 + P_v V^2 + (P_u + Q_v)UV + \frac{Q_{uu}}{2}U^3 + \frac{P_{vv}}{2}V^3$$
$$+ \left(\frac{P_{uu}}{2} + Q_{uv}\right)U^2 V + \left(\frac{Q_{vv}}{2} + P_{uv}\right)UV^2$$
$$- K^2(D_u + D_v)UV.$$

Proceeding in similar manner, we obtain the dynamical equations for third-order perturbation from (5.17) as follows

$$\begin{aligned}
(U^3)_t &= 3P_u U^3 + 3P_v U^2 V - 3K^2 D_u U^3, \\
(V^3)_t &= 3Q_v V^3 + 3Q_u UV^2 - 3K^2 D_v V^3, \\
(U^2 V)_t &= Q_u U^3 + \left(2P_u + Q_v - 2D_u K^2 - D_v K^2\right)U^2 V + 2P_v UV^2, \\
(UV^2)_t &= P_v V^3 + 2Q_u U^2 V + \left(P_u + 2Q_v - D_u K^2 - 2D_v K^2\right)UV^2.
\end{aligned} \tag{5.18}$$

In this way, we can form an infinite hierarchy but we need to truncate the hierarchy by truncating the fourth and higher order terms in Taylor series expansion and this capture the leading order nonlinearity [142].

Thus, the equations (5.17)-(5.18) forms a set of linear equations which can be written as follows:

$$\frac{d}{dt}\mathbb{X} = \mathbb{M}\mathbb{X}, \tag{5.19}$$

where $\mathbb{X} = [U, V, U^2, V^2, UV, U^3, V^3, U^2 V, UV^2]^T$ and

$$\mathbb{M} = \begin{pmatrix}
m_{11} & P_v & \frac{P_{uu}}{2} & \frac{P_{vv}}{2} & P_{uv} & \frac{P_{uuu}}{6} & \frac{P_{vvv}}{6} & \frac{P_{uuv}}{2} & \frac{P_{uvv}}{2} \\
Q_u & m_{22} & \frac{Q_{uu}}{2} & \frac{Q_{vv}}{2} & Q_{uv} & \frac{Q_{uuu}}{6} & \frac{Q_{vvv}}{6} & \frac{Q_{uuv}}{2} & \frac{Q_{uvv}}{2} \\
0 & 0 & m_{33} & 0 & 2P_v & P_{uu} & 0 & 2P_{uv} & P_{vv} \\
0 & 0 & 0 & m_{44} & 2Q_u & 0 & Q_{vv} & Q_{uu} & 2Q_{uv} \\
0 & 0 & Q_u & P_v & m_{55} & \frac{Q_{uu}}{2} & \frac{P_{vv}}{2} & \frac{P_{uu}}{2}+Q_{uv} & \frac{Q_{vv}}{2}+P_{uv} \\
0 & 0 & 0 & 0 & 0 & m_{66} & 0 & 3P_v & 0 \\
0 & 0 & 0 & 0 & 0 & 0 & m_{77} & 0 & 3Q_u \\
0 & 0 & 0 & 0 & 0 & Q_u & 0 & m_{88} & 2P_v \\
0 & 0 & 0 & 0 & 0 & 0 & P_v & 2Q_u & m_{99}
\end{pmatrix},$$

with

$$m_{11} = P_u - K^2, \; m_{22} = Q_v - D_v K^2, \; m_{33} = 2(P_u - K^2),$$
$$m_{44} = 2(Q_v - D_v K^2), \; m_{55} = P_u + Q_v - K^2(D_u + D_v),$$
$$m_{66} = 3(P_u - D_u K^2), \; m_{77} = 3(Q_v - D_v K^2),$$
$$m_{88} = 2P_u + Q_v - K^2(2D_u + D_v), \; m_{99} = 2Q_v + P_u - K^2(D_u + 2D_v).$$

Table 5.1: *Description of the model (5.6) parameters and their values.*

Parameter	Description	Value	Source
r_0	growth rate of prey population	$(0, 0.1)$	[116]
γ	decay rate due to intra-species competition	0.01	[88, 116]
δ_1	natural death rate of prey	0.015	[116]
β	rate of predation	0.5	[88, 116, 143]
ξ	prey handling time	0.6	[88, 116]
θ	conversion efficiency of prey to predator biomass	0.4	[88, 116]
δ_2	natural death rate of predator	0.05	[116]
α	level of fear	0.2	[88, 116]
η	minimum level of fear	0.1	[116]

Considering $\mathbb{X} \sim e^{\lambda t}$ as a solution of (5.19), we obtain the characteristic equation of $\mathbb{M}$ as follows

$$|\mathbb{M} - \lambda I_9| = 0, \tag{5.20}$$

where I_9 is the identity matrix of order nine and $\lambda \equiv \lambda(K)$ are the eigenvalues of $\mathbb{M}$. Hence, the condition for instability is $Re(\lambda_i(K)) > 0$ at least for one $i = 1, 2, 3, \ldots 9$. This shows that the spatiotemporal perturbation $U(t, x, y)$ and $V(t, x, y)$ diverge with the progression of time. We are unable to find the eigenvalues of the matrix $\mathbb{M}$ analytically as the structure of the matrix $\mathbb{M}$ is too complicated. Numerical illustrations will aid in finding the eigenvalues and to proceed further analysis with higher order terms. Numerically, we have plotted the max $Re(\lambda)$ and $Im(\lambda)$ for the characteristic equation (5.20) over a range of K for different value of r_0 in the figure of dispersion relation. The max $Re(\lambda)$ for linear and higher order remains positive simultaneously.

5.6 Numerical simulation

In this section, we support our analytical findings by using extensive numerical simulations with the aid of MATLAB. The system of nonlinear ordinary differential equations (5.6) is solved by 4th order Runge-Kutta method. Due to the unavailability of real field observed data, we used hypothetical value for the system parameters based on the existing literature. The assumed parameters value are listed in the Table 5.1.

5.6.1 Local stability of the equilibria

The vector flow of the system (5.6) has been shown in the Fig. 5.2 by red color vector field for different values of the prey growth rate r_0 and other

system parameters value are listed in the Table 5.1. The equilibrium points for the assumed value of r_0 are shown by solid circles in the sub-figures: 5.2(a) the trivial equilibrium point $E_0(0,0)$ by black color solid circle for $r_0 = 0.01$, 5.2(b) the axial equilibrium point $E_1(\hat{u}, 0)$ by magenta color solid circle for $r_0 = 0.018$, 5.2(c) the co-existing equilibrium point $E^*(u^*, v^*)$ by green color solid circle for $r_0 = 0.03$ and 5.2(d) the co-existing equilibrium point $E^*(u^*, v^*)$ by green color solid circle for $r_0 = 0.07$. The prey and predator isoclines are drawn by the black dashed line and solid black curve, respectively, in the Fig. 5.2(c) and Fig. 5.2(d).

In the Fig. 5.2(a), the vector field indicates the stability of the trivial equilibrium point $E_0(0,0)$ and the phase portraits with initial population size are $(0.8, 0.03)$, $(0.6, 0.125)$, $(0.6, 0.2)$, $(0.8, 0.3)$ and $(0.9, 0.3)$ converge to the trivial equilibrium point $E_0(0,0)$ and this ensures the local asymptotic stability of the trivial equilibrium point $E_0(0,0)$ with assumed system parameters. Again in the Fig. 5.2(b), the vector field indicates the stability of the axial equilibrium point $E_1(\hat{u}, 0)$ and the phase portraits with initial population size $(0.8, 0.03)$, $(0.6, 0.125)$, $(0.6, 0.2)$, $(0.8, 0.3)$ and $(0.9, 0.3)$ converge to the axial equilibrium point $E_1(\hat{u}, 0)$ and this ensures the local asymptotic stability of the axial equilibrium point $E_1(\hat{u}, 0)$ with assumed system parameters. The vector field in the Fig. 5.2(c), indicates the stability of the co-existing equilibrium point $E^*(u^*, v^*)$ and the phase portraits with initial population size $(0.8, 0.3)$ converge to the co-existing equilibrium point $E^*(u^*, v^*)$ and this ensures the local asymptotic stability of the co-existing equilibrium point $E^*(u^*, v^*)$. The phase portraits with other initial conditions are also converge to $E^*(u^*, v^*)$ but in the Fig. 5.2(c), the phase portrait diagram shows only for one initial condition to make the figure more clear. Again in the Fig. 5.2(d), the vector field indicates a limit cycle oscillation and the phase portrait ensures the limit cycle oscillation of the system (5.6) around the co-existing equilibrium point $E^*(u^*, v^*)$ for $r_0 = 0.07$.

5.6.2   Numerical simulation of transcritical bifurcation

Numerical simulation for the transcritical bifurcation is shown in the Fig. 5.3. The prey growth rate (r_0) is varied from 0 to 0.025 and the other system parameters value are listed in Table 5.1. Fig. 5.3 shows the change of stability between the equilibrium point $E_0(0,0)$ and $E_1(\hat{u}, 0)$ of the system (5.6) when $r_0 = r_0^{tc} = 0.015$. Hence, the system (5.6) undergoes a transcritical bifurcation around $E_0(0,0)$ at $r_0 = r_0^{tc} = 0.015$. The solid red line represents the stable trivial equilibrium point $E_0(0,0)$ and the red dashed line represents the unstable trivial equilibrium point $E_0(0,0)$. Again, the solid blue line represents the stable axial equilibrium point $E_1(\hat{u}, 0)$ and the dashed blue
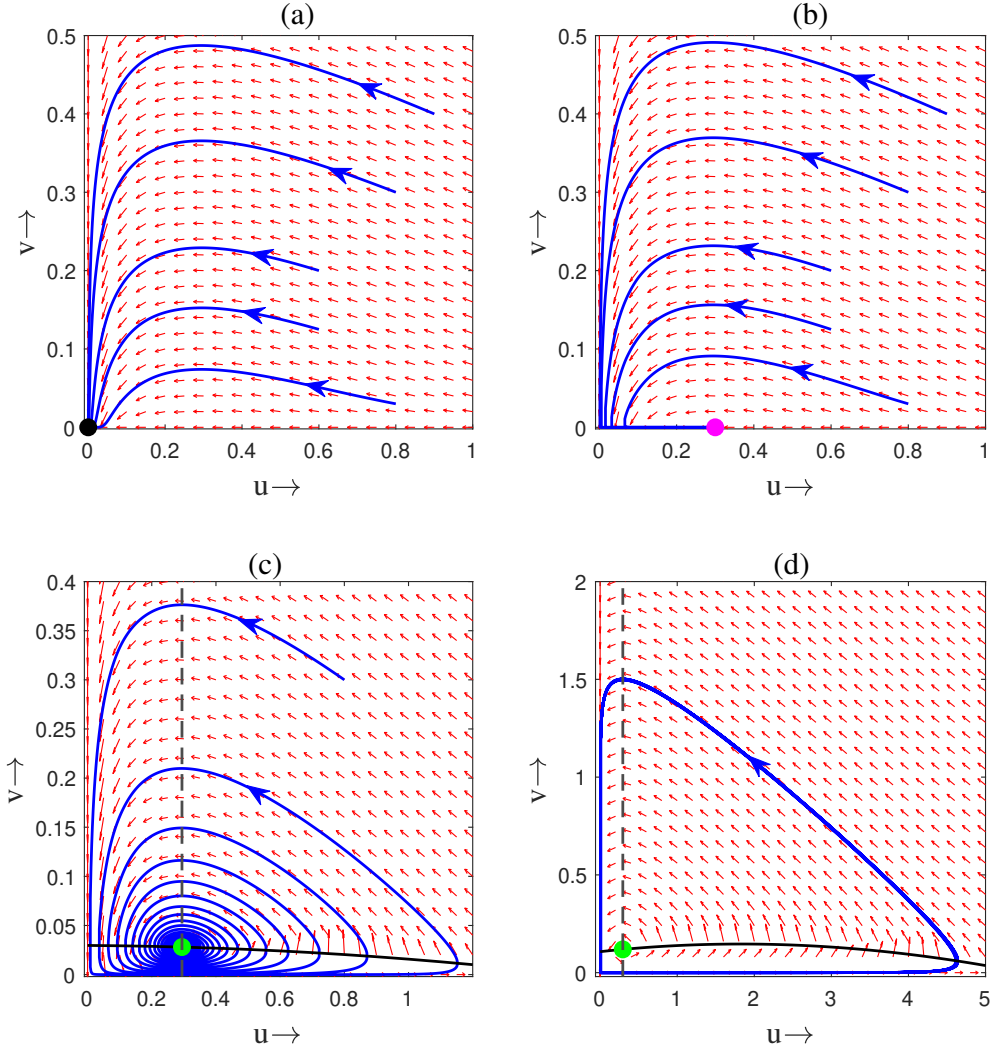
Figure 5.2: Phase portraits of the system (5.6) for $\eta = 0.10$, $\alpha = 0.2$, $\delta_1 = 0.015$, $\gamma = 0.01$, $\beta = 0.5$, $\xi = 0.6$, $\theta = 0.4$, $\delta_2 = 0.05$ and for different value of r_0: **(a)** $r_0 = 0.01$, **(b)** $r_0 = 0.018$, **(c)** $r_0 = 0.03$ and **(d)** $r_0 = 0.07$. Black dashed line (in (c) and (d)) is the prey isocline and the solid black curve (in (c) and (d)) is the predator isocline. The solid black circle (in (a)) and magenta circle (in (b)) are the location of trivial equilibrium E_0 and axial equilibrium E_1, respectively. The solid green circles (in (c) and (d)) are the location of co-existing equilibrium E^*. The red colored vector field is the flow field of the system (5.6).
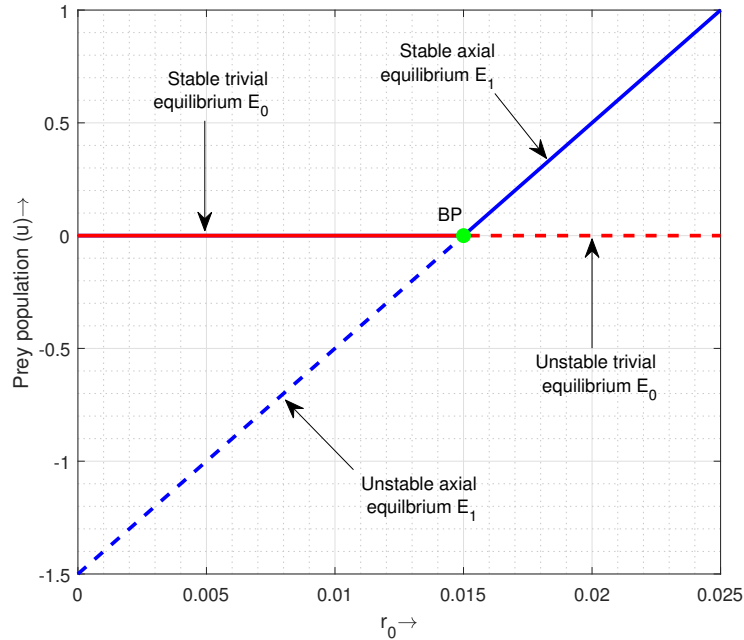
Figure 5.3: Transcritical bifurcation diagram for the system (5.6) with respect to prey growth rate r_0. The stability exchanged between E_0 and E_1 at the bifurcation point $r_0 = r_0^{tc} = 0.015$.

line represents the unstable axial equilibrium point $E_1(\hat{u}, 0)$. The solid green circle in the Fig. 5.3 represents the transcritical bifurcation point of the system (5.6).

5.6.3 Numerical simulation of Hopf bifurcation

Fig. 5.4(a) and 5.4(b) represents the bifurcation diagram with respect to prey growth rate r_0. We varied the parameter r_0 from 0.025 to 0.15 and the other system parameters value as listed in the Table 5.1. The stable co-existing equilibrium point $E^*(u^*, v^*)$ exists for the smaller value of r_0 but $E^*(u^*, v^*)$ looses its stability as r_0 increases and a stable limit cycle oscillation emerges as r_0 is increased further. When r_0 passes through the critical value $r_0^* \approx 0.04$, then the system (5.6) undergoes on a stable periodic oscillation, which is known as Hopf bifurcation that has been stated in the Theorem 5.4.6.

We also plot the bifurcation diagram with respect to the level of fear α to observe the effect of fear on a system which oscillates periodically though we have not shown the bifurcation with respect to α analytically.
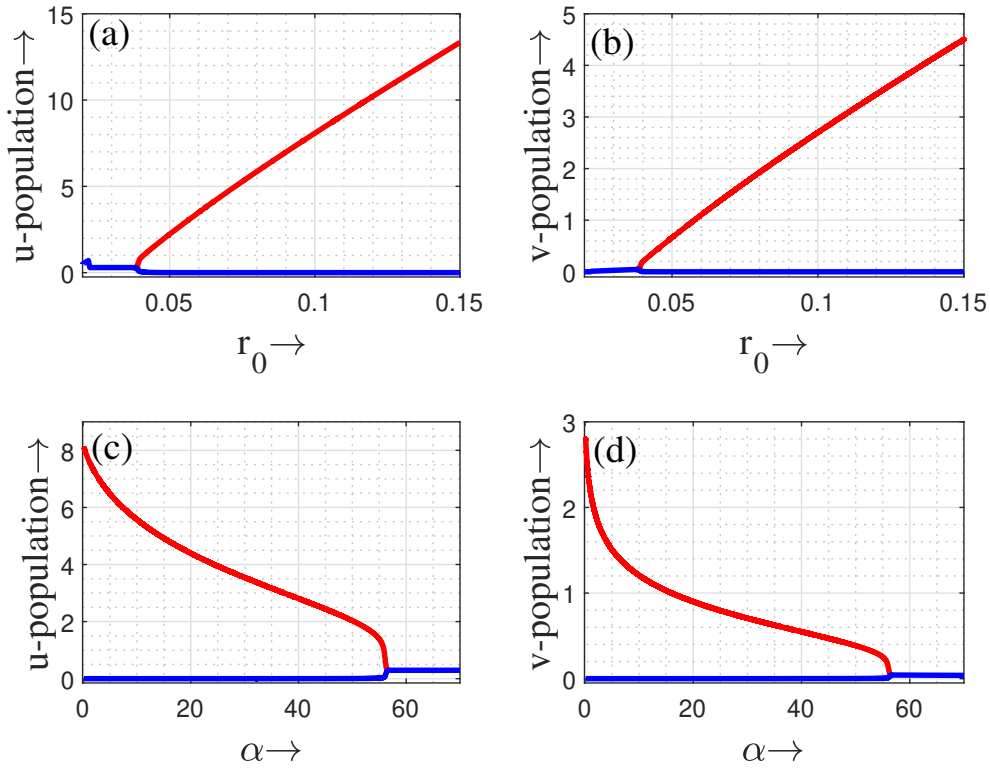
Figure 5.4: Hopf bifurcation diagram of the system (5.6) for the interior equilibrium point E^* considering r_0 ((a) and (b)) and α ((c) and (d)) as bifurcation parameters. Other parameters value are $\eta = 0.10$, $\delta_1 = 0.015$, $\gamma = 0.01$, $\beta = 0.5$, $\xi = 0.6$, $\theta = 0.4$, $\delta_2 = 0.05$, $\alpha = 0.2$ (for bifurcation diagram with respect to r_0) and $r_0 = 0.1$ (for bifurcation diagram with respect to α).

We fix the value of $r_0 = 0.1$ (which ensures periodic oscillation in the system (5.6)) and vary the level of fear α from 0 to 70; other system parameters value are listed in Table 5.1. The bifurcation diagram with respect to α is shown in the Fig. 5.4(c) and Fig. 5.4(d). As the level of fear increases the co-existing equilibrium point $E^*(u^*, v^*)$ become stable as α crosses the critical value $\alpha^* \approx 56.63$. Few steps of analytical calculations shows the occurrence of Hopf bifurcation at $\alpha = \alpha^* = [r_0 - \delta_1 - \gamma u^* - (\beta v^*)/(1 + \xi u^*)] \left[(\beta v^{*2})/(1 + \xi u^*) + (\delta_1 + \gamma u^*)v^* - r_0 \eta v^* \right]^{-1}$, where $u^* = \delta_2/(\theta \beta - \xi \delta_2)$ and $v^* = \gamma(1 + \xi u^*)^2/(\beta \xi)$. We also found that $\alpha^* \approx 56.63$ for assumed parameters value. Thus, if the level of fear increases, then the unstable oscillating system become stable around the co-existing equilibrium point $E^*(u^*, v^*)$.

172

5.6.4 Numerical illustrations for the existence of Turing pattern

To prove the existence of Turing instability for the reaction-diffusion system (5.12), we plot the polynomial $H(K^2)$ for different values of diffusion coefficient D_v and the prey growth rate r_0. The plot of the polynomial $H(K^2)$ is shown in the Fig. 5.5. In the Fig. 5.5(a), we plot $H(K^2)$ vs K^2 for different values of D_v with $r_0 = 0.1$, $D_u = 0.01$ and other parameters value as listed in Table 5.1. Fig. 5.5(a) shows that for increasing the value of D_v, the range of values of K increases for which $H(K^2)$ remains negative and hence the possibility for existence of Turing instability. Again the Fig. 5.5(b) shows that as r_0 increases, the range of value of K increases for which $H(K^2)$ remains negative and hence the possibility for the existence of Turing instability.

We plot the dispersion relation in Fig. 5.6 for different values of r_0 with $D_u = 0.01$, $D_v = 7.5$ and other system parameters as listed in Table 5.1. The solid curves for characteristic equation (5.10) and dashed curve for the characteristic equation (5.20). Turing instability occurs for $r_0 > 0.0565$ in the system (5.12). Turing instability increases as r_0 increases. The range of K become wider as the value of r_0 increases.

Now, we will show the Turing space geometrically in the Fig. 5.7 on the $D_u - D_v$-plane. Turing bifurcation occurs when $Im(\lambda(K_{cr})) = 0$ and $Re(\lambda(K_{cr})) = 0$ for $K_{cr}^2 = \frac{a_{11}}{2D_u} \neq 0$. The Turing space of the system (5.12) is shown in Fig. 5.7 for $r_0 = 0.1$ and other system parameters as listed in Table 5.1. The Turing bifurcation curve is an oblique straight line. The Turing bifurcation breaks the spatial symmetry and leads to form patterns which are oscillatory in space and stationary in time. Considering the values of D_u and D_v from the Turing space we focus on the spatial patterns.

5.6.5 Turing pattern formation

In this section, we performed numerical simulations of the proposed diffusive predator-prey system (5.12) with the effect of fear in two-dimensional space to support our theoretical analysis. All our numerical simulations of the system (5.12) are performed with zero-flux boundary condition in the 200×200 spatial domain with $\triangle x = \triangle y = 1$. To generate the pattern formation, we used the following three types of initial conditions:

(i) $u_{i,j}^0 = 1.0$, $v_{i,j}^0 = 0.2$ if $(x_i - 100)^2 + (y_j - 100)^2 < 200$, otherwise $u_{i,j}^0 = 0$, $v_{i,j}^0 = 0$.

(ii) $u_{i,j}^0 = u^* + 0.2\cos(\pi x_i/16)$, $v_{i,j}^0 = v^* + 0.4\sin(\pi x/16)$.

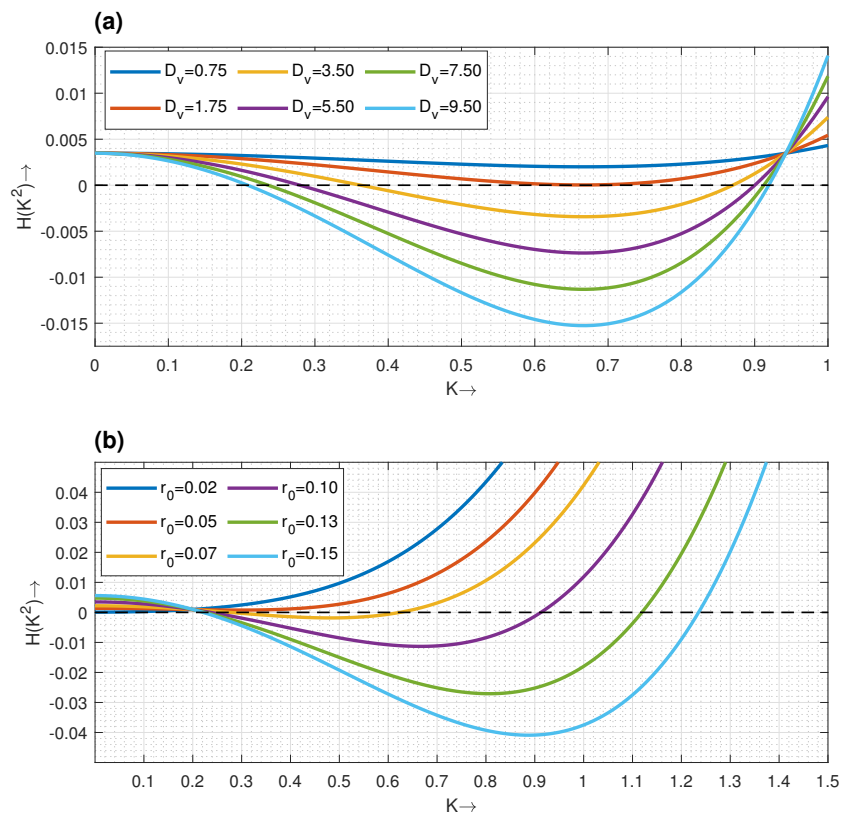Figure 5.5: Plot of $H(k^2)$ vs k **(a)** for different values of D_v and **(b)** for different values of r_0.
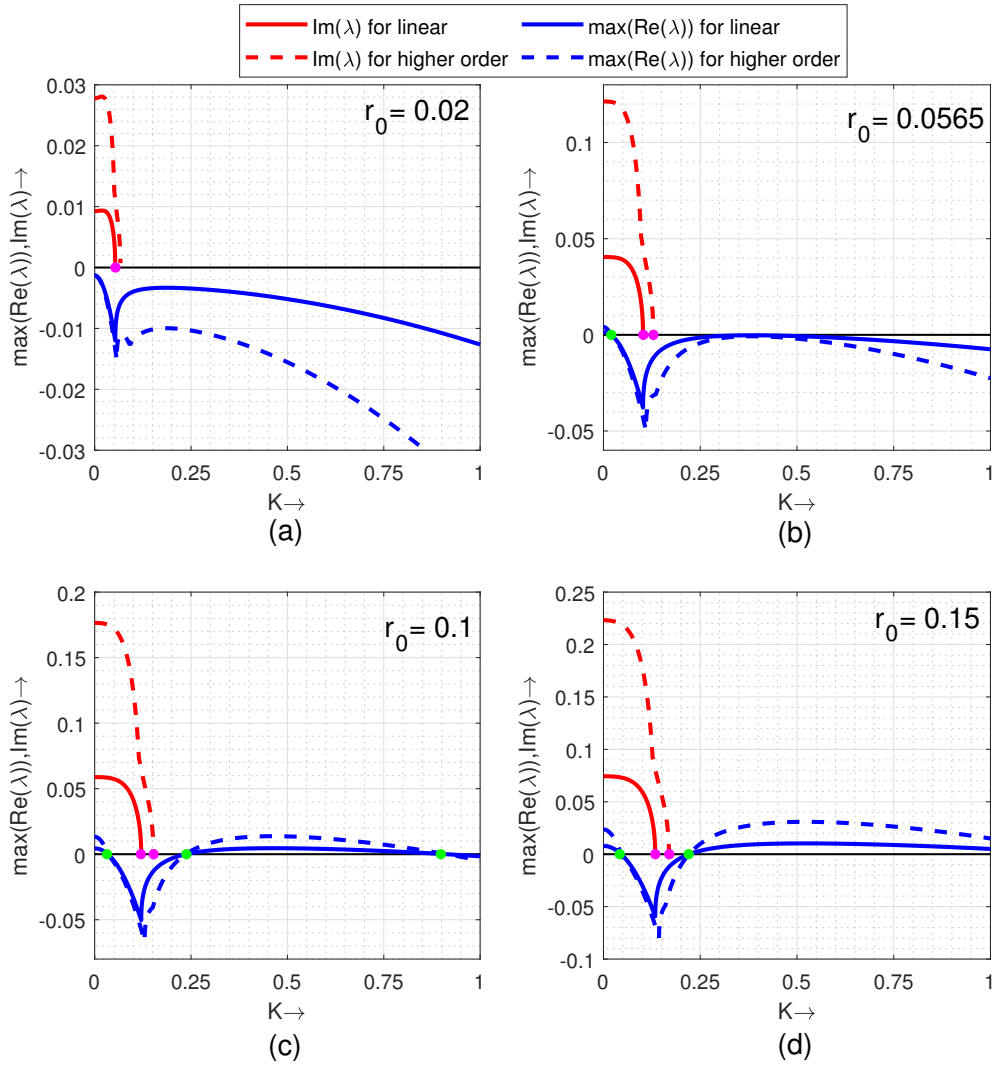
Figure 5.6: Variation of dispersion relation of the system (5.12) for different values of r_0 and the other system parameters value as: $\eta = 0.10$; $\alpha = 0.20$; $\delta_1 = 0.015$, $\gamma = 0.01$, $\beta = 0.5$, $\xi = 0.6$ $\theta = 0.4$, $\delta_2 = 0.05$, $D_u = 0.01$ and $D_v = 7.5$. Imaginary part of the eigenvalue is represented by red color (solid curve for linear system and dashed curve for nonlinear system) and the maximum of real part is represented by blue color (solid curve for linear system and dashed curve for nonlinear system).

Figure 5.7: Turing bifurcation diagram of the system (5.12) with $r_0 = 0.1$ and other system parameters as listed in Table 5.1.

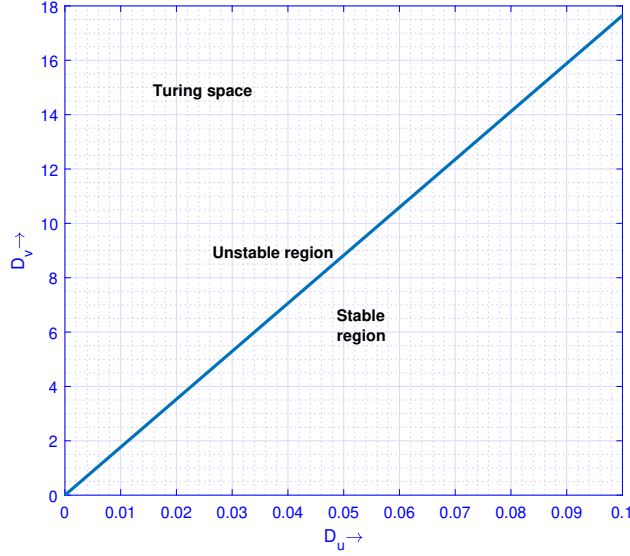(iii) $u_{i,j}^0 = u^* + 0.01\Theta_{i,j}$, $v_{i,j}^0 = v^* + 0.01\Phi_{i,j}$, where $\Theta_{i,j}$ and $\Phi_{i,j}$ are the Gaussian white noise $\delta-$correlated in space.

Forward Euler integration is used for the numerical illustrations of the diffusive predator-prey system (5.12) with $\triangle x = \triangle y = 1$, $\triangle t = 1/20$ and standard five-point approximation for the two-dimensional Laplacian system. The iteration formula for the $(n+1)$-th time step at the mesh position (x_i, y_j) are as follows:

$$U_{i,j}^{n+1} = U_{i,j}^n + \triangle t D_u \triangle_h U_{i,j}^n + \triangle t F_1(U_{i,j}^n, V_{i,j}^n),$$

$$V_{i,j}^{n+1} = V_{i,j}^n + \triangle t D_v \triangle_h V_{i,j}^n + \triangle t F_2(U_{i,j}^n, V_{i,j}^n),$$

with the Laplacian defined by

$$\triangle_h U_{i,j}^n = \frac{U_{i+1,j}^n + U_{i-1,j}^n + U_{i,j+1}^n + U_{i,j-1}^n - 4U_{i,j}^n}{h^2},$$

$$\triangle_h V_{i,j}^n = \frac{V_{i+1,j}^n + V_{i-1,j}^n + V_{i,j+1}^n + V_{i,j-1}^n - 4V_{i,j}^n}{h^2},$$

where the space step size is given by $h = \triangle x = \triangle y = 1$.

Fig. 5.8 shows the time evolution of pattern formation for prey (first and third row) and predator (second and fourth row) distribution over two-dimensional spatial domain with $r_0 = 0.1$, $D_u = 0.01$, $D_v = 7.5$ and other

system parameters as listed in Table 5.1. The system (5.12) takes long time to produce steady state warm spot pattern with initial data (i). The time steps are as follows: (a), (d) $t = 0$; (b), (e) $t = 250$; (c), (f) $t = 500$; (g), (j) $t = 3000$; (h), (k) $t = 5000$; (i), (l) $t = 500000$.

Fig. 5.9 shows the time evolution of pattern formation for prey (first & third row) and predator (second & fourth row) distribution over two dimensional spatial domain with $r_0 = 0.1$, $D_u = 0.01$, $D_v = 7.5$ and other system parameters as listed in Table 5.1. The system (5.12) produce steady state warm spot pattern with initial data (ii). It can be observed that similar warm spot pattern observed for both the initial data (i) and (ii). The steady state produced faster for the initial data (ii) than the pattern for initial data (i). The time steps are as follows: (a), (d) $t = 0$; (b), (e) $t = 250$; (c), (f) $t = 500$; (g), (j) $t = 1000$; (h), (k) $t = 3000$; (i), (l) $t = 6000$.

Fig. 5.10 shows the time evolution of pattern formation for prey (first and third row) and predator (second and fourth row) distribution over two-dimensional spatial domain with $r_0 = 0.1$, $D_u = 0.01$, $D_v = 7.5$ and other system parameters as listed in Table 5.1. The system (5.12) produce steady state warm spot pattern with initial data (iii). It can also be noticed that similar warm spot pattern observed for all the three initial data. The steady state produced slower for the initial data (iii) than the pattern for the initial data (ii). The time steps are as follows: (a), (d) $t = 0$; (b), (e) $t = 250$; (c), (f) $t = 500$; (g), (j) $t = 1000$; (h), (k) $t = 3000$; (i), (l) $t = 15000$. It is worthy in mentioning that we obtain similar type of warm spot pattern for three different types of initial conditions for our proposed reaction-diffusion predator-prey system.

Next, we simulate the pattern for different values of the diffusion coefficient D_u with $D_v = 2.0$. Fig. 5.11 shows the time evolution of pattern formation for prey (first and third row) and predator (second and fourth row) distribution over two-dimensional spatial domain with $r_0 = 0.1$, $D_u = 0.01$, $D_v = 2.0$ and other system parameters as listed in Table 5.1. Warm spot pattern is being formed in the Turing region as time progresses.

To investigate how the effect of fear can influence the spatiotemporal pattern formation, we consider $\alpha = 5.0$ and simulated the reaction-diffusion system for pattern with initial data (iii). Fig. 5.12 shows the time evolution of pattern formation for prey (first and third row) and predator (second and fourth row) distribution over two-dimensional spatial domain with $r_0 = 0.1$, $\alpha = 5.0$, $D_u = 0.01$, $D_v = 7.5$ and other system parameters as listed in Table 5.1. Warm spot pattern is being formed in Turing region as time progresses. If α increases then system takes more time to form the warm spot pattern for the prey species. For $\alpha = 0.2$ warm spot pattern in prey species is observed for $t = 3000$ onward (see Fig. 5.10) but for $\alpha = 5.0$ warm spot pattern in

prey observed for $t = 12000$ onward.

5.6.6 Non-Turing pattern formation

Here, we describe the non-Turing spatiotemporal pattern formation for the diffusive predator-prey system (5.12). Turing instability criterion failed here and is known as non-Turing instability and their associated patterns are named as non-Turing patterns. The non-Turing pattern occurs due to Hopf bifurcation, wave instability, or mixture of at least any two of Hopf criterion, wave and Turing instabilities. Hopf-Turing instability occurs for the model (5.12) when the condition (5.14) does not satisfied. Now, we simulate the pattern for different values of the diffusion coefficient $D_u = 0.1$ and $D_v = 1.5$ from the stable region of bifurcation diagram Fig. 5.7 (we have taken the diffusion coefficients from the Non-Turing space or stable region) for all three types of initial conditions and for time steps: $t = 2000$ and $t = 200000$. Fig. 5.13 shows the time evolution of prey (first and third row) and predator (second and fourth row) distribution over two-dimensional spatial domain with $r_0 = 0.1$, $D_u = 0.1$, $D_v = 1.5$ and other system parameters as listed in Table 5.1. The snapshots for the initial data (i) are shown in (a), (c) for $t = 2000$ and (g), (j) for $t = 200000$. The snapshots for the initial data (ii) are shown in (b), (e) for $t = 2000$ and (h), (k) for $t = 200000$. The snapshots for the initial data (iii) are shown in (c), (f) for $t = 2000$ and (i), (l) for $t = 200000$.

5.7 Discussion

The ecological scenarios for the predator-prey interplay is ubiquitous in terrestrial as well as in aquatic ecological community. Behavioral attributes for both the predator and prey species can influence this interplay and kinetics. By taking into account such behavioral responses, different types of mathematical models have been developed and analyzed to express the underlying dynamics of the predator-prey interactions. As for example, looking the predator species interference, the typical prey-dependent response function was adopted by Beddington [75] and DeAngelis et al. [76] and then by Arditi & Ginzburg [144]. Such type of mutual interference among predator species was studied in the response function as a fraction of prey species to predator species [144]. It is worthy in mentioning that the predator-prey system with ratio-dependent response function does not exhibit two paradoxes, namely, the paradox of enrichment and biological control paradox, as noticed in the predator-prey system with prey-dependent response function [144, 145].

Figure 5.8: Snapshots of the spatial distributions of prey (first and third rows) and predator (second row fourth rows) population at different time steps: **(a), (d)** $t = 0$; **(b), (e)** $t = 250$; **(c), (f)** $t = 500$; **(g), (j)** $t = 3000$; **(h), (k)** $t = 5000$; **(i), (l)** $t = 500000$. The system parameters value are $r_0 = 0.1$, $\eta = 0.10$, $\alpha = 0.20$, $\delta_1 = 0.015$, $\gamma = 0.01$, $\beta = 0.5$, $\xi = 0.6$, $\theta = 0.4$, $\delta_2 = 0.05$, $D_u = 0.01$, $D_v = 7.5$ with initial data: $u_{i,j}^0 = 1.0$, $v_{i,j}^0 = 0.2$ if $(x_i - 100)^2 + (y_j - 100)^2 < 200$, otherwise $u_{i,j}^0 = 0$, $v_{i,j}^0 = 0$. Warm spot pattern form in Turing region as time increases.
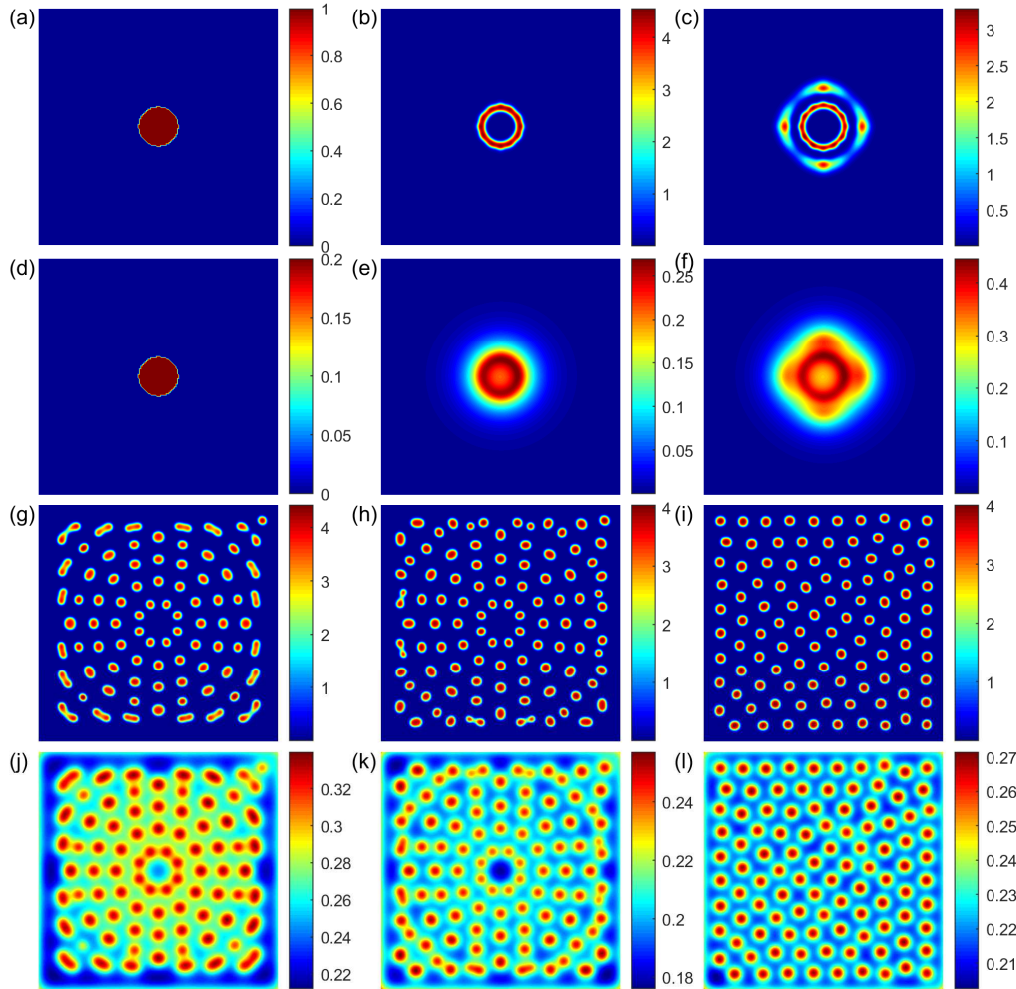
Figure 5.9: Snapshots of the spatial distributions of prey (first and third rows) and predator (second and fourth rows) population at different time steps: **(a), (d)** $t = 0$; **(b), (e)** $t = 250$; **(c), (f)** $t = 500$; **(g), (j)** $t = 1000$; **(h), (k)** $t = 3000$; **(i), (l)** $t = 6000$. The system parameters value are $r_0 = 0.1$, $\eta = 0.10$, $\alpha = 0.20$, $\delta_1 = 0.015$, $\gamma = 0.01$, $\beta = 0.5$, $\xi = 0.6$, $\theta = 0.4$, $\delta_2 = 0.05$, $D_u = 0.01$, $D_v = 7.5$ with initial data: $u_{i,j}^0 = u^* + 0.2\cos(\pi x_i/16)$, $v_{i,j}^0 = v^* + 0.4\sin(\pi x/16)$. Warm spot pattern form in Turing region as time increases.

Figure 5.10: Snapshots of the spatial distributions of prey (first and third rows) and predator (second and fourth rows) population at different time steps: **(a), (d)** $t = 0$; **(b), (e)** $t = 250$; **(c), (f)** $t = 500$; **(g), (j)** $t = 1000$; **(h), (k)** $t = 3000$; **(i), (l)** $t = 15000$. The system parameters value are $r_0 = 0.1$, $\eta = 0.10$, $\alpha = 0.20$, $\delta_1 = 0.015$, $\gamma = 0.01$, $\beta = 0.5$, $\xi = 0.6$, $\theta = 0.4$, $\delta_2 = 0.05$, $D_u = 0.01$, $D_v = 750$ with initial data: $u_{i,j}^0 = u^* + 0.01\Theta_{i,j}$, $v_{i,j}^0 = v^* + 0.01\Phi_{i,j}$, where $\Theta_{i,j}$ and $\Phi_{i,j}$ are Gaussian white noise $\delta-$ correlated in space. Warm spot pattern form in Turing region as time increases.
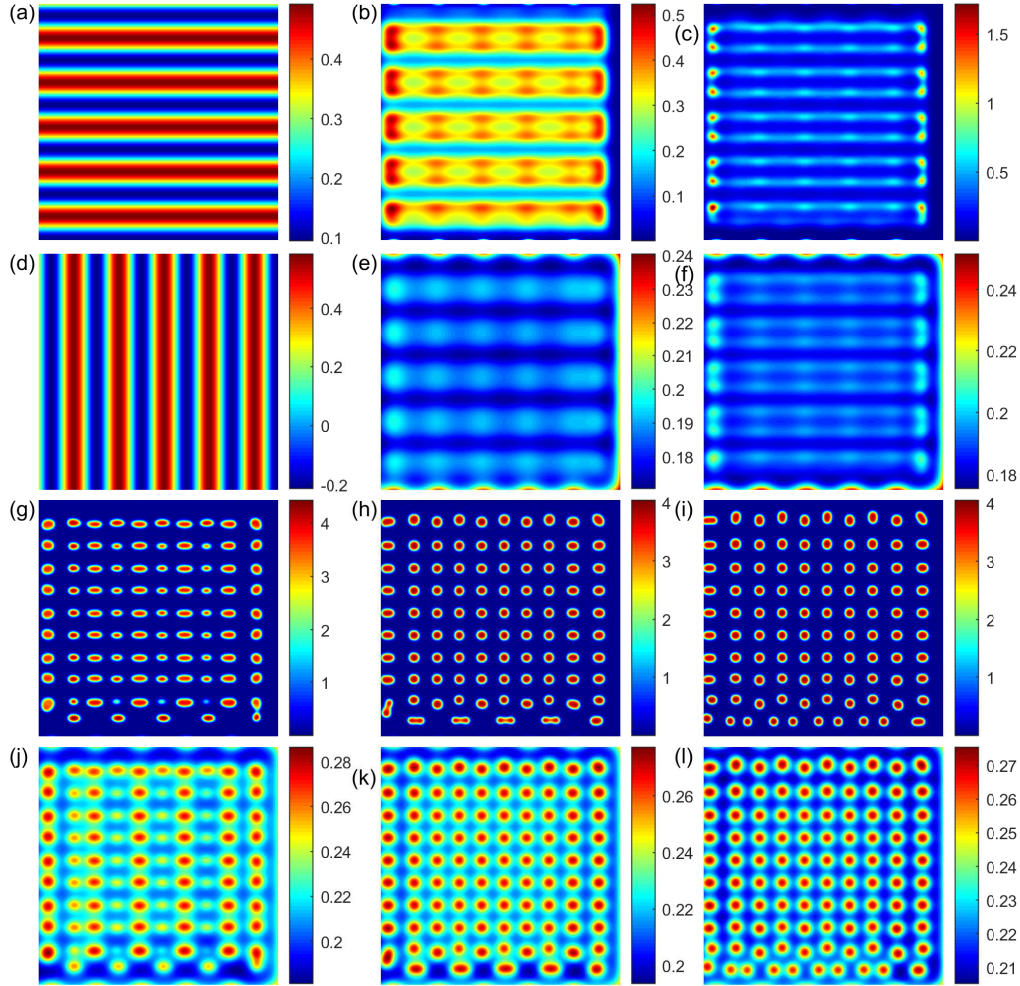
Figure 5.11: Snapshots of the spatial distributions of prey (first and third rows) and predator (second and fourth rows) population at different time steps: **(a), (d)** $t = 250$; **(b), (e)** $t = 500$; **(c), (f)** $t = 25000$; **(g), (j)** $t = 100000$; **(h), (k)** $t = 500000$; **(i), (l)** $t = 1500000$. The system parameters value are $r_0 = 0.1$, $\eta = 0.10$, $\alpha = 0.20$, $\delta_1 = 0.015$, $\gamma = 0.01$, $\beta = 0.5$, $\xi = 0.6$, $\theta = 0.4$, $\delta_2 = 0.05$, $D_u = 0.01$, $D_v = 2.0$ with initial data: $u_{i,j}^0 = u^* + 0.01\Theta_{i,j}$, $v_{i,j}^0 = v^* + 0.01\Phi_{i,j}$ where $\Theta_{i,j}$ and $\Phi_{i,j}$ are Gaussian white noise $\delta-$ correlated in space. Warm spot pattern form in Turing region as time increases
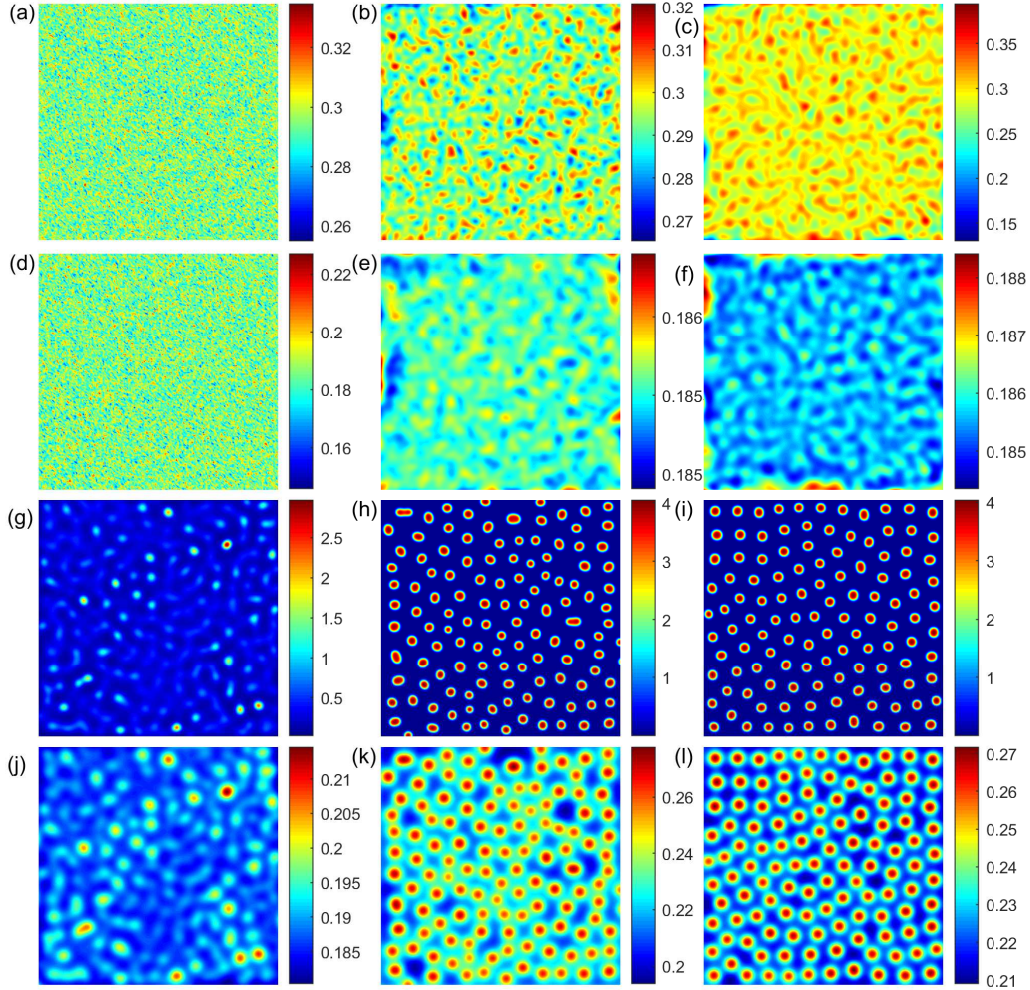
Figure 5.12: Snapshots of the spatial distributions of prey (first and third rows) and predator (second and fourth rows) population at different time steps: **(a), (d)** $t = 250$; **(b), (e)** $t = 500$; **(c), (f)** $t = 3000$; **(g), (j)** $t = 6000$; **(h), (k)** $t = 8000$; **(i), (l)** $t = 12000$. The system parameters value are $r_0 = 0.1$, $\eta = 0.10$, $\alpha = 5.0$, $\delta_1 = 0.015$, $\gamma = 0.01$, $\beta = 0.5$, $\xi = 0.6$, $\theta = 0.4$, $\delta_2 = 0.05$, $D_u = 0.01$, $D_v = 7.5$ with initial data: $u_{i,j}^0 = u^* + 0.01\Theta_{i,j}$, $v_{i,j}^0 = v^* + 0.01\Phi_{i,j}$, where $\Theta_{i,j}$ and $\Phi_{i,j}$ are Gaussian white noise $\delta-$ correlated in space. Warm spot pattern form in Turing region as time increases.
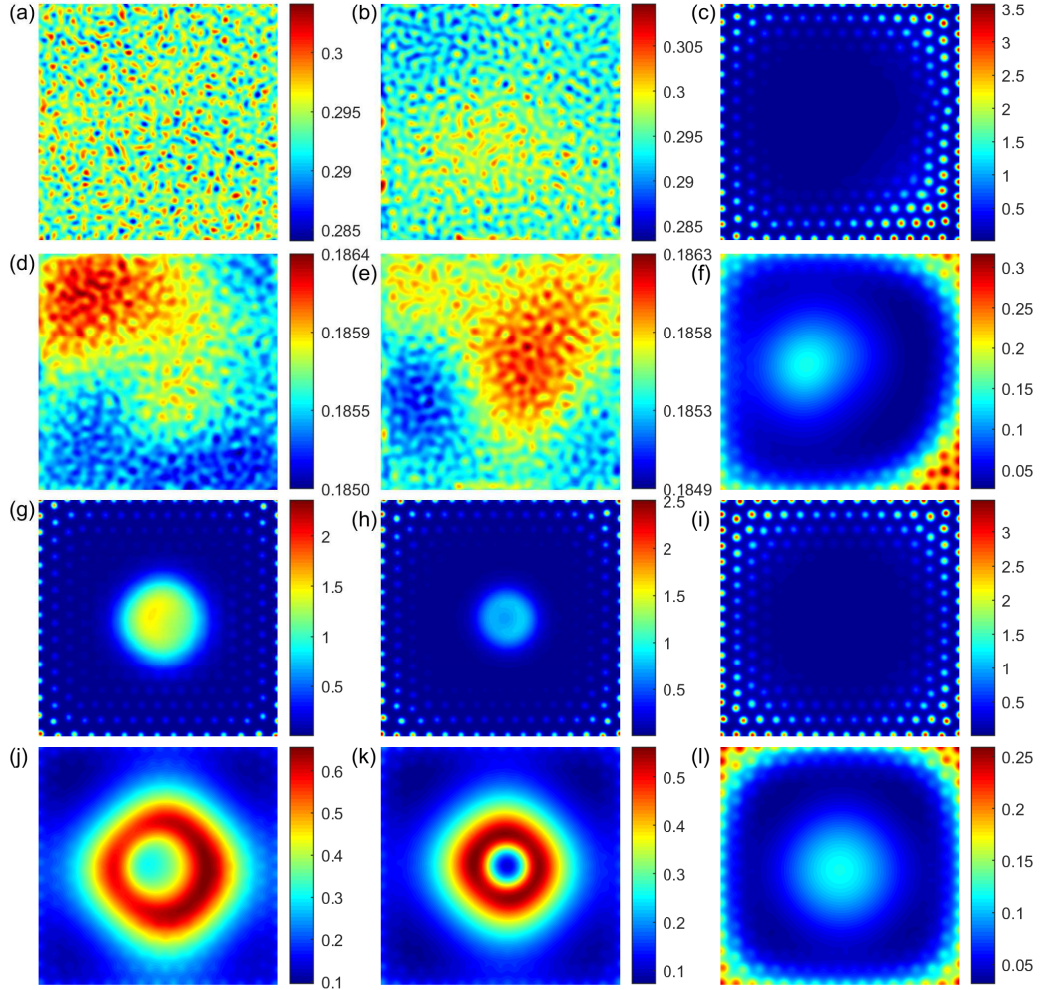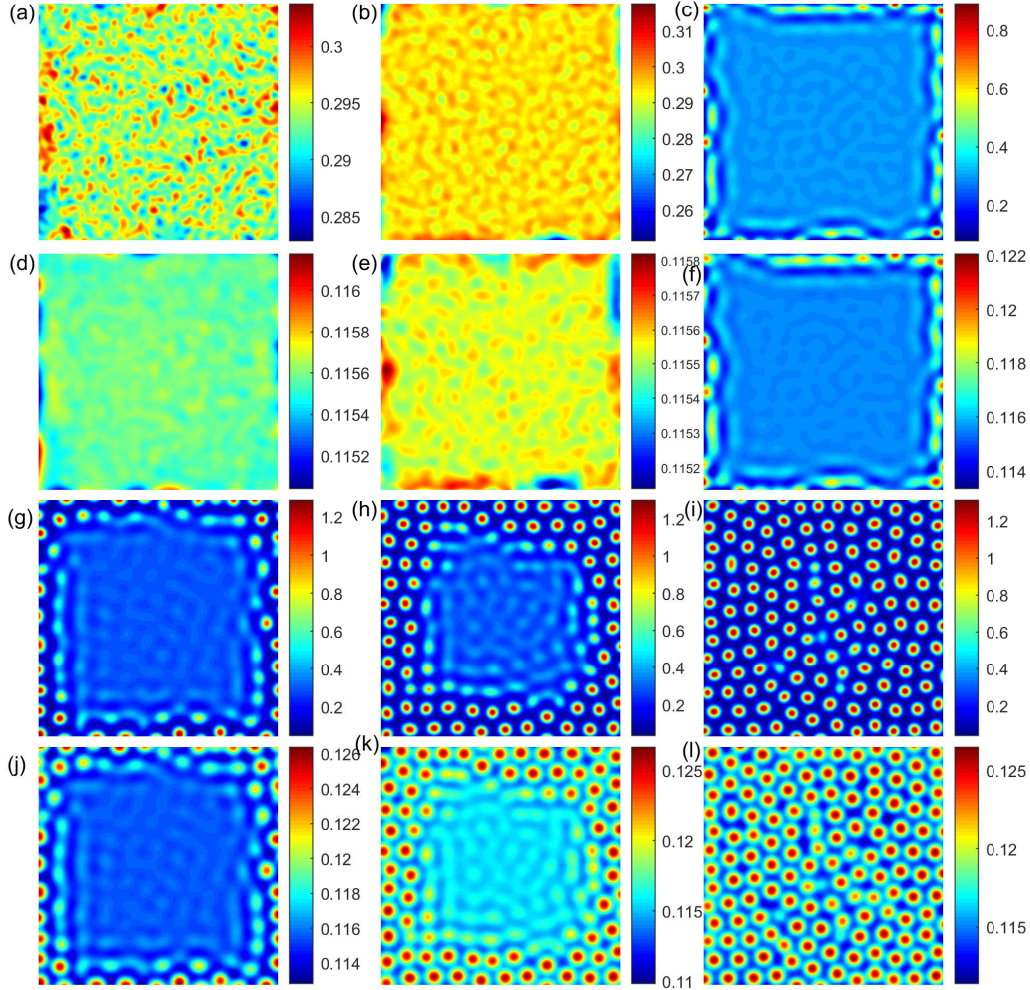
183
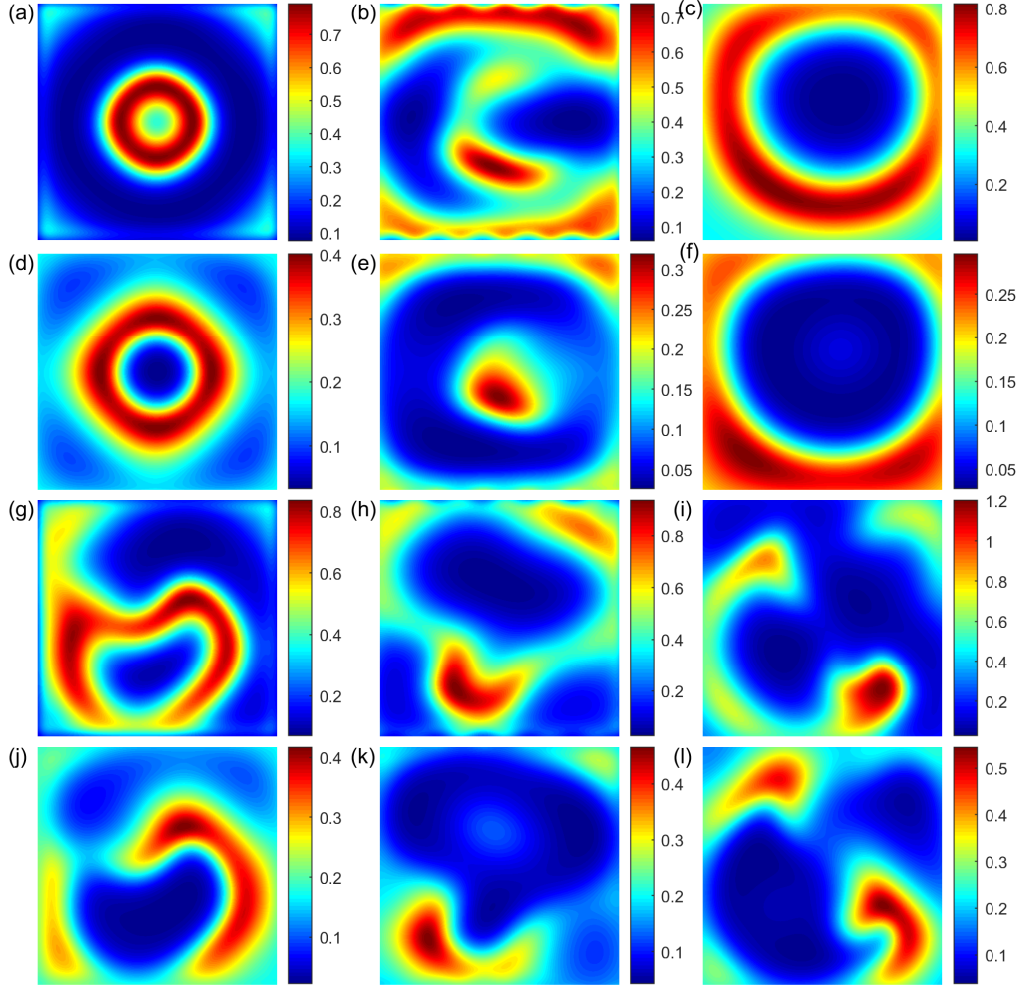
Figure 5.13: Snapshots of the spatial distributions of prey (first and third rows) and predator (second and fourth rows) population at different time steps: $t = 2000$ and $t = 200000$ and for different initial values. The system parameters value are $r_0 = 0.1$, $\eta = 0.10$, $\alpha = 0.20$, $\delta_1 = 0.015$, $\gamma = 0.01$, $\beta = 0.5$, $\xi = 0.6$, $\theta = 0.4$, $\delta_2 = 0.05$, $D_v/D_u = 15$. The snapshots for the initial data: $u^0_{i,j} = 1.0$, $v^0_{i,j} = 0.2$ if $(x_i - 100)^2 + (y_j - 100)^2 < 200$ otherwise $u^0_{i,j} = 0$, $v^0_{i,j} = 0$ are shown in **(a), (c)** for $t = 2000$ and **(g), (j)** for $t = 200000$. The snapshots for the initial data: $u^0_{i,j} = u^* + 0.2\cos(\pi x_i/16)$, $v^0_{i,j} = v^* + 0.4\sin(\pi x/16)$ are shown in **(b), (e)** for $t = 2000$ and **(h), (k)** for $t = 200000$. The snapshots for the initial data: $u^0_{i,j} = u^* + 0.01\Theta_{i,j}$, $v^0_{i,j} = v^* + 0.01\Phi_{i,j}$ where $\Theta_{i,j}$ and $\Phi_{i,j}$ are Gaussian white noise $\delta-$ correlated in space are shown in **(c), (f)** for $t = 2000$ and **(i), (l)** for $t = 200000$.

184

Recently, one more behavioral alteration in prey species was delineated by Zanette et al. [7] due to fear for predator population. Because of fear due to predators, demography for prey species was noticed to decrease substantially due to the cost of anti-predator attributes. The fear factor decreases the prey steady state density. Previously, it can be noticed that the mutual interference among predator species may generate Turing patterns due to diffusion-induced instability. For this situation, the homogeneous steady state loses its stability and generates heterogeneity in the species of a predator-prey system in space and time; howbeit, the predator-prey system with a similar prey-dependent response function unable to generate such patchiness [146].

Herein, we investigate a reaction-diffusion predator-prey model with fear effect due to predator species in addition to Turing and non-Turing spatiotemporal pattern formation. Both the prey and predator population are entitled to move in a closed domain, where population cannot leave the domain. At first, we have recapitulated a wide variety of dynamics of the predator-prey system corresponding to the non-spatial model (5.6) in terms of both the theoretical and numerical illustrations. We performed the qualitative properties of the model (5.6) including positivity, boundedness, local stability of the feasible equilibrium points, existence of Transcritical bifurcation and Hopf bifurcation with respect to the growth rate r_0 of the prey population. Extensive numerical illustrations with system parameters demonstrate that the stable interior equilibrium state alters the stable oscillatory co-existence for increased value of prey growth rate r_0. Moreover, numerical illustrations for the same parameters value reveal that the stable oscillatory interior steady state disappears through Hopf bifurcation for a sufficiently large value of the parameter α. The parameter α designates the level of fear for prey species due to predator species. Extinction of both the prey and predator species due to the level of fear for prey species is a landmark characteristic for predator-prey competitive system. The extinction phenomena due to level of fear α is delineated by the competition between prey and predators for the models with homogeneous population distribution.

Linear amplitude technique is used by considering multiscale perturbation method for the reaction-diffusion system (5.12). This study is performed with respect to the two most significant parameters, namely r_0 (growth rate of prey population) and α (level of due to predator). There are few reasons behind the selection of these two parameters. Firstly, the stability of the non-diffusive system recognized r_0 is the key parameter for the existence of the Transcritical bifurcation (see Theorem 5.4.5) and the

185

stability of E_1 depends on r_0. Secondly, the growth rate of prey species r_0 influenced the spatiotemporal pattern formation (see the Fig. 5.7). Thirdly, the level of fear has an impact on spatiotemporal pattern formation. For increasing the level of fear α, the diffusive system (5.12) takes more time for the warm spot pattern (see Fig. 5.12). Also, the parameter r_0 plays an important role in stability switching through Hopf bifurcation and the interior steady state loses its stability when the r_0 crosses the threshold value r_0^*.

Diffusion-induced instability happens when the system (5.12) is stable without diffusion and unstable in presence of diffusion. The sufficient conditions for the diffusion-driven instability is discussed in our study. Different types of instability may happen depending on the nature of the roots for the dispersion curve for the reaction-diffusion system that leads to the creation of different types of spatiotemporal pattern. Our model simulation illustrates that variation of the prey growth rate r_0 and the level of fear α causes turing pattern. The range of r_0 and α in each of the instability region, howbeit, relies on the wave number. We also numerically illustrates our diffusive system with three different initial values and observed various instabilities including Turing and non-Turing criterion. In our simulations, we noticed stationary patterns like hot spot, warm spot, mix-spots and cold spots for three different initial values. At hot spots, density of population is relatively high and thus the species will diffuse from these positions. On the other hand, density of the species is low at cold spot and the population will diffuse to these positions from the neighboring. Our investigation showed that the diffusive predator-prey model demonstrates different spatiotemporal patterns under the effect of ecological parameters as well as different initial conditions.

More investigations are essential to explore the dynamical behavior of more complicated spatiotemporal models such as predator-prey system with discrete time lag and environmental fluctuation. It would be fascinating to determine in future the spatiotemporal complexity and spatiotemporal chaos in a discrete extension of our continuous predator-prey system with the impact of fear.

Chapter 6

Mathematical modeling of carbon-phytoplankton-zooplankton dynamics and the influence of global warming

6.1 Introduction

Carbon dioxide constantly gets exchanged between the earth's atmosphere, land surface, and oceans as it is produced and absorbed by various animals, plants, and microorganisms. Atmospheric carbon dioxide increased nearly 40% over the past 250 years [51]. This increase is mainly caused by human fossil fuel combustion and deforestation [52]. In absence of anthropogenic activity, removal and emissions of CO_2 by these natural procedure tend to balance the level of CO_2. Anthropogenic activities have contributed significantly to the global warming by adding CO_2 and other green house gases to the atmosphere after the Industrial Revolution [53]. Burning of fossil fuels (e.g. natural gas, oil and coal) for energy, chemical reactions (e.g. cement manufacturing) and deforestation are the leading human activity that releases CO_2 in the atmosphere. Thus, the anthropogenic activities are responsible for an intensive emission of CO_2 and other greenhouse gases to the atmosphere [147, 148]. In marine environment, phytoplankton are the main consumer of carbon during the photosynthesis. Hence, the dynamics of carbon-phytoplankton-zooplankton system becomes very important to the researchers.

Researchers are interested in studying the interactions of species in marine systems through mathematical models. Along with the experimental stud-

ies, mathematical modeling is one of the powerful tools to understand the plankton dynamics. Sekerci and Petrovskii [149] developed a mathematical model for plankton-oxygen dynamics in a marine ecosystem introducing the effect of climate change. Their investigation demonstrates that the depletion of oxygen and plankton extinction occurs due to the effect of climate changing. Upadhyay et al. [150] developed a reaction-diffusion system to study the microalgae in marine system and found that spatial density of microalgae varies chaotically. Edwards and Brindley [151] studied the plankton-nutrient dynamics but did not take into account the consumption of CO_2. A significant number of research has been done by considering various characteristic of phytoplankton and zooplankton dynamics with space and time [152–156], but there is relatively few research considered the effect of CO_2 consumption.

The main objective of this study is to understand the interactive dynamics of carbon with phytoplankton and zooplankton in temporal and spatial pattern formation. We have considered both ordinary and partial differential equation to better visualize the carbon-phytoplankton-zooplankton dynamics. At first, we considered a deterministic model based on ordinary differential equations and studied plankton dynamics with time. Next, the model is upgraded to the spatial process by considering reaction-diffusion equations.

The rest of the chapter is organized in the following way. In Section 6.2, we proposed a carbon-phytoplankton-zooplankton model. In Section 6.3, we studied the positivity, boundedness, PRCC sensitivity and existence of biologically feasible equilibrium points. Local stability of the system abound the equilibria and the existence of Hopf bifurcation is studied in Section 6.4. We considered spatiotemporal model and studied its stability in Section 6.5. Numerical simulations have been performed to validate our analytical findings and the effect of global warming is studied in Section 6.6. Finally, a discussion in Section 6.7 concludes the chapter.

6.2 Formulation of the model

Marine ecosystem is an aquatic environment containing many nonlinear interacting species, inorganic and organic substances. Differential equations are efficient tools to describe the interactive dynamics of an ecosystem [149]. A realistic mathematical model of the marine ecosystem consist of many equations. Our aim in the formulation of a mathematical model is to permit sufficient complexity in such a way that the model will qualitatively create ecologically observed patterns, while it concurrently maintains sufficient simplicity to admit analysis. For our model formulation, we consider the interplay between dissolve carbon dioxide (for the sake of simplicity we write

"carbon" instead of "dissolve carbon dioxide") and phytoplankton as the carbon is consumed by phytoplankton during photosynthesis. We also include zooplankton in our model as the zooplankton consumes phytoplankton and produces carbon during metabolism. Following assumptions are made to construct the mathematical model:

- The atmospheric carbon dioxide continuously mixing with ocean water at a constant rate C_0.

- Carbon is consumed by phytoplankton during photosynthesis and released during respiration.

- Zooplankton consume phytoplankton and produce carbon during respiration.

- Sufficient amount of oxygen is available in the ocean for respiration.

- Consumption of carbon by phytoplankton is higher than the production of carbon by phytoplankton.

Based on the above assumptions, the interaction of the population of the proposed carbon-phytoplankton-zooplankton system is shown schematically in Fig. 6.1. The interplay among carbon, phytoplankton and zooplankton have been presented in the following coupled system of nonlinear ordinary differential equations:

$$\frac{dC}{dt} = \text{Atmospheric carbon dioxide flux} + \text{Respiration} - \text{Photosynthesis}$$
$$- \text{Natural Decay},$$
$$\frac{dP}{dt} = \text{Growth} - \text{Mortality} - \text{Consumption by zooplankton},$$
$$\frac{dZ}{dt} = \text{Growth} - \text{Mortality}, \tag{6.1}$$

where C represents the concentration of carbon, P represents the phytoplankton biomass and Z represents zooplankton biomass. The proposed carbon-phytoplankton-zooplankton (or CPZ) system (6.1) can be expressed mathematically as follows:

$$\frac{dC}{dt} = C_0 + r_1 P + r_2 Z - f(C)g(P) - \delta_1 C,$$
$$\frac{dP}{dt} = \theta_1 f(C)g(P) - h(P,Z) - \delta_2 P, \tag{6.2}$$
$$\frac{dZ}{dt} = \theta_2 h(P,Z) - \delta_3 Z.$$

The interpretation of the functions and parameters are given in Table 6.1 and Table 6.2, respectively. We assume that the phytoplankton (P) can grow logistically, which can be represented as $g(P) = \alpha P - \beta P^2$, where α represents the growth rate and α/β represents the carrying capacity. The function $f(C)$ describes the carbon uptake due to phytoplankton. To understand the properties of the function $f(C)$, we must take into account the effect of photosynthesis process. Carbon is consumed by phytoplankton during daytime to synthesis food in the process of photosynthesis and carbon is release by phytoplankton during their metabolism. The function $h(P, Z)$ describes the consumption of phytoplankton by zooplankton. Now, we consider the following functional form

$$
\begin{aligned}
f(C) &= \frac{\alpha_1 C}{K_1 + C}, \\
g(P) &= \alpha P - \beta P^2, \\
h(P, Z) &= \frac{\alpha_2 P Z}{K_2 + P}.
\end{aligned}
\tag{6.3}
$$

Thus, the proposed system (6.2) takes the following form

$$
\begin{aligned}
\frac{dC}{dt} &= C_0 + r_1 P + r_2 Z - \frac{\alpha_1 C}{K_1 + C}(\alpha P - \beta P^2) - \delta_1 C, \\
\frac{dP}{dt} &= \frac{\theta_1 \alpha_1 C}{K_1 + C}(\alpha P - \beta P^2) - \frac{\alpha_2 P Z}{K_2 + P} - \delta_2 P, \\
\frac{dZ}{dt} &= \frac{\theta_2 \alpha_2 P Z}{K_2 + P} - \delta_3 Z,
\end{aligned}
\tag{6.4}
$$

with non-negative initial values: $C(0) = C_0 \geq 0$, $P(0) = P_0 \geq 0$ and $Z(0) = Z_0 \geq 0$.

6.3   Theoretical study

In this section, positivity and boundedness of the system (6.4) are established. The positivity and boundedness of the system (6.4) ensures the long-term existence of all the populations. Existence of equilibria are also established in this section.

6.3.1   Positive invariance

The positivity of the proposed system (6.4) investigated with non-negative initial values as for any time $t > 0$, the biomass of any population cannot
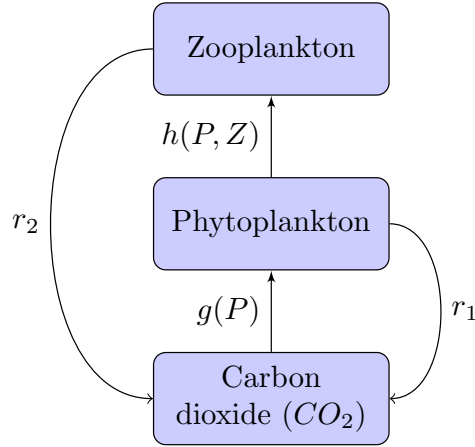
Figure 6.1: Schematic diagram of the proposed model (6.2) describing the interaction between carbon, phytoplankton and zooplankton.

Table 6.1: *Biological meaning of the functions used in the model with sources.*

Function	Biological meaning	Functional form	Source
$f(C)$	Carbon dioxide uptake by Phytoplankton	$\frac{\alpha_1 C}{K_1+C}$	Assumed
$g(P)$	Phytoplankton growth function	$\alpha P - \beta P^2$	[157]
$h(P,Z)$	Phytoplankton uptake by zooplankton	$\frac{\alpha_2 PZ}{K_2+P}$	[158]

be negative. Now, we shall show that all the population remains positive in the interior of $\mathbb{R}^3_+$, where $\mathbb{R}^3_+ = \{(C,P,Z) \in \mathbb{R}^3 : C \geq 0, P \geq 0, Z \geq 0\}$ that means any solution starting in $\mathbb{R}^3_+$ remains in $\mathbb{R}^3_+$ for a finite time. The system (6.4) can be written as $\dot{V} = \mathcal{F}(V)$ with $V(0) = V_0 \in \mathbb{R}^3_+$, where $V = (C,P,Z)^T \in \mathbb{R}^3_+$ and $\mathcal{F}(V)$ is given by

$$\mathcal{F}(V) = \begin{bmatrix} C_0 + r_1 P + r_2 Z - \frac{\alpha_1 C}{K_1+C}(\alpha P - \beta P^2) - \delta_1 C \\ \frac{\theta_1 \alpha_1 C}{K_1+C}(\alpha P - \beta P^2) - \frac{\alpha_2 PZ}{K_2+P} - \delta_2 P \\ \frac{\theta_2 \alpha_2 PZ}{K_2+P} - \delta_3 Z \end{bmatrix},$$

where $\mathcal{F} : C_+ \to \mathbb{R}^3$ and $\mathcal{F} \in C^\infty(\mathbb{R}^3)$.

Table 6.2: *Biological meaning of the model parameters and functions. Estimated parameters value with their sources.*

Par.	Biological meaning	Ranges	Default value	Dimension	Source
C	Dissolved carbon dioxide			Mass	
P	Phytoplankton biomass			Mass	
Z	Zooplankton biomass			Mass	
r_1	Respiration of phytoplankton	$(0, 0.05)$	0.01	Time^{-1}	[159]
r_2	Respiration of zooplankton	$(0.008, 50.8)$	0.01	Time^{-1}	[160]
α_1	Carbon capturing coefficient	$(0, 1.83)$	0.30	-	[158, 161, 162]
α_2	Phytoplankton capturing rate	$(0, 0.7)$	0.15	Time^{-1}	[158, 163]
δ_1	Natural decay rate of carbon	$(0, 0.03)$	0.01	Time^{-1}	[164]
δ_2	Natural mortality rate of phytoplankton	$(0, 0.1)$	0.01	Time^{-1}	[149]
δ_3	Natural mortality rate of zooplankton	$(0, 0.1)$	0.01	Time^{-1}	[149, 163]
θ_1	Conversion coefficient of carbon to phytoplankton biomass	$(0, 1.0)$	0.75	-	Assumed
θ_2	Conversion coefficient of phytoplankton biomass to zooplankton biomass	$(0, 0.25)$	0.20	-	[163, 165]
C_0	Emission rate of carbon from natural sources	-	0.05	MassTime^{-1}	Assumed
α	Linear growth of phytoplankton	$(0, 0.3)$	0.25	Time^{-1}	[163]
β	Intraspecific competition of phytoplankton	-	0.24	Mass^{-1}Time^{-1}	Assumed
K_1	Half saturation constant	$(0, 0.25)$	0.20	Mass	[166, 167]
K_2	Half saturation constant	$(0, 4.0)$	0.40	Mass	[164, 166]

It is easy to verify that whenever $V(0) \in \mathbb{R}_+^3$, such that $V_i = 0$, then $\mathcal{F}(V) \mid_{V_i=0} \geq 0$ for all $i = 1, 2, 3$. Hence, any solution $V(t) = V(t, V_0)$ of $\dot{V} = \mathcal{F}(V)$ with $V_0 \in \mathbb{R}_+^3$ is such that $V(t) \in \mathbb{R}_+^3$ for all $t > 0$ [168, 169].

6.3.2 Boundedness

In terms of ecology, boundedness of (6.4) implies that for any time t, none of the interacting population will grow exponentially or unboundedly. The biomass of each of the population remains bounded due to limited resources.

Theorem 6.3.1. *All the solution of (6.4) with non-negative initial conditions (C_0, P_0, Z_0), which starts in $\mathbb{R}_+^3$ are uniformly bounded.*

Proof. Let $(C(t), P(t), Z(t))$ be any solution of (6.4) with positive initial condition (C_0, P_0, Z_0). To prove the boundedness of (6.4), we consider the following function

$$W(t) = C(t) + \frac{1}{\theta_1}P(t) + \frac{1}{\theta_1\theta_2}Z(t).$$

After differentiation, we get

$$\begin{aligned}
\frac{dW}{dt} &= \frac{dC}{dt} + \frac{1}{\theta_1}\frac{dP}{dt} + \frac{1}{\theta_1\theta_2}\frac{dZ}{dt} \\
&= C_0 - \delta_1 C - (\frac{\delta_2}{\theta_1} - r_1)P - (\frac{\delta_3}{\theta_1\theta_2} - r_2)Z \\
&= C_0 - \delta_1 C - \frac{1}{\theta_1}(\delta_2 - r_1\theta_1)P - \frac{1}{\theta_1\theta_2}(\delta_3 - r_2\theta_1\theta_2)Z \\
&\leq C_0 - \rho\left[C(t) + \frac{1}{\theta_1}P(t) + \frac{1}{\theta_1\theta_2}Z(t)\right],
\end{aligned}$$

where $\rho = \min\{\delta_1, \delta_2 - r_1\theta_1, \delta_3 - r_2\theta_1\theta_2\}$. Therefore, we have

$$\frac{dW}{dt} + \rho W \leq C_0.$$

Using the theory of differential inequality for $W(t)$, we obtain

$$0 < W(C, P, Z) \leq \frac{C_0}{\rho}(1 - e^{-\rho t}) + W(C(0), P(0), Z(0))e^{-\rho t},$$

for $t \rightarrow \infty$, we have $0 < W < \frac{C_0}{\rho}$. Hence, all the solutions of (6.4) that initiating in $\mathbb{R}^3_+$ are confined in the region $\mathbb{S} = \left\{(C, P, Z) \in \mathbb{R}^3_+ : W = \frac{C_0}{\rho} + \epsilon, \text{ for any } \epsilon > 0\right\}$. $\qquad\square$

6.3.3 PRCC sensitivity analysis

Sensitivity analysis determine the most influential system parameters with respect to the state variable. The partial rank correlation coefficient (PRCC), a global sensitivity analysis is a powerful and reliable sampling based method used to identify the most effective system parameters. PRCC computes the effect of changes for each system parameters on model output [170]. For the input system parameters, we have conducted Latin hypercube sampling (LHS) without substitution to estimate the PRCC [133]. The sampling is conducted autonomously and the range for every system parameter is $\pm 25\%$ of the nominal values. The PRCC computed with reference to carbon (C). The PRCC values for all the fourteen system parameters is illustrated by bar diagram in Fig. 6.2 for 50, 75, 100, 125 and 150 days. If the value of the PRCC is positive then the parameter has positive correlation with the model output, that is, positive changes in the system parameters will increase the model output. Again if the value of the PRCC is negative

then the parameter has negative correlation with the model output, that is, negative changes in the parameter will decrease the model output. The value of PRCC lies between -1 to $+1$. A value $+1$ (or -1) of PRCC indicates that perfect positive (or negative) linear relationship between the system output and the corresponding system parameter. Again a value near 0 of PRCC indicates no relationship between the system output and the corresponding system parameter. If the PRCC value of r_1 is 0.8, then increase of r_1 by 10% will increase the value of the population by 8%.

From the Fig. 6.2, we found that the most influential parameters are the emission rate of carbon from natural sources (C_0), intra-specific competition of phytoplankton (β) and phytoplankton capturing rate (α_2). The most negatively influential parameters are natural decay rate of carbon (δ_1), linear growth rate of phytoplankton (α) and carbon capturing coefficient (α_1). It is important to identify these key parameters as they influence more in the system dynamics.
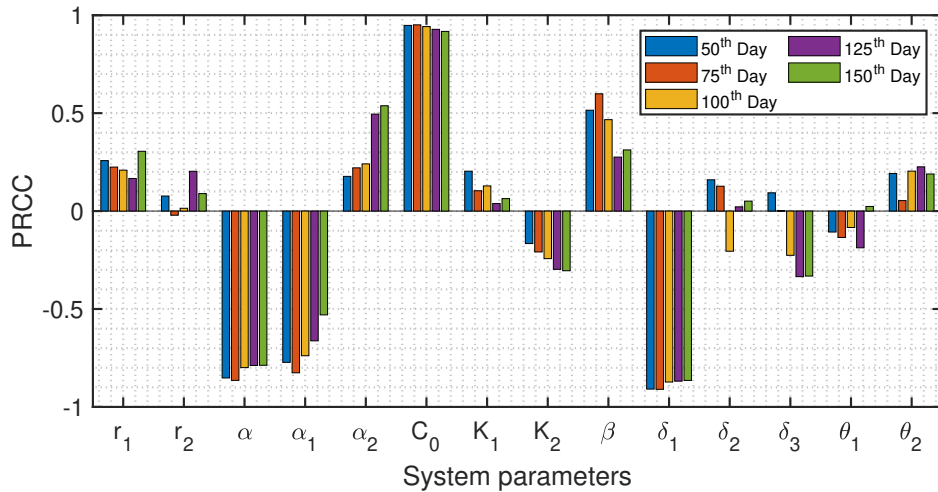

Figure 6.2: PRCC for the parameters of the system (6.4) for different times with $p < 0.001$.

6.3.4 Equilibria

Biologically feasible equilibrium points are the point of intersections of the following zero-growth isoclines in the non-negative octant $\mathbb{R}^3_+ = \left\{ \big(C(t), P(t), Z(t)\big) : C(t), P(t), Z(t) \geq 0 \right\}$, where

$$C_0 + r_1 P + r_2 Z - \frac{\alpha_1 C}{K_1 + C}(\alpha P - \beta P^2) - \delta_1 C = 0,$$

$$\frac{\theta_1 \alpha_1 C}{K_1 + C}(\alpha P - \beta P^2) - \frac{\alpha_2 P Z}{K_2 + P} - \delta_2 P = 0, \qquad (6.5)$$

$$\frac{\theta_2 \alpha_2 P Z}{K_2 + P} - \delta_3 Z = 0.$$

The carbon nullcline surface, phytoplankton nullcline surface and the zooplankton nullcline surfaces are represented by the first, second and third equations of (6.5), respectively. The model system (6.4) has three biologically feasible equilibrium points, namely

(i) phytoplankton and zooplankton-free equilibrium $E_0(\frac{C_0}{\delta_1}, 0, 0)$,

(ii) zooplankton-free equilibrium $E_1(\bar{C}, \bar{P}, 0)$ where $\bar{C} = \dfrac{K_1 \delta_2}{\theta_1 \alpha_1 (\alpha - \beta \bar{P}) - \delta_2}$, which is feasible for $\delta_2 < \theta_1 \alpha_1 (\alpha - \beta \bar{P})$ and $\bar{P}$ is the positive root(s) of the quadratic equation

$$P^2 + \sigma_1 P + \sigma_2 = 0,$$

where

$$\sigma_1 = \frac{C_0 \theta_1^2 \alpha_1 \beta - (r_1 \theta_1 - \delta_2)(\alpha \alpha_1 \theta_1 - \delta_2)}{\theta_1 \alpha_1 \beta (r_1 \theta_1 - \delta_2)} \text{ and}$$

$$\sigma_2 = \frac{K_1 \delta_1 \delta_2 - C_0 (\alpha \alpha_1 \theta_1 - \delta_2)}{\alpha_1 \beta (r_1 \theta_1 - \delta_2)}.$$

Hence $\bar{P} = \dfrac{-\sigma_1 \pm \sqrt{\sigma_1^2 - 4\sigma_2}}{2}$, which is real for

$$\left[C_0 \theta_1^2 \alpha_1 \beta - (r_1 \theta_1 - \delta_2)(\alpha \alpha_1 \theta_1 - \delta_2) \right]^2 >$$

$$4\theta_1^2 \alpha_1 \beta (r_1 \theta_1 - \delta_2) \left[K_1 \delta_1 \delta_2 - C_0 (\alpha \alpha_1 \theta_1 - \delta_2) \right].$$

Now, if $\sigma_2 < 0$ then $\bar{P}$ has a unique positive root, that is, $\bar{P} = \dfrac{-\sigma_1 + \sqrt{\sigma_1^2 - 4\sigma_2}}{2}$. Again if $\sigma_2 > 0$ and $\sigma_1 < 0$ then $\bar{P}$ has two positive values $\bar{P} = \dfrac{-\sigma_1 \pm \sqrt{\sigma_1^2 - 4\sigma_2}}{2}$.

(iii) Co-existing equilibrium $E^*(\tilde{C}, \tilde{P}, \tilde{Z})$, where $\tilde{P} = \dfrac{K_2 \delta_3}{\theta_2 \alpha_2 - \delta_3}$,

$$\tilde{Z} = \frac{\theta_1 \alpha_1 \tilde{C}(\alpha - \beta \tilde{P})(K_2 + \tilde{P}) - \delta_2(K_1 + \tilde{C})(K_2 + \tilde{P})}{\alpha_2(K_1 + \tilde{C})}$$

and $\tilde{C}$ is the positive root of the equation

$$\tau_1 C^2 + \tau_2 C + \tau_3 = 0,$$

where

$$\tau_1 = \delta_1 \alpha_2,$$
$$\tau_2 = K_1 \delta_1 \alpha_2 + \alpha_1 \alpha_2 (\alpha \tilde{P} - \beta \tilde{P}^2) + r_2 \delta_2(K_2 + \tilde{P})$$
$$- \alpha_2(C_0 + r_1 \tilde{P}) - \theta_1 \alpha_1 r_2 (\alpha - \beta \tilde{P})(K_2 + \tilde{P})$$
$$\text{and } \tau_3 = K_1 r_2 \delta_2 (K_2 + \tilde{P}) - K_1 \alpha_2 (C_0 + r_1 \tilde{P}).$$

Here, $\tilde{P}$ and $\tilde{Z}$ will be feasible when $\theta_2 \alpha_2 > \delta_3$ and $\theta_1 \alpha_1 \tilde{C}(\alpha - \beta \tilde{P})(K_2 + \tilde{P}) > \delta_2(K_1 + \tilde{C})(K_2 + \tilde{P})$. Now, if $\tau_3 < 0$, then $\tilde{P}$ has unique positive value

$$\tilde{P} = \frac{-\tau_2 + \sqrt{\tau_2^2 - 4\tau_1 \tau_3}}{2\tau_1}$$

provided $\tau_2^2 > 4\tau_1 \tau_3$. Again if $\tau_3 > 0$ and $\tau_2 < 0$, then $\tilde{P}$ has two positive values

$$\tilde{P} = \frac{-\tau_2 \pm \sqrt{\tau_2^2 - 4\tau_1 \tau_3}}{2\tau_1}$$

provided $\tau_2^2 > 4\tau_1 \tau_3$.

6.3.5   Nullclines

The nullcline surfaces of the CPZ system (6.4) are

$$f_1 \equiv C_0 + r_1 P + r_2 Z - \frac{\alpha_1 C}{K_1 + C}(\alpha P - \beta P^2) - \delta_1 C = 0,$$
$$f_2 \equiv \frac{\theta_1 \alpha_1 C}{K_1 + C}(\alpha P - \beta P^2) - \frac{\alpha_2 P Z}{K_2 + P} - \delta_2 P = 0$$
$$\text{and } f_3 \equiv \frac{\theta_2 \alpha_2 P Z}{K_2 + P} - \delta_3 Z = 0$$

with $C - P$ co-ordinate plane (that is, $Z = 0$), $P - Z$ co-ordinate plane (that is, $C = 0$) and $Z - C$ co-ordinate plane (that is, $P = 0$). The nullcline

surfaces of the CPZ system (6.4) are shown in Fig. 6.3 in the C-P-Z space. In the nullcline plot, the carbon nullcline is represented by red surface, the phytoplankton nullcline is represented by blue surface and the green surface represents the zooplankton nullcline. The dotted grid lines represent the co-ordinate planes. The black curve is the intersection of the carbon nullcline surface and phytoplankton nullcline surface, carbon nullcline surface and zoo-plankton nullcline surface intersect through the green curve and the red curve is the intersection of phytoplankton nullcline surface and zooplankton null-cline surface. The parameters are used to draw the Fig. 6.3 and presented in Table 6.2. The phytoplankton and zooplankton-free equilibrium $E_0(5, 0, 0)$ is represented by solid black circle and the zooplankton-free equilibrium $E_1(4.7171, 0.8486, 0)$ is represented by solid green circle. The interior equilibrium point $E^*(4.1769, 0.2000, 0.1335)$ is the point of intersection of black, red and green curve. The interior equilibrium point $E^*(4.1769, 0.2000, 0.1335)$ is represented by solid red circle.

6.4 Local stability analysis

In this section, the local asymptotic stability of the equilibrium points are analyzed. To do this, we compute the variational matrix (J_E) of the system (6.4) around each of the equilibrium point $E(C, P, Z)$ as follows:

$$
J_E = \begin{bmatrix}
-\frac{\alpha_1 K_1}{(K_1+C)^2}(\alpha P - \beta P^2) - \delta_1 & r_1 - \frac{\alpha_1 C}{K_1+C}(\alpha - 2\beta P) & r_2 \\
\frac{\theta_1 \alpha_1 K_1}{(K_1+C)^2}(\alpha P - \beta P^2) & \frac{\theta_1 \alpha_1 C}{K_1+C}(\alpha - 2\beta P) - \frac{\alpha_2 K_2 Z}{(K_2+P)^2} - \delta_2 & -\frac{\alpha_2 P}{K_2+P} \\
0 & \frac{\theta_2 \alpha_2 K_2 Z}{(K_2+P)^2} & \frac{\theta_2 \alpha_2 P}{K_2+P} - \delta_3
\end{bmatrix}.
$$

The stability criterion of the biologically feasible steady states E_0, E_1 and E^* are delineated in the following Theorems.

Theorem 6.4.1. *The necessary condition for the system (6.4) to be locally asymptotically stable around the phytoplankton and zooplankton-free equilibrium $E_0(\frac{C_0}{\delta_1}, 0, 0)$ is $\frac{\alpha \alpha_1 \theta_1 C_0}{C_0 + K_1 \delta_1} < \delta_2$, otherwise unstable.*

Proof. The variational matrix of the system (6.4) at the phytoplankton and zooplankton-free equilibrium point E_0 is

$$
J(E_0) = \begin{bmatrix}
-\delta_1 & r_1 - \frac{\alpha \alpha_1 C_0}{C_0 + K_1 \delta_1} & r_2 \\
0 & \frac{\alpha \alpha_1 C_0 \theta_1}{C_0 + K_1 \delta_1} - \delta_2 & 0 \\
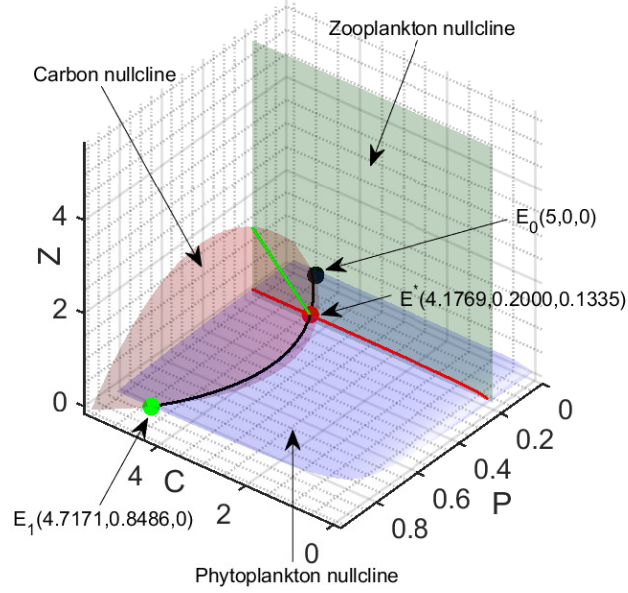0 & 0 & -\delta_3
\end{bmatrix}.
$$

Figure 6.3: Nullcline surfaces of the CPZ system (6.4). The red surface represents the carbon nullcline, phytoplankton nullcline is represented by the blue surface and the green surface represents the zooplankton nullcline. The phytoplankton and zooplankton-free equilibrium $E_0(5, 0, 0)$ are represented by solid black circle. The zooplankton-free equilibrium $E_1(4.7171, 0.8486, 0)$ is represented by solid green circle and the interior equilibrium $E^*(4.1769, 0.2000, 0.1335)$ is represented by solid red circle. The parameters value are listed in Table 6.2.

The eigenvalues of the above matrix are $-\delta_1$, $-\delta_3$ and $\frac{\alpha\alpha_1\theta_1 C_0}{C_0+K_1\delta_1} - \delta_2$. Here all the parameters are non-negative, therefore the equilibrium point $E_0(\frac{C_0}{\delta_1}, 0, 0)$ of the system (6.4) will be locally asymptotically stable if $\frac{\alpha\alpha_1\theta_1 C_0}{C_0+K_1\delta_1} < \delta_2$, that is, the mortality rate of phytoplankton grater than some threshold value. $\square$

Theorem 6.4.2. *The zooplankton-free equilibrium $E_1(\bar{C}, \bar{P}, 0)$ of the system (6.4) is locally asymptotically stable if $\varphi_1 > 0$, $\varphi_3 > 0$ and $\varphi_1\varphi_2 - \varphi_3 > 0$, where φ_i (for i =1, 2, 3) are defined in the proof.*

Proof. The variational matrix of the system (6.4) around the zooplankton-free equilibrium point E_1 is

$$J(E_1) = \begin{bmatrix} -\frac{\alpha_1 K_1}{(K_1+\bar{C})^2}(\alpha\bar{P} - \beta\bar{P}^2) - \delta_1 & r_1 - \frac{\alpha_1\bar{C}}{K_1+\bar{C}}(\alpha - 2\beta\bar{P}) & r_2 \\ \frac{\theta_1\alpha_1 K_1}{(K_1+\bar{C})^2}(\alpha\bar{P} - \beta\bar{P}^2) & \frac{\theta_1\alpha_1\bar{C}}{K_1+\bar{C}}(\alpha - 2\beta\bar{P}) - \delta_2 & -\frac{\alpha_2\bar{P}}{K_2+\bar{P}} \\ 0 & 0 & \frac{\theta_2\alpha_2\bar{P}}{K_2+\bar{P}} - \delta_3 \end{bmatrix}.$$

The characteristic equation of the variational matrix $J(E_1)$ is

$$\lambda^3 + \varphi_1 \lambda^2 + \varphi_2 \lambda + \varphi_3 = 0,$$

where

$$\varphi_1 = \delta_1 + \delta_2 + \delta_3 + \frac{\alpha_1 K_1}{(K_1 + \bar{C})^2}(\alpha\bar{P} - \beta\bar{P}^2) - \frac{\theta_1 \alpha_1 \bar{C}}{K_1 + \bar{C}}(\alpha - 2\beta\bar{P}) - \frac{\theta_2 \alpha_2 \bar{P}}{K_2 + \bar{P}},$$

$$\varphi_2 = \left[\delta_3 - \frac{\theta_2 \alpha_2 \bar{P}}{K_2 + \bar{P}}\right]\left[\delta_1 + \delta_2 + \frac{\alpha_1 K_1}{(K_1 + \bar{C})^2}(\alpha\bar{P} - \beta\bar{P}^2) - \frac{\theta_1 \alpha_1 \bar{C}}{K_1 + \bar{C}}(\alpha - 2\beta\bar{P})\right]$$

$$- \left[\frac{\theta_1 \alpha_1 \delta_1 \bar{C}}{K_1 + \bar{C}}(\alpha - 2\beta\bar{P}) - \frac{\alpha_1 K_1 \delta_2}{(K_1 + \bar{C})^2}(\alpha\bar{P} - \beta\bar{P}^2)\right.$$

$$\left. - \delta_1 \delta_2 + \frac{\theta_1 \alpha_1 K_1 r_1}{(K_1 + \bar{C})^2}(\alpha\bar{P} - \beta\bar{P}^2)\right] \text{ and}$$

$$\varphi_3 = \left[\frac{\theta_2 \alpha_2 \bar{P}}{K_2 + \bar{P}} - \delta_3\right]\left[\frac{\theta_1 \alpha_1 \delta_1 \bar{C}}{K_1 + \bar{C}}(\alpha - 2\beta\bar{P}) - \frac{\alpha_1 K_1 \delta_2}{(K_1 + \bar{C})^2}(\alpha\bar{P} - \beta\bar{P}^2)\right.$$

$$\left. - \delta_1 \delta_2 + \frac{\theta_1 \alpha_1 K_1 r_1}{(K_1 + \bar{C})^2}(\alpha\bar{P} - \beta\bar{P}^2)\right].$$

Due to well-known Routh-Hurwitz criteria, we have that the system (6.4) is locally asymptotically stable around the zooplankton-free equilibrium $E_1(\bar{C}, \bar{P}, 0)$ if $\varphi_1 > 0$, $\varphi_3 > 0$ and $\varphi_1 \varphi_2 - \varphi_3 > 0$. $\qquad\square$

Theorem 6.4.3. *The co-existing equilibrium $E^*(\tilde{C}, \tilde{P}, \tilde{Z})$ of the system (6.4) is locally asymptotically stable if $\mu_1 > 0$, $\mu_3 > 0$ and $\mu_1 \mu_2 - \mu_3 > 0$, where μ_i (for i =1, 2, 3) are defined in the proof.*

Proof. The variational matrix of the system (6.4) around the co-existing equilibrium point $E^*(\tilde{C}, \tilde{P}, \tilde{Z})$ is

$$J(E^*) = \begin{bmatrix} J_{11} & J_{12} & J_{13} \\ J_{21} & J_{22} & J_{23} \\ J_{31} & J_{32} & J_{33} \end{bmatrix}, \tag{6.6}$$

where

$$J_{11} = -\frac{\alpha_1 K_1}{(K_1 + \tilde{C})^2}(\alpha\tilde{P} - \beta\tilde{P}^2) - \delta_1, \quad J_{12} = r_1 - \frac{\alpha_1 \tilde{C}}{K_1 + \tilde{C}}(\alpha - 2\beta\tilde{P}),$$

$$J_{13} = r_2, \quad J_{21} = \frac{\theta_1 \alpha_1 K_1}{(K_1 + \tilde{C})^2}(\alpha\tilde{P} - \beta\tilde{P}^2),$$

$$J_{22} = \frac{\theta_1 \alpha_1 \tilde{C}}{K_1 + \tilde{C}}(\alpha - 2\beta\tilde{P}) - \frac{\alpha_2 K_2 \tilde{Z}}{(K_2 + \tilde{P})^2} - \delta_2,$$

$$J_{23} = -\frac{\alpha_2 \tilde{P}}{K_2 + \tilde{P}}, \quad J_{31} = 0, \quad J_{32} = \frac{\theta_2 \alpha_2 K_2 \tilde{Z}}{(K_2 + \tilde{P})^2}, \text{ and } J_{33} = 0.$$

The characteristic equation of the variational matrix $J(E^*)$ is given by

$$\lambda^3 + \mu_1\lambda^2 + \mu_2\lambda + \mu_3 = 0, \tag{6.7}$$

where

$$\mu_1 = -(J_{11} + J_{22})$$
$$= \delta_1 + \delta_2 + \frac{\alpha_1 K_1}{(K_1 + \tilde{C})^2}(\alpha\tilde{P} - \beta\tilde{P}^2) + \frac{\alpha_2 K_2 \tilde{Z}}{(K_2 + \tilde{P})^2}$$
$$- \frac{\theta_1 \alpha_1 \tilde{C}}{K_1 + \tilde{C}}(\alpha - 2\beta\tilde{P}),$$

$$\mu_2 = -J_{23}J_{32} + (J_{11}J_{22} - J_{12}J_{21})$$
$$= \frac{\theta_2 \alpha_2^2 K_2 \tilde{P}\tilde{Z}}{(K_2 + \tilde{P})^3} - \frac{\theta_1 \alpha_1 K_1 r_1}{(K_1 + \tilde{C})^2}(\alpha\tilde{P} - \beta\tilde{P}^2)$$
$$+ \frac{\theta_1 \alpha_1^2 K_1 \tilde{C}}{(K_1 + \tilde{C})^3}(\alpha - 2\beta\tilde{P})(\alpha\tilde{P} - \beta\tilde{P}^2)$$
$$+ \left[\delta_1 + \frac{\alpha_1 K_1}{(K_1 + \tilde{C})^2}(\alpha\tilde{P} - \beta\tilde{P}^2)\right]\left[\delta_2 + \frac{\alpha_2 K_2 \tilde{Z}}{(K_2 + \tilde{P})^2}\right.$$
$$\left. - \frac{\theta_1 \alpha_1 \tilde{C}}{K_1 + \tilde{C}}(\alpha - 2\beta\tilde{P})\right],$$

$$\mu_3 = J_{11}J_{23}J_{32} - J_{13}J_{21}J_{32}$$
$$= \left[\delta_1 + \frac{\alpha_1 K_1}{(K_1 + \tilde{C})^2}(\alpha\tilde{P} - \beta\tilde{P}^2)\right]\frac{\theta_2 \alpha_2^2 K_2 \tilde{P}\tilde{Z}}{(K_2 + \tilde{P})^3}$$
$$- \frac{\theta_1 \theta_2 \alpha_1 \alpha_2 K_1 K_2 r_2}{(K_1 + \tilde{C})^2 (K_2 + \tilde{P})^2}(\alpha\tilde{P} - \beta\tilde{P}^2)\tilde{Z}.$$

Due to the Routh-Hurwitz criterion, the system (6.4) is locally asymptotically stable around the co-existing equilibrium $E^*(\tilde{C}, \tilde{P}, \tilde{Z})$ if $\mu_1 > 0$, $\mu_3 > 0$ and $\mu_1\mu_2 - \mu_3 > 0$. Hence, the co-existing equilibrium of the system (6.4) is locally asymptotically stable under this condition. $\qquad\square$

6.4.1 Stability region

To investigate the complex dynamics of the CPZ system (6.4), the stability regions are plotted in $(\alpha_1 - \theta_1)$ and $(\alpha_1 - C_0)$ parameters space for all the equilibrium points (see Fig. 6.4). The stability regions for the three equilibrium points of the CPZ system (6.4) have been shown by different colored and remain the same color for each equilibrium points in both the sub-figures. In the Fig. 6.4(a), α_1 is varied from 0 to 2.5, θ_1 is varied from 0 to 1 and other system parameters are listed in the Table 6.2. In the Fig. 6.4(b), α_1 is varied from 0 to 0.5, C_0 is varied from 0 to 0.5 and other system parameters are listed in the Table 6.2. In the region R_1, phytoplankton and zooplankton-free equilibrium point $E_0(C_0/\delta_1, 0, 0)$ is locally asymptotic stable but zooplankton-free equilibrium point $E_1(\bar{C}, \bar{P}, 0)$ and co-existing equilibrium point $E^*(\tilde{C}, \tilde{P}, \tilde{Z})$ are unstable. In the region R_2, zooplankton-free equilibrium point $E_1(\bar{C}, \bar{P}, 0)$ is locally asymptotic stable but phytoplankton and zooplankton-free equilibrium point $E_0(C_0/\delta_1, 0, 0)$ and co-existing equilibrium point $E^*(\tilde{C}, \tilde{P}, \tilde{Z})$ are unstable. In region R_3, co-existing equilibrium point $E^*(\tilde{C}, \tilde{P}, \tilde{Z})$ is stable but phytoplankton and zooplankton-free equilibrium point $E_0(C_0/\delta_1, 0, 0)$ and zooplankton-free equilibrium point $E_1(\bar{C}, \bar{P}, 0)$ are unstable. In region R_4, all the equilibrium points are unstable.

6.4.2 Analysis of Hopf bifurcation

Hopf bifurcation of the system (6.4) with respect to carbon capturing coefficient (α_1) by the phytoplankton is analyzed in this section. The system (6.4) undergoes Hopf bifurcation around the co-existing equilibrium point $E^*(\tilde{C}, \tilde{P}, \tilde{Z})$ when the characteristic equation (6.7) of the variational matrix (6.6) have complex conjugate eigenvalues. The following theorem states the existence of Hopf bifurcation of the system (6.4) with respect to the parameter α_1.

Theorem 6.4.4. *The necessary and sufficient condition to occur Hopf bifurcation are that there exists $\alpha_1 = \alpha_1{}^*$ such that*

(i) $\mu_i(\alpha_1{}^*) > 0$, $i = 1, 2, 3$,

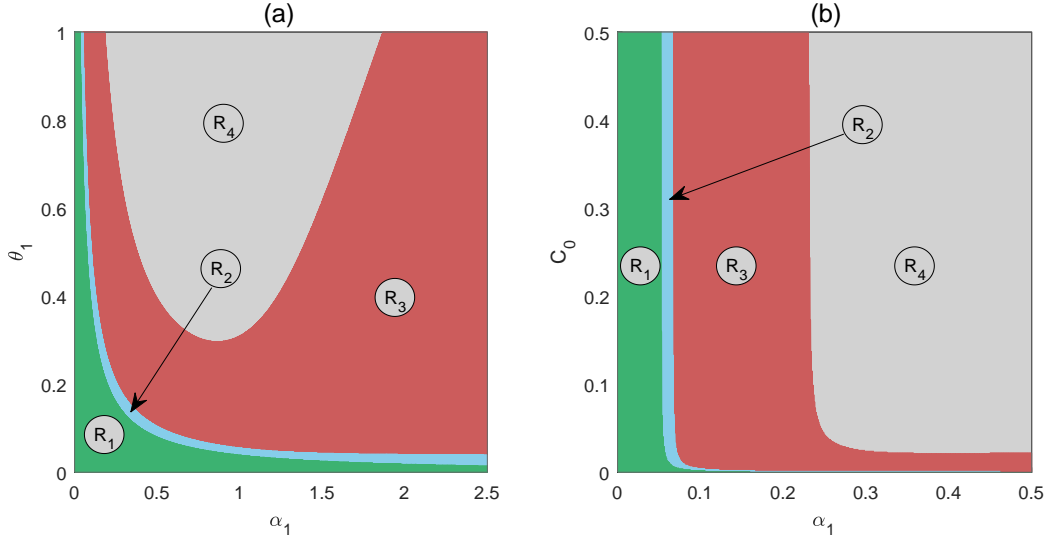*(ii) $\mu_1(\alpha_1{}^*)\mu_2(\alpha_1{}^*) - \mu_3(\alpha_1{}^*) = 0$,*

Figure 6.4: Numerical illustrations of the stability regions of $E_0(C_0/\delta_1, 0, 0)$, $E_1(\bar{C}, \bar{P}, 0)$ and $E^*(\tilde{C}, \tilde{P}, \tilde{Z})$ are denoted by R_1, R_2 and R_3, respectively. In the region R_4, all the equilibrium points are unstable.

(iii) $\left[\frac{d}{d\alpha_1}(Re(\lambda_i))\right]_{\alpha_1=\alpha_1{}^*} \neq 0, \; i = 1, 2,$

where μ_1, μ_2 and μ_3 are defined in the proof of the Theorem 6.4.3.

Proof. Here, $\mu_i(\alpha_1{}^*) > 0$ for $\alpha_1 = \alpha_1{}^*$ and $i = 1, 2, 3$, then there exists an interval $(\alpha_1{}^* - \zeta_i, \; \alpha_1{}^* + \zeta_i)$ containing $\alpha_1{}^*$ where $i = 1, 2, 3$. Now, we consider $0 < \zeta < \min\{\zeta_i : i = 1, 2, 3\}$ in such a way that $\alpha_1{}^* - \zeta > 0$ and $\mu_i(\alpha_1) > 0$ for $\alpha_1 \in (\alpha_1{}^* - \zeta_i, \; \alpha_1{}^* + \zeta_i)$ with $i = 1, 2, 3$. For $\alpha_1 = \alpha_1{}^*$, $\mu_1(\alpha_1{}^*)\mu_2(\alpha_1{}^*) - \mu_3(\alpha_1{}^*) = 0$ and the characteristic equation (6.7) can be written as

$$(\lambda^2 + \mu_2)(\lambda + \mu_1) = 0.$$

The roots of the above equation are $\lambda_1 = i\sqrt{\mu_2}$, $\lambda_2 = -i\sqrt{\mu_2}$ and $\lambda_3 = -\mu_1$. Now, for any $\alpha_1 \in (\alpha_1{}^* - \zeta, \; \alpha_1{}^* + \zeta)$, the roots can be expressed in the form

$$\lambda_1(\alpha_1) = \phi_1(\alpha_1) + i\phi_2(\alpha_1),$$
$$\lambda_2(\alpha_1) = \phi_1(\alpha_1) - i\phi_2(\alpha_1),$$
$$\lambda_3(\alpha_1) = -\mu_1(\alpha_1).$$

Now, we shall verify the transversality condition

$$\left[\frac{d}{d\alpha_1}(Re(\lambda_i))\right]_{\alpha_1=\alpha_1{}^*} \neq 0, \quad i = 1, 2.$$

By substituting $\lambda_i(\alpha_1) = \phi_1(\alpha_1) + i\phi_2(\alpha_1)$ in the characteristic equation (6.7) and differentiating with respect to α_1, we obtain

$$\begin{aligned}
P(\alpha_1)\phi_1{}'(\alpha_1) - Q(\alpha_1)\phi_2{}'(\alpha_1) + R(\alpha_1) = 0, \\
Q(\alpha_1)\phi_1{}'(\alpha_1) + P(\alpha_1)\phi_2{}'(\alpha_1) + S(\alpha_1) = 0,
\end{aligned} \tag{6.8}$$

where

$$\begin{aligned}
P(\alpha_1) &= 3\phi_1{}^2(\alpha_1) - 3\phi_2{}^2(\alpha_1) + 2\mu_1(\alpha_1)\phi_1(\alpha_1) + \mu_2(\alpha_1), \\
Q(\alpha_1) &= 6\phi_1(\alpha_1)\phi_2(\alpha_1) + 2\mu_1(\alpha_1)\phi_2(\alpha_1), \\
R(\alpha_1) &= \mu_1{}'(\alpha_1)\phi_1{}^2(\alpha_1) - \mu_1{}'(\alpha_1)\phi_2{}^2(\alpha_1) + \mu_2{}'(\alpha_1)\phi_1(\alpha_1) + \mu_3{}'(\alpha_1), \\
S(\alpha_1) &= 2\mu_1{}'(\alpha_1)\phi_1(\alpha_1)\phi_2(\alpha_1) + \mu_2{}'(\alpha_1)\phi_2(\alpha_1).
\end{aligned}$$

It can be noticed that $\phi_1(\alpha_1{}^*) = 0$ and $\phi_2(\alpha_1{}^*) = \sqrt{\mu_2(\alpha_1{}^*)}$, we have

$$\begin{aligned}
P(\alpha_1{}^*) &= -2\mu_2(\alpha_1{}^*), \quad Q(\alpha_1{}^*) = 2\mu_1(\alpha_1{}^*)\sqrt{\mu_2(\alpha_1{}^*)}, \\
R(\alpha_1{}^*) &= -\mu_1{}'(\alpha_1{}^*)\mu_2(\alpha_1{}^*) + \mu_3{}'(\alpha_1{}^*), \quad S(\alpha_1{}^*) = \mu_2{}'(\alpha_1{}^*)\sqrt{\mu_2(\alpha_1{}^*)}.
\end{aligned}$$

Thus, the transversality condition becomes

$$\begin{aligned}
\left[\frac{d}{d\alpha_1}(Re(\lambda_i))\right]_{\alpha_1=\alpha_1{}^*} &= \phi_1{}'(\alpha_1{}^*) \\
&= -\left[\frac{P(\alpha_1)R(\alpha_1) + Q(\alpha_1)S(\alpha_1)}{P^2(\alpha_1) + Q^2(\alpha_1)}\right]_{\alpha_1=\alpha_1{}^*} \\
&= -\frac{\mu_1(\alpha_1{}^*)\mu_2{}'(\alpha_1{}^*) - \mu_3{}'(\alpha_1{}^*) + \mu_1{}'(\alpha_1{}^*)\mu_2(\alpha_1{}^*)}{2\left(\mu_2(\alpha_1{}^*) + \mu_1{}^2(\alpha_1{}^*)\right)} \\
&\neq 0,
\end{aligned}$$

provided that $\mu_1(\alpha_1{}^*)\mu_2{}'(\alpha_1{}^*) - \mu_3{}'(\alpha_1{}^*) + \mu_1{}'(\alpha_1{}^*)\mu_2(\alpha_1{}^*) \neq 0$ and $\mu_2(\alpha_1{}^*) + \mu_1{}^2(\alpha_1{}^*) \neq 0$. Therefore, the transversality condition is satisfied and Hopf bifurcation occur at $\alpha_1 = \alpha_1{}^*$. $\qquad\square$

6.5   Spatial structure

To better visualize the carbon-phytoplankton-zooplankton model, we incorporate the spatial effect of our temporal CPZ system (6.4) through reaction-diffusion equations. We consider the reaction-diffusion system is bounded in

a domain $\Omega \subset \mathbb{R}^3$ with boundary $\partial\Omega$. Let $C(x, y, t)$, $P(x, y, t)$ and $Z(x, y, t)$ denotes carbon, phytoplankton and zooplankton densities, respectively, at time t and at spatial location $(x, y) \in \Omega$. Thus, the spatiotemporal model for carbon, phytoplankton and zooplankton is given by the following reaction-diffusion equations:

$$
\begin{aligned}
\frac{\partial C}{\partial t} &= C_0 + r_1 P + r_2 Z - \frac{\alpha_1 C}{K_1 + C}(\alpha P - \beta P^2) - \delta_1 C + d_C\left(\frac{\partial^2 C}{\partial x^2} + \frac{\partial^2 C}{\partial y^2}\right), \\
\frac{\partial P}{\partial t} &= \frac{\theta_1 \alpha_1 C}{K_1 + C}(\alpha P - \beta P^2) - \frac{\alpha_2 P Z}{K_2 + P} - \delta_2 P + d_P\left(\frac{\partial^2 P}{\partial x^2} + \frac{\partial^2 P}{\partial y^2}\right), \\
\frac{\partial Z}{\partial t} &= \frac{\theta_2 \alpha_2 P Z}{K_2 + P} - \delta_3 Z + d_Z\left(\frac{\partial^2 Z}{\partial x^2} + \frac{\partial^2 Z}{\partial y^2}\right),
\end{aligned}
\tag{6.9}
$$

where d_C, d_P and d_Z are the diffusion coefficients for carbon, phytoplankton and zooplankton, respectively. The system (6.9) is satisfied subject to non-negative initial conditions: $C(x, y, 0) \equiv C_0(x, y) \geq 0$, $P(x, y, 0) \equiv P_0(x, y) \geq 0$ and $Z(x, y, 0) \equiv Z_0(x, y) \geq 0$ for all $(x, y) \in \Omega$ with zero-flux boundary conditions $\frac{\partial C}{\partial \hat{n}} = \frac{\partial P}{\partial \hat{n}} = \frac{\partial Z}{\partial \hat{n}} = 0$, where $\hat{n}$ is the outward drawn unit normal vector on the boundary $\partial\Omega$.

6.5.1 Stability analysis of the spatial system

To study the stability of the spatial system (6.9), we consider small perturbations $c \equiv c(x, y, t)$, $p \equiv p(x, y, t)$ and $z \equiv z(x, y, t)$ of C, P and Z, respectively. Then, we linearized the system (6.9) about the co-existing equilibrium $E^*(\tilde{C}, \tilde{P}, \tilde{Z})$ by setting $C = \tilde{C} + c$, $P = \tilde{P} + p$ and $Z = \tilde{Z} + z$ and neglecting the second and higher order terms. We obtain the following linearized system of equations:

$$
\begin{aligned}
\frac{\partial c(x, y, t)}{\partial t} &= J_{11}c + J_{12}p + J_{13}z + d_C\left(\frac{\partial^2 c}{\partial x^2} + \frac{\partial^2 c}{\partial y^2}\right), \\
\frac{\partial p(x, y, t)}{\partial t} &= J_{12}c + J_{22}p + J_{23}z + d_P\left(\frac{\partial^2 p}{\partial x^2} + \frac{\partial^2 p}{\partial y^2}\right), \\
\frac{\partial z(x, y, t)}{\partial t} &= J_{31}c + J_{32}p + J_{33}z + d_Z\left(\frac{\partial^2 z}{\partial x^2} + \frac{\partial^2 z}{\partial y^2}\right),
\end{aligned}
\tag{6.10}
$$

where J_{ij} for $i, j = 1, 2, 3$ are defined in the proof of Theorem 6.4.3.

Let us consider the solutions of the system (6.10) is given by

$$\begin{pmatrix} c \\ p \\ z \end{pmatrix} = \begin{pmatrix} l_1 \\ l_2 \\ l_3 \end{pmatrix} e^{\lambda_k t} \cos(k_x x) \cos(k_y y),$$

where l_1, l_2 and l_3 are sufficiently small constants, λ_k represents the wave length with k_x and k_y are the components of wave number (k) along x and y directions, respectively. The Jacobian matrix of the linearized system (6.10) is given by

$$J = \begin{pmatrix} J_{11} - d_C k^2 & J_{12} & J_{13} \\ J_{21} & J_{22} - d_P k^2 & J_{23} \\ 0 & J_{32} & J_{33} - d_Z k^2 \end{pmatrix},$$

where k denotes the wave number, with $k^2 = k_x^2 + k_y^2$ and the characteristic equation of the Jacobian matrix J is given by

$$\lambda^3 + A_1 \lambda^2 + A_2 \lambda + A_3 = 0, \tag{6.11}$$

where

$$A_1 = (d_C + d_P + d_Z)k^2 + \mu_1,$$
$$A_2 = (d_C d_P + d_C d_Z + d_P d_Z)k^4$$
$$\quad - \left[d_C(J_{22} + J_{33}) + d_P(J_{11} + J_{33}) + d_Z(J_{11} + J_{22}) \right] k^2 + \mu_2,$$
$$A_3 = d_C d_P d_Z k^6 - (J_{11} d_P d_Z + J_{22} d_C d_Z + J_{33} d_C d_P)k^4$$
$$\quad + \left[d_C(J_{22}J_{33} - J_{23}J_{32}) + d_P J_{11}J_{33} + d_Z(J_{11}J_{22} - J_{12}J_{21}) \right] k^2$$
$$\quad + \mu_3,$$
$$A_1 A_2 - A_3 = B_0 + B_1 k^2 + B_2 k^4 + B_3 k^6,$$

with

$$B_0 = \mu_1 \mu_2 - \mu_3,$$
$$B_1 = \mu_2(d_C + d_P + d_Z) - \mu_1 \left\{ d_C(J_{22} + J_{33}) + d_P(J_{11} + J_{33}) + d_Z(J_{11} + J_{22}) \right\}$$
$$\quad - d_C(J_{22}J_{33} - J_{23}J_{32}) - d_P J_{11}J_{33} - d_Z(J_{11}J_{22} - J_{12}J_{21}),$$
$$B_2 = J_{11}d_P d_Z + J_{22}d_C d_Z + J_{33}d_C d_P + \mu_1(d_C d_P + d_C d_Z + d_P d_Z)$$
$$\quad - (d_C + d_P + d_Z) \left\{ d_C(J_{22} + J_{33}) + d_P(J_{11} + J_{33}) + d_Z(J_{11} + J_{22}) \right\},$$
$$B_3 = (d_C + d_P + d_Z)(d_C d_P + d_C d_Z + d_P d_Z) - d_C d_P d_Z.$$

Due to the well-known Routh-Hurwitz criterion, the spatiotemporal system (6.9) become stable if

$$A_1 > 0, \quad A_3 > 0 \text{ and } A_1 A_2 - A_3 > 0. \tag{6.12}$$

Theorem 6.5.1. *If the co-existing equilibrium point $E^*(\tilde{C}, \tilde{P}, \tilde{Z})$ become locally asymptotically stable for non-spatial system (6.4), then $E^*(\tilde{C}, \tilde{P}, \tilde{Z})$ become locally asymptotically stable for spatiotemporal system (6.9) if (6.12) holds.*

Proof. The proof of the theorem is omitted as it directly follows from the Routh-Hurwitz criterion. □

6.5.2 Turing instability

Turing instability occurs when a stable homogeneous steady-state (which is stable under small amplitude of homogeneous perturbation) becomes unstable under small amplitude of inhomogeneous perturbation. First, we analyzed the non-spatial system (6.4) and concluded that the interior equilibrium $E^*(\tilde{C}, \tilde{P}, \tilde{Z})$ is asymptotically stable if and only if $\mu_1 > 0$, $\mu_3 > 0$ and $\mu_1\mu_2 - \mu_3 > 0$. The system (6.4) become unstable due to diffusion if any of the conditions $A_1 > 0$, $A_3 > 0$ and $A_1A_2 - A_3 > 0$ fails to hold. If the real part of one of the eigenvalues of the characteristic equation (6.11) passes through zero while other two eigenvalues still have negative real parts, then the diffusion driven instability occur [54, 171, 172]. We assume that λ_1, λ_2 and λ_3 are the roots of (6.11), then we obtain the following relation between roots and coefficients of a polynomial equation as

$$
\begin{aligned}
\lambda_1 + \lambda_2 + \lambda_3 &= -A_1(k^2), \\
\lambda_1\lambda_2 + \lambda_2\lambda_3 + \lambda_3\lambda_1 &= A_2(k^2), \\
\lambda_1\lambda_2\lambda_3 &= -A_3(k^2), \\
-(\lambda_1 + \lambda_2)(\lambda_2 + \lambda_3)(\lambda_3 + \lambda_1) &= A_1(k^2)A_2(k^2) - A_3(k^2).
\end{aligned}
$$

Now at the Turing threshold $k = k_{cr}$, one of the eigenvalues of the characteristic equation (6.11) is equal to zero and real part of other two eigenvalues still remains negative and without any loss of generality, we assume that

$$
\lambda_1(k^2 = k_{cr}^2) = 0, \;\; Re\left[\lambda_2(k^2 = k_{cr}^2)\right] < 0, \;\; Re\left[\lambda_3(k^2 = k_{cr}^2)\right] < 0. \quad (6.13)
$$

Hence, $A_3(k_{cr}^2) = 0$ and considering the Turing instability conditions in (6.13), we obtain $A_1(k_{cr}^2) > 0$, $A_2(k_{cr}^2) > 0$ and $A_1(k_{cr}^2)A_2(k_{cr}^2) - A_3(k_{cr}^2) > 0$. Hence, the system remain stable if $A_3(k_{cr}^2) > 0$ holds for all real k and the system become Turing unstable if $A_3(k_{cr}^2) < 0$ for at least one k. We rewrite the expression of $A_3(k_{cr}^2)$ as follows

$$
A_3(k^2) = \varrho_1(k^2)^3 + \varrho_2(k^2)^2 + \varrho_3(k^2) + \varrho_4, \quad\quad (6.14)
$$

206

where

$$\varrho_1 = d_C d_P d_Z,$$
$$\varrho_2 = -(J_{11} d_P d_Z + J_{22} d_C d_Z + J_{33} d_C d_P),$$
$$\varrho_3 = d_C(J_{22} J_{33} - J_{23} J_{32}) + d_P J_{11} J_{33} + d_Z(J_{11} J_{22} - J_{12} J_{21}),$$
$$\varrho_4 = \mu_3 = -J_{11}(J_{22} J_{33} - J_{23} J_{32}) + J_{12} J_{21} J_{33} - J_{13} J_{21} J_{32}.$$

Here, $\varrho_1 > 0$ as the diffusion coefficients d_C, d_P and d_Z are positive and $\varrho_4 > 0$ from the condition of stability of the co-existing equilibrium point $E^*(\tilde{C}, \tilde{P}, \tilde{Z})$. The minimum value of $A_3(k^2)$ occurs at

$$k_{cr}^2 = \frac{-\varrho_2 + (\varrho_2 - 3\varrho_1\varrho_3)^{1/2}}{3\varrho_1},$$

and $\frac{dA_3}{d(k^2)} = 0$ and $\frac{d^2 A_3}{d(k^2)^2} > 0$ holds at $k = k_{cr}$. Now k_{cr}^2 is positive if $\varrho_3 < 0$ or $\varrho_2 < 0$ and $\varrho_2^2 > 3\varrho_1\varrho_3$. Hence, we obtain the Turing bifurcation boundary is as follows

$$2\varrho_2^3 - 9\varrho_1\varrho_2\varrho_3 - 2(\varrho_2^2 - 3\varrho_1\varrho_3)^{3/2} + 27\varrho_1^2\varrho_4 = 0.$$

Thus, the conditions for Turing instability are obtained.

6.6 Numerical simulation

In this section, we used extensive numerical simulations to support our previous analytical findings. The system of nonlinear ordinary differential equations (6.4) is solved by 4th order Runge-Kutta method. We used hypothetical value for the system parameters based on the existing literature due to unavailability of real data. The assumed parameters value are listed in Table 6.2. We assumed initial population size as $C(0) = 4.5$, $P(0) = 0.3$ and $Z(0) = 0.1$; and same initial population size is used for all numerical simulations.

6.6.1 Local stability of the equilibria

The time series solution and phase portrait analysis of the CPZ system (6.4) are shown in Fig. 6.5 for $\alpha_1 = 0.11$ (see sub-figures (a) and (b)) and $\alpha_1 = 0.30$ (see sub-figures (c) and (d)). For $\alpha_1 = 0.11$, we have $\mu_1 = 1.18 \times 10^{-2} > 0$, $\mu_3 = 4.01 \times 10^{-7} > 0$ and $\mu_1\mu_2 - \mu_3 = 2.88 \times 10^{-7} > 0$, which satisfied the conditions (Routh-Hurwitz criterion) for the stability of the interior equilibrium $E^*(4.7974, 0.2000, 0.0240)$. The time series solution (see Fig.

6.5(a)) and phase portrait diagram (see Fig. 6.5(b)) shows that the system (6.4) is locally asymptotically stable around the coexisting equilibrium $E^*(4.7974, 0.2000, 0.0240)$. Again, for $\alpha_1 = 0.30$, $\mu_1 = 9.30 \times 10^{-3} > 0$ and $\mu_3 = 2.25 \times 10^{-6} > 0$ but $\mu_1\mu_2 - \mu_3 = -2.25 \times 10^{-7} < 0$. Hence, the stability criterion of the coexisting equilibrium $E^*(4.1769, 0.2000, 0.1335)$ is failed. The time series (see Fig. 6.5(c)) and phase portrait (see Fig. 6.5(c)) shows periodic oscillation around the coexisting equilibrium $E^*(4.1769, 0.2000, 0.1335)$.
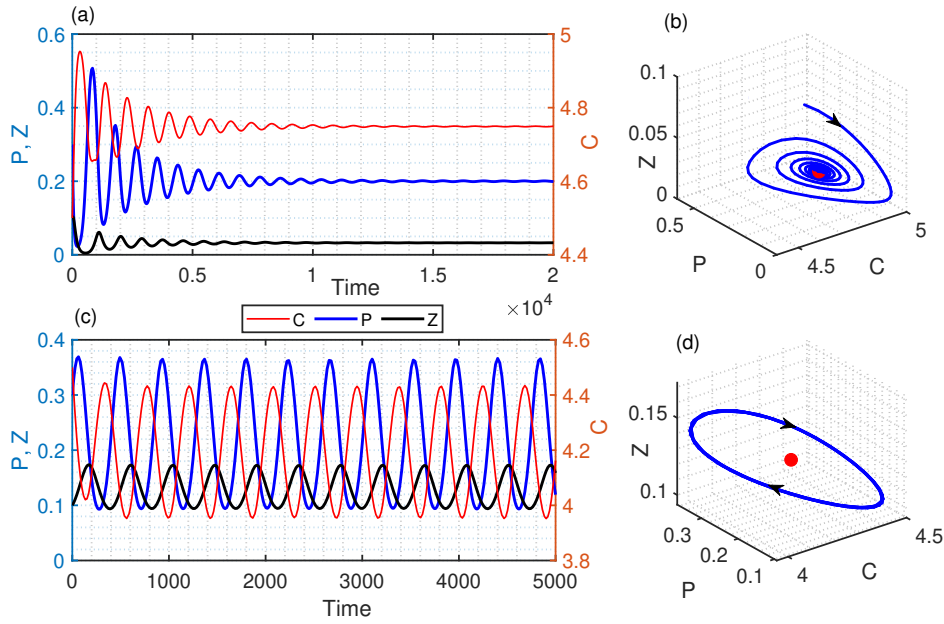

Figure 6.5: Time series evolution and phase portrait diagram of the system (6.4) for different values of α_1. The sub-figures **(a)** and **(b)** shows local asymptotic stability of (6.4) around the coexisting equilibrium $E^*(4.7974, 0.2000, 0.0240)$ (shown by solid red circle) for $\alpha_1 = 0.11$. The sub-figures **(c)** and **(d)** shows limit cycle oscillation of the system (6.4) around the coexisting equilibrium $E^*(4.1769, 0.2000, 0.1335)$ (shown by solid red circle) for $\alpha_1 = 0.30$. Other system parameters are listed in Table 6.2.

6.6.2 Numerical simulation of Hopf bifurcation

The carbon capturing coefficient (α_1) is one of the most influential system parameters as we have observed in the PRCC sensitivity analysis. If the value of α_1 is increased, then more carbon will be synthesized by phytoplankton, that is, more carbon will be removed from the environment. Thus, to understand

the dynamics of the CPZ system in response to carbon capturing coefficient become very crucial. In this section, we observed local asymptotic stability of the system (6.4) depending on the carbon capturing coefficient (α_1). The bifurcation diagram is shown in Fig. 6.6 by varying α_1 which gives an overview of how carbon, phytoplankton and zooplankton population changes and different dynamics occur with variation of α_1. The parameter α_1 varies from 0 to 2.5 and other system parameters value as listed in Table 6.2. The red curve represents the unstable steady state. The Fig. 6.6 shows that the system (6.4) remains stable for lower value of α_1 ($\alpha_1 < 0.23$). Further increased the value of α_1 results in Hopf bifurcation and the system (6.4) shows limit cycle oscillation for $\alpha_1 \in (0.23, 1.65)$. However, for higher value of α_1 ($\alpha_1 > 1.65$), the system (6.4) again becomes stable.
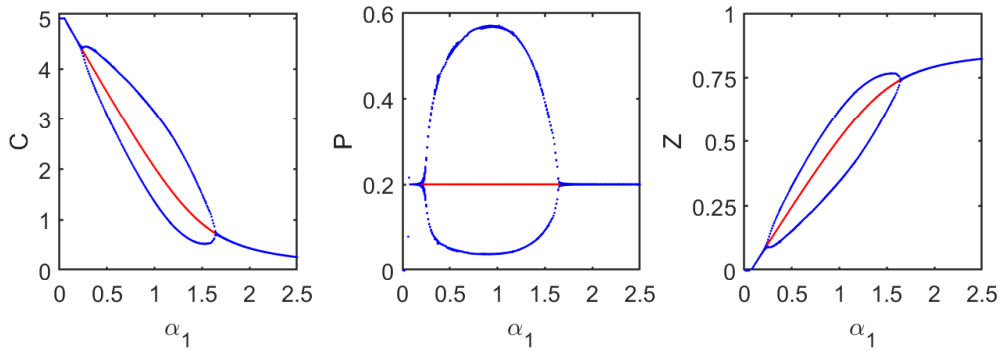

Figure 6.6: Bifurcation diagram of the system (6.4) with respect to carbon capturing coefficient (α_1). Here, α_1 varies from 0 to 2.5 and other system parameters value are listed in Table 6.2. Red curve represents the unstable steady state.

6.6.3 Pattern formation

In this section, we performed numerical simulations of the proposed diffusive CPZ system (6.9) in two-dimensional space to support our theoretical analysis. To ensure the existence of Turing instability for the reaction-diffusion system (6.9), we plot the polynomial $A_3(k^2)$ as defined in (6.14) for different values of diffusion coefficient d_Z and carbon capturing coefficient α_1. The plot of $A_3(k^2)$ is shown in Fig. 6.7 for different values of d_Z with $\alpha_1 = 0.3$ and other parameters as listed in Table 6.2. The Fig. 6.7 shows that for increasing value of d_Z, the length of the interval of k for which $A_3(k^2)$ remains negative and hence the possibility for existence of Turing instability. Again the plot of $A_3(k^2)$ is also shown in Fig. 6.8 for different values of d_Z

with $\alpha_1 = 0.6$ and other parameters as listed in Table 6.2. The Fig. 6.8 shows that for increasing value of d_Z, the length of the interval of k for which $A_3(k^2)$ remains negative increases and hence the possibility for existence of the Turing instability.
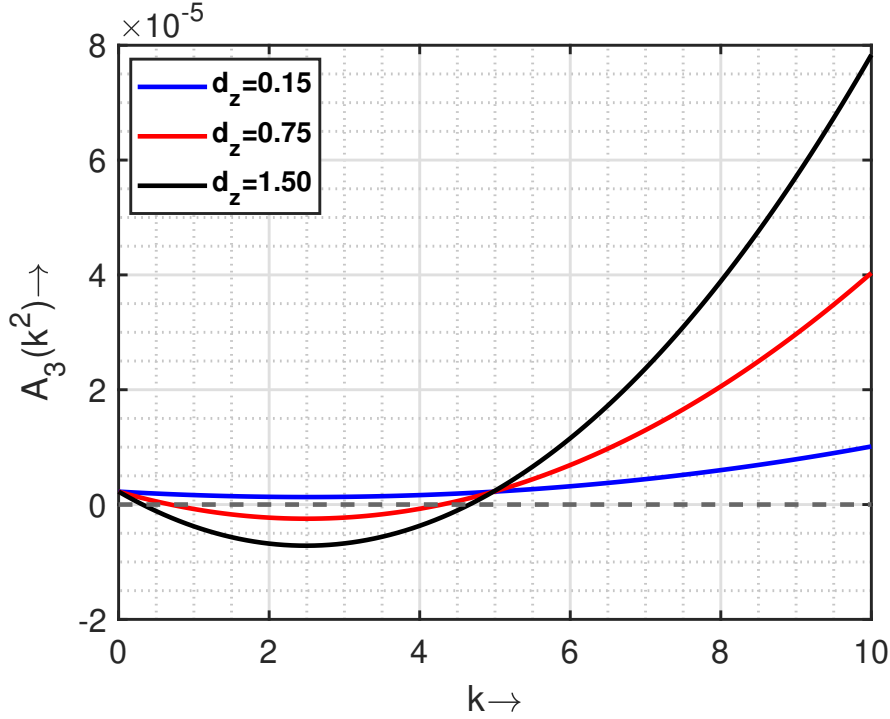

Figure 6.7: Plot of $A_3(k^2)$ for different values of d_Z with $\alpha_1 = 0.3$, $d_C = 0.00005$, $d_Z = 0.0001$ and other system parameters as listed in Table 6.2.

All our numerical simulations of the system (6.9) are performed with zero-flux boundary condition in the 200×200 spatial domain with $\triangle x = \triangle y = 1$. To generate the pattern formation, we used the following initial conditions $C_{i,j}^0 = \tilde{C} + 0.01\Theta_{i,j}$, $P_{i,j}^0 = \tilde{P} + 0.01\Phi_{i,j}$ and $Z_{i,j}^0 = \tilde{Z} + 0.01\Upsilon_{i,j}$, where $\Theta_{i,j}$, $\Phi_{i,j}$ and $\Upsilon_{i,j}$ are the Gaussian white noise $\delta-$correlated in space. Forward Euler integration is used for the numerical illustrations of the diffusive system (6.9) with $\triangle x = \triangle y = 1$, $\triangle t = 1/100$ and standard five-point approximation for the two dimensional Laplacian system. The iteration formula for the $(n+1)$-th time step at the mesh position (x_i, y_j) are as follows:

$$
\begin{aligned}
C_{i,j}^{n+1} &= C_{i,j}^n + \triangle t\, d_C\, \triangle_h C_{i,j}^n + \triangle t\, f_1(C_{i,j}^n, P_{i,j}^n, Z_{i,j}^n), \\
P_{i,j}^{n+1} &= P_{i,j}^n + \triangle t\, d_P\, \triangle_h P_{i,j}^n + \triangle t\, f_2(C_{i,j}^n, P_{i,j}^n, Z_{i,j}^n), \\
Z_{i,j}^{n+1} &= Z_{i,j}^n + \triangle t\, d_Z\, \triangle_h Z_{i,j}^n + \triangle t\, f_3(C_{i,j}^n, P_{i,j}^n, Z_{i,j}^n),
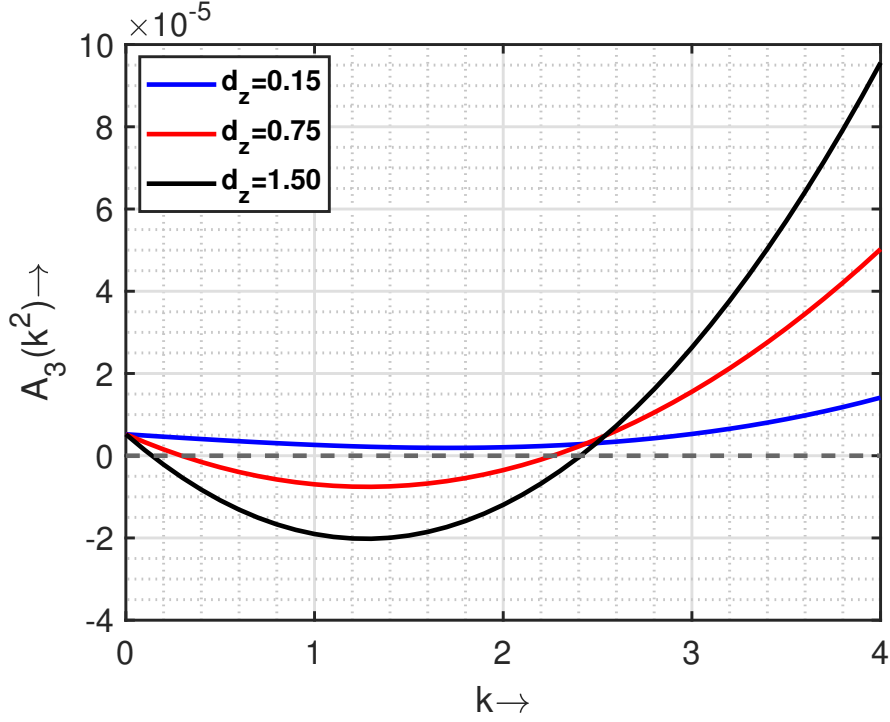\end{aligned}
$$

Figure 6.8: Plot of $A_3(k^2)$ for different values of d_Z with $\alpha_1 = 0.6$, $d_C = 0.002$, $d_Z = 0.001$ and other system parameters as listed in Table 6.2.

with the Laplacian defined by

$$
\triangle_h C_{i,j}^n = \frac{C_{i+1,j}^n + C_{i-1,j}^n + C_{i,j+1}^n + C_{i,j-1}^n - 4C_{i,j}^n}{h^2},
$$

$$
\triangle_h P_{i,j}^n = \frac{P_{i+1,j}^n + P_{i-1,j}^n + P_{i,j+1}^n + P_{i,j-1}^n - 4P_{i,j}^n}{h^2},
$$

$$
\triangle_h Z_{i,j}^n = \frac{Z_{i+1,j}^n + Z_{i-1,j}^n + Z_{i,j+1}^n + Z_{i,j-1}^n - 4Z_{i,j}^n}{h^2},
$$

where the space step size is given by $h = \triangle x = \triangle y = 1$.

Fig. 6.9 shows the time evolution of pattern formation for carbon (first column), phytoplankton (second column) and zooplankton (third column) distribution over two dimensional spatial domain with $\alpha_1 = 0.3$, $d_C = 0.00005$, $d_P = 0.0001$, $d_Z = 1.5$ and other system parameters as listed in Table 6.2.

Fig. 6.10 shows the time evolution of pattern formation for carbon (first column), phytoplankton (second column) and zooplankton (third column) distribution over two dimensional spatial domain with $\alpha_1 = 0.6$, $d_C = 0.002$, $d_P = 0.001$, $d_Z = 1.5$ and other system parameters as listed in Table 6.2.
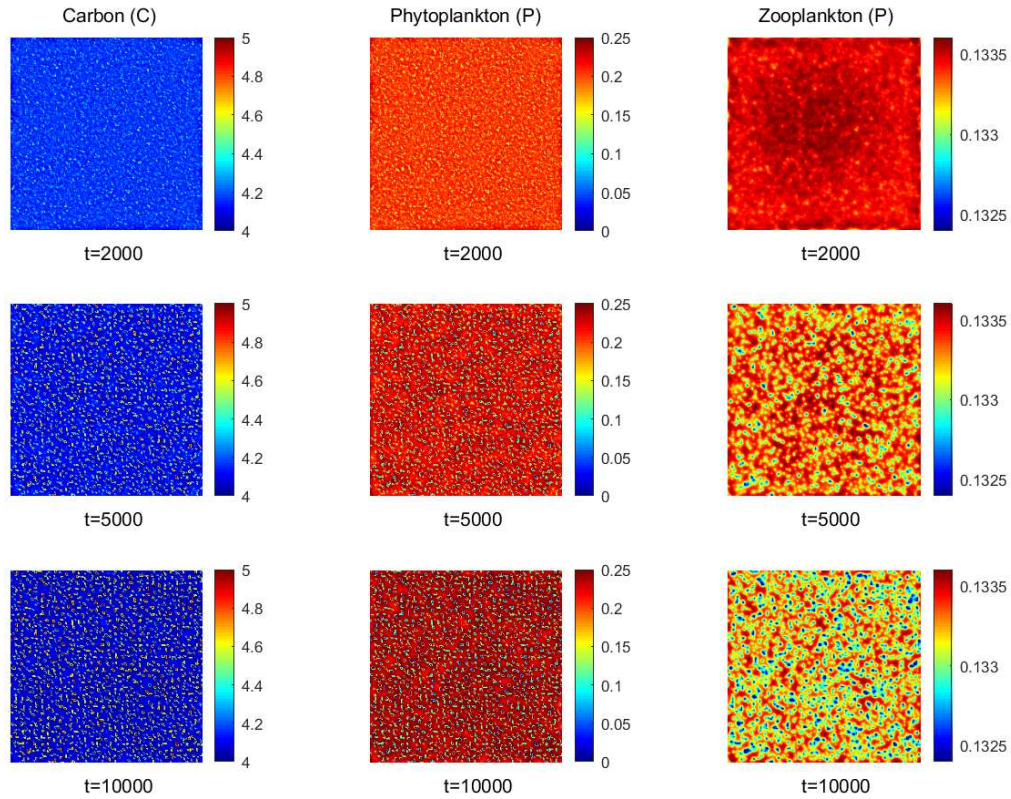
Figure 6.9: Spatial distribution of the densities of carbon (first column), phytoplankton (second column) and zooplankton (third column) densities at different time steps with $\alpha_1 = 0.3$, $d_C = 0.00005$, $d_P = 0.0001$, $d_Z = 1.5$ and other parameters are listed in Table 6.2.

6.6.4 Effect of the global warming in the CPZ system

In the introduction section, we have discussed that due to anthropogenic activities, CO_2 and other green house gases produced extensively, which causing change of the climate. In our model (6.2), the emission rate of carbon from atmosphere to ocean is estimated by the parameter C_0. In order to implement the effect of global warming in the CPZ system (6.4), we consider the parameter C_0 as a function of CO_2. Consequently, the carbon is a function of time; therefore C_0 becomes a function of time too. Hence, we assume $C_0 = C_0(t)$ and other system parameters are fixed for simplicity. As the level of carbon increased in ocean water, pH of ocean water decreases, which resulting in reduction of phytoplankton biomass [173]. For the sake of simplicity of the mathematical model, we have not considered the effect of water pH in our proposed model. The interaction of carbon with phyto-
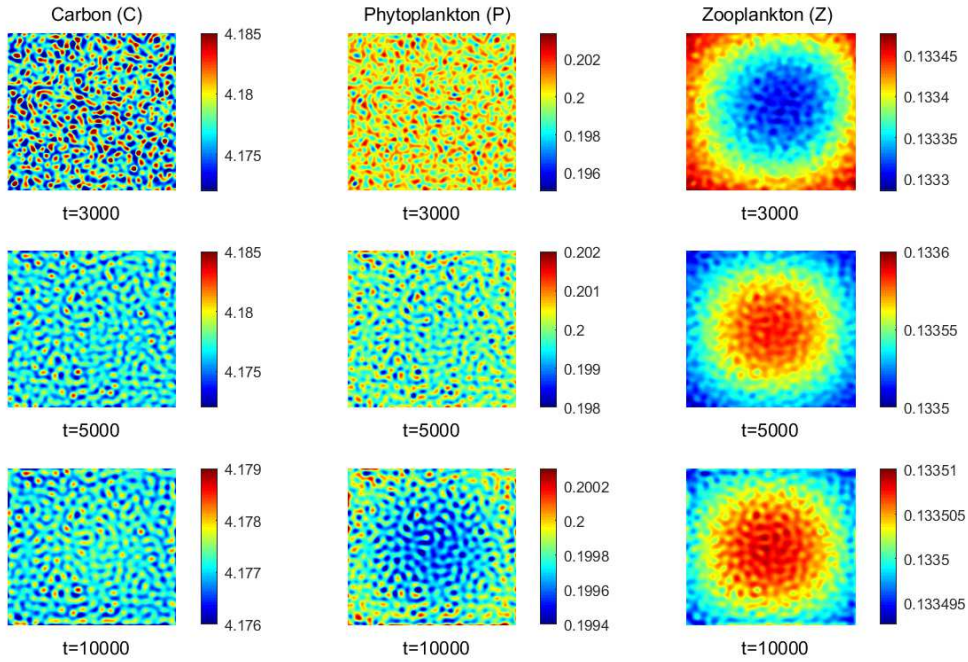
Figure 6.10: Spatial distribution of the densities of carbon (first column), phytoplankton (second column) and zooplankton (third column) densities at different time steps with $\alpha_1 = 0.6$, $d_C = 0.002$, $d_P = 0.001$, $d_Z = 1.5$ and other parameters are listed in Table 6.2.

plankton is very complicated by considering all the environmental factors. Thus the functional form of $C_0(t)$ will be very complicated. The main aim of this study is to understand the effect of global warming conceptually. Hence, we consider the simplest linear functional form of $C_0(t)$ and we define $C_0(t)$ as follows:

$$C_0(t) = \begin{cases} C_0^{cr} & \text{if } t < t_0, \\ C_0^{cr} + \omega(t - t_0) & \text{if } t \geq t_0. \end{cases} \qquad (6.15)$$

Here t_0 is the time when global warming started, C_0^{cr} is the emission rate of the carbon from atmosphere to ocean before the global warming and the rate of global warming quantified by the term ω. After assuming the expression of $C_0(t)$ as defined in (6.15), the CPZ system (6.4) become non-autonomous. Due to lack of experimental data, we assume hypothetical value of the system parameters to quantify the effect of global warming in the proposed CPZ system (6.4). As the global warming is very slow process, we assume a very small value of ω, that is, $\omega \ll \min\{r_1, r_2, \alpha_1, \alpha_2, \delta_1, \delta_2, \delta_3, \theta_1, \theta_2, C_0, \alpha, \beta, K_1, K_2\}$. Before the global warming, we assumed that the ecosystem in the ocean was in a state that the coexisting equilibrium E_3 is either locally asymptotically

213

stable or unstable surrounded by a stable limit cycle oscillation. Hence, we choose $C_0^{cr} = 0.05$ and the value of α_1 as 0.11 and 0.30 for locally asymptotically stable and limit cycle oscillation, respectively.

We assume $C_0^{cr} = 0.05$, $\alpha_1 = 0.11$ and for different values of ω, we numerically solved the CPZ system (6.4) with C_0 as defined in (6.15) and the numerical simulation is displayed in Fig. 6.11. The CPZ system (6.4) is locally asymptotically stable and the system does not remain locally asymptotically stable after introducing the effect of global warming as the density of carbon is increasing with time. Again, we assumed $C_0^{cr} = 0.05$ and $\alpha_1 = 0.3$, then the system (6.4) shows stable limit cycle oscillation around the coexisting equilibrium $E^*(4.1769, 0.2000, 0.1335)$ but after introduction of the effect of global warming the system oscillates with semi-stable limit cycle (see Fig. 6.12). We have shown the global atmospheric carbon dioxide and oceanic pCO_2 in Fig. 6.12(d). Increase in oceanic CO_2 over the past 30 years is consistent with the atmospheric CO_2 increase. We observed similar type of oscillation of carbon in our model simulation after introducing the effect of global warming. The phytoplankton and zooplankton density is replotted for the time interval 18000 to 20000 in Fig. 6.12(e) and Fig. 6.12(f), respectively. Shift in oscillations (or phase difference) of phytoplankton and zooplankton density are observed after introduction of the effect of global warming in the system (6.4). Experimental studies were also observed the shift in oscillations (that is, shifts in seasonal dynamics) of the density of phytoplankton [174–176]. Due to the effect of global warming spring bloom of phytoplankton occured 1 to 1.5 days earlier in response to per degree of temperature increase [175, 176]. No significant difference in duration of bloom was observed. Response of global warming in zooplankton was more strong, some species of zooplankton hatched up to 9 days earlier per degree of temperature increased [175, 176]. Thus, our mathematical model nicely captured the shifts in oscillation of phytoplankton and zooplankton density. Also, we have shown the plot of phase difference vs ω in Fig. 6.12(g). The phase difference rises as the effect of global warming increases but eventually levels off at a plateau (or asymptote) at which the phase difference remains almost constant regardless of increases in the effect of global warming. We also observe 4.4% increase of amplitude in phytoplankton density and 6.2% increase of amplitude in zooplankton density after introducing the effect of global warming though we have not considered the factors limiting net production such as sea water acidification, light, temperature etc.
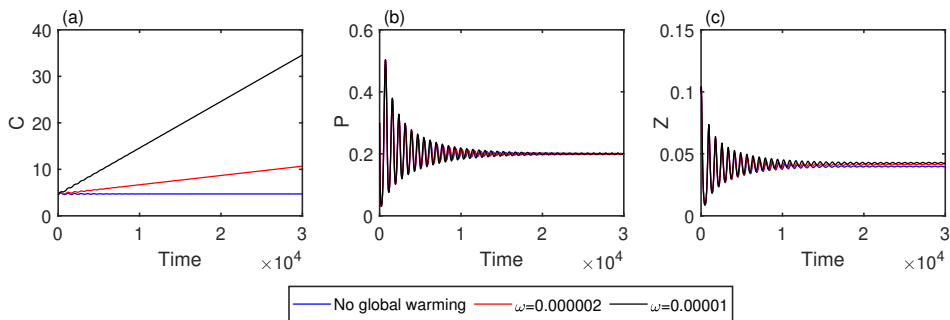
Figure 6.11: Time series evolution of the system (6.4) for different values of ω with $C_0 = 0.05$, $\alpha_1 = 0.11$ and other system parameters are listed in Table 6.2.

6.7 Discussion and concluding remarks

Understanding the effect of global warming is an important issue nowadays. The effect of global warming on the interactive dynamics of phytoplankton and zooplankton in marine environment [177, 178]. However, more research is needed to get a better understanding about the worst danger due to global warming. The increase in water temperature can disrupt phytoplankton's photosynthesis, which affects the total oxygen and carbon budgets in the ocean [149, 167].

In this chapter, we proposed and analyzed a carbon-phytoplankton-zooplankton system in a marine environment by introducing the effect of global warming. Our model takes into account the effect of carbon fixation by phytoplankton during photosynthesis, zooplankton predation on phytoplankton, respiration of phytoplankton and zooplankton (see Fig. 6.1). The mathematical model is described by a system of coupled ordinary differential equations in the non-spatial and reaction-diffusion partial differential equations in the spatial extension of the system. We investigate the qualitative properties of the non-spatial CPZ system (6.4), including boundedness and positivity of the solutions. Theoretically, we obtained three biologically feasible equilibrium points, namely, phytoplankton and zooplankton-free equilibrium point, zooplankton-free equilibrium point and coexisting equilibrium point. We investigated the local asymptotic stability of the equilibrium points and considering the Routh-Hurwitz criterion for stability. To better visualize the system dynamics, we have plotted the stability region in $\alpha_1 - \theta_1$ and $\alpha_1 - C_0$ parameter space.

We gradually increased the value of the carbon capturing coefficient α_1 to observe the effect of carbon capture by the phytoplankton in the CPZ
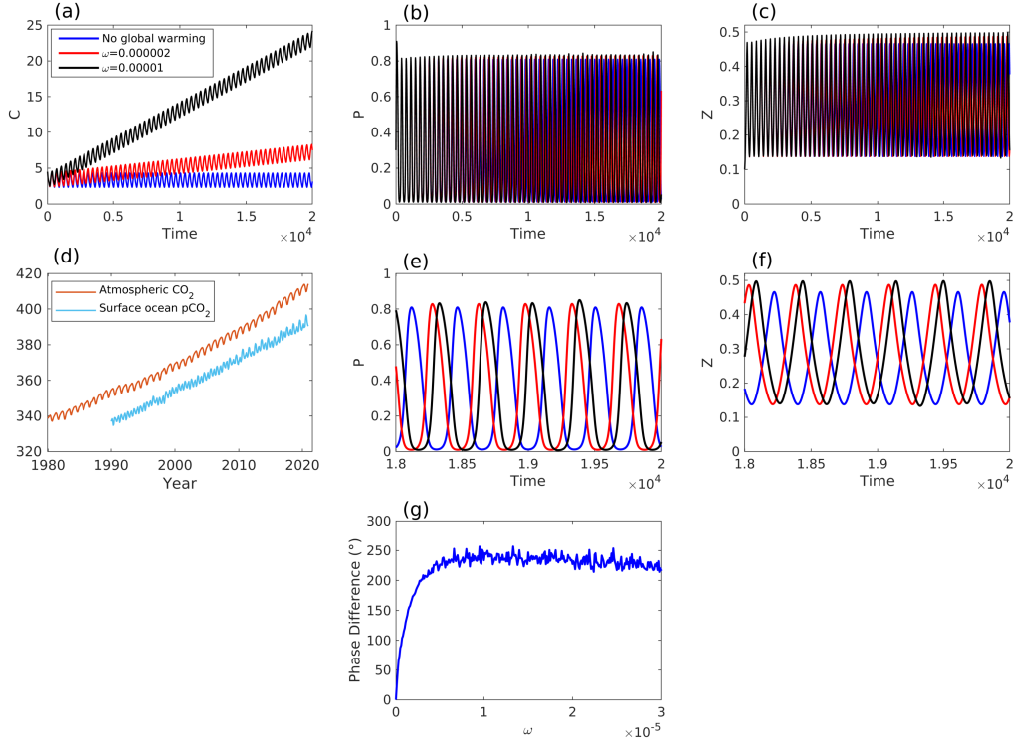
Figure 6.12: Time series evolution of the system (6.4) for different values of ω with $C_0 = 0.05$, $\alpha_1 = 0.3$ and other system parameters are listed in Table 6.2. Time series of phytoplankton and zooplankton are replotted for $t = 18000$ to $t = 20000$ in (e) and (f), respectively. Shifts in oscillations of phytoplankton and zooplankton are observed after the introduction of the effect of global warming. Time series of globally averaged monthly mean atmospheric CO_2 (in parts per million) and globally averaged monthly mean of surface ocean pCO_2 (in μatm) is shown in (d). The atmospheric CO_2 data obtained from NOAA global monitoring laboratory [179] and the pCO_2 obtained from JMA Ocean CO_2 map product [180].

system (6.4). We found that the CPZ system (6.4) remains stable for lower values for $\alpha_1(< 0.23)$ and the CPZ system (6.4) shows limit cycle oscillation around the coexisting equilibrium for further increase in the value of α_1 ($0.23 < \alpha_1 < 1.65$). Again, the CPZ system (6.4) become stable for higher values of $\alpha_1(> 1.65)$ but then the magnitude of carbon become lower though magnitude of phytoplankton remains same but magnitude of zooplankton increases. Thus, the level of carbon can be reduced by increasing phytoplankton carbon capturing coefficient (α_1). In a marine ecosystem, the

carbon capturing coefficient can be increased by providing nutrients for phytoplankton. Iron is one of the most important nutrients for phytoplankton in carbon fixation. The European Iron Fertilization Experiment (EIFEX) was carried out from 11 February 2004 to 20 March 2004 in the Southern ocean and observed that iron addition generates phytoplankton bloom [177].

Our study also focused on the pattern formation in the CPZ system as it is well known from previous studies that pattern formation can enhance a system's sustainability [58]. The spatial extension of the CPZ system (6.9) exhibits complicated spatiotemporal dynamics resulting in transient patchy pattern formation. Plankton patchiness commonly observed in marine ecosystem and the reaction-diffusion system for plankton dynamics describes this phenomenon [150]. We have studied the stability of the reaction-diffusion system (6.9) by considering small perturbation about the coexisting equilibrium. The population density plots are shown in Fig. 6.9 and Fig. 6.10, which shows complex spatial patterns.

In this study, we aimed to understand the implication of global warming in plankton dynamics by using mathematical modeling as it has been used as a powerful tool. We have considered the effect of global warming in the CPZ system (6.4) and our CPZ model simulation shows shifts in plankton seasonal dynamics, which was experimentally observed by Sommer et al. [175] and Lewandowska et al. [176]. Our research appears to leave many unanswered questions. Arguably, the main question is whether an increase in amplitude of phytoplankton and zooplankton oscillation can happen in reality as the carbon concentration increases due to global warming. According to some studies, as carbon levels increased, the pH of the water decreased, resulting in low phytoplankton biomass production [173]. Hence, more research needs to be carried out considering the effect of pH in the CPZ system.

In summary, we conclude that increase in carbon capturing by phytoplankton lowers the density of carbon in the marine ecosystem. Global warming is causing changes in plankton seasonal dynamics. We conducted our research using hypothetical data because data for all system parameters is limited. This research will benefit the researcher who is conducting an observational/experimental study. In our future study, we can investigate environmental factors such as temperature, light, pH, in the plankton dynamics.

Chapter 7

Conclusion and future directions

7.1 Conclusion

In this thesis, we studied predator-prey system and introduced the effect of fear on prey due to the presence of predators. The effect of fear is also incorporated in an eco-epidemiological system as the infected prey become more vulnerable to predators. A delayed eco-epidemiological system also studied in this thesis as the infection in a population is not an instantaneous process and followed by some time lag(s). We have also investigated the influence of global warming in a carbon-phytoplankton-zooplankton system. Then, we extended our study from time domain to space and investigated Turing and non-Turing pattern formation for the proposed predator-prey system. The summary of the results are given sequentially.

� In this thesis, we have developed a mathematical model for predator-prey dynamics using nonlinear ordinary differential equations. We investigated the role of three different types of functional responses, namely Beddington-DeAngelis, Holling type-I and Holling type-II, on the dynamics of predator-prey system. Positivity, boundedness and uniform persistence of the system is established. We investigate the biologically feasible equilibrium points and their stability analysis. The dynamical behavior of the system remains unaltered for different type of functional responses but the position of the bifurcation points altered.

✥ We proposed a fear function and incorporated the effect of fear in the predator-prey system with Holling type-II response function. We inves-

tigated biologically feasible equilibrium points and their stability. The predator-prey system undergoes Hopf bifurcation with respect to prey growth rate and death rate of predator. Strong anti-predator responses can stabilize the predator-prey system by ignoring the existence of periodic behavior.

✤ Next, we considered an eco-epidemiological system with disease in prey and incorporated the effect of fear on prey population due to the presence of predator population. Due to the fear effect, the prey population become more vigilant and moves away from suspected predators. Such foraging activity of prey, decreases the contact of susceptible prey with infected prey and therefore reduces the chance of infection among susceptible prey. Effect of fear on infected prey is not considered as they are more vigilant. Analytically, we established the positivity of solutions, boundedness of the model system, local stability analysis of the biologically feasible equilibrium points. The system shows Hopf bifurcation with respect to the level of fear. As the level of fear increases, the system moves toward the steady state from limit cycle oscillation. The disease can not be wiped out from the system by increasing the level of fear, but amplitude of the infected prey decreases as the level of fear increases.

✤ Uninfected prey population become infected after infection of the disease, but this is not an instantaneous process. There is a time lag after infection to become infected population. Thus, we have incorporated the effect of time delay in the eco-epidemiological system with disease in prey and weak Allee effect in predator population. The PRCC sensitivity analysis is conducted to identify most sensitive system parameters. Positivity, boundedness of solutions of the delayed eco-epidemiological system are established. Local stability of equilibrium points and the conditions for Hopf bifurcation are established. The delayed eco-epidemiological system shows chaotic behavior with respect to the time delay parameter and disease transmission rate.

✤ Next, we have proposed a modified and more realistic fear function and incorporated this fear function in a predator-prey system. We performed theoretical analysis of the model including positivity and boundedness of solutions, existence of critical points and their local stability analysis, existence of transcritical and Hopf bifurcation. The predator-prey system shows Hopf bifurcation with respect to prey growth rate and level of fear. The transcritical bifurcation is analyzed by varying the growth rate of the prey population. In the spatially

extended system, mutual interaction of population create various spatiotemporal patterns in population distribution. Spatiotemporal pattern formation becomes slower as the level of fear becomes higher.

✳ Concentration of carbon dioxide in atmosphere is rapidly increasing after industrial revolution around the year 1750. Anthropogenic activity such as burning fossils fuel causing emission of greenhouse gases, among which carbon dioxide is a component. Deforestation is one of the major factor increasing carbon dioxide concentration in the atmosphere. Carbon dioxide is continuously exchanging among the earth's atmosphere, ocean and land surface. In the process of ocean "biological pump," inorganic carbon is fixed into organic carbon by phytoplankton via photosynthesis and a portion of organic carbon transported into the deep ocean. Thus, studying a carbon-phytoplankton-zooplankton system become very important and our study describes the dynamics of mutual interaction of carbon, phytoplankton and zooplankton. Our mathematical model simulation shows shifts in plankton seasonal dynamics, which was experimentally observed by Sommer & Lengfellner [175] and Lewandowska & Sommer [176]. In the spatially extended system, mutual interaction of carbon-phytoplankton-zooplankton create various spatiotemporal patterns in their distribution.

7.2   Future directions

Our future study will focus on, but not limited to, the following topics:

✳ The effect of stochasticity can be employed to better understand the existence and extinction of the predator-prey system.

✳ More comprehensive study of the predator-prey system introducing the effect of global warming and validating the analytical results with observed data.

✳ The effect of fear on zooplankton in a carbon-phytoplankton-zooplankton system.

✳ Geometric approach can be used for global asymptotic stability (higher dimensional Bendixson criterion). This might be quite challenging due to complexity of higher order matrices in ecological models.

Publications from the content of the Thesis

Published:

1. **Kankan Sarkar**, Subhas Khajanchi, Prakash Chandra Mali and J.J. Nieto (2020): **Rich Dynamics of a Predator-Prey System with Different Kinds of Functional Responses**, Complexity, 2020, `https://doi.org/10.1155/2020/4285294`

2. **Kankan Sarkar** and Subhas Khajanchi (2020): **Impact of fear effect on the growth of prey in a predator-prey interaction model**, Ecological Complexity, 42:100826, `https://doi.org/10.1016/j.ecocom.2020.100826`

3. **Kankan Sarkar**, Subhas Khajanchi (2022): **An eco-epidemiological model with the impact of fear**, Chaos, 32:083126, `https://doi.org/10.1063/5.0099584`

4. **Kankan Sarkar**, Subhas Khajanchi, Prakash Chandra Mali (2022): **A delayed eco-epidemiological model with weak Allee effect and disease in prey**, International Journal of Bifurcation and Chaos, 32(8):2250122, `https://doi.org/10.1142/S021812742250122X`

Communicated:

1. **Kankan Sarkar**, Subhas Khajanchi: **Spatiotemporal dynamics of a predator-prey system with fear effect** (Communicated)

2. **Kankan Sarkar**, Subhas Khajanchi, Prakash Chandra Mali: **Mathematical modeling of carbon-phytoplankton-zooplankton dynamics and the influence of global warming** (Communicated)

Bibliography

[1] Berryman, A.A., 1992. The origins and evolution of predator–prey theory. Ecology 73(5), 1530–1535.

[2] Creel, S., Christianson, D., 2008. Relationships between direct predation and risk effects. Trends. Ecol. Evolut. 23, 194–201.

[3] Lima, S., Dill, L.M., 1990. Behavioral decisions made under the risk of predation: A review and prospectus. Can. J. Zool. 68, 619–640.

[4] Cresswell, W., 2011. Predation in bird populations. J. Ornithol. 152(1), 251–263.

[5] Preisser, E.L., Bolnick, D.I., 2008. The many faces of fear: comparing the pathways and impacts of non-consumptive predator effects on prey populations. PLoS One 3(6), e2465.

[6] Creel, S., Christianson, D., Liley, S., Winnie, J.A., 2007. Predation risk affects reproductive physiology and demography of Elk. Science 315(5814), 960.

[7] Zanette, L.Y., White, A.F., Allen, M.C., Clinchy, M., 2011. Perceived predation risk reduces the number of offspring songbirds produce per year. Science 334(6061), 1398-1401.

[8] Eggers, S., Griesser, M., Nystrand, M., Ekman, J., 2006. Predation risk induces changes in nest-site selection and clutch size in the Siberian jay. Proc R Soc B Biol Sci. 273(1587), 701–706.

[9] Ghalambor, C.K., Peluc, S.I., Martin, T.E., 2013. Plasticity of parental care under the risk of predation: how much should parents reduce care?. Biol. Lett. 9(4), 20130154.

[10] Hua, F., Sieving, K.E., Fletcher, R.J., Wright, C.A., 2014. Increased perception of predation risk to adults and offspring alters avian reproductive strategy and performance. Behav Ecol. 25(3), 509–519.

[11] Fontaine, J.J., Martin, T.E., 2006. Parent birds assess nest predation risk and adjust their reproductive strategies. Ecol. Lett. 9(4), 428–434.

[12] Sheriff, M.J., Krebs, C.J., Boonstra, R., 2009. The sensitive hare: sublethal effects of predator stress on reproduction in snowshoe hares. J. Anim. Ecol. 78(6), 1249–1258.

[13] Wirsing, A.J., Ripple, W.J., 2011. A comparison of shark and wolf research reveals similar behavioural responses by prey. Front. Ecol. Environ. 9(6), 335–341.

[14] Elliott, K.H., Betini, G.S., Norris, D.R., 2017. Fear creates an Allee effect: experimental evidence from seasonal populations. Proc. R. Soc. Lond. B 284, 20170878.

[15] Anderson, R.M., May, R.M., 1986. The invasion, persistence, and spread of infectious diseases within animal and plant communities. Philos. Trans. R. Soc. Lond. B 314, 533–570.

[16] Bairagi, N., Roy, P.K., Chattopadhyay, J., 2007. Role of infection on the stability of a predator–prey system with several response functions—A comparative study. J. Theor. Biol. 248, 10–25.

[17] Bairagi, N., Adak, D., 2015. Complex dynamics of a predator–prey–parasite system: An interplay among infection rate, predator's reproductive gain and preference. Ecol. Complex. 22, 1–22.

[18] Chattopadhyay, J., Arino, O., 1999. A predator-prey model with disease in the prey. Nonlinear Anal. Theory Methods Appl. 36, 747–766.

[19] Venturino, E., 2002. Epidemics in predator-prey models: disease in the predators. IMA J. Math. Appl. Med. Biol. 19, 185–205.

[20] Freedman, H.I., 1990. A model of predator–prey dynamics as modified by the action of parasite. Math. Biosci. 99, 143–155.

[21] Area, I., Fernández, F.J., Nieto, J.J., Tojo, F.A.F., 2022. Concept and solution of digital twin based on a Stieltjes differential equation. Math Meth Appl Sci. 45, 7451–7465.

[22] Lafferty, K.D., Morris, A.K., 1996. Altered behaviour of parasitized killifish increases susceptibility to predation by bird final hosts. Ecology 77, 1390–1397.

[23] McCallum, H., Gerber, L., Jani, A., 2005. Does infectious diseases influence the efficacy of marine protected areas? A theoretical framework. J. Appl. Ecol. 42, 688–698.

[24] Hudson, P.J., Newborn, D., Dobson, A.P., 1992. Regulation and stability of a free-leaving host–parasite system, Trichostrongylus tenuis in red grouse. I. Monitoring and parasite reduction experiment. J. Anim. Ecol. 61, 477–486.

[25] Hudson, P.J., Dobson, A.P., Newborn, D., 1998. Prevention of population cycles by parasite removal. Science 282, 2256–2258.

[26] Jones, G.A., Sievingy, K.E., Averyz, M.L., Meagher, R.L., 2005. Parasitized and nonparasitized prey selectivity by an insectivorous bird. Crop. Prot. 24, 185–189.

[27] Meyling, N.V., Pell, J.K., 2006. Detection and avoidance of an entomopathogenic fungus by a generalist insect predator. Ecol. Entomol. 31, 162–171.

[28] Brown, J.S., Laundre, J.W., Gurung, M., 1999. The ecology of fear: optimal foraging, game theory, and trophic interactions. J. Mammal. 80, 385–399.

[29] Sha, A., Samanta, S., Martcheva, M., Chattopadhyay, J., 2019. Backward bifurcation, oscillations and chaos in an eco-epidemiological model with fear effect. J. Biol. Dyn. 13(1), 301–327.

[30] Hossain, M., Pal, N., Samanta, S., 2020. Impact of fear on an eco-epidemiological model. Chaos Solit. Fractals 134, 109718.

[31] Beretta, E., Kuang, Y., 1996. Convergence results in a well-known delayed predator-prey system. J. Math. Anal. Appl. 204, 840–853.

[32] Beretta, E., Kuang, Y., 1998. Modelling and analysis of a marine bacteriophage infection. Math. Biosci. 149, 57–76.

[33] Cushing, J.M., 1997. Periodic time-dependent predator-prey systems. SIAM J. Appl. Math. 32, 82–95.

[34] Ghosh, D., Khajanchi, S., Mangiarotti, S., Denis, F., Dana, S.K., Letellier, C., 2017. How tumor growth can be influenced by delayed interactions between cancer cells and the microenvironment?. BioSystems 158, 17–30.

[35] Khajanchi, S., Perc, M., Ghosh, D., 2018. The influence of time delay in a chaotic cancer model. Chaos 28, 103101.

[36] Khajanchi, S., Baneerjee, S., 2018. Influence of multiple delays in brain tumor and immune system interaction with T11 target structure as a potent stimulator. Math. Biosci. 302, 116–130.

[37] Khajanchi, S., 2017. Uniform persistence and global stability for a brain tumor and immune system interaction. Biophys. Rev. Lett. 12(4), 187–208.

[38] Misra, A.K., Singh, R.K., Tiwari, P.K., Khajanchi, S., Kang, Y., 2020. Dynamics of algae blooming: effects of budget allocation and time delay. Nonlinear Dyn 100, 1779–1807.

[39] Ruan, S., Wei, J., 2003. On the zeros of transcendental functions with applications to stability of delay differential equations with two delays. Dyn. Contin. Discrete Impuls. Syst. Ser. A 10, 863–874.

[40] Tang, X.H., Zou, X., 2003. Global attractivity of non-autonomous Lotka-Volterra competition system without instantaneous negative feedback. J. Differ. Equations 192(2), 502–535.

[41] Tiwari, P.K., Singh, R.K., Khajanchi, S., Kang, Y., Misra, A.K., 2021. A mathematical model to restore water quality in urban lakes using Phoslock. Discrete Continuous Dyn. Syst. Ser. B 26(6), 3143–3175.

[42] Khajanchi, S., 2015. Bifurcation analysis of a delayed mathematical model for tumor growth. Chaos Soliton. Fract. 77, 264–276.

[43] Khajanchi, S., 2020. Chaotic dynamics of a delayed tumor immune interaction model. Int. J. Biomath. 13(2), 2050009.

[44] Sardar, M., Biswas, S., Khajanchi, S., 2021. The impact of distributed time delay in a tumor-immune interaction system. Chaos Solitons Fractals 142, 110483.

[45] Sardar, M., Khajanchi, S., Biswas, S., Abdelwahab, S.F., Nisar, K.S., 2021. Exploring the dynamics of a tumor-immune interplay with time delay. Alex. Eng. J. 60(5), 4875–4888.

[46] Khajanchi, S., 2016. Bifurcations and oscillatory dynamics in a tumor immune interaction model. BIOMAT 2015: International Symposium on Mathematical and Computational Biology 241–259.

225

[47] Sasmal, S.K., Ghosh, D., 2017. Effect of dispersal in two-patch prey-predator system with positive density dependence growth of preys. BioSyst. 151, 8–20.

[48] Freedman, H.I., 1987. Deterministic mathematical models in population ecology. HIFR Consulting Ltd., Edmonton.

[49] Kuang, Y., 1993. Delay differential equation with applications in population dynamics. Academic Press, New York.

[50] Shi, X., Zhou, X., Song, X., 2010. Dynamical properties of a delay prey-predator model with disease in the prey species only. Discret. Dyn. Nat. Soc. 10, 196–204.

[51] Solomon, S., Qin, D., Manning, M., Chen, Z., Marquis, M., et al. 2007. Climate change 2007: The physical science basis: Contribution of working group I to the fourth assessment report of the intergovernmental panel on climate change. New York: Cambridge Univ. Press.

[52] Doney, S.C., Schimel, D.S., 2007. Carbon and climate system coupling on timescales from the Precambrian to the Anthropocene. Annu. Rev. Environ. Resour. 32, 31–66.

[53] Hansen, J., Sato, M., Ruedy, R., Kharecha, P., Lacis, A., Miller, R., Nazarenko, L., Lo, K., Schmidt, G.A., Russell, G., et al. 2007. Climate simulations for 1880–2003 with GISS modelE. Clim. Dyn. 29, 661–696.

[54] Turing, A.M., 1952. The chemical basis of morphogenesis. Philos. Trans. R. Soc. Lond. B 237, 37–72.

[55] Cross, M.C., Hohenberg, P.C., 1993. Pattern formation outside of equilibrium. Rev. Mod. Phys. 65, 851–1112.

[56] Murray, J.D., 1989. Mathematical biology II : Spatial Models and Biomedical Applications. Springer, Heidelberg.

[57] Khajanchi, S., Nieto, J.J., 2021. Spatiotemporal dynamics of a glioma immune interaction model. Sci. Rep. 11, 22385.

[58] Malchow, H., Petrovskii, S.V., Venturino, E., 2008. Spatiotemporal patterns in ecology and epidemiology. Chapman & Hall, U.K.

[59] Medvinsky, A., Petrovskii, S., Tikhonova, I., Malchow, H., Li, B.L., 2002. Spatiotemporal complexity of plankton and fish dynamics. SIAM Rev. 44, 311–370.

[60] Aslanidi, O.V., Clayton, R.H., Holden, A.V., Phillips, H.K., Ward, R.J., 2003. Vulnerability to reentry, and drift, stability and breakdown of spiral waves in a linear gradient of G_K in a Luo-Rudy 1 virtual ventricular tissue. Int. J. Bifurc. Chaos 13, 3865–3871.

[61] Barkley, D., 1992. Linear stability analysis of rotating spiral waves in excitable media. Phys. Rev. Lett. 68, 2090–2093.

[62] Tyson, J.J., Keener, J.P., 1988. Singular perturbation theory of traveling waves in excitable media (a review). Physica D 32, 327–361.

[63] Ghosh, S., Ray, D.S., 2015. Selecting spatio-temporal patterns by substrate injection in a reaction-diffusion system. Eur. Phys. J. B 99, 1–7.

[64] Okubo, A., Levin, S.A., 2001. Diffusion and Ecological Problems: Modern Perspectives, vol. 14 Springer, New York.

[65] Segel, L.A., Jackson, J.L., 1972. Dissipative structure: an explanation and an ecological example. J. Theor. Biol. 37(3), 545–559.

[66] Levin, S.A., Segel, L.A., 1976. Hypothesis for origin of planktonic patchiness. Nature 259, 659.

[67] Baurmann, M., 2004. Turing instabilities and pattern formation in a benthic nutrient-microorganism system. Math. Biosci. Eng. 1(1), 111–130.

[68] Banerjee, M., Banerjee, S., 2012. Turing instabilities and spatio-temporal chaos in ratio-dependent Holling-Tanner model. Math. Biosci. 236, 64–76.

[69] Banerjee, M., 2011. Spatial pattern formation in ratio-dependent model: higher-order stability analysis. Math Med Biol 28, 111–128

[70] Petrovskii, S.V., Malchow, H., 1999. A minimal model of pattern formation in a prey-predator system. Math. Comput. Model. 29, 49–63.

[71] Sherratt, J.A., Lewis, M.A., Fowler, A.C., 1995. Ecological chaos in the wake of invasion. Proc. Natl. Acad. Sci. 92, 2524–2528.

[72] Upadhyay, R.K., Volpert, V., Thakur, N.K., 2012. Propagation of Turing pattern in a plankton model. J. Biol. Dynam. 6, 524–538.

[73] Ginzburg, L.R., 1998. Assuming reproduction to be a function of consumption raises doubts about some popular predator-prey models. J Anim Ecol 67(2), 325–327.

[74] Holling, C.S., 1965. The functional response of predator to prey density and its role in mimicry and population regulation. Mem. Ent. Soc. Can. 97(S45), 5–60.

[75] Beddington, J.R., 1975. Mutual interference between parasites or predators and its effect on searching efficiency. J Anim Ecol 44, 331–340.

[76] DeAngelis, D.L., Goldstein, R.A., O'Neill, R.V., 1975. A model for trophic interaction. Ecology, 56, 881–892.

[77] Anderson, T.W., 2001. Predator responses, prey refuges and density-dependent mortality of a marine fish. Ecology 82(1), 245–257.

[78] Allee, W.C., 1931. Animal aggregations. A study in general sociology. University of Chicago Press, Chicago.

[79] Dennis, B., 1989. Allee effects: population growth, critical density, and the chance of extinction. Nat. Resour. Model. 3, 481–538.

[80] McCarthy, M.A., 1997. The Allee effect, finding mates and theoretical models. Ecol. Model. 103, 99–102.

[81] Scheuring, I., 1999. Allee effect increases the dynamical stability of populations. J. Theor. Biol. 199, 407–414.

[82] Wang, M., Kot, M., 2001. Speeds of invasion in a model with strong or weak Allee effects. Math. Biosci. 171, 83–97.

[83] Courchamp, F., Clutton-Brock, T., Grenfell, B., 1999. Inverse density dependence and the Allee effect. Trends Ecol. Evol. 14(10), 405–410.

[84] Courchamp, F., Clutton-Brock, T., Grenfell, B., 2000. Multipack dynamics and the Allee effect in the African wild dog, *Lycaon pictus*. Anim. Conserv. 3(4), 277–285.

[85] Kuussaari, M., Saccheri, I., Camara, M., Hanski, I., 1998. Allee effect and population dynamics in the Glanville fritillary butterfly. Oikos 82(2), 384–392.

[86] Groom, M., 1998. Allee effects limit population viability of an annual plant. Am. Nat. 151(6), 487–496.

[87] Elliott, K.H., Betini, G.S., Dworkin, I., Norris, D.R., 2016. Experimental evidence for within- and cross-seasonal effects of fear on survival and reproduction. J. Anim. Ecol. 85, 507–515.

[88] Wang, X., Zanette, L., Zou, X., 2016. Modelling the fear effect in predator-prey interactions. J. Math. Biol. 75(5), 1179–1204.

[89] Sardar, M., Khajanchi, S., 2021. Is the allee effect relevant to stochastic cancer model?. J. Appl. Math. Comput. 68, 2293—2315.

[90] Wang, X., Zou, X., 2017. Modeling the fear effect in predator-prey interactions with adaptive avoidance of predators. Bull. Math. Biol. 79, 13–25.

[91] Wang, J., Cai, Y., Fu, S., Wang, W., 2019. The effect of the fear factor on the dynamics of a predator-prey model incorporating the prey refuge. Chaos 29, 83109.

[92] Mondal, S., Maiti, A., Samanta, G.P., 2018. Effects of fear and additional food in a delayed predator-prey model. Biophys. Rev. Lett. 13(04), 157–177.

[93] Das, A., Samanta, G.P., 2018. Modeling the fear effect on a stochastic prey-predator system with additional food for the predator. J. Phys. A: Math. Theor. 51, 465601.

[94] Zhanga, H., Cai, Y., Fu, S., Wan, W., 2019. Impact of the fear effect in a prey-predator model incorporating a prey refuge. Appl. Math. Comput. 356, 328-337.

[95] Banerjee, S., 2014. Mathematical Modeling: Models, Analysis and Applications (1st ed.). Chapman and Hall/CRC.

[96] Murray, J.D., 2002. Mathematical Biology I. An Introduction. Springer-Verlag, New York.

[97] Gopalsamy, K., 1992. Stability and Oscillations in Delay Differential Equations of Population Dynamics. Kluwer Academic Publishers, Boston.

[98] Seo, G., Kot, M.A., 2008. Comparison of two predator-prey models with Holling type-I functional response. Math. Biosci. 212(2), 161–179.

[99] Hsu, S.B., Hwang, T.W., Kuang, Y., 2001. Global analysis of the Michaelis-Menten-type ratio-dependent predator-prey system. J. Math. Biol., 42(6), 489–506.

[100] Lv, Y., Chen, L., Chen, F., 2020. Stability and bifurcation in a single species logistic model with additive Allee effect and feedback control. Adv Differ Equ 129(2020).

[101] Khajanchi, S., 2017. Modeling the dynamic of stage-structure predator-prey system with Monod-Haldane type response function. Appl. Math. Comput. 302, 122–143.

[102] Cantrell, R.S., Cosner, C., 2001. On the dynamics of predator-prey models with the Beddington-DeAngelis functional response. J. Math. Anal. Appl. 257(1), 206–222.

[103] Chen, L., Chen, F., Chen, L., 2010. Qualitative analysis of a predator-prey model with Holling type II functional response incorporating a constant prey refuge. Nonlinear Anal. Real World Appl. 11(1), 246–252.

[104] Khajanchi, S., 2018. Modeling the dynamics of glioma-immune surveillance. Chaos Solitons Fractals 114, 108–118.

[105] Li, H., Takeuchi, Y., 2011. Dynamics of the density dependent predator-prey system with Beddington-DeAngelis functional response. J. Math. Anal. Appl. 374(2), 644–654.

[106] Khajanchi, S., 2019. Stability analysis of a mathematical model for glioma-immune interaction under optimal therapy. Int. J. Nonlinear Sci. Numer. Simul. 20(3-4), 269–285.

[107] Guckenheimer, J., Holmes, P.J., 1983. Nonlinear Oscillations, Dynamical Systems and Bifurcation of Vector Fields. Springer, New York.

[108] Gard, T., Hallam, T., 1979. Persistence in food webs-Lotka-Volterra food chains. Bull. Math. Biol. 41(6), 877–891.

[109] Kuang, Y., Freedman, H.I., 1988. Uniqueness of limit cycles in Gause-type models of predator-prey systems. Math. Biosci. 88(1), 67-84.

[110] Hassard, B.D., Kazarinoff, Y.H., Wan, Y.H., 1981. Theory and Applications of Hopf bifurcation. Cambridge University Press, Cambridge.

[111] Rosenzweig, M.L., 1971. Paradox of Enrichment: Destabilization of exploitation ecosystems in ecological time. Science 171(3969), 385–387.

[112] Gilpin, M.E., Rosenzweig, M.L., 1972. Enriched Predator-Prey Systems: Theoretical Stability. Science 177(4052), 902–904.

[113] Smith, J.A., Wang, Y., Wilmers, C.C., 2015. Top carnivores increase their kill rates on prey as a response to human-induced fear. Proc. Royal Soc. B 282, 20142711.

[114] Liu, J., Liu, B., Lv, P., Zhang, T., 2021. An eco-epidemiological model with fear effect and hunting cooperation. Chaos Solit. Fractals 142, 110494.

[115] Hamilton, W.D., Axelrod, R., Tanese, R., 1990. Sexual reproduction as an adaptation to resist parasites (a review). Proc. Natl. Acad. Sci. U.S.A. 87(9), 3566–3573.

[116] Sarkar, K., Khajanchi, S., 2020. Impact of fear effect on the growth of prey in a predator-prey interaction model. Ecol. Complex. 42, 100826.

[117] Xiao, Y., Chen, L., 2001. Modeling and analysis of a predator prey model with disease in the prey. Math. Biosci. 171, 59–82.

[118] Beaumont, R.A., Pierce, R.S., 1963. The Algebraic Foundations of Mathematics Reading MA. Addison-Wesley.

[119] Kar, T.K., Ghorai, A., Jana, S., 2012. Dynamics of pest and its predator model with disease in the pest and optimal use of pesticide. J. Theor. Biol. 310, 187–198.

[120] Hadeler, K.P., Freedman, H.I., 1989. Predator-prey populations with parasitic infection. J. Math. Biol. 27, 609–631.

[121] Stephens, P.A., Sutherland, W.J., 1999. Consequences of the Allee effect for behaviour, ecology and conservation. Trends Ecol. Evol. 14, 401–405.

[122] Hilker, F.M., Langlais, M., Petrovskii, S.V., Malchow, H., 2007. A diffusive SI model with Allee effect and application to FIV. Math. Biosci. 206, 61–80.

[123] Burrows, R., Hofer, H., East, M.L., 1995. Population dynamics, intervention and survival in African wild dogs (Lycaon pictus). Proc. R. Soc. B Biol. Sci. 262, 235–245.

[124] Angulo, E., Roemer, G.W., Berec, L., Gascoigen, J., Courchamp, F., 2007. Double Allee effects and extinction in the island fox. Conserv. Biol. 21(4), 1082–1091.

[125] Tian, X., Guo, S., 2021. Spatio-temporal patterns of predator-prey model with Allee effect and constant stocking rate for predator. Int. J. Bifurc. Chaos 31(16), 2150249.

[126] Zhu, Z., Chen, Y., Li Z., Chen, F., 2022. Stability and bifurcation in a Leslie-Gower predator-prey model with Allee effect. Int. J. Bifurc. Chaos 32(3), 2250040.

[127] Wang, L., Qiu, Z., Feng, T., Kang, Y., 2022. An eco-epidemiological model with social predation subject to a component Allee effect. Appl. Math. Model. 101, 111–131.

[128] Berec, L., Bernhauerová, V., Boldin, B., 2018. Evolution of mate-finding Allee effect in prey. J. Theor. Biol. 441, 9–18.

[129] Sasmal, S.K., 2018. Population dynamics with multiple Allee effects induced by fear factors – A mathematical study on prey-predator interactions. Appl. Math. Model. 64, 1–14.

[130] Hethcote, H.W., Wang, W., Han, L., Ma, Z., 2004. A predator-prey model with infected prey. Theor. Popul. Biol. 66, 259–268.

[131] Khajanchi, S., 2014. Dynamic behavior of a Beddington–DeAngelis type stage structured predator–prey model. Appl. Math. Comput. 244, 344–360.

[132] MacDonald, M., 1978. Time delays in biological models. Springer, Heidelberg.

[133] Marino, S., Hogue, I.B., Ray, C.J., Kirschner, D.E., 2008. A methodology for performing global uncertainty and sensitivity analysis in systems biology. J Theor Biol 254(1), 178–96.

[134] Freedman, H., Rao, V., 1983. The trade-off between mutual interference and time lags in predator-prey systems. Bull. Math. Biol. 45(6), 991–1004.

[135] Hale, J.K., Waltman, P., 1989. Persistence in infinite-dimensional systems. SIAM J. Math. Anal. 20(2), 388–395.

[136] Chen, F., 2005. On a nonlinear nonautonomous predatorprey model with diffusion and distributed delay. J Comput Appl Math 180(1), 33–49.

[137] Nyquist, H., 1932. Regeneration theory. Bell. Syst. Tech. J. 11(1), 126–147.

[138] Jafari, A., Hussain, I., Nazarimehr, F., Golpayegani, S.M.R.H., Jafari, S., 2021. A simple guide for plotting a proper bifurcation diagram. Int. J. Bifurc. Chaos 31(1), 2150011.

[139] Wolf, A., Swift, J.B., Swinney, H.L., Vastano, J.A., 1985. Determining Lyapunov exponents from a time series. Phys. D: Nonlinear Phenom. 16(3), 285–317.

[140] Holling, C.S., 1959. The components of predation as revealed by a study of small-mammal predation of the European Pine Sawfly. Can. Entomol. 91(5), 293–320.

[141] Perko, L., 2001. Differential Equations and Dynamical Systems. Springer Science & Business Media, New York.

[142] Riaz, S.S., Sharma, R., Bhattacharya, S.P., Ray, D.S., 2007. Instability and pattern formation in reaction-diffusion systems: a higher order analysis. J. Chem. Phys. 127, 064503.

[143] Sasmal, S.K., Takeuchi, Y., 2020. Dynamics of a predator-prey system with fear and group defense. J. Math. Anal. Appl. 481(1), 123471.

[144] Arditi, R., Ginzburg, L.R., 1989. Coupling in predator–prey dynamics: ratio-dependence. J. Theor. Biol. 139(3), 311–326.

[145] Berezovskaya, F., Karev, G., Arditi, R., 2001. Parametric analysis of the ratio-dependent predator-prey model. J. Math. Biol. 43, 221–246.

[146] Alonso, D., Bartumeus, F., Catalan, J., 2002. Mutual interference between predators can give rise to Turing spatial patterns. Ecology 83, 28–34.

[147] Crutzen, P.J., Stoermer, E.F., 2000. Global Change Newslett. 41, 12.

[148] Sabine, C.L., Feely, R.A., Gruber, N., Key, R.M., Lee, K., Bullister, J.L., Wanninkhof, R., Wong, C.S., Wallace, D.W.R., Tilbrook, B., Millero, F.J., Peng, T.H., Kozyr, A., Ono, T., Rios, A.F., 2004. The oceanic sink for anthropogenic CO_2. Science 305(5682), 367–371.

[149] Sekerci, Y., Petrovskii, S., 2015. Mathematical modelling of plankton–oxygen dynamics under the climate change. Bull. Math. Biol. 77, 2325–2353.

[150] Upadhyay, R.K., Kumari, S., Kumar, P., Rai, V., 2019. Spatial distribution of microalgae in marine systems: A reaction–diffusion model. Ecol. Complex. 39, 100771.

[151] Edwards, A.M., Brindley, J., 1999. Zooplankton mortality and the dynamical behavior of plankton population models. Bull. Math. Biol., 61, 303–339.

[152] Zhang, T., Wang, W., 2012. Hopf bifurcation and bistability of a nutrient–phytoplankton–zooplankton model. Appl. Math. Model. 36, 6225–6235.

[153] Janga, S.R.-J., Baglama, J., Rick, J., 2006. Nutrient-phytoplankton-zooplankton models with a toxin. Math Comput Model 43, 105-118.

[154] Franks, P.J.S., 2002. NPZ Models of Plankton dynamics: Their construction, coupling to physics, and Application. J. Oceanogr. 58, 379-387.

[155] Sekerci, Y., Ozarslan, R., 2020. Oxygen-plankton model under the effect of global warming with nonsingular fractional order. Chaos Solit. Fractals 132, 109532.

[156] Zhao, Q., Liu, S., Niu, X., 2020. Effect of water temperature on the dynamic behavior of phytoplankton–zooplankton model. Appl. Math. Comput. 378, 125211.

[157] Arditi, R., Lobry, C., Sari, T., 2015. Is dispersal always beneficial to carrying capacity? New insights from the multi-patch logistic equation. Theor. Popul. Biol. 106, 45-59.

[158] Pal, P.J., Saha, T., Sen, M., Banerjee, M., 2012. A delayed predator–prey model with strong Allee effect in prey population growth. Nonlinear Dyn. 68, 23–42.

[159] Groeger, A.W., Kimmel, B.L., 1989. Relationship between photosynthetic and respiratory carbon metabolism in freshwater phytoplankton. Hydrobiologia 173, 107-117.

[160] Mayzaud, P., Boutoute, M., Gasparini, S., Mousseau, L., 2005. Respiration in marine zooplankton—the other side of the coin: CO_2 production. Limnol. Oceanogr. 50(1), 291–298.

[161] Wai Yan Cheah, Pau Loke Show, Jo-Shu Chang, Tau Chuan Ling, Joon Ching Juan, 2015. Biosequestration of atmospheric CO_2 and flue gas-containing CO_2 by microalgae. Bioresour. Technol. 184, 190-201.

234

[162] Ho, S.-H., Chen, C.-Y., Lee, D.-J., Chang, J.-S., 2010. Perspectives on microalgal CO_2-emission mitigation systems - a review. Biotechnol. Adv. 29(2), 189–198.

[163] Freund, J.A. Mieruch, S., Scholze, B., Wiltshire, K., Feudel, U., 2006. Bloom dynamics in a seasonally forced phytoplankton–zooplankton model: Trigger mechanisms and timing effects. Ecol. Complex. 3(2), 129-139.

[164] Six, K.D., Maier-Reimer, E., 1996. Effects of plankton dynamics on seasonal carbon fluxes in an ocean general circulation model. Global Biogeochem Cycles, 10(4), 559-583.

[165] Edwards, A.M., 2001. Adding detritus to a nutrient–phytoplankton–zooplankton model:A dynamical-systems approach. J. Plankton Res. 23(4), 389–413.

[166] Rehim, M., Zhang, Z., Muhammadhaji, A., 2016. Mathematical analysis of a nutrient–plankton system with delay. SpringerPlus 5, 1055.

[167] Petrovskii, S.V., Sekerci, Y., Venturino, E., 2017. Regime shifts and ecological catastrophes in a model of plankton-oxygen dynamics under the climate change. J. Theor. Biol. 424, 91–109.

[168] Nagumo, M., 1942. Über die Lage der Integralkurven gewöhnlicher Differentialgleichungen. Proc. Phys. Math. Soc. Jpn. 24, 551–559.

[169] Sahoo, B., Poria, S., 2013. Disease control in a food chain model supplying alternative food. Appl. Math. Model. 37(8), 5653-5663.

[170] McKay, M.D., Beckman, R.J., Conover, W.J., 1979. A comparison of three methods for selecting values of input variables in the analysis of output from a computer code. Technometrics 21(2), 239–245.

[171] White, K.A.J., Gilligan, C.A., 1997. Spatial heterogeneity in three-species, plant-parasite-hyperparasite, systems. Phil. Trans. R. Soc. Lond. B 353(1368), 543–557.

[172] Mukherjee, N., Ghorai, S., Banerjee, M., 2019. Detection of turing patterns in a three species food chain model via amplitude equation. Commun Nonlinear Sci Numer Simul 69, 219-236.

[173] Bates, N.R., Best, M.H.P., Neely, K., Garley, R., Dickson, A.G., Johnson, R.J., 2012. Detecting anthropogenic carbon dioxide uptake and ocean acidification in the North Atlantic Ocean. Biogeosciences 9, 2509–2522.

[174] Winder, M., Sommer, U., 2012. Phytoplankton response to a changing climate. Hydrobiologia 698, 5–16.

[175] Sommer, U., Lengfellner, K., 2008. Climate change and the timing, magnitude, and composition of the phytoplankton spring bloom. Glob Chang Biol 14, 1199–1208.

[176] Lewandowska, A., Sommer, U., 2010. Climate change and the spring bloom: a mesocosm study on the influence of light and temperature on phytoplankton and mesozooplankton. Mar Ecol Prog Ser 405, 101–111.

[177] Smetacek, V., Klaas, C., Strass, V. et al. 2012. Deep carbon export from a Southern Ocean iron-fertilized diatom bloom. Nature 487, 313–319.

[178] Nguyen, K.D.T., Morley, S.A., Lai, C-H, Clark, M.S., Tan, K.S., Bates A.E., et al. 2011. Upper temperature limits of tropical marine ectotherms: Global warming implications. PLoS ONE 6(12), e29340.

[179] NOAA atmospheric CO_2 data: `https://gml.noaa.gov/ccgg/trends/gl_trend.html` (accessed 20 August, 2022)

[180] JMA ocean pCO_2 data: `https://www.data.jma.go.jp/gmd/kaiyou/english/co2_flux/co2_flux_data_en.html` (accessed 20 August, 2022)